HYBRID MODELING AND ANALYSIS OF MULTISCALE BIOCHEMICAL REACTION NETWORKS

A Thesis
Presented to
The Academic Faculty

by

Jialiang Wu

In Partial Fulfillment
of the Requirements for the Degree
PhD in Bioinformatics in the
School of Mathematics

Georgia Institute of Technology
October 2011

HYBRID MODELING AND ANALYSIS OF MULTISCALE BIOCHEMICAL REACTION NETWORKS

HYBRID MODELING AND ANALYSIS OF MULTISCALE BIOCHEMICAL REACTION NETWORKS

Approved by:

Dr. Eberhard O. Voit, Advisor
The Wallace H. Coulter Department of Biomedical Engineering
Georgia Institute of Technology and Emory University

Dr. Leonid Bunimovich
School of Mathematics
Georgia Institute of Technology

Dr. Yi Jiang
Mathematical Modeling and Analysis
Los Alamos National Laboratory

Dr. Howard Weiss
School of Mathematics
Georgia Institute of Technology

Dr. Melissa Kemp
The Wallace H. Coulter Department of Biomedical Engineering
Georgia Institute of Technology and Emory University

Dr. Robert Butera
The Wallace H. Coulter Department of Biomedical Engineering
Georgia Institute of Technology and Emory University

Date Approved:

This dissertation is dedicated to God
the Father, the Son and the Holy Spirit.
I would also like to thank my parents
Xingfa and Zhonghao, and my fiancée Carolyn Taylor.

ACKNOWLEDGEMENTS

My sincere thanks go to my advisor, Dr. Eberhard Voit, who gave me his patient guidance and high-standard level of training. He helped me to grow in independence, persistence and passion for excellence. His wisdom of, "Never waste any of your work," will be a lifelong asset to me. I will continue to do my best to uphold his standard in the coming years. I am also tremendously grateful to Dr. Yi Jiang. She has provided for me technical insights, connecting me to useful resources, as well as demonstrated to me an outstanding example of integrity and excellence in her own work. Many thanks go to Dr. Leonid Bunimovich. Thank you Leonid very much, for recruiting me into your math-team for bio-exploration. From you, I have received undying support and much encouragement! Also my appreciation goes to Dr. Brani Vidacovi, Dr. Melissa Kemp, Dr. Robert Butera, Dr. Luca Dieci and Dr. Howie Weiss. I know that you have invested your time and effort into my works as well as improving this dissertation. Thank you.

To whom I owe great gratitude, I want to thank my parents, Xingfa Wu and Zhonghao Li. Without exception they have stood beside me with strong support! I want to thank them for their prayers and practical guidance over the years. I could not have made it successfully to the finish line without them.

I also want to give credit to my fiancée and best friend, Carolyn Taylor Shurtz. I see her as a gift from God to me. She has been with me through every struggle in this past season of my life. When there seems to be "no light at the end of the tunnel," her gentleness has been my strength; and her sweetness wipes away the weariness of life. I know that her prayers have helped me tremendously in the technical advancements I have made in this period. On this journey of free running (one of my favorite sports), I see

Taylor as a help to view every obstacle in this life as a joy to overcome. The answer is there; it is just waiting to be discovered. Every problem can be answered with creativity and exploration of new ideas and solutions much like the sport I enjoy. Whether in relationships, work, responsibilities or the mundane in life, our faith will always be a cornerstone on which we can build. We will continue this journey together; and I am blessed and thankful to have her in my life.

I especially want to thank my many good, trial-tested and trustworthy friends whom I have served together with in the Lord: Shaun Wang and Esther Yang, Yonghui Lim, Maureen Leardini, Debra Stoner, Roy and Bessie Rhodes, Glenn and Shelley Hall, Johnny and Elizabeth Enlow, Julia Simmer, Mark and Elizabeth Roots, Jim and Paula Pendleton, Changsheng Lin and Biyun Ke. These are my true spiritual fathers and mothers and sisters and brothers. We have shed tears together, encouraged one another and sowed seeds of faith, hope and love. Thank you very much for being in my bigger family!

Above all I want to thank my Heavenly Father, who knows me and loves me greater and deeper than I have ever known of love before. Even before the earth was formed, He had given me a great calling in Him, full of purpose, meaning and life. His tender love dispels all fears; and in Him I find love of acceptance and forgiveness. He is my source of hope above all confusions, and peaceful joy within me that flows like living streams of water. He is always near, keeping His eyes on me and directing my path. These couple years at Tech were not lack of trials and difficulties, but I have found it worthy. He takes every opportunity to mold me into His image, giving me life and life abundant. Thank you Abba! I have victory in You!

TABLE OF CONTENTS

Page

ACKNOWLEDGEMENTS iv

LIST OF TABLES vii

LIST OF FIGURES xii

SUMMARY xvi

CHAPTER

Chapter 1 Introduction 1

1. Overall goal and specific aims of hybrid modeling 1

2. Background and significances 4

2.1. Biochemical Systems Theory; GMA Systems and S-systems 4

2.2. Hybrid Functional Petri Net 7

2.3. Agent Base Modeling in Systems Biology 10

2.4. Significance of extending BST to HFPN and ABM frameworks 13

References 17

Chapter 2 Hybrid Modeling in Biochemical Systems Theory by Means of Functional Petri Nets 23

Abstract 24

1. Introduction 25

2. Methods 26

2.1. Biochemical Systems Theory (BST) 28

2.2. Hybrid Functional Petri Nets (HFPN) 32

2.3. Implement of BST models as Petri Nets 34

2.4. Representation of stochasticity in HFPN 35

2.5. Approximation of various types of delays by ODEs 38

3. Results 42

Example 1: A generic pathway system 42

Example 2: An auto-repressive gene regulatory network 49

4. Discussion 56

4.1. BST and Petri Nets 57

4.2. Reformulation of different types of delays within BST (or other ODE frameworks) 57

4.3. Switches and stochasticity in BST 57

4.4. Stochasticity and delays 57

4.5.Design and operating principles 58

Acknowledgements 59

References 60

Chapter 3 Integrative Biological Systems Modeling: Challenges and Opportunities 64

Abstract 65

1. Introduction 66

1.1. Stochasticity of biochemical reaction in vivo 67

1.2. Accounting for multiple time scales in biological systems 69

1.3. Combined models of continuous and discrete components in intracellular systems 69

2.Methods 70

2.1. Biochemical Systems Theory; GMA systems and S-systems 70

2.2. Petri Net modeling 72

2.3. Implementing a BST model in HFPN 72

3.Illustration: genetic toggle switch 73

4.Challenges and future developments 81

Challenge 1: Analysis of functional properties of hybrid systems 83

Challenge 2: Parameter estimation 84

Challenge 3: Computational efficiency of hybrid modeling 84

Challenge 4: Discovery of design principles 85

Acknowledgements 85

References 85

Chapter 4 Impacts of Delays and Noise on Dopamine Signal Transduction 90

Abstract 91

1. Introduction 91

2. Methods 96

2.1. Biochemical Systems Theory 97

2.2. Implementation of a GMA model as a Hybrid Functional Petri Net 98

2.3. Representation of delays and noise in the model of dopamine dynamics 99

2.4. Simulation of dopamine flux in response to calcium signals 101

3.Results 102

3.1. Effects of different delays 102

3.2. Effects of stochastic noise 106

3.3. Combined effects of delays and noise 109

4.Discussion 111

Acknowledgements 114

References 114

Chapter 5 Constructing Stochastic Models from Deterministic Process Equations by Propensity Adjustment 122

Abstract 124

1. Background 125

1.1. Representations of systems of biochemical reactions 127

1.2. Motivation for the power-law formalism: reactions in crowded media 129

1.3. The Generalized Mass Action (GMA) format 132

1.4. Proper use of equation-based functions for stochastic simulations 133

2. Method 134

2.1. Deriving the mean and variance of a power-law function of random variables 134

2.2. Deriving proper propensity functions for stochastic simulations from differential equation-based models 136

2.3.Calculation of $\mathrm{cov}\left[\log X_i(t), \log X_j(t)\right]$ 147

2.4.Statistic criteria for propensity adjustment 149

3. Result 150

3.1. Generic special cases 150

3.2. Power-law representation of a reversible reaction with feedback controls 153

3.3. Repressilator 157

3.4. Enzymatic reaction using a quasi-steady state assumption (QSSA) 163

3.5. Stochastic focusing 166

4. Discussion and conclusion 166

Authors' contributions 174

Acknowledgements 174

References 176

Chapter 6 Stochastic 3D Simulations of Diffusion-Controled Reactions with Concentration Dependent Kinetics Rate in Crowded Environments 180

Abstract 182

1. Introduction 182

2. Methods 187

Motivation for power-law representations in crowded medium 187

Extensions of strict ODE representation 190

Method 1: Extending a reaction-kinetic ODE to spatial stochastic modeling 191

i) Association reaction 191

ii) Dissociation reaction 195

iii) Particle-based diffusion 197

Method 2: An ODE for diffusion-controlled reactions in a homogeneous system 202

3. Results 207

3.1. Distinction between Method 1 and 2: theoretical considerations 207

3.2. Numerical Validation of Method 1 and 2 210

Numerical Validation for association reactions 210

Numerical Validation for dissociation reactions 212

Numerical Validation for reversible reactions 213

3.3. Models of reaction in virtual crowded media 214

Creating crowded medium with Netlogo 215

Diffusion in crowded medium 215

3.4. Quantifying crowding effects 216

Quantifying crowding effects within the framework of Method 216

Quantifying crowding effects within the framework of Method 221

3.5. Application to binding of Dansylamide and Carbonic Anhydrase in a crowed medium 224

4. Conclusion 227

Authors' contributions 230

Acknowledgements 230

References 230

Chapter 7 Summary, Conclusions and Future Works 255

APPENDIX A: Derivation of the mean and variance of a power-law function of random variables 265

APPENDIX B: Computation of approximate mean and covariance for a generic propensity function to be used in stochastic simulations 271

LIST OF TABLES

Page

Table 4.1: The number of effective responses changes with different delays 105

Table 6.1: Numerical values of parameters used in Fig.6 236

Table 6.2:
Kinetic parameters obtained by weighted least-squares fitting of the GMA model in eqn.

(73) for crowded and non-crowded media 237

LIST OF FIGURES

Page

Figure 1.1: Representations of a biochemical reaction 5

Figure 1.2: An illustrative HFPN model of transcription and translation 8

Figure 2.1: An illustrative HFPN model of transcription and translation 33

Figure 2.2: GMA system and its HFPN representation 35

Figure 2.3: Implementation of monomolecular and bimolecular reactions in a discrete Petri Net 36

Figure 2.4: A generic system with one inhibitory feedback loop and two delays: standard diagram and its corresponding HFPN representation 43

Figure 2.5: Comparisons between the solutions obtained with established methods 44

Figure 2.6: Generic biochemical system with random delays 46

Figure 2.7: Generic biochemical system with noise, delays and feedback loop 47

Figure 2.8: Auto-repressive gene expression system and initial parts of its HFPN representation 50

Figure 2.9: Auto-repressive gene regulatory network in a single cell 51

Figure 2.10: Auto-repressive gene regulatory network in a single cell 52

Figure 2.11: Auto-repressive gene regulatory network in a single cell 54

Figure 3.1: GMA system and its HFPN representation 73

Figure 3.2: Genetic toggle switch associated with the SOS signaling pathway 75

Figure 3.3: HFPN representation the ODE portion of the toggle switch 76

Figure 3.4: HFPN representation the stochastic portion of the toggle switch 77

Figure 3.5: Simulations of the genetic toggle switch as it is affected by the SOS signaling pathway 78

Figure 3.6: Alternative HFPN model of the toggle switch with direct implementation of Gaussian noise, asdepicted by Cell Illustrator 79

Figure 3.7: Simulations of the toggle switch with the alternate HFPN model in Fig. 5 80

Figure 4.1: The chemical synapse of a dopaminergic neuron and its role in signal transduction 95

Figure 4.2: Generic GMA system and its HFPN representation 99

Figure 4.3: Implementation of noisy and delayed processes in a hybrid GMA-HFPN model 100

Figure 4.4: Effects of different delays on dopamine signaling 104

Figure 4.5: Effects of delays when signals are sparse 105

Figure 4.6: Statistics of effective responses in dopamine signaling systems subjected to noise of various amplitudes and frequencies 108

Figure 4.7: Signaling dynamics of dopamine systems subjected to noise 109

Figure 4.8: Combined effects of different delays and noise 110

Figure 5.1: Scheme of reversible reaction with feedback controls 154

Figure 5.2: Reversible reaction with feedback controls 156

Figure 5.3: Reaction scheme of the repressilator 158

Figure 5.4: Scaling of the repressilator equations changes the oscillation period in the stochastic simulation 159

Figure 5.5: Power-law approximation of $p(x_i)^{-1}$ 161

Figure 5.6: A comparison of the dynamics of repressilator using the original ODEs, GMA

approximation and its corresponding moment-based ODEs 163

Figure 5.7: Stochastic focusing 169

Figure 6.1: Spatial stochastic simulations of a homogeneous diffusion-reaction system238

Figure 6.2: The dissociation reaction in eqn.(47) is concentration dependent, but diffusion independent 240

Figure 6.3: Comparison of spatial stochastic simulations of a homogeneous, reversible diffusion-reaction system with predictions from two ODEs models 241

Figure 6.4: Creating a virtual, crowded medium by filling a reaction volume with inert blocks 243

Figure 6.5: Enzymatic reaction-diffusion system in crowded media 244

Figure 6.6: Detailed quantification of crowding effects 246

Figure 6.7: The two GMA models (for dilute and sucrose media) are not affected significantly by the diffusion rate 247

Figure 6.8a: The GMA model (for dilute conditions) are not affected significantly by a wide range of crowding parameters 249

Figure 6.8b: Two GMA models (for dilute and sucrose conditions) are not affected significantly by awide range of crowding parameters 251

Figure 6.9: Comparison of diluted mass action models (left panel) and diluted GMA models (right panel) with escalated association rates under different degrees of crowding. 253

Figure 6.10: Diluted mass action models with escalated association rate are affected significantly by high crowdedness 254

SUMMARY

This dissertation addresses the development of integrative modeling strategies capable of combining deterministic and stochastic, discrete and continuous, as well as multi-scale features. The first set of studies combines the purely deterministic modeling methodology of Biochemical Systems Theory (BST) with a hybrid approach, using Functional Petri Nets, which permits the account of discrete features or events, stochasticity, and different types of delays. The efficiency and significance of this combination is demonstrated with several examples, including generic biochemical networks with feedback controls, gene regulatory modules, and dopamine based neuronal signal transduction.

A study expanding the use of stochasticity toward systems with small numbers of molecules proposes a rather general strategy for converting a deterministic process model into a corresponding stochastic model. The strategy characterizes the mathematical connection between a stochastic framework and the deterministic analog. The deterministic framework is assumed to be a generalized mass action system and the stochastic analogue is in the format of the chemical master equation. The analysis identifies situations where internal noise affecting the system needs to be taken into account for a valid conversion from a deterministic to a stochastic model. The conversion procedure is illustrated with several representative examples, including elemental reactions, Michaelis-Menten enzyme kinetics, a genetic regulatory motif, and stochastic focusing.

The last study establishes two novel, particle-based methods to simulate biochemical diffusion-reaction systems within crowded environments. These simulation methods effectively simulate and quantify crowding effects, including reduced reaction volumes, reduced diffusion rates, and reduced accessibility between potentially reacting

particles. The proposed methods account for fractal-like kinetics, where the reaction rate depends on the local concentrations of the molecules undergoing the reaction. Rooted in an agent based modeling framework, this aspect of the methods offers the capacity to address sophisticated intracellular spatial effects, such as macromolecular crowding, active transport along cytoskeleton structures, and reactions on heterogeneous surfaces, as well as in porous media.

Taken together, the work in this dissertation successfully develops theories and simulation methods which extend the deterministic, continuous framework of Biochemical Systems Theory to allow the account of delays, stochasticity, discrete features or events, and spatial effects for the modeling of biological systems, which are hybrid and multiscale by nature.

CHAPTER 1

INTRODUCTION

1. Overall goal and specific aims of hybrid modeling

Most biological systems are by nature hybrids consisting of interacting discrete and continuous components, which may even operate at different spatiotemporal scales. It is therefore desirable to establish modeling frameworks that are capable of combining deterministic and stochastic, discrete and continuous, as well as multi-scale features. An example for the need of such a combination is the investigation of integrated biological pathways that contain gene regulatory, metabolic and signaling components, some of which involve on-off decisions as well as stochastic effects imposed by heterogeneous environments. The implementation of an integrated hybrid system is not trivial because most software is limited to one or the other of the dichotomies above. It is also well recognized that hybrid systems are notoriously difficult to set up and analyze.

The goal of this dissertation is to develop integrative modeling strategies that combine the purely deterministic modeling methodology of Biochemical Systems Theory (BST) with hybrid approaches, such as Petri Nets and Agent Based Modeling (ABM). The efficiency and significance of these combinations is demonstrated with different representative examples, such as generic biochemical networks with feedback controls, gene regulatory modules, and dopamine based neuronal signal transduction. The details of this work are structured according to the following specific aims, and presented in Chapters 2 to 6. The work in these chapters has been (or is being) published in professional journals and is reproduced in the published format.

Specific Aim 1: Implement BST in a hybrid functional Petri net (HFPN) framework.

Chapter 2 extends BST to hybrid modeling within the framework of Hybrid Functional Petri Nets (HFPN). First I show how the canonical GMA and S-system models in BST can be directly implemented in a standard Petri Net framework. In a second step I demonstrate how to account for different types of time delays as well as for discrete, stochastic and switching effects. Using representative test cases, I validate the hybrid modeling approach through comparative analyses and simulations with other approaches and highlight the feasibility, quality and efficiency of the hybrid method. Continuing in Chapter 3, by using the example of a toggle switch, I demonstrate the flexibility of this hybrid modeling framework through two modeling approaches. Moreover, some significant challenges and future opportunities in hybrid modeling are discussed.

Specific Aim 2: Build hybrid model for dopamine based neuronal signal transduction.

Utilizing the methods developed in Specific Aim 1, a hybrid model for dopamine based neuronal signal transduction is established in Chapter 4. Dopamine is a critical neurotransmitter for the normal functioning of the central nervous system. Abnormal dopamine signal transmission in the brain has been implicated in diseases such as Parkinson's disease (PD) and schizophrenia, as well as in various types of drug addiction. It is therefore important to understand the dopamine signaling dynamics in the presynaptic neuron of the striatum and the synaptic cleft, where dopamine synthesis, degradation, compartmentalization, release, reuptake, and numerous regulatory processes occur. The biochemical and biological processes governing this dynamics consist of interacting discrete and continuous components, operate at different time scales, and must function effectively in spite of intrinsic stochasticity and external perturbations. Not

fitting into the realm of purely deterministic phenomena, the hybrid nature of the system requires special means of mathematical modeling, simulation and analysis. I show in this part of the dissertation how hybrid functional Petri-nets (HFPNs) and the software Cell Illustrator® facilitate computational analyses of systems that simultaneously contain deterministic, stochastic, and delay components. I evaluate the robustness of dopamine signaling in the presence of delays and noise and discuss implications for normal and abnormal states of the system.

Specific Aim 3: Mathematical foundation and method to construct stochastic models from deterministic process equations.

Chapter 5 discusses a rather general strategy for converting a deterministic process model into a corresponding stochastic model. The strategy characterizes the mathematical connection between a stochastic framework and the deterministic analog. The deterministic framework is assumed to be a generalized mass action system and the stochastic analogue is in the format of the chemical master equation. The analysis identifies situations where internal noise affecting the system needs to be taken into account for a valid conversion from a deterministic to a stochastic model. The conversion procedure is illustrated with several representative examples, including elemental reactions, Michaelis-Menten enzyme kinetics, a genetic regulatory motif, and stochastic focusing.

Specific Aim 4: Develop ABM methods for investigating biochemical reactions in heterogeneous intracellular environments.

Chapter 6 establishes two novel, particle-based methods to simulate biochemical diffusion-reaction systems within crowded environments. These simulation methods effectively simulate and quantify crowding effects, including reduced reaction volumes, reduced diffusion rates, and reduced accessibility between potentially reacting particles. The proposed methods account for fractal-like kinetics, where the reaction rate depends

on the local concentrations of the molecules undergoing the reaction. Rooted in an agent based modeling framework, this aspect of the methods offers the capacity to address sophisticated intracellular spatial effects, such as macromolecular crowding, active transport along cytoskeleton structures, and reactions on heterogeneous surfaces, as well as in porous media.

2. Background and Significance

2.1. Biochemical Systems Theory; GMA Systems and S-systems

Modeling a network requires a sufficiently accurate, mathematically feasible description of all critical components and their interactions. Two "extreme" conceptual frameworks for mathematical pathway modeling that are commonly used are: a) Deterministic kinetic models, represented by differential equations and often formulated as generalized mass action systems, where reaction rates depend continuously on changes in the participating species over time. b) Stochastic models and simulations of biochemical reaction networks ultimately based on the Chemical Master Equation (Gillespie 2007) for homogeneous systems and Reaction Diffusion Master Equation for heterogeneous ones. Among the deterministic models, *Biochemical Systems Theory* (BST) is one of the best established and most general modeling frameworks (Savageau 1969 a; Savageau 1969 b; Savageau 1976; Voit 2000). The basis of BST is the use the power-law functions to approximate enzyme-catalyzed reactions that may be regulated or modulated by other components of the system under study. Canonical methods have been developed for representations such as S-systems and Generalized Mass Action (GMA) models within BST. These representations have the formats shown in Figure 1.

$$\dot{X}_i = \sum_{j=1}^{p} v_{ij}^{+} - \sum_{j=1}^{q} v_{ij}^{-} = V_i^{+} - V_i^{-}, \quad i = 1, \cdots, n.$$

$$\dot{X}_i = \sum_{p=1}^{P_i} \left[\pm \gamma_{ip} \prod_{j=1}^{n} X_j^{f_{ipj}} \right], \qquad i = 1, \cdots, n.$$

$$\dot{X}_i = \alpha_i \prod_{j=1}^{n} X_j^{g_{ij}} - \beta_i \prod_{j=1}^{n} X_j^{h_{ij}}, \qquad i = 1, \cdots, n.$$

Figure 1.1 Representations of a biochemical reaction. Upper panel: generic model; middle panel: GMA system; lower panel: S-system.

A GMA model is based on a multivariate power-law representation that may be developed *de novo* or as an approximation of some other nonlinear rate laws. Formulated as shown in Fig.1, the rate of change within a specific pool X_j, which could represent a gene activity, metabolite, or protein level, is determined by the difference between incoming (production) fluxes and outgoing (degradation) fluxes. Each incoming or outgoing flux is individually represented by a product of power-law functions. The rate constants γ_{ip} are positive or zero and the kinetic orders f_{ipj} have real values; both types of parameters are to be estimated from observations. The positive terms represent the production of pool X_j, while negative terms describe degradation.

While a GMA model requires each input or output flux to be represented by one power-law term, an S-system model combines all input fluxes into one power-law term and all the output fluxes into a second term, with the result that S-system equations contain at most one positive and one negative power-law term. This difference in format leads to differences in mathematical features, which have been compared and discussed many times (*e.g.*, (Voit 2000)). A main advantage of the GMA format is its closeness to biological intuition, because each process is mapped, one-to-one, onto a specific mathematical term. The aggregation of terms in the S-system format somewhat clouds

this intuition, but has significant mathematical advantages, such as the algebraic computability of steady states, along with straightforward methods of stability and sensitivity analysis (Savageau 1969 b; Savageau 1976). I will use the GMA format in the following illustrations.

The translation of a graphical pathway representation into a GMA model is straightforward. Consider any dependent variable X_i in the pathway map. The arrows pointing toward X_i represent the flows of material contributing to the production of X_i. For each entering flow, one lists all variables that directly affect the flow (by contributing material or a signal), which enter the power law term of X_i, with their own kinetic order f_{ipj}. The first index of the kinetic order i refers to the dependent variable being produced, the second index p refers to the index of the flow, and the third index j refers to the variable contributing to the production. The rate constant γ_{ip} is included after all variables are listed as a product. The degradation of X_i is formulated in the same way. The construction of equations is repeated for all dependent variables. Finally, the initial values of the dependent variables, values for all independent variables, and all rate constants and kinetic orders need to be set.

Other biological formalisms based on ordinary differential equations (ODEs) have been developed for pathway representation and simulation, including mass action, lin-log (Hatzimanikatis and Bailey 1996; Visser and Heijnen 2002), and SC methods (Albert, Benito et al. 2007). Their translation into Petri Nets and ABM is similar, and I will focus here exclusively on BST models. Among differently structured types of approaches of network analysis, Boolean methods (Kauffman, Peterson et al. 2003), graph methods (Aittokallio and Schwikowski 2006), and Petri Nets (Chaouiya 2007) have received some attention. Since Boolean methods do not appropriately represent cycles or feedback and graph methods usually require linearity, I will not pursue these approaches. Moreover,

partial differential equations (PDE) have been used to describe the spatial distribution of species or force fields; however, it is very difficult to account for biologically commonplace spatial effects such as macromolecular crowding and highly structured intracellular environments. Therefore, I will use agent based modeling, which offers a very flexible approach to addressing these complicated spatial effects.

In the following chapters, I will show in a hierarchical fashion how to include delays, discrete features or events, stochasticity and spatial effects into an initial ODE based model. The sequence of models will be:

- ODEs
- ODEs with delays
- HFPN framework to include delays, discrete features or events and stochasticity
- ABM framework to include delays, discrete features or events, stochasticity and spatial effects

2.2. Hybrid Functional Petri Net (HFPN)

A Petri Net is a graphical and mathematical formalism for systems with concurrent processes and properties that may be continuous or discrete. Petri Nets have been applied to such diverse disciplines as manufacturing and communication (Reisig 1985) and were apparently first applied to biological systems by Reddy and collaborators in 1993 (Reddy, Mavrovouniotis et al. 1993). To meet various needs, Petri Nets have been extended into different directions: Stochastic Petri Nets include randomness; Colored Petri Nets add a color feature to tokens and thus allow, in the same model, the representation of different dynamic behaviors that are modeled by different token colors; Hybrid Petri Nets allow the simultaneous investigation of discrete and continuous processes; Functional Petri Nets permit dynamic modifications of system parameters. Hardy and Robillard (Hardy

and Robillard 2004) recently reviewed the advantages of specific Petri Net formalisms for qualitative or quantitative analyses. Of particular importance here is the Hybrid Functional Petri Net (HFPN) format.

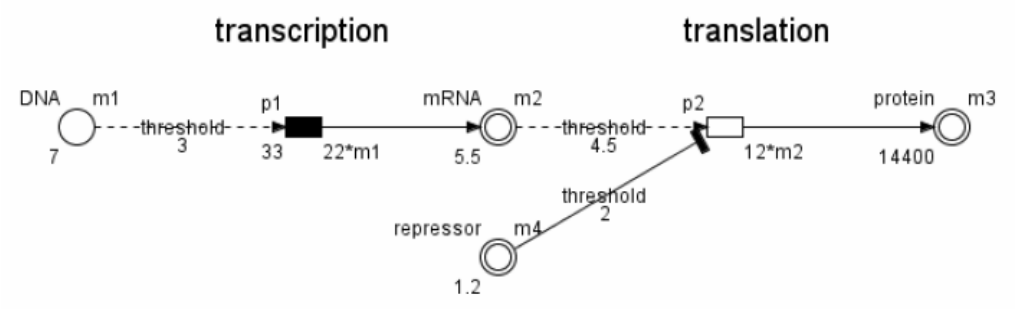

Figure 1.2 An illustrative HFPN model of transcription and translation (as depicted in Cell Illustrator (Miyano 2008)). Test arcs are used as input arcs because DNA (mRNA) is not consumed by the process of transcription (translation). The effect of a repressor element is described by an inhibitory arc. Here $m1$ is the number of DNA molecules with initial value 7; $m2$ is the mRNA concentration with initial value 5.5; $m3$ is the protein concentration with initial value 14,400; $m4$ is the repressor concentration with initial value 1.2. The discrete transition $p1$ represents the transcription, which is fired with the speed of $22 \cdot m1$ per time unit and with delay 33; the continuous transition $p2$ describes the translation and is fired with speed $12 \cdot m2$ per time unit. Translation occurs only if the mRNA concentration $m2$ is greater than or equals to the test arc weight 4.5 and if the repressor concentration $m4$ is less than or equal to the inhibitory arc weight 2.0. (from (Wu and Voit 2009 a))

HFPN is an extended functional Petri Net that accounts for both discrete and continuous events within the same model system (Matsuno, Tanaka et al. 2003) and has been implemented in the software package Cell Illustrator (Miyano 2008). HFPN consists of three types of process elements: places, transitions, and arcs (Figure 2). Places appear graphically as single (discrete type) or double (continuous type) lined circles that represent the states of the modeled system. In terms of biochemical pathways, places usually represent molecular species such as chemical substrates or enzymes. A discrete place contains an integer number of tokens which represents the number of molecules,

while a continuous place contains a positive real number representing the substrate concentration. The number of tokens in discrete places and the concentration in continuous places define the *marking* of the system. Transitions (filled or empty rectangles) represent (discrete or continuous) *actions* of the modeled system, such as biochemical reactions, protein binding, transcription, translation, or translocation. Both types of transitions have the property *speed*, which is a function of the marking of the system, whereas only a discrete transition has the property *delay*, which quantifies the time interval between consequent tokens to be processed by the transition. An arc is used to connect a place with a transition. (It is not allowed to use an arc to connect between places or between transitions.) An arc from a place to a transition is called an *input arc*, and one from a transition to a place is called an *output arc*. There are three types of arcs: *normal*, *inhibitory*, and *testing*. All three types of arcs may be used as input arcs, while only a normal arc is allowed to be used as an output arc. Each arc has the property *weight*, which is the minimum amount of flux required for the arc to function. A transition is *enabled* only if the content in all source places (there may be only one source place) is equal to or exceeds the weight of the input arc(s). When a transition is *fired*, the content in each source place is taken off the arc weight amount and, through a normal arc, the output arc weight amount of content is added to each sink place. An inhibitory arc with weight w enables a transition to fire only if the content of the source place is less than or equal to w. For instance, an inhibitory arc can be used to represent a repressor in gene regulation. A test arc does not consume any content of the source place by firing, but is used, for instance, to represent an enzyme catalyzing a reaction without being consumed (Figure 1.2).

2.3. Agent Based Modeling in Systems Biology

Agent based modeling (ABM) is a rule-based computational modeling methodology where the constituents of a real system are treated as unique individuals (called *agents*) residing in an *environment* where agents interact with one another and with the environment by specific if-then *rules*, thereby allowing complex system behaviors to be generated in a very intuitive manner (Bankes 2002; Bonabeau 2002; Grimm, Revilla et al. 2005).

One important, generic goal of systems biology is to understand how the interactions of microscopic components in a biological system can give rise to a system's macroscopic functioning and behavior. In contrast to the paradigm of reductionism which attempts to reduce a phenomenon to a set of fundamental components by "taking things apart," systems biology focuses on how system level properties emerge from the interactions of individuals by "putting things together." Thus, a central piece of systems biology is to integrate *in vitro* and *in vivo* biological data into mathematical or computational models in order to achieve a comprehensive and unified understanding of the biological phenomenon. While many analytical methods focus on characterizing the equilibria of systems, ABM allows investigations of how these equilibria are generated and is in some way complementary to strictly analytical methods. More specifically, the following characteristics of systems biology are directly in line with the ABM philosophy, making ABM an appealing modeling framework for the development, analysis and utilization of systems models.

1. **Complexity.** Systems biology investigates biological systems which are by nature complex in structure, function, dynamical history and environments. For instance, intracellular biochemical reactions often occur in a non-homogeneous and highly structured environment; enzymatic biochemical reactions frequently occur at the surface of intracellular organelles, instead of a homogeneous 3D space that is present *in vitro*; the

function of proteins is affected by their spatial conformation and location and thus highly sensitive to effects of macromolecular crowding. The complexity in systems modeling can be addressed in ABM as follows:

Structural complexity: Besides defining local interaction rules at the individual level, ABM is capable of imposing constraints on parts of the system or the whole system, thus allowing maximum control on system structure specification.

Functional complexity: The interaction rules for agents can be made up of thousands of lines of computational script, thereby enabling agents to achieve sophisticated functionality such as memory and adaptation. Expressed differently, what an agent can do is determined by the modeling objectives, and the flexibility in interaction rule specification can lead to distinctly different levels of functional abstractions.

Dynamical complexity: Agents are equipped with state variables, each of which is a specific function of the agent and its interaction history. Therefore an agent's current behavior depends on its unique history. Moreover, the congregated behaviors of all agents give rise to the system's history, which in turn can feed back to restrain the current behavior of an individual agent. ABM can record the dynamical history of both individual agents and the whole system, and therefore provides maximum capacity to interrogate, explain and understand the system dynamics.

Environmental complexity: ABMs allow for spatial features, and ABM software is often equipped with primitives for the construction of desired spatial structures. As a result, it is relatively easy even for non-experts to reconstruct a realistic reaction environment with complicated geometry and topology. Examples include a 2D surface with blocks positioned on it and a 3D space filled with microskeletons.

2. **Emergence.** Systems biology explores how novel properties, patterns and functions at the system level arise from dynamical interactions of relatively simple entities at lower levels. ABM specifies the interactions at the individual level as agent rules and instantiates the rules' consequences by simulation. Compared with the traditional analytic methods, which focus on characterizing the behavioral patterns of a system, agent based models allow us to explore the possible causal factors generating these patterns or to test the veracity of a set of identified/presumed mechanisms in a system, thereby fitting the goal of systems biology.

3. **Integration.** One major challenge for systems biology is the integration of biological data of multiple scales and formats into a single model to gain a comprehensive and unified understanding. These data can be qualitative as well as quantitative, thus making equation-based methods alone insufficient. The ABM framework is powerful for integration because it can incorporate a rule-based paradigm with an equation-based paradigm by assigning to agents *if-then* logical rules while updating the state variables of the environment or agent with equations. As illustrated by an ABM model of chemotaxis (Guo, Sloot et al. 2008), this feature also allows ABM to incorporate data of multiple scales. In this particular model, cells are modeled by agents while molecules are represented by variables, thereby successfully integrating the cell migration dynamics with a scale of micrometer per minute with molecular reaction-diffusion dynamics in the range of nanometers per millisecond. Because the behaviors of a system ultimately arise from the interactions among its constituents, and in turn feed back to restrain an individual's dynamics, the ABM multi-scale capacity becomes very attractive, especially for continual integration of new research findings, as demanded by biological system modeling.

2.4. Significance of Extending BST to HFPN and ABM Hybrid Frameworks

While BST models have been successfully applied in a variety of biological fields, their structure as systems of ordinary differential equations imposes limits on their scope. The following issues cannot be directly modeled in BST (and the same is true for all other modeling approaches that are anchored in ordinary differential equations): discrete features or events, stochasticity, delays and spatial effects. The first three can be addressed by HFPN techniques and all of them can be represented in ABM, thereby making these hybrid frameworks significant for biological systems modeling. However, the advantages of HFPN and ABM do not come for free. In particular, it is extremely difficult to perform analytical tasks on rule-based ABM structures, and the characterization of features like stability, sensitivities, and bifurcations must rely on simulations.

1. Discrete features or events. In addition to continuous changes, biological systems are frequently exposed to external or internal switches. In the former case, the environment may abruptly change, whereas an example for the latter is the turning on or off of the expression of some gene. External switches are easy to implement through a segmentation of the time scale, whereas internal switches are much more complicated because they depend on the internal state of the system and are therefore difficult to predict. Modeling of hard internal switches thus requires some approximation with a "softened" continuous switch (Voit 2005) or if-then statements (Savageau 2001). By contrast, discrete features and if-then rules are native features of rule-based HFPN and ABM representations.

2. Stochasticity. Most metabolic analyses implicitly assume that thousands of molecules are available to participate in an enzymatic reaction. However, this is not necessarily the case if pathways outside the organism's central metabolism are under investigation. If only relatively few molecules are present, the assumptions underlying essentially all continuous rate laws are questionable. The kinetic conversions become strings of discrete events that happen randomly, with some (possibly time dependent) probability, and it seems that the dynamics is better formulated as a stochastic process. The best known formulation of this type of approach is Gillespie's "stochastic simulation algorithm" (Gillespie 1977), which has triggered the development of numerous variations (Gillespie 2000; Gillespie 2001; Gillespie 2001). Wolkenhauer (Wolkenhauer, Ullah et al. 2004) recently reviewed the progression of approximations, starting with a true stochastic process, via the Chemical Master Equations and Langevin's formulation, and ultimately resulting in typical continuous rate laws. However, Gillespie methods do not address stochasticity resulting from spatial effects and the computational cost even for single reactions is substantial. It is therefore hardly feasible to implement realistic systems such as large metabolite networks in crowded intracellular environments. In HFPN, a random number generator and various probability functions are available, thereby allowing actualization of stochastic components, whether these are continuous (in the form of stochastic equations) or discrete. By contrast, stochasticity from both small numbers of reactants and environmental uncertainties can be naturally addressed by ABM: each reactant is represented by an agent and the perturbation from the environment can be incorporated into the agent's interaction rules, such as the reaction probability between reacting agents.

3. Delays. All typical metabolic models assume that the reaction speed depends directly on the current state of the system. In reality, there may be significant delays, for instance, between the up-regulation of a gene and its ultimate metabolic effect, or the reception of

an external signal and the effect of the transduced signal on genome expression. The natural choice for mathematically representing delays in continuous systems is the format of Delay Differential Equations (DDEs), whose theoretical foundation is well established (Hale and Lunel 1993). An impediment to the practical use of DDEs is the fact that their analysis requires specialized software, which is distinct from standard software for ODEs. Moreover, if delays are to be combined with discrete or stochastic effects, software for analysis is essentially lacking and must be designed from scratch. While models within BST consist entirely of ODEs, Mocek *et al*. showed that processes with a constant delay can be approximated with arbitrary accuracy within the BST format (Mocek, Rudnicki et al. 2005). This approximation is accomplished through the introduction of auxiliary variables and equations, which however do not require additional biological parameters. Wu and Voit further extended Mocek's method to allow for multiple delays of different types, including discrete, distributed, time dependent, and random delays (Wu and Voit 2009 a; Wu and Voit 2009 b). For HFPN, a delay is an imbedded function for a discrete process, while delays in continuous processes can be implemented by the techniques for ODEs described above. Compared with equation based methods where delays need to be implemented by auxiliary processes, delays in ABM originate naturally, for instance, from the time needed by agents for migration (through diffusion or facilitated flow) and from agent interaction processes, since in an agent based model, agents mimic the real system constituents and their interactions mimic the real systems dynamics.

4. Spatial Effects. Most metabolic models assume spatial homogeneity, even though it is known that the organization of cells is highly compartmentalized. This is a very difficult problem, and even partial differential equation (PDE) models are not always appropriate, because the underlying mechanisms, such as active transport and the use of scaffolds, are intrinsically different from diffusion processes that are better amenable to PDE methods.

While HFPN can only deal with non-spatial issues, ABM was designed specifically to account for spatial heterogeneity as described in the previous sections.

As soon as switches, delays, stochasticity and spatial effects are significant within the same system of interest, none of the traditional modeling frameworks are sufficient. However, it is desirable to address them concurrently within one package, for instance, to answer the question: What is the significance of a delay in a stochastic system? This is not an artificially construed question, because it was recently shown, for instance, that although transcription may be highly erratic, metabolite levels are very well buffered (Ishii, Nakahigashi et al. 2007). Explanations of this observation require the simultaneous modeling of both, stochastic effects and time delays. Moreover, the stochastic effects originating from spatial features and from small number reactants have been known to incur important biological consequences. This complexity has been demonstrated with numerous examples, such as microtubule formation (Dogterom and Leibler 1993), ultrasensitive modification and de-modification reactions (Berg, Paulsson et al. 2000), plasmid copy number control (Paulsson and Ehrenberg 2001), noise-induced oscillations (Vilar, Kueh et al. 2002) and metabolite dynamics (Elf, Paulsson et al. 2003). I will show in the following how these types of questions can be addressed when I embed BST in HFPN and ABM frameworks. I use for all demonstrations the HFPN software Cell Illustrator® (Miyano 2008) and the ABM software Netlogo (Wilensky 1999). While I primarily focus on BST, other ODE formulations could be addressed similarly.

References

Aittokallio, T. and B. Schwikowski (2006). "Graph-based methods for analysing networks in cell biology." Brief Bioinform **7**(3): 243-255.

Albert, S., H.-B. Benito, et al. (2007). "Cooperativity and saturation in biochemical networks: A saturable formalism using Taylor series approximations." Biotechnology and Bioengineering **97**(5): 1259-1277.

Alves, R. and M. A. Savageau (2000). "Effect of overall feedback inhibition in unbranched biosynthetic pathways." Biophysical Journal **79** 2290-2304.

Bankes, S. C. (2002). "Agent-based modeling: A revolution?" Proceedings of the National Academy of Sciences of the United States of America **99**(Suppl 3): 7199-7200.

Berg, O. G., J. Paulsson, et al. (2000). "Fluctuations and quality of control in biological cells:

zero-order ultrasensitivity reinvestigated.". Biophys J **79**: 1228-1236.

Bonabeau, E. (2002). "Agent-based modeling: Methods and techniques for simulating human systems." Proceedings of the National Academy of Sciences of the United States of America **99**(Suppl 3): 7280-7287.

Chaouiya, C. (2007). "Petri net modelling of biological networks." Brief Bioinform: bbm029.

Dogterom, M. and S. Leibler (1993). "Physical aspects of the growth and regulation of microtubule

structures." Physical Review Letters **70**: 1347-1350.

Elf, J., J. Paulsson, et al. (2003). "Near-critical phenomena in intracellular metabolite pools." Biophys J **84**: 154-170.

Fell, D. A. (1997). Understanding the Control of Metabolism, Portland Press, London.

Gillespie, D. T. (1977). "Exact stochastic simulation of coupled chemical reactions " Journal of Physical Chemistry **81**(25): 2340-2361.

Gillespie, D. T. (2000). "The chemical Langevin equation." The Journal of Chemical Physics **113**(1): 297-306.

Gillespie, D. T. (2001). "Approximate accelerated stochastic simulation of chemically reacting systems." Journal of chemical physics **115**: 1716-1733.

Gillespie, D. T. (2001). "Approximate accelerated stochastic simulation of chemically reacting systems." Journal of Chemical Physics **115**: 1716.

Gillespie, D. T. (2001). "Approximate accelerated stochastic simulation of chemically reacting systems." J. Chem. Phys. **115**: 1716.

Gillespie, D. T. (2002). "The chemical Langevin and Fokker-Planck equations for the reversible isomerization reaction." Journal of Physical Chemistry A **106**: 5063.

Gillespie, D. T. (2007). "Stochastic simulation of chemical kinetics." Annual Review of Physical Chemistry **58**: 35-55.

Goss, P. J. E. and J. Peccoud (1998). "Quantitative modeling of stochastic systems in molecular biology by using stochastic Petri nets." Proceedings of the National Academy of Sciences **95**: 6750-6755.

Grimm, V., E. Revilla, et al. (2005). "Pattern-Oriented Modeling of Agent-Based Complex Systems: Lessons from Ecology." Science **310**(5750): 987-991.

Guo, Z., P. M. A. Sloot, et al. (2008). "A hybrid agent-based approach for modeling microbiological systems." Journal of Theoretical Biology **255**(2): 163-175.

Hale, J. and S. Lunel (1993). Introduction to Functional Differential Equations. 1st ed: . New York, Springer-Verlag.

Hale, J. and S. M. V. Lunel Introduction to Functional Differential Equations, Springer.

Hardy, S. and P. N. Robillard (2004). "Modeling and simulation of molecular biology systems using Petri nets: Modeling goals of various approaches." Journal of Bioinformatics and Computational Biology **2**(4): 619-637.

Hatzimanikatis, V. and J. Bailey (1996). "MCA has more to say." Journal of Theorectical Biology **182**: 233-242.

Hatzimanikatis, V. and J. E. Bailey (1996). "MCA Has More to Say." Journal of Theoretical Biology **182**(3): 233-242.

Henri, M. V. (1903). "Lois générales de l'action des diastases." Paris, Hermann.

Hlavacek, W. S. and M. A. Savageau (1996). "Rules for coupled expression of regulator and effector genes in inducible circuits." J Mol Biol **255** 121-139.

Irvine, D. H. and M. A. Savageau (1985). "Network regulation of the immune response: alternative control points for suppressor modulation of effector lymphocytes." Journal of Immunology **134** 2100-2116.

Ishii, N., K. Nakahigashi, et al. (2007). "Multiple high-throughput analyses monitor the response of E. coli to perturbations." Science **316**(5824): 593-597.

Kauffman, S., C. Peterson, et al. (2003). "Random Boolean network models and the yeast transcriptional network." Proceedings of the National Academy of Sciences of the United States of America **100**(25): 14796-14799.

Lipniacki, T., P. Paszek, et al. (2006). "Transcriptional stochasticity in gene expression." Journal of Theorectical Biology **238**(2): 348-367.

Longo, D. and J. Hasty (2006). "Dynamics of single-cell gene expression." Molecular Systems Biology **2**.

Lotka, A. (1924). Elements of Physical Biology. Baltimore, Williams and Wilkins

Maheshri, N. and E. K. O Shea (2007). "Living with Noisy Genes: How Cells Function Reliably with Inherent Variability in Gene Expression." Annual Review of Biophysics and Biomolecular Structure **36**(1): 413-434.

Matsuno, H., Y. Tanaka, et al. (2003). "Biopathways representation and simulation on hybrid functional Petri net." In Silico Biol **3**: 389-404.

May, R. E. (1976). Theoretical Ecology: Principles and Applications. Oxford, Blackwell.

Michaelis, L. and M. L. Menten (1913). "Die Kinetik der Invertinwirkung." Biochem. Zeitschrift **49**: 333-369.

Miyano, S. (2008). Cell Illustrator.

Miyano, S. (2008). "Cell Illustrator website." http://www.cellillustrator.com/.

Mocek, W. T., R. Rudnicki, et al. (2005). "Approximation of delays in biochemical systems." Mathematical Biosciences **198**(2): 190-216.

Mocek, W. T., R. Rudnicki, et al. (2005). "Approximation of delays in biochemical systems." Math Biosci **198**(2): 190-216.

Monk, N. A. M. (2003). "Oscillatory expression of Hes1, p53, and NF-kappaB driven by transcriptional time delays." Curr. Biol. **13**: 1409.

Nagasaki, M., R. Yamaguchi, et al. (2006). "Genomic data assimilation for estimating hybrid functional Petri net from time-course gene expression data." Genome Informatics **17**(1): 46-61.

Paulsson, J. and M. Ehrenberg (2001). "Noise in a minimal regulatory network: plasmid copy number

control. ." Q Rev Biophys **34**: 1-59

Reddy, V. N., M. L. Mavrovouniotis, et al. (1993). "Petri net representations in metabolic pathways." Proc. Int. Conf. Intell. Syst. Mol. Biol.: 328-336.

Reisig, W. (1985). Petri Nets: An Introduction, Springer Verlag.

Savageau, M. A. (1969 a). "Biochemical systems analysis. I. Some mathematical properties of the rate law for the component enzymatic reactions." Journal of Theorectical Biology **25**(3): 365-369.

Savageau, M. A. (1969 b). "Biochemical systems analysis. II. The steady-state solutions for an n-pool system using a power-law approximation." Journal of Theorectical Biology **25**(3): 370-379.

Savageau, M. A. (1976). Biochemical systems analysis. A study of function and design in molecular biology, Addison-Wesley.

Savageau, M. A. (1985). "A theory of alternative designs for biochemical control systems." Biomed Biochim Acta **44**(6): 875-880.

Savageau, M. A. (2001). "Design principles for elementary gene circuits: Elements, methods, and examples." Chaos **11**: 142-159.

Savageau, M. A. and E. O. Voit (1987). "Recasting nonlinear differential equations as S-systems: a canonical nonlinear form." Mathematical Biosciences **87**(1): 31-113.

Tian, T. and K. Burrage (2006). "Stochastic models for regulatory networks of the genetic toggle switch." Proceedings of the National Academy of Sciences **103**(22): 8372-8377.

Tian, T., K. Burrage, et al. (2007). "Stochastic delay differential equations for genetic regulatory networks." The Journal of Computational and Applied Mathematics **205**(2): 696-707.

Vilar, J. M., H. Y. Kueh, et al. (2002). "Mechanisms of noise-resistance in genetic oscillators." Proc Natl Acad Sci U S A **99**: 5988-5992.

Visser, D. and J. J. Heijnen (2002). "The mathematics of metabolic control analysis revisited." Metab Eng **4**(2): 114-123.

Visser, D. and J. J. Heijnen (2002). "The Mathematics of Metabolic Control Analysis Revisited." Metabolic Engineering **4**(2): 114-123.

Voit, E. (2005). "Smooth bistable S-systems." IEE Proc Systems Biol **152**: 207-213.

Voit, E. O. (1993). "S-system modeling of complex systems with chaotic input." Environmetrics **4**(2): 153-186.

Voit, E. O. (2000). Computational analysis of biochemical systems: a practical guide for biochemists and molecular biologists, Cambridge University Press.

Voit, E. O. (2005). "Smooth bistable S-systems." IEE Proc. Systems Biol **152**: 207-213.

Volterra, V. (1926). "Variazioni e fluttuazioni del numero d'individui in specie animali conviventi." Mem. R. Accad. dei Lincei. **2**.

Wilensky, U. (1999). NetLogo, Center for Connected Learning and Computer-Based Modeling, Northwestern University. Evanston, IL.

Wolkenhauer, O., M. Ullah, et al. (2004). "Modelling and Simulation of IntraCellular Dynamics: Choosing an Appropriate Framework " IEEE Transactions on NanoBioscience **3**: 200-207.

Wu, J. and E. Voit (2009 a). "Hybrid modeling in biochemical systems theory by means of functional petri nets." Journal of bioinformatics and computational biology **7**(1): 107-134.

Wu, J. and E. Voit (2009 b). "Integrative biological systems modeling: challenges and opportunities." Frontiers of Computer Science in China **3**(1): 92-100.

PAPER 1

CHAPTER 2

Hybrid modeling in biochemical systems theory by means of Functional petri nets

Jialiang Wu and Eberhard O. Voit

Journal of bioinformatics and computational biology 2009 a. **7**(1): p. 107-34.

Hybrid modeling in biochemical systems theory by means of Functional petri nets

JIALIANG WU

Department of Mathematics, Bioinformatics Program, Georgia Institute of Technology, Atlanta, GA 30332, USA
gtg337v@mail.gatech.edu

EBERHARD VOIT[1]

Integrative BioSystems Institute and
The Wallace H. Coulter Department of Biomedical Engineering, Georgia Institute of Technology
Atlanta, GA 30332, USA
eberhard.voit@bme.gatech.edu

Abstract

Many biological systems are genuinely hybrids consisting of interacting discrete and continuous components and processes that often operate at different time scales. It is therefore desirable to create modeling frameworks capable of combining differently structured processes and permitting their analysis over multiple time horizons. During the past forty years, Biochemical Systems Theory (BST) has been a very successful approach to elucidating metabolic, gene regulatory and signaling systems. However, its foundation in ordinary differential equations has precluded BST from directly addressing problems containing switches, delays, and stochastic effects. In this study, we extend BST to hybrid modeling within the framework of Hybrid Functional Petri Nets (HFPN). First we show how the canonical GMA and S-system models in BST can be directly implemented in a standard Petri Net framework. In a second step we demonstrate how to account for different types of time delays as well as for discrete, stochastic and switching effects. Using representative test cases, we validate the

[1] Corresponding author

hybrid modeling approach through comparative analyses and simulations with other approaches and highlight the feasibility, quality and efficiency of the hybrid method.

Keywords: Biochemical Systems Theory; BST; Delay; Hybrid Functional Petri Nets; HFPN; Hybrid modeling; GMA system; Stochastic modeling; S-system.

Introduction

Integrative biology endeavors to understand how the components of biological systems interact and how these interactions give rise to emerging functions and behaviors at the systemic level. Supporting this endeavor are experiments that produce comprehensive datasets at different levels of organization, including the genome, proteome, and metabolome, as well as novel computational techniques and the creation of innovative devices. In some sense, the centerpiece of these diverse techniques is a mathematical model that utilizes the experimentally observed data and formulates them as theoretical structures that can be assessed and interpreted with computational means. Corresponding to the predominantly reductionist methods of traditional experimental biology, mathematical models have in the past usually focused on a single biological level, such as gene expression or enzyme kinetics. As it is becoming possible to generate data that simultaneously shed light on several levels, models also have to be able to bridge between genomic, proteomic, metabolomic, and higher-order, physiological phenomena. A key challenge for such multi-level models is that processes tend to occur at different time scales and that effects due to stochasticity and time delays become so crucial that standard approximations are no longer valid. In this study, we propose a hybrid modeling methodology that allows combinations of deterministic and stochastic, discrete and continuous effects. The proposed hybrid approach uses features of classical dynamical modeling, based on ordinary differential equations (ODEs), and combines them with modeling strategies for discrete events and stochastic effects. Specifically, we use, as a

representative default for dynamical approaches in biology, the well-established modeling framework of Biochemical Systems Theory (BST) (Savageau 1969 a; Savageau 1969 b; Savageau 1976; Voit 2000), which we extend here by embedding it into Hybrid Functional Petri Nets (HPFN) (Matsuno, Tanaka et al. 2003). The result permits the simultaneous analysis of continuous, discrete, deterministic and stochastic processes along with different types of time delays. The hybrid approach is implemented in the software Cell Illustrator (Miyano 2008). We illustrate the proposed methodology with BST and other models that describe metabolic processes and gene regulatory networks. The same methods are similarly applicable to other levels of organization, from cellular to ecological systems.

Methods

The construction of models for biological systems has traditionally occurred from the bottom up. Namely, individual processes were characterized biologically, then formulated mathematically, and finally all process descriptions were merged into a comprehensive differential equation model. For instance, in the context of metabolic pathway systems, one measured the features of all catalyzing enzymes involved, translated them into Henri-Michaelis-Menten rate laws (Henri 1903; Michaelis and Menten 1913), and entered these rate laws as flux descriptions into dynamic models. Indeed, many *in vitro* studies have suggested that these types of rate laws are often reasonable representations. Nonetheless, while conceptually straightforward, this procedure of dynamic model construction often runs into discrepancies between observed and modeled behaviors at the systems level. Some of the discrepancies are due to the lack of data, information originating from different organisms or experimental conditions, or invalid mathematical representations. In particular, if processes are more convoluted and not consistent with the assumptions underlying enzyme catalyzed mechanisms, no guidelines are available for even starting the modeling process.

To remedy this situation, different types of approximations were explored over the years. It was clear that linear models would be of limited validity, because biological systems are seldom linear in their responses. Nonlinear approximation techniques yielded different types of "canonical models." These provided strong, and badly needed, guidance for setting up model equations and identifying their parameters and suggested custom tailored techniques for numerical integration, diagnostics and interpretation. Furthermore, these canonical models allowed better insights into the functioning of complex systems and were easily scalable to larger systems with tens or hundreds of reactions, at least in principle. At this point, prominent canonical models in biology are Lotka-Volterra models in ecology (Lotka 1924; Volterra 1926; May 1976) and power-law models in molecular biology. Among the latter, BST (Savageau 1976; Voit 2000) have become in some sense a default, Although Metabolic Control Analysis is popular for steady-state analyses (Fell 1997) and has more recently been augmented with log-linear process descriptions for dynamic considerations (Hatzimanikatis and Bailey 1996; Visser and Heijnen 2002). Canonical models are no panacea, because they are based on approximations, which are by nature limited in their ranges of valid representations. However, all other models are approximations as well, and the challenge to the modeler is to select the most suitable model for a given situation. Thus, if a proven mechanistic model is at hand, and if it is mathematically and computationally tractable, it should probably be the top choice. However, if no such model is a clear "winner" among the infinite possible mathematical structures, a canonical model is an excellent default, because it offers very specific guidelines for streamlined model design, diagnostics, model utilization, and the exploration of design and operating principles (Voit 2000). We focus here primarily on BST, because it is the most developed canonical modeling framework in molecular biology and because it lends itself to extensions, for instance,

with respect to delays. Nevertheless, we also show that the same philosophy of hybrid model construction may be applied to other dynamical modeling strategies.

2.1 Biochemical systems theory (BST)

The generic design of a BST model typically begins with a diagram showing all components, the fluxes of material between the components, and the regulatory effects that some of the components have on some of the processes in the system. Focusing on one node X_i at a time, one lists all processes augmenting X_i and all processes degrading X_i. Under the not very restrictive assumption that no changes happen within the node, a generic equation is directly obtained from the stoichiometry of the system and reads:

$$dX_i/dt = \dot{X}_i = \sum v_{ij}^{+} - \sum v_{ij}^{-} = V_i^{+} - V_i^{-} \qquad X_i(0) = X_{i0} \ . \tag{1}$$

With only slight variations, this general representation is the same for very many systems descriptions in biological systems analysis. The basis of BST is the use the power-law functions for the representation of the functions in Eq. 1. Thus, each process v_{ij} (or V_i) in Eq. 1 is represented in the generic format

$$v_i \approx \gamma_i \prod_{j=1}^{n+m} X_j^{f_{ij}}, \tag{2}$$

where γ_i is the rate constant of the process and each kinetic order f_{ij} quantifies the effect the variable X_j has on the process v_i. If the effect is activating or augmenting, the kinetic order is positive. If the effect is inhibiting or diminishing, the kinetic order is negative. If X_j has no effect on v_i, f_{ij} is zero. While variables X_1, …, X_n are state variables that may

change under the action of the system, the remaining variables X_{n+1}, …, X_{n+m} are independent variables that are independent of the dynamics of the system and that are usually constant.

In the General Mass Action (GMA) representation within BST, each v_{ij}^{+} or v_{ij}^{-} is represented by a product of power-law functions, as indicated in Eq. 2, and the result is a system description in the format

$$\dot{X}_i = \gamma_{i1} \prod_{j=1}^{n+m} X_j^{f_{ij1}} \pm \gamma_{i2} \prod_{j=1}^{n+m} X_j^{f_{ij2}} \pm \ldots \pm \gamma_{ik} \prod_{j=1}^{n+m} X_j^{f_{ijk}} \pm \ldots \; . \qquad (3)$$

As an alternative, all incoming and all outgoing processes v_{ij}^{+} or v_{ij}^{-} may be aggregated into one term each, given in Eq. 1 as V_i^{+} and V_i^{-}, respectively, which leads to the S-system format

$$\dot{X}_i = \alpha_i \prod_{j=1}^{n+m} X_j^{g_{ij}} - \beta_i \prod_{j=1}^{n+m} X_j^{h_{ij}} ,$$

GMA and S-system models have different mathematical features that have been compared and discussed many times (*e.g.*, (Voit 2000)). A main advantage of the GMA format is its closeness to biological intuition, because each process is mapped, one-to-one, onto a specific mathematical term. The aggregation of terms in the S-system format somewhat clouds this intuition, but has significant mathematical advantages, such as the algebraic computability of steady states (Savageau 1969 b). We will use the GMA format in the following illustrations.

BST models have been successfully applied in a variety of biological fields and also in non-biological areas (*e.g.*, see (Voit 2000)). Nonetheless, their structure as systems of ordinary differential equations imposes limits on their scope. The following issues cannot be directly modeled in BST, and the same is true for all other modeling approaches that are anchored in ordinary differential equations.

1. Discrete events. In addition to continuous changes, biological systems are frequently exposed to external or internal switches. In the former case, the environment may abruptly change, whereas an example for the latter is the turning on or off of the expression of some gene. External switches are easy to implement through a segmentation of the time scale, whereas internal switches are much more complicated because they depend on the internal state of the system and are therefore difficult to predict. Modeling of hard internal switches thus requires if-statements (Savageau 2001) or some approximation with a "softened" continuous switch (Voit 2005).

2. Stochasticity. Most metabolic analyses implicitly assume that thousands of molecules are available to participate in an enzymatic reaction. However, this is not necessarily the case if pathways outside the organism's central metabolism are under investigation. If only relatively few molecules are present, the assumptions underlying essentially all continuous rate laws are questionable. The kinetic conversions become strings of discrete events that happen randomly, with some (possibly time dependent) probability, and it seems that the dynamics is better formulated as a stochastic process. The best known formulation of this type of approach is Gillespie's "stochastic simulation algorithm" (Gillespie 1977), which has triggered the development of numerous variations (Gillespie 2000; Gillespie 2001). Wolkenhauer (Wolkenhauer, Ullah et al. 2004) recently reviewed the progression of approximations, starting with a true stochastic process, via the Chemical Master Equations and Langevin's formulation, and ultimately resulting in typical continuous rate laws.

3. Delays. All typical metabolic models assume that reaction speed depends on the current state of the system. In reality, there may be significant delays, for instance, between the up-regulation of a gene and its ultimate metabolic effect, or the reception of an external signal and the effect of the transduced signal on the genome. The natural

choice for mathematically representing delays in continuous systems is the format of Delay Differential Equations (DDEs), whose theoretical foundation is well established (Hale and Lunel). An impediment to the practical use of DDEs is the fact that their analysis requires specialized software, which is distinct from standard software for ODEs. Moreover, if delays are to be combined with discrete or stochastic effects, software for analysis is essentially lacking and must be designed from scratch. Mocek *et al.* (Mocek, Rudnicki et al. 2005) recently described a suitable ODE approximation within BST for systems with a single delay, which thus bridges one of the above divides. Other types of delays have not been supported by canonical modeling software and require the writing of specific code, for instance, in Matlab. We show in a later section that these delays can also be formulated as ODE approximations within BST.

4. Spatial Effects. Most metabolic models assume spatial homogeneity, even though it is known that the organization of cells is highly compartmentalized. This is a very difficult problem, and even partial differential equations (PDEs) models are not always appropriate, because the underlying mechanisms, such as active transport and the use of scaffolds, are intrinsically different from diffusion processes that are amenable to PDE methods. Instead, it might be necessary to use agent based or object-oriented modeling techniques for spatial models. We do not discuss this issue here.

As soon as switches, stochastic effects and delays are significant within the same system of interest, none of the existing modeling frameworks are sufficient. However, it is desirable to address all within one package, for instance, to answer the question: What is the significance of a delay in a stochastic system? This is not an artificially construed question, because it was recently shown that although transcription may be highly erratic, metabolite levels are very well buffered (Ishii, Nakahigashi et al. 2007). Explanations of

this observation require the simultaneous modeling of both, stochastic effects and time delays. We will show in the following how these types of questions can be addressed when we embed BST in a Hybrid Functional Petri Net (HFPN). We use for our demonstration the HFPN software Cell Illustrator (Miyano 2008), which *per se* does not allow the modeling of delays, but can capture delays through the method of Mocek *et al.* (Mocek, Rudnicki et al. 2005) and some additional strategies outlined later in this article. While we primarily focus on BST, other ODE formulations could be addressed similarly.

2.2 *Hybrid functional Petri net (HFPN)*

A Petri Net is a graphical and mathematical formalism of a system with concurrent processes and properties that may be continuous or discrete. Petri Nets have been applied to such diverse disciplines as manufacturing and communication (Reisig 1985) and were apparently first applied to biological systems by Reddy and collaborators in 1993 (Reddy, Mavrovouniotis et al. 1993). To meet various needs, Petri Nets have been extended into different directions: Stochastic Petri Nets include randomness; Colored Petri Nets add a color feature to tokens and thus allow representing, in the same model, different dynamic behaviors that are modeled by different token colors; Hybrid Petri Nets allow the simultaneous investigation of discrete and continuous processes; Functional Petri Nets permit dynamic modifications of system parameters. Hardy and Roillard (Hardy and Robillard 2004) recently reviewed the advantages of specific Petri Net formalisms for qualitative or quantitative analyses. Of particular importance here is the Hybrid Functional Petri Net (HFPN) format.

HFPN is an extended functional Petri Net that accounts for both discrete and continuous events within the same model system (Matsuno, Tanaka et al. 2003) and has been implemented in the software package Cell Illustrator (Miyano 2008). HFPN consists of

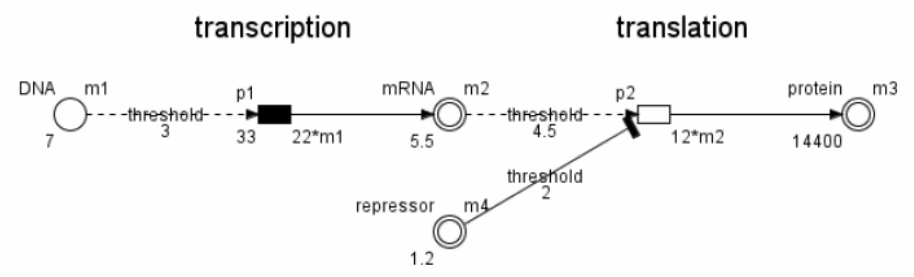

Fig.2.1 An illustrative HFPN model of transcription and translation, as depicted in Cell Illustrator (Miyano 2008). Test arcs are used as input arcs because DNA (mRNA) is not consumed by the process of transcription (translation). The effect of a repressor element is described by an inhibitory arc. Here $m1$ is the number of DNA molecules with initial value 7; $m2$ is the mRNA concentration with initial value 5.5; $m3$ is the protein concentration with initial value 14,400; $m4$ is the repressor concentration with initial value 1.2. The discrete transition $p1$ represents the transcription, which is fired with the speed of $22 \cdot m1$ per time unit and with delay 33; the continuous transition $p2$ describes the translation and is fired with speed $12 \cdot m2$ per time unit. Translation occurs only if the mRNA concentration $m2$ is greater than or equals to the test arc weight 4.5 and if the repressor concentration $m4$ is less than or equal to the inhibitory arc weight 2.0.

three types of process elements: places, transitions, and arcs (Fig.1). Places appear graphically as single (discrete type) or double (continuous type) lined circles that represent the states of the modeled system. In terms of biochemical pathways, places usually represent molecular species such as chemical substrates or enzymes. A discrete place contains an integer number of tokens which represents the number of molecules, while a continuous place contains a positive real number representing the substrate concentration. The number of tokens in discrete places and the concentration in continuous places define the *marking* of the system. Transitions (filled or empty rectangles) represent (discrete or continuous) *actions* of the modeled system, such as biochemical reactions, protein binding, transcription, translation, or translocation. Both types of transitions have the property *speed*, which is a function of the marking of the system, whereas only a discrete transition has the property *delay*, which quantifies the time interval between consequent tokens to be processed by the transition. An arc is used

to connect a place with a transition. (It is not allowed to use an arc to connect between places or between transitions.) An arc from a place to a transition is called an *input arc*, and one from a transition to a place is called an *output arc*. There are three types of arcs: *normal*, *inhibitory*, and *testing*. All three types of arcs may be used as input arcs, while only a normal arc is allowed to be used as an output arc. Each arc has the property *weight*, which is the minimum amount of flux required for the arc to function. A transition is *enabled* only if the content in all source places (there may be only one source place) is equal to or exceeds the weight of the input arc(s). When a transition is *fired*, the content in each source place is taken off the arc weight amount and, through a normal arc, the output arc weight amount of content is added to each sink place. An inhibitory arc with weight *w* enables a transition to fire only if the content of the source place is less than or equal to *w*. For instance, an inhibitory arc can be used to represent a repressor in gene regulation. A test arc does not consume any content of the source place by firing, but is used, for instance, to represent an enzyme catalyzing a reaction without being consumed (Fig.1).

2.3. *Implement of BST models as Petri Nets*

It is relatively straightforward to translate a GMA system into a Petri Net model (Fig.2). Each dependent and independent variable in the GMA is represented in the Petri Net model by a continuous place with the species' name. Every positive term in the GMA differential equations translates into the speed of an input transition and every negative term into the speed of an output transition. Direct connectivity is only built between places where mass is conserved between them. However, there is an exception: when a place represents a constant input, it does not connect with any other place as to keep its

content unaltered. We do not connect places that are related through signals only. Examples will be shown in the Results section.

In addition to being capable of representing continuous and deterministic ODE models, Petri Nets can actualize stochastic components, whether these are continuous (in the form of stochastic equations) or discrete. The Petri Net framework permits several realizations of a stochastic model.

2.4. *Representation of stochasticity in HFPN*

2.4.1. Construction of a discrete stochastic model according to reaction type

Besides spontaneous transitions, HFPN provides the option of *timed transitions*, where an enabled transition fires with randomly determined time delay d. This feature can be used to model random events in biological process systems. The random time follows a specified probability density function such as the most commonly used exponential distribution, where d satisfies $Prob(d<t)=1-\exp(-\beta t)$. The rate β is related to the deterministic rate parameter and the number of available reactant molecules. For a first-order reaction of the form

$$A \xrightarrow{k} B,$$

we have $\beta=k$, where k is the deterministic rate constant. For a reaction of the form

$$A + B \xrightarrow{k} C,$$

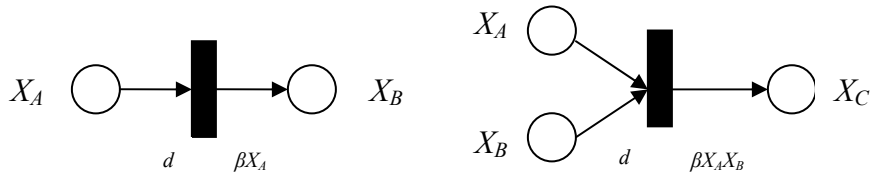

Fig.2.2 Implementation of monomolecular and bimolecular reactions in a discrete Petri Net. Here X_A, X_B, and X_C are the molecular amounts of species A, B, and C, respectively; d is the transition delay; βX_A and $\beta X_A X_B$ are the transition speeds for monomolecular reaction and bimolecular reaction, respectively.

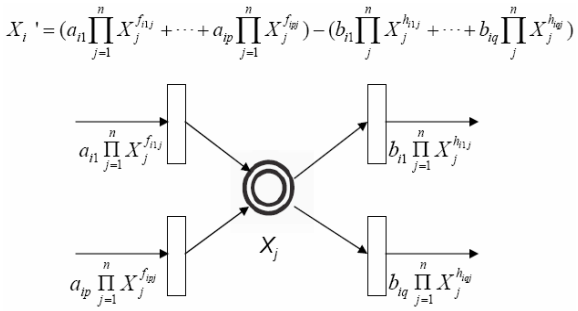

Fig. 2.3 GMA system and its HFPN representation.

we have $\beta = k/(V N)$, where V is the cell volume and N is Avogadro's number.
If the reactions are different than these two simple types, they need to be reduced to these base types, and the stochastic construction is more complicated (Goss and Peccoud 1998).

2.4.2. *Construction of a discrete stochastic model from a deterministic ODE model*

The so-called τ-leap method within Gillespie's method for stochastic modeling (Gillespie 2007) connects stochastic simulations of biochemical reaction systems to the

Euler method for solving ODEs. Tian and Burrage (Tian and Burrage 2006) developed a more general technique to construct stochastic models from deterministic models described by ODEs. Suppose a reaction can be described by the deterministic ODE model

$$\frac{d\,\underline{x}_i}{dt} = f_i(\underline{x}_1,...,\underline{x}_N) - g_i(\underline{x}_1,...,\underline{x}_N), i = 1,...,N, \tag{5}$$

where $f_i(\underline{x}_1,...,\underline{x}_N)\tau$ and $g_i(\underline{x}_1,...,\underline{x}_N)\tau$ are the synthesis and degradation of species S_i respectively, and $\underline{x}_i$ represents the concentration of species S_i in the deterministic model. The corresponding discrete stochastic model is

$$x_i(t+\tau) = x_i(t) + P(f_i(x_1,...,x_N)\,\tau) - P(g_i(x_1,...,x_N)\,\tau), \tag{6}$$

where x_i is the number of molecules of species S_i, Eq. 6 describes how increases and decreases in x_i within a time interval $[t,\ t+\tau)$ can be seen as samples of Poisson random variables with means $f_i(x_1,...,x_N)\tau$ and $g_i(x_1,...,x_N)\tau$, respectively. Thus, without requiring detailed knowledge of biochemical reactions, kinetic rates or molecular numbers, a discrete stochastic model can be constructed from the conventional deterministic ODE model.

2.4.3. *Construction of continuous stochastic models*

Noting the mathematical fact that a Poisson variable with a particular mean and variance that is much greater than 1 can be approximated by a Gaussian random variable with the same mean and variance, one can further approximate Eq. 6 as

$$\begin{aligned} x_i(t+\tau) &\approx x_i(t) + N(f_i\tau, f_i\tau) - N(g_i\tau, g_i\tau) \\ &= x_i(t) + [f_i\tau + \sqrt{f_i\tau}N_1(0,1)] - [g_i\tau + \sqrt{g_i\tau}N_2(0,1)] \end{aligned} \tag{7}$$

For continuous Markov processes, it can be shown (Gillespie 2001; Gillespie 2002) that Eq. 7 is mathematically equivalent to an equation with white noise of the form

$$x_i'(t) = [f_i + \sqrt{f_i}\Gamma_1(t)] - [g_i + \sqrt{g_i}\Gamma_2(t)], \quad (8)$$

where $\Gamma(t)$ is the Gaussian white-noise process satisfying $\langle \Gamma_i(t)\Gamma_j(t')\rangle = \delta_{ij}\delta(t-t')$; the first delta function is Kronecker's and the second is Dirac's. Eq. 7 represents a general way to construct continuous stochastic models from deterministic models, either with or without delays (Tian, Burrage et al. 2007).

The HFPN software Cell Illustrator (Miyano 2008) is equipped with a random number generator, which facilitates the modeling of basic stochastic effects, such as Gaussian noise. Poisson process can be implemented through a programming option. In the Results section, we demonstrate the ease with which noise and delay effects can be modeled and simulated in this setting.

Specially, if we can find $N_1, \cdots, N_n$ such that $\tau_1/N_1 = \cdots = \tau_n/N_n$, *i.e.*, every discretization step in the derivative approximation has the same size, then we only need a system of $\max\{N_1, \cdots, N_n\} + 1 = N_{\max} + 1$ additional ODEs of the form

2.5 Approximation of various types of delays by ODEs

Although the HFPN software Cell Illustrator is equipped with a delay function for discrete transitions, it provides no means to actualize delay effects in continuous systems. The typical mathematical formulation of delays in continuous systems with multiple time scales is a system of delay differential equations (DDEs). Since ODEs, in contrast to DDEs, are easily represented within the framework of HFPN, it is useful to explore what types of delays can be represented as ODEs in an approximate, yet valid fashion.

The simplest case of a single delay was addressed with a discretization method proposed by Mocek *et al*. (Mocek, Rudnicki et al. 2005). This method includes a normalization step, which is inconvenient here and will be removed in the following.

2.5.1. Approximation of multiple constant delays by ODEs

Consider a system with (one or) multiple constant delays of the form

where $Y(t)$ is a vector function and $\tau_1, \cdots, \tau_n$ are distinct discrete delays. We choose n positive integers $N_1, \cdots, N_n$ and define the following auxiliary variables:

$$\begin{aligned} Y'(t) &= f(Y(t), Y(t-\tau_1), ..., Y(t-\tau_n)) \\ Y(t) &= \phi(t), t \in [-h, 0], \end{aligned} \tag{9}$$

$$x_{ij}(t) = Y(t - i\frac{\tau_j}{N_j}), 0 \le i \le N_j, j = 1, \cdots, n. \tag{10}$$

Particularly, the definition implies that

$$x_{0j}(t) = Y(t), x_{N_j j}(t) = Y(t-\tau_j), j \in \{1, ...n\}. \tag{11}$$

The derivative of x_{ij} can be approximated as

$$\begin{aligned} x_{ij}' &\approx [x_{ij}(t + \frac{\tau_j}{N_j}) - x_{ij}(t)] / \frac{\tau_j}{N_j} \\ &= \frac{N_j}{\tau_j}[x_{(i-1)j}(t) - x_{ij}(t)], t > \frac{i}{N_j}. \end{aligned} \tag{12}$$

Thus the DDE (Eq.9) can be approximated by a system of $\sum N_j + 1$ additional ODEs

$$\begin{aligned} Y'(t) &= f(Y(t), x_{N_1}(t), ..., x_{N_n}(t)) \\ x_{ij}' &= \frac{N_j}{\tau_j}[x_{(i-1)j}(t) - x_{ij}(t)] \\ x_{ij}(0) &= \phi(-i/N_j), 1 \le i \le N_j, j = 1, ..., n. \end{aligned} \tag{13}$$

Specially, if we can find $N_1, \cdots, N_n$ such that $\tau_1 / N_1 = \cdots = \tau_n / N_n$, *i.e.*, every discretization step in the derivative approximation has the same size, then we only need a system of $\max\{N_1, \cdots, N_n\} + 1 = N_{\max} + 1$ additional ODEs of the form

In contrast to a fixed delay, the state of the system may also depend on its recent history, where, for instance, the most recent events have a higher impact than events that

happened a longer time ago. A system affected by its history in the past interval [*t*-*L*, *t*] may be represented in two ways that are mathematically equivalent. The first option is the integro-differential equation

$$\begin{aligned} Y'(t) &= f(Y(t), x_{N_1}(t), ..., x_{N_n}(t)) \\ x_i' &= \frac{N_{\max}}{\tau_{\max}}[x_{(i-1)}(t) - x_i(t)] \\ x_i(0) &= \phi(-i / N_{\max}), 1 \le i \le N_{\max}, \end{aligned} \tag{14}$$

where $\tau_{\max}$ is the delay corresponding to $N_{\max}$.

2.5.2. Approximation of distributed delay by ODEs

In contrast to a fixed delay, the state of the system may also depend on its recent history, where, for instance, the most recent events have a higher impact than events that happened a longer time ago. A system affected by its history in the past interval [*t*-*L*, *t*] may be represented in two ways that are mathematically equivalent. The first option is the integro-differential equation

$$Y'(t) = F(Y(t), \int_0^L Y(t-s) f(s) ds), \tag{15}$$

where *f* is the function characterizing the distributed delay and satisfying $\int_0^L f(s) ds = 1$.

The second option is

$$Y'(t) = F(Y(t), \int_{t-L}^{t} Y(s) f(s) ds), \tag{16}$$

where *f* is a periodic distribution function with period *L*. To convert the distributed delay to a constant delay, we use the second representation. Introducing an auxiliary variable

$$z(t) = \int_{t-L}^{t} Y(s) f(s) ds\ , \tag{17}$$

we differentiate it to yield an ODE with a singular discrete delay

$$\frac{dz(t)}{dt} = Y(t)f(t) - Y(t-L)f(t). \tag{18}$$

Applying the earlier discretization method again, we obtain

$$\begin{aligned} Y'(t) &= F(Y(t), z(t)) \\ z'(t) &= Y(t)f(t) - x_N(t)f(t) \\ x_i'(t) &= \frac{N}{L}[x_{i-1}(t) - x_i(t)], \qquad 1 \le i \le N. \end{aligned} \tag{19}$$

2.5.3. Approximation of time dependent delays by ODEs

A delay system with a bounded time-dependent delay can be represented by

$$Y'(t) = F(Y(t), Y(t-\tau(t))), \tag{20}$$

where the time dependent delay is a positive differentiable function $\tau(t) \in [a,b]$. Based on the discretization approach, Eq. 19 can be approximated by

$$\begin{aligned} Y'(t) &= F(Y(t), x_N(t)) \\ x_i'(t) &= N\frac{1-\tau'(t)}{\tau(t)}[x_{i-1}(t) - x_i(t)], \qquad 1 \le i \le N. \end{aligned} \tag{21}$$

2.5.4. Approximation of systems with random delay

We consider a system with a bounded random delay of the form

$$Y'(t) = F(Y(t), Y(t-\tau(t))), \tag{22}$$

where the delay $\tau(t) \in [a,b]$ is a bounded discrete stochastic process. Based on the discretization approach, the system can be approximated by

where τ_{rv} is the value of the corresponding random variable sampled at time t and remains that constant in the window of $[t, t+\Delta t]$. In light of the possible distraction from the main theme and also the rather modest need for continuous random delays in biological systems analysis, we limit ourselves here to discrete random delays, which can be easily implemented in the Cell Illustrator, and will explore the more complicated issue

of continuous stochastic delays at a later time. We will show in the Results section how these approximations can be seamlessly implemented in the HFPN framework.

$$
\begin{aligned}
&Y'(t) = F(Y(t), x_N(t)) \\
&x_i(t+\Delta t) = x_i(t) + \frac{N}{\tau_{rv}}[x_{i-1}(t) - x_i(t)]\Delta t, \qquad 1 \le i \le N,
\end{aligned}
\tag{23}
$$

3. Results

To test the validity of the above approximations, we apply the proposed methods to two simple yet generic systems and compare our simulation results with those obtained with established methods.

Example 1: A generic pathway system

This first example was inspired by a combination of experimental findings. Namely, it has been observed that gene transcription and translation are often quite erratic, which may be due to fluctuations in the availability of ribosomes and/or particular puridines, pyrimidines, or amino acids (*e.g.*, (Maheshri and O Shea 2007)). At the same time, Ishii *et al.* (Ishii, Nakahigashi et al. 2007) observed that metabolite concentrations are surprisingly constant even if transcription and translation are strongly affected, for instance, by special diets, such as amino acid starvation. The combination of stochastic production and smooth availability of metabolites begs the question of whether the delays between gene activation and metabolite generation buffer the observed stochasticity. Because the complete transcription, translation, and metabolite production process is complex, we study a very much simplified, yet for our purposes representative, generic pathway system with respect to buffering per delays and feedback.

Effects of Delays. We consider a generic branched system (Fig. 4) with four time dependent variables ($y_1, \ldots, y_4$) and one constant supply (y_5). The downstream component

y_3 inhibits the production of upstream component y_1 through negative feedback, and two delays exist between y_2 and y_3, and between y_2 and y_4. A direct example for such a structure is a metabolic pathway. As an illustration, we test the following four cases:

(1) Two different constant delays τ_1 and τ_2.

(2) Two non-constant delays: the first is a distributed delay in the window $[\tau_1 - d, \tau_1 + d]$ with kernel function $f(t)$, and second is a time dependent delay $\tau_2(t)$.

(3) The delays are given as two uniform random variables whose values are taken from the windows $[\tau_1 - d_1, \tau_1 + d_1]$ and $[\tau_2 - d_2, \tau_2 + d_2]$, respectively.

(4) The delays are Gaussian random variables with means τ_1 and τ_2 and standard deviation (stddev) d_1 and d_2, respectively.

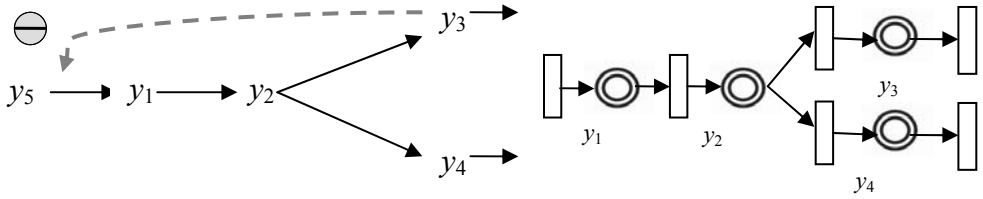

Fig.2.4 A generic system with one inhibitory feedback loop and two delays: standard diagram and its corresponding HFPN representation.

As a specific example, consider the (almost arbitrarily chosen) numerical implementation of the (delayed) GMA representation of the pathway in Fig. 4, which is given in Eq. 24.

$$
\begin{aligned}
y_1' &= y_3^{-0.2}\, y_5 - 3 y_1^{0.7} \\
y_2' &= 3 y_1^{0.7} - y_2(t-\tau_1)^{0.2} - y_2(t-\tau_2)^{0.2} \\
y_3' &= y_2(t-\tau_1)^{0.2} - 2\, y_3^{0.6} \\
y_4' &= y_2(t-\tau_2)^{0.2} - 0.6\, y_4^{0.4} \\
y_1(t) &= 1, y_2(t) = 2, y_3(t) = 3, y_4(t) = 4, t \in [-\max(\tau_1, \tau_2), 0] \\
y_5 &= 2.5
\end{aligned}
\qquad (24)
$$

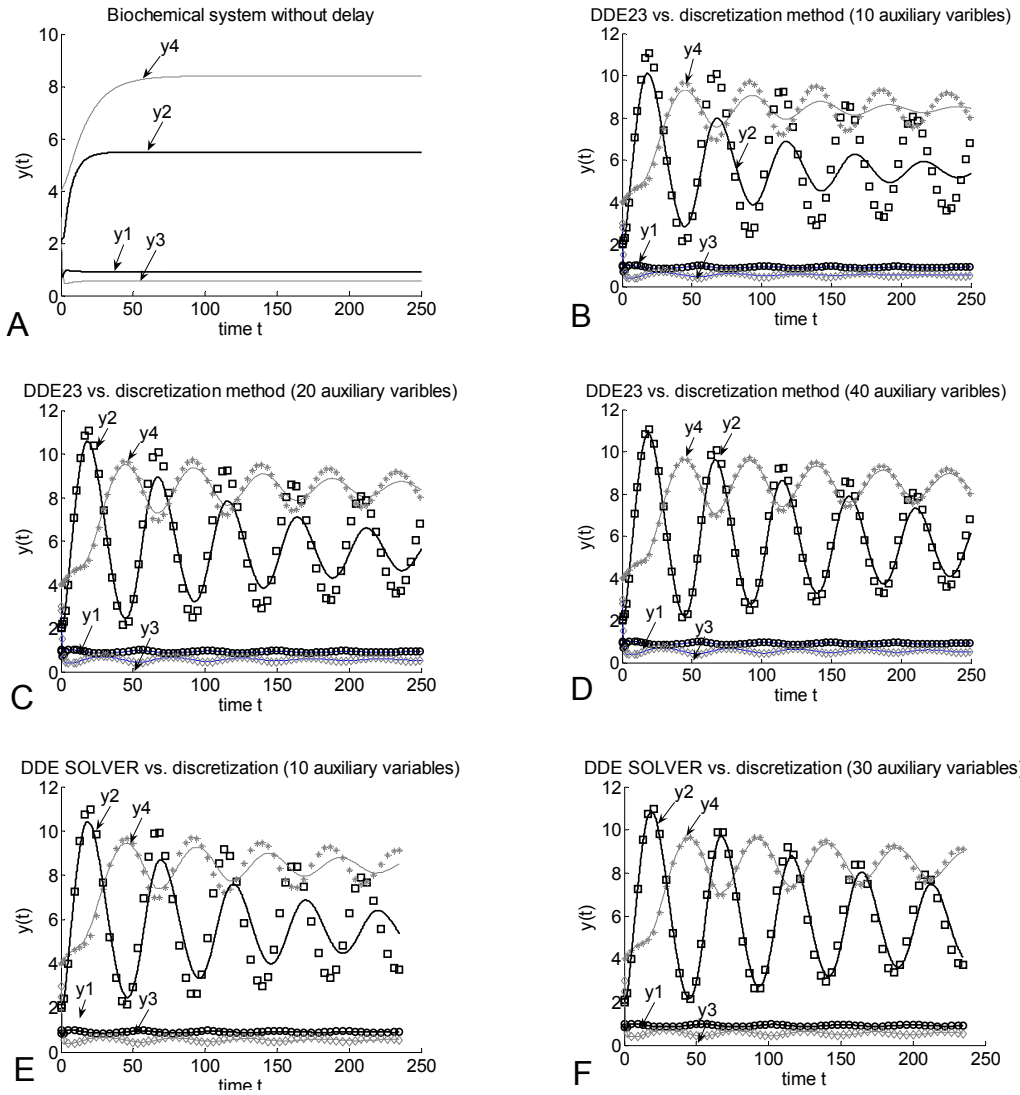

Fig.2.5 Comparisons between the solutions obtained with established methods (DDE23 in MatLab and DDE SOLVER in Fortran), shown with symbols, and the proposed discretization, implemented in Cell Illustrator and shown as solid lines. (A) Responses of the generic system in Fig.4 without delay. (B, C, D) Cases with two constant delays τ_1=9, τ_2=15 and different numbers of auxiliary variables (N=10, 20 and 40, respectively). (E, F) Cases with two non-constant delays: a distributed delay in the window [7.5,10.5] with kernel $\pi/6\ |\sin(t\ \pi\ /3)|$, and a time dependent delay τ =15+sin$t$; numbers of auxiliary variables are N=10 and 30, respectively.

For cases involving fixed, deterministic delays we can easily compare our solutions with solutions from algorithms such as DDE23 in MatLab and the DDE SOLVER in Fortran. The results show that a moderate number of auxiliary variables is sufficient for a

relatively accurate discretization (Fig.5). Not being restricted to deterministic delays, the discretization method can also be applied to systems with random delays. For such systems, no standard method is available for comparisons, and we execute the comparison instead with the case of constant delays. Figs. 6 A and B show that, with 10 and 30 auxiliary variables applied respectively, the dynamics of systems with uniform random delays is very close to results with the corresponding constant delays. Again, the more auxiliary variables are used, the more accurate the simulation will be. Moreover, relatively small numbers of auxiliary variables already produce accurate simulations, and this conclusion also holds for the Gaussian case. The results suggest that the system behavior is robust with respect to the ranges and (A, B, C) and distribution types (D) of the random delays, and that the dynamic responses are mainly determined by the mean values of the random delays. This finding implies that irregular delays *in vivo* may in most cases be modeled by the corresponding constant mean delays.

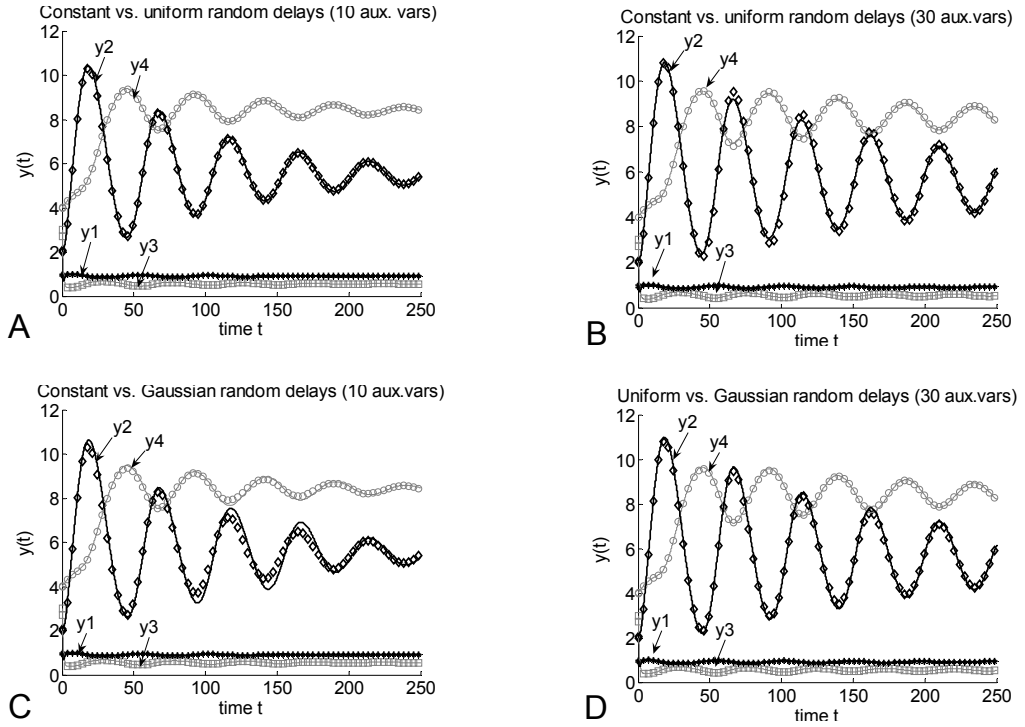

Fig.2.6 Generic biochemical system with random delays. (A, B) Delays are implemented as two uniform random variables with values sampled from [5,13] and [11,19], respectively. Solid lines result from uniform random delays and discrete symbols from two constant delays τ_1=9, τ_2=15. Numbers of auxiliary variables are N=10 and 30 for A and B, respectively. (C) Delays are Gaussian random variables with means 9 and 15, respectively, and both with standard deviation 8. Solid lines result from Gaussian random delays and discrete symbols from two constant delays τ_1=9, τ_2=15. N=10. (D) Delays are taken from different distributions; namely Gaussian (solid lines) versus uniform delays (discrete symbols). The two distributions have the same means (9 and 15 respectively for the two delays); Gaussian random delays have the same standard deviation 8 and uniform random delays have the same window width 8; N=30.

Effects of Stochasticity. We now consider the effects of stochasticity, which we implement and interpret as two types of internal noise, namely additive Gaussian and multiplicative noise.

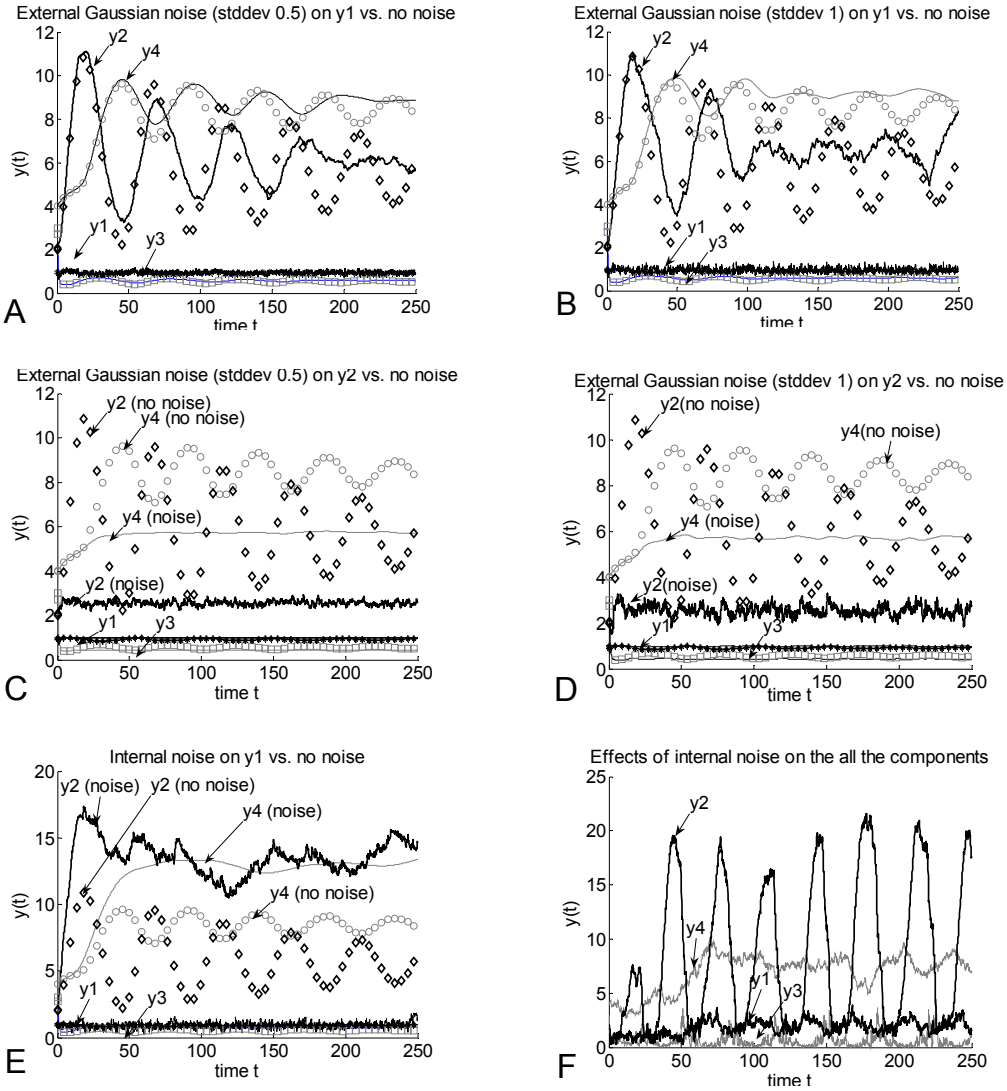

Fig.2.7 Generic biochemical system with noise, delays and feedback loop. (A,B) external Gaussian noise G(0,0.5) and G(0,1) are added to $y1$ respectively. (C,D) external Gaussian noise G(0,0.5) and G(0,1) are added to $y2$ respectively. (E, F) internal noise is added to $y1$ and the entire system, respectively. All scenarios use two constant delays τ_1=9, τ_2=15 and 40 auxiliary variables. Different symbols represent the noise free dynamics (stars for $y1$, diamonds for $y2$, squares for $y3$, circles for $y4$) and solid lines describe the noisy dynamics.

When 50% Gaussian noise is added to variable y_1, the intermediate metabolite directly following y_1, namely y_2, is numerically affected, but its oscillation frequency and amplitude are qualitatively retained. The downstream products y_3 and y_4 are relatively

smooth and seem to converge to the stationary states of the noise-free system (Fig.7. A). If the amplitude of the external noise in y_1 is increased to 100% (Fig.7. B), the oscillation in y_2 is more strongly affected, while the dynamics of y_3 and y_4 are not too different from the previous case. Compared with y_1, the impact of noise in y_2 is more severe. The variable itself, as well as y_4, both deviate considerably from their trajectory in the original noise-free system, while the dynamics of y_1 and y_3 are roughly retained (Figs.7. C, D). The smoothness of y_3 and y_4 in all these cases clearly suggests that the external noise in the substrates y_1 and y_2 is rather effectively buffered by the delays. Moreover, notice that y_1, y_2 and y_3 are connected through mass fluxes and through the negative feedback control of y_1 by y_3, while the pathway composed by y_1, y_2 and y_4 has no such controlling mechanism. As a consequence, the responses are different: the negative feedback loop together with delay efficiently dampens the external noise and retains the integrity of the system behavior.

Fig.7. E and F demonstrate that internal noise implemented through multiplicative terms has a stronger impact on this particular system than additive external noise. When internal noise is restricted to y_1 only, y_1's direct successor y_2 deviates far from the original noise-free trajectory, and the same effect is seen in the following metabolite y_4. By contrast, y_3, maintains more or less the same dynamics as its noise-free counterpart, which is probably again due to the combination of the negative feedback loop with the delay. When internal noise terms are added to all metabolites, all components in the closed pathway consisting of y_1, y_2 and y_3 exhibit undamped oscillations, and the dynamics of all components is distinctly different from that of the noise-free system. Taken together the results indicate that the combination of negative feedback with delay can substantially affect noise and either buffer or amplify oscillations, depending on the specifics of the system.

Example 2: An auto-repressive gene regulatory network

As a second example we consider an auto-repressive gene regulatory network in a single cell as studied previously by (Lipniacki, Paszek et al. 2006; Tian, Burrage et al. 2007), but with generalizations that account for the effects of a discrete switch, delays, and noise in the system (Fig.8). Suppose there are H homogeneous copies of a certain gene in a cell. Each gene copy switches independently between an active and an inactive state. The period that the gene remains on or off is a Gaussian random variable with the same mean and variance. The activated genes are transcribed into mRNAs and these are consequently translated into proteins. Both transcription and translation are relatively time consuming multi-stage processes, which are modeled through time delays. When exceeding some concentration threshold, the resulted protein acts as a repressor: it reduces the rate of gene activation by shortening the period during which the gene is active, and also reduces the production rate of the corresponding mRNA. The system is a hybrid that contains stochastic discrete switches and delays that are difficult to model within traditional software systems and benefits from our implementation of discrete and continuous features in Cell Illustrator. The model system can be formulated as

$$\begin{aligned}
&\text{InactiveGene}(I) \underset{Gaussian(k_A G_2(p))}{\overset{Gaussian(k_I)}{\rightleftarrows}} \text{ActiveGene}(A)\\
&g(t, p(\bullet)) = \sum_{i=1}^{H} g_i, \quad g_i(I) = 0, g_i(A) = 1,\\
&m(t)' = \alpha_m G_1(p(t-\tau_m)) g(t-\tau_m, p(\bullet)) - \beta_m m(t),\\
&p(t)' = \alpha_p m(t-\tau_p) - \beta_p p(t),
\end{aligned} \tag{25}$$

where *g, m* and *p* are amounts (concentrations) of active gene, mRNA and protein, respectively; k_I and k_A are the periods during which the gene remains active and inactive, respectively; τ_m and τ_p are time delays for transcription and translation, respectively; and

a and β are rates of synthesis and degradation, respectively. $G(p)=1/(1+p^n/p_0^n)$ is a Hill function representing the inhibitory effect of the protein, with Hill coefficient n characterizing the strength of association and p_0 representing the repression threshold of the protein. It is straightforward to recast this function as a power-law model within BST (Savageau and Voit 1987; Voit 2005), but we skip this step here because it would not yield genuinely new insights. Instead, retaining the Hill function also shows that the proposed hybrid method applies to non-BST dynamical representations as well.

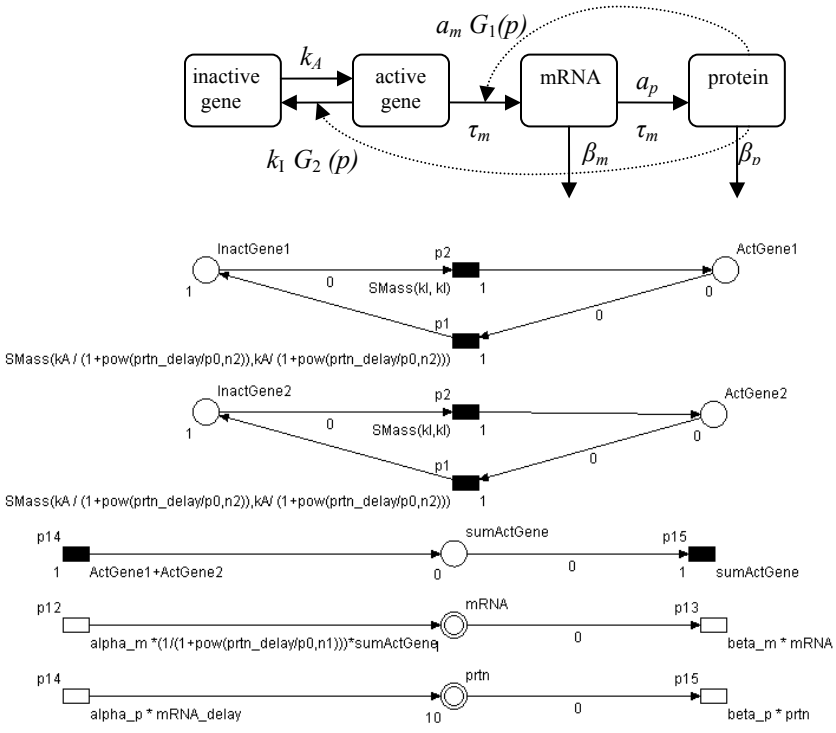

Fig.2.8 Auto-repressive gene expression system and initial parts of its HFPN representation.

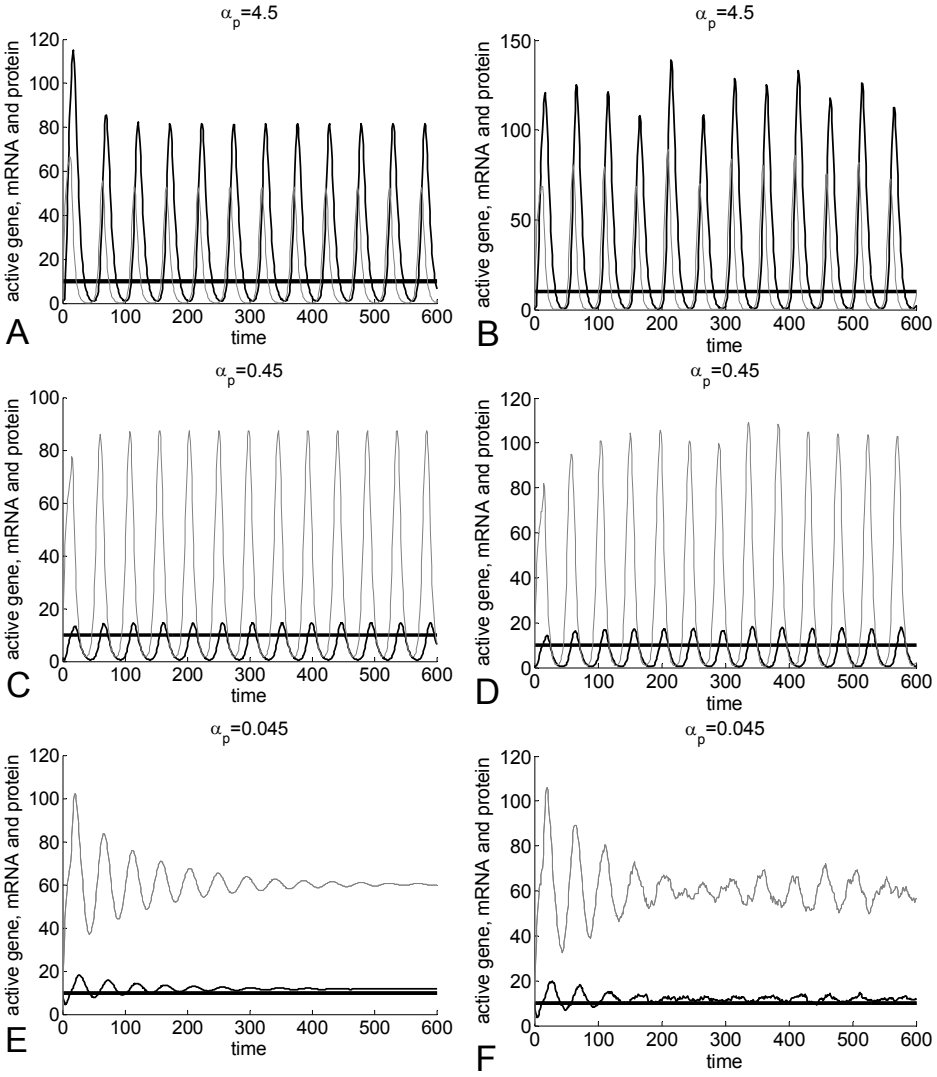

Fig.2.9 Auto-repressive gene regulatory network in a single cell: comparisons of effects of noise, assuming that the system has a constantly activated gene, $g(t)$=1. a_p =4.5, 0.45, 0.045 for the first, the second and third rows respectively. Left column figures are without noise, right columns are from systems with internal noise. p(t)=10, $t \in [-2.8, 0]$; $m(t) = 1$, $t \in [-12, 0]$; N=2, $\alpha_m = 33$, $\beta_m = \beta_p = 0.23$, $\tau_m = 12$, $\tau_p = 2.8$. $p_0 = 10$, $n = 2$. (bold line: active gene scaled by 10 fold; grey line: mRNA; black line: protein scaled by 0.1 fold, except for E and F.)

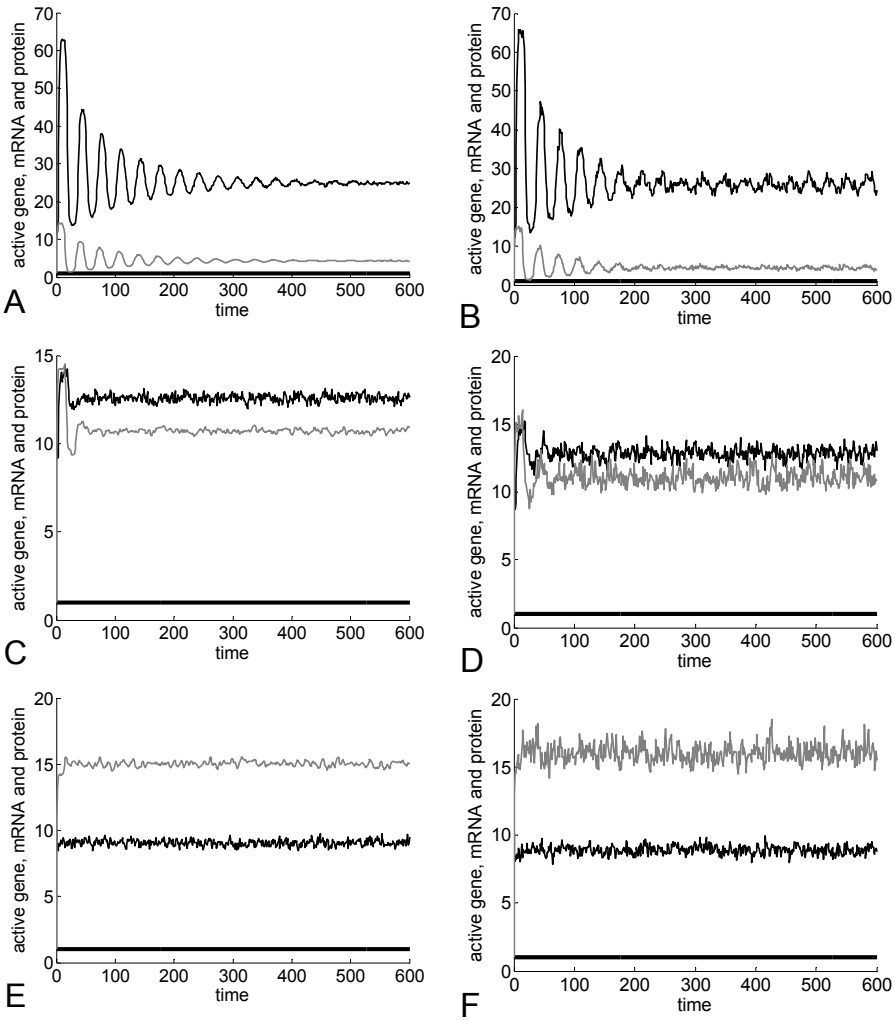

Fig.2.10 Auto-repressive gene regulatory network in a single cell: comparison of systems exposed to external noise and those exposed to external and internal noise. It is assumed that the system has a constantly activated gene, $g(t)$=1. $\alpha_p = 4.5, 0.45, 0.045$ for the first, the second and third rows respectively. Panels in left column: systems with external noise (10% of initial values); panels in right column: systems with external and internal noise. Other parameter values are the same as in Fig.9. (bold line: active gene; grey line: mRNA; black line: protein)

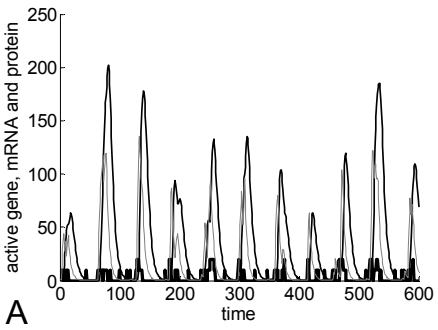
active gene, mRNA and protein
time
0
50
100
150
200
250
0
100
200
300
400
500
600

A

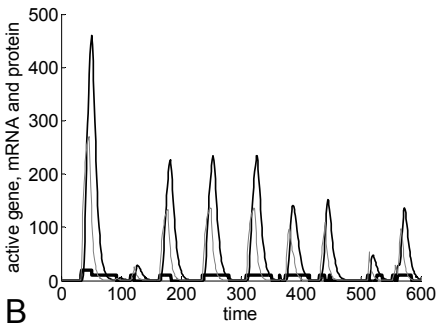
active gene, mRNA and protein
time
0
100
200
300
400
500
0
100
200
300
400
500
600

B

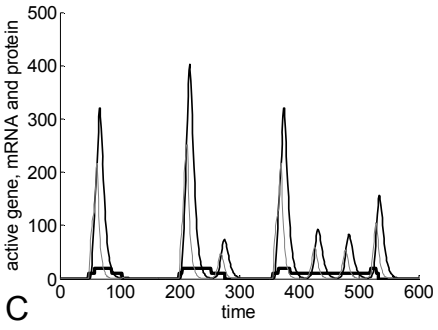
active gene, mRNA and protein
time
0
100
200
300
400
500
0
100
200
300
400
500
600

C

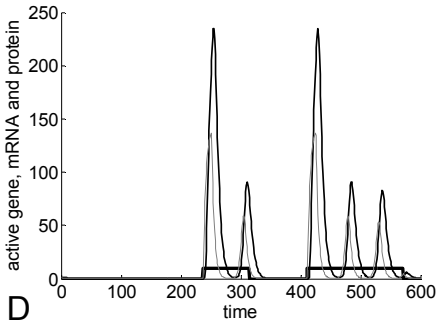
active gene, mRNA and protein
time
0
50
100
150
200
250
0
100
200
300
400
500
600

D

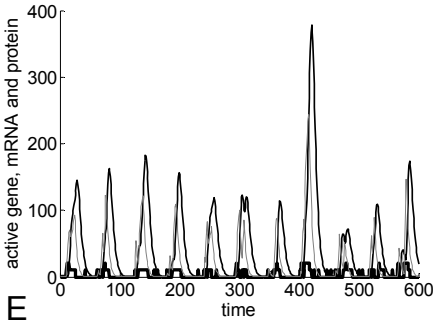
active gene, mRNA and protein
time
0
100
200
300
400
0
100
200
300
400
500
600

E

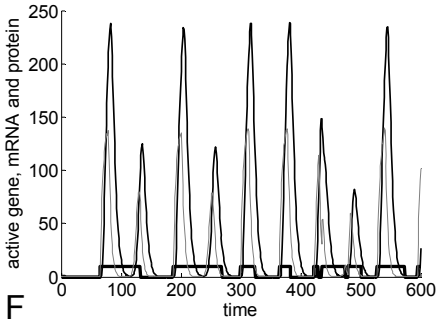
active gene, mRNA and protein
time
0
50
100
150
200
250
0
100
200
300
400
500
600

F

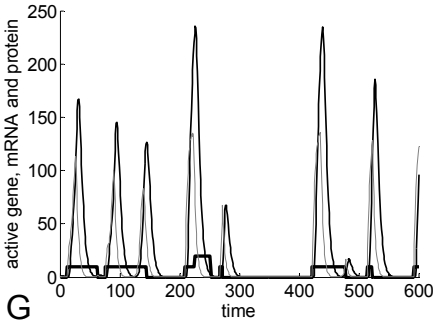
active gene, mRNA and protein
time
0
50
100
150
200
250
0
100
200
300
400
500
600

G

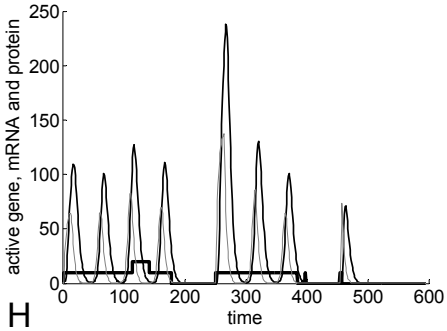
active gene, mRNA and protein
time
0
50
100
150
200
250
0
100
200
300
400
500
600

H

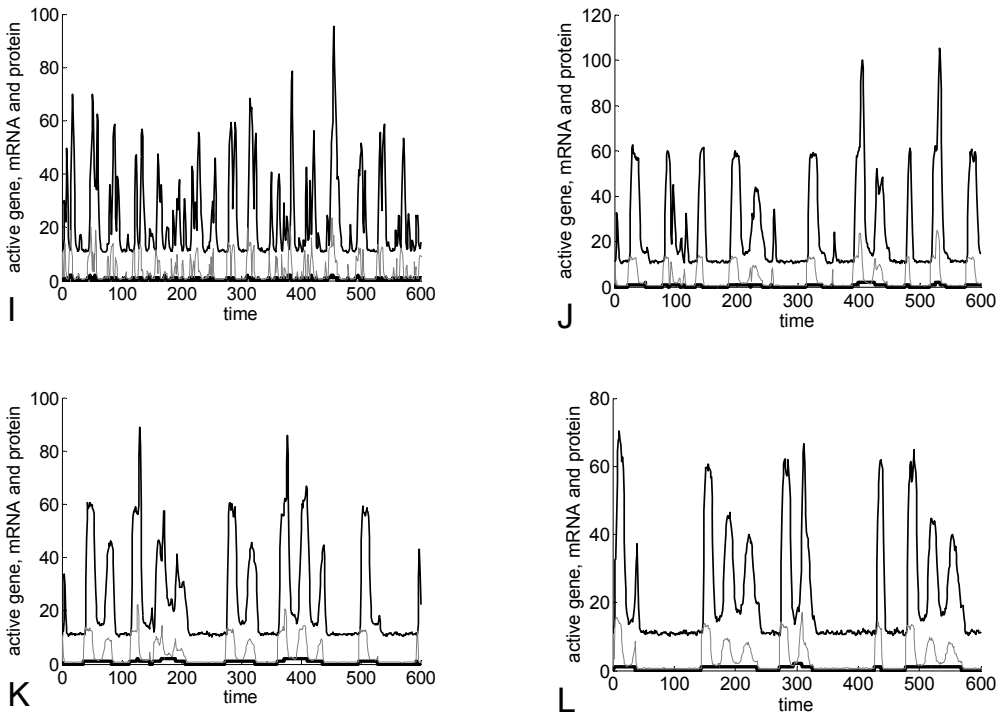

Fig. 2.11 Auto-repressive gene regulatory network in a single cell. (A, B, C, D) Randomness originates only from the genetic switch; $k_A = k_I = 6, 30, 60, 120$ minutes, respectively. (E, F, G, H) randomness arise from genetic switch and internal noise in both mRNA and protein. $k_A = k_I = 6, 30, 60, 120$ minutes respectively. (I, J, K, L) randomness arises from genetic switch and noise (both internal and external) in transcription and translation. $k_A = k_I = 6, 30, 60, 120$ minutes respectively. For all scenarios, $\alpha_p = 4.5,$ and the two Hill functions are identical. Other parameters are the same as those in Fig.9. (bold line: active gene scaled 10 fold; grey line: mRNA; black line: protein scaled by 0.1 fold; data are not scaled in I, J , K and L)

We studied the individual and cooperative effects of negative feedback loops, switches, delays and noise in three steps: in the first two steps we only considered stochasticity in transcription and translation while fixing the activated gene number as 1; in the third step we expanded our scope by including randomness in the activated gene.

To study the combined effects of negative feedback and internal noise, we performed simulations with different protein synthesis rates while all other parameters were kept the same (Figs. 9). The simulation results were consistent with those by Tian *et al.* (Tian, Burrage et al. 2007): the oscillations in the deterministic model are robust with respect to the protein synthetic rate α_P; the stochastic nature in gene expression can clearly amplify the amplitudes of the oscillation, while the oscillatory period roughly remains the same; even if there is a 100-fold decrease in the protein synthesis rate, the stochastic system can maintain the oscillation while the deterministic system produces a damped oscillation (E, F). However, using the results from the MatLab algorithm DDE23 as a base for comparison, our method shows greater accuracy than (Tian, Burrage et al. 2007) in simulating the delay differential equation in the noise free case (result not shown).

After numerically establishing the accuracy of our method in the first step, we compared the effects of internal noise, external noise and their combination. Fig.10 shows that, instead of amplifying the oscillation as internal noise does, even small amounts of external noise (10% of the initial values) can significantly dampen the oscillation (A, C, E): the amplitude of the oscillation is greatly reduced, and the oscillation period also decreases from ~50 min in the noise free case (Fig.9 A) to ~30 min (Fig.10 A); when the system is simulated with both eternal and internal noise, the oscillation is not sustainable, and both mRNA and protein concentrations are close to some constant levels. This comparison shows the dominating effects of external noise over internal noise, and it provides a clue to the question why it is rare (Monk 2003) to observe oscillations in gene expression in most auto-repressive system.

Finally we include a genetic switch in our system (Figs.11). Whenever the gene is switched on, bursts in mRNA and protein appear after some delay; if the gene remains active long enough, both mRNA and protein exhibit oscillations. However, when the

active period of the gene is less than the period of the oscillation, Figs.11 A, E and I show that only parameters k_I and k_A (the gene's mean periods of being active or inactive, respectively) affect the frequency of mRNA and protein production. When only internal noise is added to mRNA and protein, the system dynamics is not significantly different from the noise free case, as one can see from comparing the two sets of figures A~D vs. E~F, and the gene switch contributes primarily to the stochasticity in the system. However, when both internal noise and external noise are applied to mRNA and protein (I~L), the amplitudes of mRNA and protein oscillations are greatly reduced. Moreover, their concentrations maintain the initial, basal level when no activated gene is available. In summary, our study indicates that external noise and randomness in the gene switch contribute significantly to the stochasticity of gene regulatory systems, which are under the influence of both external and internal uncertainty.

4. Discussion

In the past, aspects like stochasticity, switches and delays in biological systems had to be addressed with different software packages, or it was necessary to develop new software from scratch. As a consequence, the interrelationships between such combined effects have seldom been investigated, even though they are known to occur in reality with some frequency. In this work we have developed a hybrid method that permits the simulation of biological systems containing different types of non-trivial effects, including regulation, switches, randomness, and various delays. Two simple yet generic examples from metabolism and gene regulation demonstrated the accuracy, efficiency and advantages of this hybrid approach. The proposed methodology allows the integration and analysis of the following components:

1. BST and Petri nets

Although BST and Petri nets are both over 40 years old, we have shown here for the first time how they can be merged for advanced studies in systems biology. The merger of the two frameworks makes it possible to take advantage of the features of both methodologies and to simulate within the same standard software some complicated, combined effects that up to now could only be done through programming from scratch. In particular, the strong and very valuable guidance for *de novo* model design, offered by BST, can now be extended to ODE systems that are not strictly deterministic. Furthermore, BST methods associated with the steady state are becoming applicable for delayed systems. For instance, we showed elsewhere (Mocek, Rudnicki et al. 2005) that stability in delay systems may be assessed with methods developed for ODEs.

2. Reformulation of different types of delays within BST (or other ODE frameworks)

While simple, fixed delays have been modeled in BST before (Mocek, Rudnicki et al. 2005), the repertoire of delays is vastly expanded in this work. This ability to account for different types of delays is becoming increasingly important when models in systems biology span different organizational levels and run at different time scales that lead to delayed responses.

3. Switches and stochasticity in BST

Switches and stochasticity have appeared in the BST literature (*e.g.*, (Voit 1993; Savageau 2001; Lipniacki, Paszek et al. 2006)), but never in a systematic fashion. They are now both direct variations in the HFPN formulation presented here.

4. Stochasticity and delays

The combination of stochasticity and delays appears to become more important, for instance, in fluctuations in transcription, and in studies of individual cells (Longo and

Hasty 2006). Their combination has seldom been studied in the past, because a unifying modeling framework was missing. We have proposed such a framework here.

5. Design and operating principles

Merging different aspects of biological systems, as described here, will support a major pursuit of systems biology, namely the search for general design principles, which dictate why biological systems are organized in a particular fashion (Savageau 1985). With the repertoire of tools proposed here, we will be able to answer questions such as: What are the best mechanisms to buffer stochasticity or fluctuations in the environment? Are delays necessary evils or are they integral and advantageous to particular designs? Our studies presented here provide the necessary tool to address these and other challenges that pervade integrative systems in biology. In particular, the special structure of the equations in BST system has been shown to offer an elegant manner for the elucidation of design features, called the *method of controlled mathematical comparisons* (MCMC) (Irvine and Savageau 1985; Hlavacek and Savageau 1996; Alves and Savageau 2000). According to this method, the investigated pathway is compared with an alternative, hypothetical pathway that differs in just one particular regulatory or operational feature, so that the difference in responses can be attributed solely to the feature of interest (*e.g.*, (Savageau 1985)). Even if some quantities affecting the investigated and the hypothetic models are unknown, their effects often cancel out and can then be ignored in the comparisons. Because the proposed hybrid models constitute a BST extension that permit discrete and stochastic components, it is feasible to apply MCMC to hybrid systems and to evaluate the effects of a particular feature of interest in comparison to systems without this feature. For instance, the importance of stochasticity may be assessed in comparison to the corresponding deterministic model. We are presently comparing a standard BST-GMA system of the dynamics of dopamine at synapses in the context of neurodegenerative diseases with a corresponding model that allows for delays and

stochasticity. The comparison is being executed with alternative HFPN formulations within CI, and the results will be presented elsewhere.

A remaining challenge of all modeling efforts is parameter estimation. In the case of hybrid models, it may be possible to distinguish parameters for continuous and discrete parts of a hybrid model. The details of this separation need to be worked out. A possibility may be application of a method that originated in geophysics and is called data assimilation (DA). Its authors, Nagasaki *et al.* (Nagasaki, Yamaguchi et al. 2006), estimated parameters and identified the structure of a small-sized HFPN model from time-course gene expression data. However, their approach was limited to an ODEs model, and a true hybrid model (containing discrete and continuous, deterministic and stochastic effects) has yet to be addressed. In general, structural analysis for discrete Petri Nets has proven to be very fruitful in attempts to understand the topological properties of a network and to discover biological design principles. While it is to be expected that theoretical analyses are more complicated for hybrid systems, it is also evident that hybrid systems are abundant in nature and that the development of novel methods of analysis will be rewarding. In this paper we have taken a step forward toward these types of analysis.

Acknowledgments

The authors thank Skip Thompson for his advice regarding the DDE SOLVER. Monika Bajan and Sebastian Sosnik's technical assistance with Cell Illustrator was highly appreciated. This work was supported in part by a Molecular and Cellular Biosciences Grant (MCB-0517135; E.O. Voit, PI) from the National Science Foundation. Any opinions, findings, and conclusions or recommendations expressed in this material are

those of the authors and do not necessarily reflect the views of the sponsoring institutions.

References

1. Savageau MA. Biochemical systems analysis. I. Some mathematical properties of the rate law for the component enzymatic reactions. Journal of Theoretical Biology 1969;25:365-369
2. Savageau MA. Biochemical systems analysis. II. The steady-state solutions for an n-pool system using a power-law approximation. Journal of Theoretical Biology 1969;25:370-379
3. Savageau MA. Biochemical systems analysis. A study of function and design in molecular biology: Addison-Wesley; 1976
4. Voit EO. Computational analysis of biochemical systems: a practical guide for biochemists and molecular biologists: Cambridge University Press; 2000
5. Matsuno H, Tanaka Y, Aoshima H, et al. Biopathways representation and simulation on hybrid functional Petri net. In Silico Biol 2003;3:389-404
6. Miyano S. Cell Illustrator website. http://wwwcellillustratorcom/ 2008
7. Henri MV. Lois générales de l'action des diastases. Paris, Hermann 1903
8. Michaelis L, Menten ML. Die Kinetik der Invertinwirkung. Biochem Zeitschrift 1913;49:333-369
9. Volterra V. Variazioni e fluttuazioni del numero d'individui in specie animali conviventi. Mem R Accad dei Lincei 1926;2
10. Lotka A. Elements of Physical Biology. Baltimore: Williams and Wilkins 1924
11. May RE. Theoretical Ecology: Principles and Applications. Oxford: Blackwell; 1976
12. Fell DA. Understanding the Control of Metabolism: Portland Press, London; 1997

13. Visser D, Heijnen JJ. The mathematics of metabolic control analysis revisited. Metab Eng 2002;4:114-123
14. Hatzimanikatis V, Bailey J. MCA has more to say. Journal of Theorectical Biology 1996;182:233-242
15. Savageau MA. Design principles for elementary gene circuits: Elements, methods, and examples. Chaos 2001;11:142-159
16. Voit EO. Smooth bistable S-systems. IEE Proc Systems Biol 2005;152:207-213
17. Gillespie DT. Exact stochastic simulation of coupled chemical reactions Journal of Physical Chemistry 1977;81:2340-2361
18. Gillespie DT. The chemical Langevin equation. The Journal of Chemical Physics 2000;113:297-306
19. Gillespie DT. Approximate accelerated stochastic simulation of chemically reacting systems. Journal of chemical physics 2001;115:1716-1733
20. Wolkenhauer O, Ullah M, Kolch W, Cho K-H. Modelling and Simulation of IntraCellular Dynamics: Choosing an Appropriate Framework IEEE Transactions on NanoBioscience 2004;3:200-207
21. Hale J, Lunel SMV. Introduction to Functional Differential Equations. 1st ed: Springer
22. Mocek WT, Rudnicki R, Voit EO. Approximation of delays in biochemical systems. Mathematical Biosciences 2005;198:190-216
23. Ishii N, Nakahigashi K, Baba T, et al. Multiple high-throughput analyses monitor the response of E. coli to perturbations. Science 2007;316:593-597
24. Reisig W. Petri Nets: An Introduction: Springer Verlag; 1985
25. Reddy VN, Mavrovouniotis ML, Liebman MN. Petri net representations in metabolic pathways. Proc Int Conf Intell Syst Mol Biol 1993:328-336

26. Hardy S, Robillard PN. Modeling and simulation of molecular biology systems using Petri nets: Modeling goals of various approaches. Journal of Bioinformatics and Computational Biology 2004;2:619-637

27. Goss PJE, Peccoud J. Quantitative modeling of stochastic systems in molecular biology by using stochastic Petri nets. Proceedings of the National Academy of Sciences 1998;95:6750-6755

28. Gillespie DT. Stochastic simulation of chemical kinetics. Annual Review of Physical Chemistry 2007;58:35-55

29. Tian T, Burrage K. Stochastic models for regulatory networks of the genetic toggle switch. Proceedings of the National Academy of Sciences 2006;103:8372-8377

30. Gillespie DT. Approximate accelerated stochastic simulation of chemically reacting systems. Journal of Chemical Physics 2001;115:1716

31. Gillespie DT. The chemical Langevin and Fokker-Planck equations for the reversible isomerization reaction. Journal of Physical Chemistry A 2002;106:5063

32. Tian T, Burrage K, Burrage PM, Carletti M. Stochastic delay differential equations for genetic regulatory networks. The Journal of Computational and Applied Mathematics 2007;205:696-707

33. Maheshri N, O Shea EK. Living with Noisy Genes: How Cells Function Reliably with Inherent Variability in Gene Expression. Annual Review of Biophysics and Biomolecular Structure 2007;36:413-434

34. Lipniacki T, Paszek P, Marciniak-Czochra A, Brasier AR, Kimmel M. Transcriptional stochasticity in gene expression. Journal of Theorectical Biology 2006;238:348-367

35. Savageau MA, Voit EO. Recasting nonlinear differential equations as S-systems: a canonical nonlinear form. Mathematical Biosciences 1987;87:31-113

36. Monk NAM. Oscillatory expression of Hes1, p53, and NF-kappaB driven by transcriptional time delays. Curr Biol 2003;13:1409

37. Voit EO. S-system modeling of complex systems with chaotic input. Environmetrics 1993;4:153-186

38. Longo D, Hasty J. Dynamics of single-cell gene expression. Molecular Systems Biology 2006;2

39. Savageau MA. A theory of alternative designs for biochemical control systems. Biomed Biochim Acta 1985;44:875-880

40. Irvine DH, Savageau MA. Network regulation of the immune response: alternative control points for suppressor modulation of effector lymphocytes. Journal of Immunology 1985;134 2100-2116.

41. Hlavacek WS, Savageau MA. Rules for coupled expression of regulator and effector genes in inducible circuits. J Mol Biol 1996;255 121-139

42. Alves R, Savageau MA. Effect of overall feedback inhibition in unbranched biosynthetic pathways. Biophysical Journal 2000 79 2290-2304

43. Nagasaki M, Yamaguchi R, Yoshida R, et al. Genomic data assimilation for estimating hybrid functional Petri net from time-course gene expression data. Genome Informatics 2006;17:46-61

44. Li C, Suzuki S, Ge Q-W, et al. Structural modeling and analysis of signaling pathways based on Petri nets. Journal of Bioinformatics and Computational Biology 2006;4:1119-1140

PAPER 2

CHAPTER 3

Integrative Biological Systems Modeling: Challenges and Opportunities

Jialiang Wu and Eberhard O. Voit

Frontiers of Computer Science in China, 2009 b. **3**(1): p. 92-100.

Integrative Biological Systems Modeling: Challenges and Opportunities

JIALIANG WU

Department of Mathematics, Bioinformatics Program, Georgia Institute of Technology,

Atlanta, GA 30332, USA

gtg337v@mail.gatech.edu

EBERHARD VOIT*

Integrative BioSystems Institute and

The Wallace H. Coulter Department of Biomedical Engineering, Georgia Institute of Technology

Atlanta, GA 30332, USA

eberhard.voit@bme.gatech.edu

* *Corresponding author*

Abstract

Most biological systems are by nature hybrids consist of interacting discrete and continuous components, which may even operate on different time scales. It is therefore desirable to establish modeling frameworks that are capable of combining deterministic and stochastic, discrete and continuous, as well as multi-timescale features. In the context of molecular systems biology, an example for the need of such a combination is the investigation of integrated biological pathways that contain gene regulatory, metabolic and signaling components, which may operate at different time scales and involve on-off switches as well as stochastic effects. The implementation of integrated hybrid systems is not trivial because most software is limited to one or the other of the dichotomies above. In this study, we first review the motivation for hybrid modeling. Secondly, by using the example of a toggle switch model, we illustrate a recently developed modeling framework that is based on the combination of Biochemical Systems Theory (BST) and Hybrid Functional Petri Nets (HFPN). Finally, we discuss remaining challenges and future opportunities.

1. Introduction

Several generic modeling frameworks have been developed during the past decades to predict the behavior of continuous, deterministic systems in biology and medicine. Among the best known are Biochemical Systems Theory (BST) (Savageau 1969; Savageau 1969; Savageau 1976; Voit 2000; Torres and Voit 2002), which was designed for dynamic and steady-state systems, and Metabolic Control Analysis (Kacser and Burns 1973; Heinrich and Rapoport 1974; Fell 1997), which was originally limited to responses at the steady state but later augmented with the lin-log model formulation for dynamic analyses (Hatzimanikatis and Bailey 1996 ; Visser and Heijnen 2002; Wang, Ko et al. 2007). Most dynamical approaches implicitly assume that relatively large numbers of molecules interact freely within a well-mixed medium. This assumption is important because it permits the application of methods of statistical mechanics, which allows averaged, continuous rates and, thus, the use of differential equations. However, many intracellular behaviors are discrete and some are apparently random in nature, for instance, because of low substrate concentrations or heterogeneous reaction environments. If these aspects cannot be validly ignored, the foundations of pure ordinary differential equation (ODE) representations present a significant limitation. As an alternative, some more recent modeling languages have been proposed to overcome this limitation. Examples include stochastic Petri Nets (Goss and Peccoud 1998; Haas 2002) and stochastic automata (D'Argenio and Katoen 2005). The stochastic approaches pose their own challenges and are usually less efficient than differential equation methods (Gillespie 1992; Gillespie 2007). The question thus arises of whether it is possible to combine the positive aspects of continuous, deterministic, and stochastic formulations and merge them into a unified, hybrid formalism. In this article, we discuss a promising combination of this type. We first identify more specifically the needs in integrative biological systems modeling, then outline a recently proposed, combined methodology,

based on BST and Hybrid Functional Petri Nets (HFPN) (Matsuno, Tanaka et al. 2003), and finally point out future directions and opportunities. Additional aspects and technical details, along with different types of examples, are presented elsewhere (Wu and Voit, 2009).

Rationale for Hybrid Modeling

1.1 Stochasticity of biochemical reactions *in vivo*

Deterministic modeling relies fundamentally on the law of mass action. This law is derived from the assumption that thousands of molecules interact within a well-mixed and homogeneous medium, which in some sense admits the laws governing ideal gases. Supposing that molecular reactions are essentially random processes, one infers that macroscopic systems with a large number of interacting molecules allow the randomness to be averaged out so that the overall macroscopic state of the system can be accurately approximated by the deterministic laws. However, the population sizes of some components in an individual cell are limited (sometimes numbering only a few hundreds), and reactants often interact on a small scale and within non-homogeneous cellular environments. These observations render the assumption of continuous and deterministic approaches questionable. A typical example is the regulation of gene expression where only a few transcription factors interact with DNA binding sites in the gene's regulatory sequence. Indeed, fluorescent probes have identified fluctuations at the level of individual cells (Elowitz, Levine et al. 2002; Blake, Kaern et al. 2003), and one must wonder whether it is prudent and valid if these are averaged. Similarly, McAdams and Arkin (McAdams and Arkin 1997) showed that low copy numbers of expressed RNAs can be significant for the regulation of downstream pathways. Moreover, cellular

environments are highly compartmental and structured, which is far from the homogenous, well-mixed solutions that are typical of *in vitro* experiments (Schnell and Turner 2004). A high degree of molecular crowding and the presence of endogenous obstacles in cellular media have important consequences for the thermodynamics within the cell (Minton 1993; Minton 1998) and strongly affect the diffusion processes (Luby-Phelps, Castle et al. 1987). For instance, the viscosity of the mitochondrion is 25–37 times higher than that of a typical *in vitro* experimental buffer (Scalettar, Abney et al. 1991). Diffusion of macromolecules in the cytoplasm can be 5–20 times lower than in saline solutions (Verkman 2002). Finally, rather than happening in a 3-dimensional volume, many reactions occur on two-dimensional membranes or in quasi-one-dimensional channels (Clegg, 1984; Srere, Jones et al., 1989). Thus, caution is needed when assumptions are made with regard to homogeneity and well mixing in biochemical reaction systems *in vivo*.

Stochastic approaches try to capture the inherently random nature of molecular collisions and to construct probabilistic models of the reaction kinetics (Gillespie 1976; Qian and Elson 2002). If successful, such an approach is thus inherently more appropriate than averaging methods for the small, heterogonous environments that are typical of *in vivo* conditions (Kuthan 2001). In spite of their advantages, stochastic models are still not sufficient for small-scale biological systems, because they do not explicitly account for spatial heterogeneity and are difficult to implement analytically. Furthermore, stochastic methods present major, genuine challenges. For instance, their construction requires detailed biochemical knowledge, including kinetic rates and numbers of molecules. In later sections we shall discuss to what degree HFPN is a suitable framework for implementing, simulating, and analyzing stochastic effects in biological pathway systems.

1.2 Accounting for multiple time scales in biological systems

Most models implicitly assume that the processes in biological systems run at similar time scales. If this is true, the dynamics of a system by and large depends on its current state and can be formulated with ordinary differential equations. In particular, the homogeneity of time scales implies that delay effects can be ignored. However, in reality, fast reactions (dimerization, phosphorylation, protein-DNA binding or unbinding) and slow reactions (transcription, translation, degradation) occur simultaneously, and they affect each other in multiple ways that critically influence their transient dynamics. For instance, it has been shown that delay within a feedback loop of mRNA transcription and protein expression can result in oscillatory expression patterns (Hirata, Yoshiura et al. 2002; Monk 2003). Moreover, the combination of delays and positive feedback loops has been recognized as a mechanism that is able to maintain oscillatory expression patterns in noisy systems (Tian, Burrage et al. 2007). In the absence of a unifying modeling framework, any analysis of such a combination of stochastic and deterministic features has to be addressed through programming from scratch, which is seldom done.

1.3 Combined models of continuous and discrete components in intracellular systems

Biological systems often involve continuous and discrete phenomena side by side. For instance, gene transcription is switched on or off depending on the expression levels of other genes and on the presence or absence of transcription factors in sufficient quantities. The more or less continuous change in the concentration of a protein may trigger a discrete transition, such as the onset of mitosis or cell differentiation, which in turn changes the protein concentration. Hybrid methods easily address both discrete and continuous events within the same model. A hybrid approach is usually less computationally expensive than an exact discrete-event simulation and more accurate than continuous approximations, preserving the discrete or stochastic nature of the model

where it is important. Hybrid methods also lead to models in which the sources of stochastic behavior are more transparent, because the non-stochastic components are logically and computationally separated from the stochastic components (Kiehl, Mattheyses et al. 2004). These considerations make hybrid modeling of biological processes very appealing. Nonetheless, one must also realize the challenges encountered by hybrid modeling for biological phenomenon: a) the partition of a system into discrete and continuous parts sometimes needs to be done dynamically; the hybrid modeling framework should provide automatic classification mechanisms; and b) the control of the communication between the discrete and continuous components is complicated; it should run in the background without burdening the modeler.

2. Methods

Modeling a regulated network requires a precise description of network components and their interactions. Two "extreme" conceptual frameworks for modeling mathematical pathway systems are commonly used: a) Deterministic mass action models and their generalizations, which are represented by ordinary differential equations, where reaction rates depend continuously on changes in the participating species over time. b) Stochastic models and simulations of biochemical reaction networks based on the Chemical Master Equation or stochastic differential equations (Gillespie 2007). Here we show how to merge these two streams into a synergetic uniform framework for integrative biological systems analysis.

2.1 Biochemical Systems Theory; GMA Systems and S-systems

Among the deterministic models, *Biochemical Systems Theory* (BST) is one of the best established and most general modeling frameworks (Voit 2000). The basis of BST is the use the power-law functions to approximate all processes in the system. For instance, in

metabolic systems, all enzyme-catalyzed reactions are represented as power-laws that contain a rate constant and all contributing substrates, enzymes, and modifiers, each raised to a real-valued power, the kinetic order. Most prominent among the "canonical models" within BST are Generalized Mass Action (GMA) and S-system models; their respective formats are shown in Equations (1)-(3).

Generic Model:

$$\dot{X}_i = [v_{1i} + v_{2i} + \ldots + v_{pi}] - [v_{i1} + v_{i2} + \ldots + v_{iq}] = V_i^+ - V_i^- \qquad (1)$$

GMA System*:*

$$\dot{X}_i = \sum_{p=1}^{P_i} \left(\pm \gamma_{ip} \prod_{j=1}^{n} X_j^{f_{ipj}} \right), \qquad i = 1, \ldots, n \qquad (2)$$

S-system:

$$\dot{X}_i = \alpha_i \prod_{j=1}^{n} X_j^{g_{ij}} - \beta_i \prod_{j=1}^{n} X_j^{h_{ij}}, \qquad i = 1, \ldots, n. \qquad (3)$$

While models within BST consist strictly of systems of ODEs, Mocek *et al*. showed that processes with simple, constant delays can be approximated within the BST format with arbitrary accuracy (Mocek, Rudnicki et al. 2005). Wu and Voit recently extended Mocek's method to allow delays of different types, including multiple discrete delays, distributed delays, time dependent delays and random delays (Wu and Voit, 2009).

Other biological formalisms based on differential equations have been developed for pathway representation and simulation, but we will focus here exclusively on BST models. Among non-ODE-based approaches of network analysis, Boolean methods, graph methods, and Petri Nets have received some attention. Since Boolean methods and graph methods do not appropriately represent feedback signals and other nonlinearities, we only mention these approaches here without further pursuing them.

2.2 Petri Net Modeling

A Petri Net is a mathematical construct that graphically, and then formally, depicts a system with concurrent processes and properties. Originally designed for discrete systems, Petri Nets have recently been extended to account for hybrid systems containing both discrete and continuous events. These Hybrid Functional Petri Nets (HFPN) can be simulated conveniently with the software package Cell Illustrator (Miyano 2008).

2.3 Implementing a BST Model in HFPN

As indicated in Fig.1, it is straightforward to implement a BST model in the HFPN framework: each dependent and independent variable in BST is represented in the Petri Net by a *continuous place* with the name of the molecular species. Every positive term in the BST differential equations is the *speed* of an *input transition* and every negative term the *speed* of an *output transition*. Direct connectivity is only included between places between which there is mass flow. In HFPN, a continuous place is graphically represented by double-ringed circle, and a continuous transition by an open rectangle.

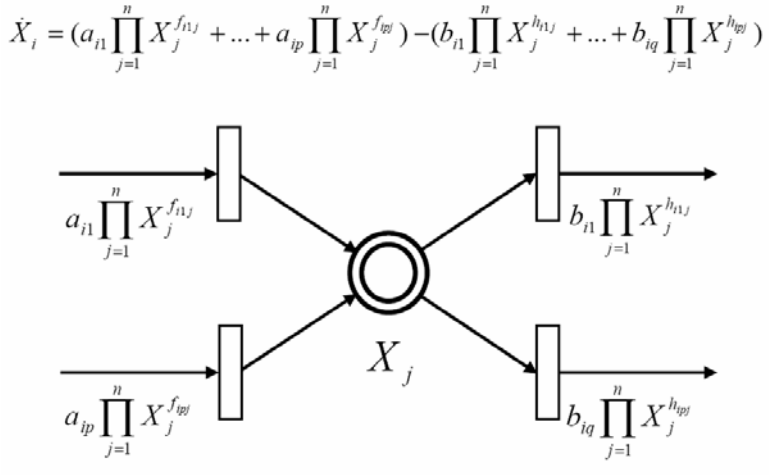

Fig. 3.1 GMA system and its HFPN representation.

In parallel work (Wu and Voit, 2009) we developed a hybrid approach combining BST and HFPN, which allows the simulation of biological systems containing different types of non-trivial effects, including feedback regulations, switches, randomness, and various delays. Here we illustrate the advantages and opportunities of this hybrid method with a generic example from the area of gene regulation.

3. Illustration: Genetic Toggle Switch

The SOS signaling pathway allows bacteria and higher organisms to respond to a variety of stresses in a coordinated fashion. Gardner *et al.* (Gardner, Cantor et al. 2000) studied this pathway in *E. coli* cells that responded to DNA damage caused by the exposure to mitomycin C (*MMC*). A critical component for the functionality of the SOS pathway is a genetic toggle switch that is composed of two genes, *lacI* and $\lambda\, cI$, which encode two repressor proteins *LacR* and $\lambda\, CI$, respectively. As sketched in Fig. 2, the *lacI* gene is expressed in the presence of promoter P_L, which is repressed by $\lambda\, CI$. Similarly, the $\lambda\, cI$ gene is expressed in the presence of promoter P_{trc}, which is repressed by *LacR*. This "symmetric" gene regulatory system has two stable steady states. When the expression level of *lacI* is high, the $\lambda\, cI$ expression level is low, and *vice versa*. An external signal

may trigger transitions between the steady states. Specifically, in the experiments of Gardner and collaborators (Gardner, Cantor et al. 2000), exposure to *MMC* leads to the activation of protein *RecA*, which in turn cleaves the repressor protein λCI, thereby releasing repression and resulting in increased expression of gene *lacI*. Under their chosen experimental conditions, due to noise, some cells will trigger the genetic switch while others don't, resulting in a bimodal population distribution. By contrast, if there is no SOS signal, noise alone rarely transfers the system from one steady state to another and a unimodal population is observed.

Gardner's goup (Gardner, Cantor et al. 2000) proposed a deterministic model (Eq. (1)) which successfully characterized the conditions under which the genetic toggle switch expresses two distinct steady states. However, being a deterministic model, the model cannot simulate experimental results where different cells undergo different genetic switching under the same experimental conditions. Based on this deterministic model, Tian and Burrage (Tian and Burrage 2006) proposed a stochastic model (Eqs.(4) and (5)) to realize experimental results with bimodal population distributions with regard to the expression levels of *LacR*. We use this model here for demonstration. Even though it is not directly in BST format, it could easily be reformulated as such (Savageau and Voit 1987; Voit 2005) and indicates the general procedure of including kinetic, dynamic modeling and stochasticity into the same HFPN framework.

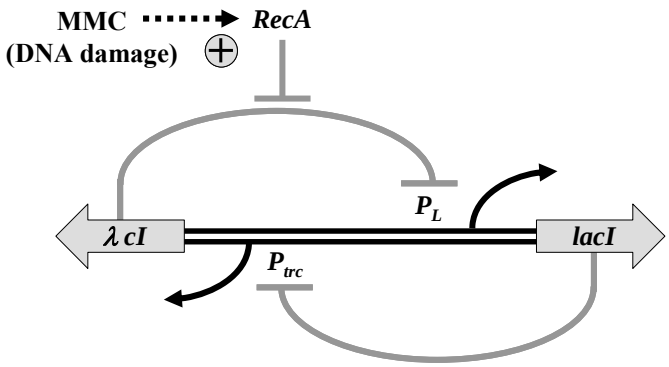

Fig. 3.2: Genetic toggle switch associated with the SOS signaling pathway (adapted from (Tian and Burrage 2006))

$$\frac{du}{dt} = \varepsilon\left(\alpha_1 + \frac{\beta_1}{1+v^3}\right) - \left(1 + \frac{\gamma^s}{1+s}\right)u, \qquad \frac{dv}{dt} = \varepsilon\left(\alpha_2 + \frac{\beta_2}{1+u^3}\right) - v. \tag{4}$$

$$\begin{aligned} u(t+\tau) &= u(t) + P\left[\varepsilon\left(\alpha_1 + \frac{\beta_1 K_1^3}{K_1^3 + v(t)^3}\right)\tau\right] - P\left[\left(d_1 + \frac{\gamma^s}{1+s}\right)u(t)\tau\right], \\ v(t+\tau) &= v(t) + P\left[\varepsilon\left(\alpha_2 + \frac{\beta_2 K_2^3}{K_2^3 + u(t)^3}\right)\tau\right] - P\left[d_2 v(t)\tau\right]. \end{aligned} \tag{5}$$

In Eqs. (4) and (5), u and v are the numbers of λCI and *LacR* molecules respectively. α_1 and $\alpha_1 + \beta_1$ represent the basal and maximal rates of λCI synthesis from the P_{trc} promoter, respectively, and α_2, $\alpha_2 + \beta_2$ are the equivalent parameters for *LacR* expression from the P_L promoter, respectively. The parameter ε is associated with the copy number of the toggle switch plasmid, while parameter s represents the effect of *MMC* on the degradation of λCI. Tian and Burrage used the following parameter values: $\alpha_1 = \alpha_2 = 0.2$ μM min^{-1}, $\beta_1 = \beta_2 = 4$ μM min^{-1}, $\varepsilon = 1$, $d_1 = d_2 = 1$ min^{-1}, $K_1 = K_2 = 1$ μM, *and* $\gamma = 1$ min^{-1}.

Fig. 3.3 HFPN representation of the ODE portion of the toggle switch (Eq.(4)), as depicted in Cell Illustrator (Miyano 2008).

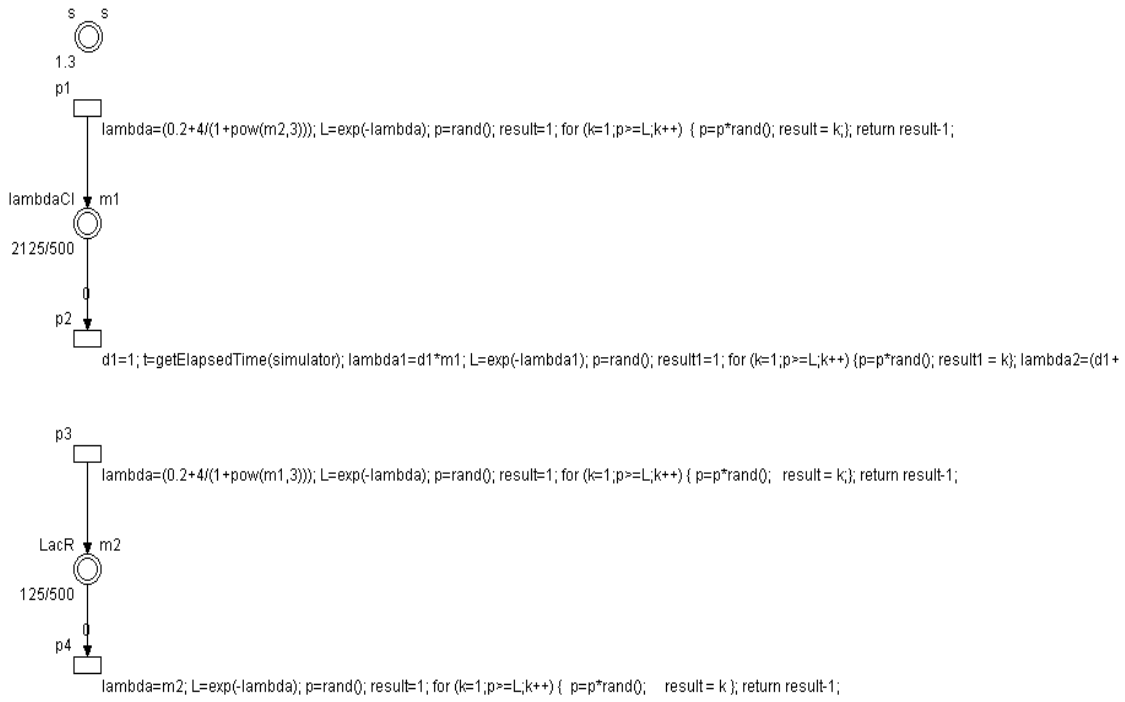

Fig. 3.4 HFPN representation the stochastic portion of the toggle switch (Eq.(5)), as depicted in Cell Illustrator (Miyano 2008).

It is fairly simple to convert Eqs. (4) and (5) into a corresponding HFPN model of the toggle switch. In Figs. 3 and 4, the transitions *p1* and *p2* are the production and degradation processes of λCI, respectively, and *p3* and *p4* are those of *LacR*, respectively. Place variables *m1* and *m2* represent the numbers of λCI and *LacR* molecules respectively, each with corresponding initial values 2125/500 and 125/500. We programmed the SOS signaling effect on the transition *p2*: when the SOS signal is applied in (60, 960), the degradation rate is $(1+\frac{1}{1+s})m1$, otherwise the degradation rate is *d1m1*. The Poisson numbers needed for the transitions *p1* through *p4* (see Fig.4) were generated by a short script.

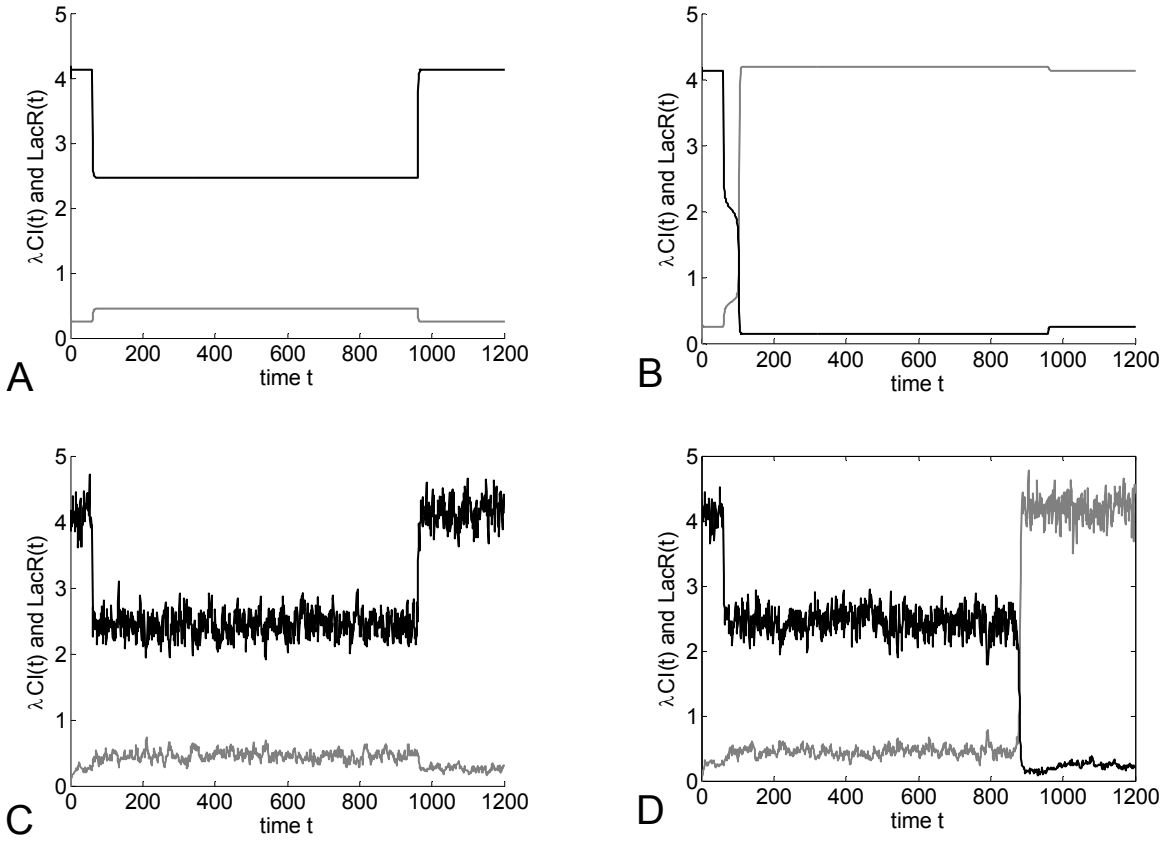

Fig. 3.5 Simulations of the genetic toggle switch as it is affected by the SOS signaling pathway (A) Deterministic model (Eq. (4)) with s=1.3 and d_1 switching at t=60 and t=960 during *MMC* exposure (see Text); no switch occurs for $s \leq 2.0$. (B) Deterministic model (Eq. (4)) with s=2.2; a single switch occurs. (C) Stochastic HFPN model (Eqs. (5)) corresponding to the deterministic model in (A); in spite of noise, no switch occurs. (D) The same stochastic HFPN model, with the same degradation rate and the same noise structure as in (C), may lead to a switch. Dark and grey lines show λ *CI* and *LacR*, respectively. The values of both λ *CI* and *LacR* are scaled by 1/500.

Corresponding to the experimental exposure regimen with various concentrations of *MMC*, the degradation rate of λ *CI* is d_1=1 when t is in [0, 60] and $t \geq 960$, and $d_1 + \gamma^s/(1+s)$ when t is in [60, 960]. The large change in rate triggers a shift in the system from the steady state to an intermediate state in both the deterministic and stochastic simulations. In the deterministic simulations, there is no genetic switching for $s \leq 2.0$, but

switching may occur for $s > 2.0$ if the concentration of λCI is below some threshold value (Fig.5 B, s= 2.2). The situation in the stochastic simulations is different: when the system enters into the unstable intermediate state where $\lambda CI \approx 2.3$ and $LacR \approx 0.5$, intrinsic noise can be sufficient to switch the system from the intermediate unstable state to the other steady state where $\lambda CI \approx 0.26$ and $LacR \approx 4.1$. For the same s=1.3, the noise may cause a genetic switch in one simulation (Fig. 5 D) but not in another (Fig. 5 C). If the transition between the steady states does not happen during [60, 960], the system will jump back to the initial steady state.

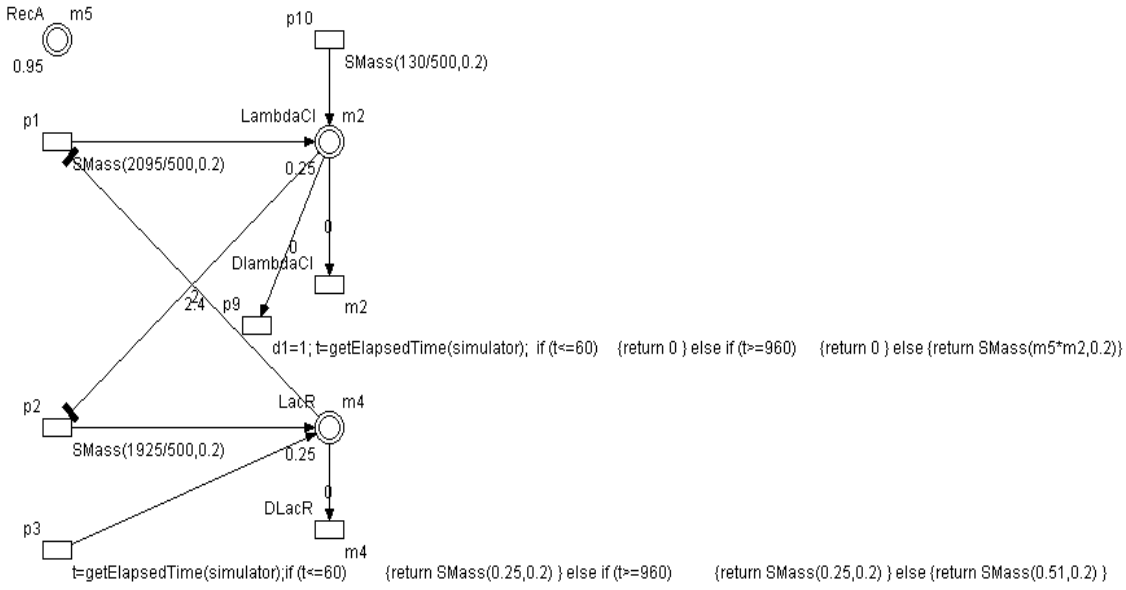

Fig. 3.6 Alternative HFPN model of the toggle switch with direct implementation of Gaussian noise, as depicted by Cell Illustrator (Miyano 2008).

Instead of setting up stochastic equations as before, it is possible to enter stochasticity directly into the HFPN model. Fig. 6 shows an alternative way to model the toggle switch through HFPN in a very intuitive way: continuous place variables *m2* and *m4* represent the numbers of λCI and *LacR* molecules respectively; transitions *p3* and *p2* respectively

describe the basal and major production of *LacR*, where "basal" is the production rate when *LacR* is inhibited by λ *CI* and "major" is the rate added to the basal part when there is no inhibition; *p10* and *p1* are equivalent transitions for λ *CI*. The degradation of λ *CI* consists of two parts: *D*λ *cI* is the degradation rate under normal physiological situation and *p9* is the additional rate during [60, 960] when *MMC* is applied and the SOS signaling is in action. (The control on *p9* is realized through a script, similar for *p3*). *DLacR* is the degradation process for *LacR*. As shown in the figure, Gaussian noise is added to the production processes of λ *CI* and *LacR* through a Cell Illustrator function *SMass*(*mean, stdv*).

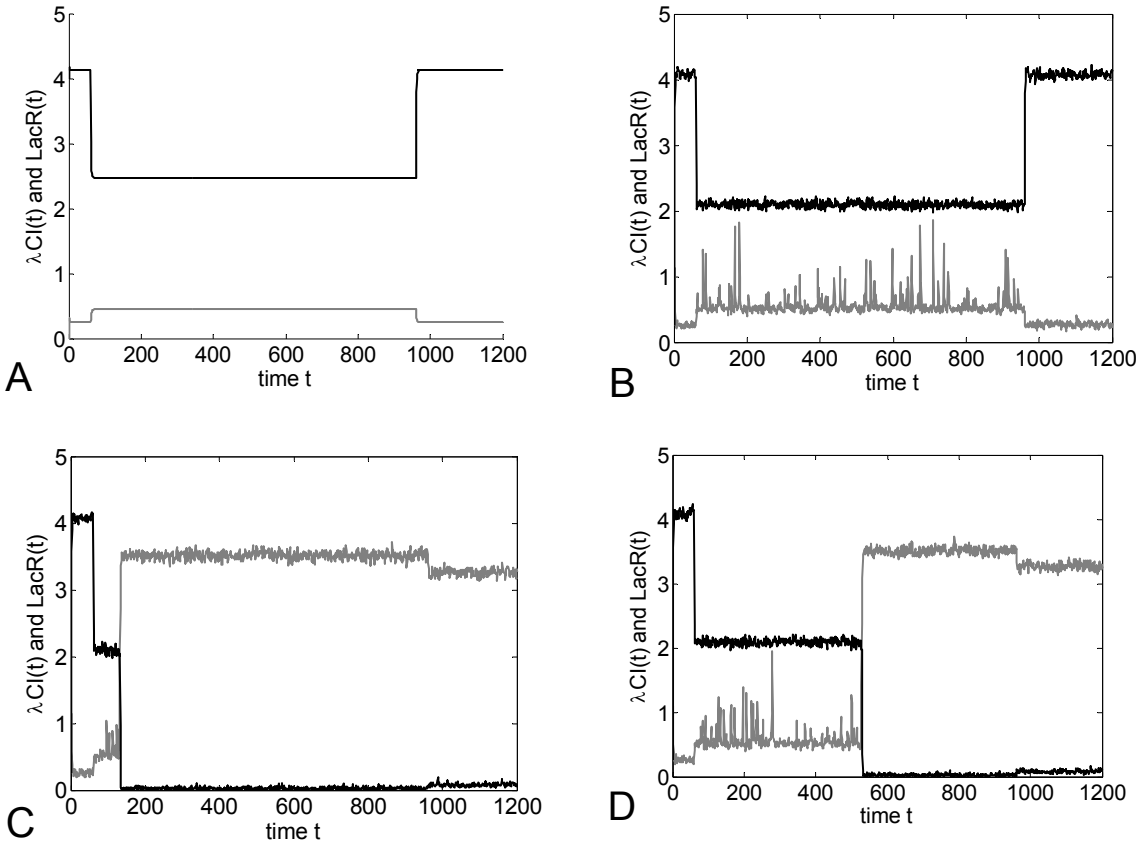

Fig. 3.7 Simulations of the toggle switch with the alternate HFPN model in Fig. 5. (A) No genetic switch occurs in the (deterministic) model without noise. (B) Even with Gaussian noise of standard

deviation 0.2, there is no switch in this simulation. (C, D) With the same Gaussian noise of standard deviation 0.2 as in (B), a switch appears in both simulations, but at different times. The dark lines are for λ *CI*, and the grey lines for *LacR*. The values of both λ *CI* and *LacR* are scaled by 1/500.

The results (Figs. 5 and 7) demonstrate the potentially crucial effects of stochasticity on the toggle switch: when the system is in an unstable intermediate state, noise may or may not cause the system to switch to a different stable state. One should note that the simulation results are strongly affected by the simulation settings. For instance, switches occur for most of the simulations for a larger sampling interval, say 0.5, where noise more easily accumulates to a degree sufficient to trigger a switch, but switches rarely appear when the sampling interval is small, say 0.01. The probable reason is that the sampling interval not only "controls the simulation accuracy and performance" so that "the smaller the sampling interval, the higher the accuracy," as mentioned in the Cell Illustrator user manual (Miyano 2008), but that it also controls the frequency of the noise: the smaller the sampling interval, the more often a stochastic sample is added to the system, resulting in a higher noise frequency. It is therefore crucial to determine simulation settings that correspond closely to the observations *in vivo*. If the settings are appropriate, the model yields the percentages of switched cells under different physiological situations or stimuli, such as the degree of noise and the effect strength of SOS signaling.

4. Challenges and Future Developments

The previous sections have indicated that hybrid BST modeling within a Petri Net framework can have significant advantages, because the ease of model design and analysis in BST is easily connected to discrete and stochastic features. For a full and effective implementation, four challenges still have to be overcome.

Challenge 1: Analysis of functional properties of hybrid systems

Once each phase of the modeling process has been formulated, the resulting hybrid model needs to be analyzed with algebraic and computational means for consistency, stability, robustness, responsiveness, and other criteria of functional effectiveness. There are powerful theorems and effective tools for linear systems, but they are much fewer for nonlinear systems, and there is an even greater need for theorems and methods for hybrid systems. This issue could be addressed in two complimentary ways: model checking and simulation.

Given experimental data, a hybrid model represents a hypothetical mechanism that results in simulation data. On one hand, due to non-deterministic features, simulations will yield different results and it is therefore impossible to check, by executing the model, whether all possible outcomes conform to the data (Clarke, Grumberg et al. 1999). Through a search strategy, model checking systematically analyzes all classes of the infinitely many possible outcomes of the computational model without executing them one by one. On the other hand, formal analysis, such as model checking, is usually restricted or unavailable for hybrid systems. In these cases, rather than performing an exhaustive analysis, it is more practical to construct a model and perform simulations. For such simulations, the accuracy and efficiency of numerical integration techniques are critical. For instance, imprecise numerical integration might cause a discrete event. Simply shrinking the step size is not a sure solution because it will greatly increase the simulation time yet does not guarantee the elimination of this kind of simulation error. Moreover, because the system could have infinite numbers of discrete transitions in finite time, the simulation may not be able to converge and hence the solution for a hybrid system may not exist or be unique. Therefore, it is necessary to develop a complementary strategy that applies model checking and simulation intelligently. In the future one should address the following problems in the HFPN

extension of BST models: how can one characterize situations where model checking and simulation can be applied respectively? What are the situations where both of these two methods can be applied to yield complementary insights? For other situations than those above, what can be done? One possible strategy will be to "divide and conquer": divide a hybrid system into deterministic and stochastic parts, analyze every part's properties and then seek to integrate the combined affects.

Challenge 2: Parameter estimation

Although many estimation methods are available for discrete or continuous models, parameter estimation remains one of the most challenging tasks for hybrid modeling efforts. A natural attempt is to distinguish parameters for the continuous and discrete parts of hybrid models. Nagasaki *et al.* (Nagasaki, Yamaguchi et al. 2006) applied a method called data assimilation (DA) to estimate parameters and identify the structure of a small-sized HFPN model from time-course gene expression data. However, their success was limited to an ODE model, and a true hybrid model (containing discrete and continuous, deterministic and stochastic effects) has yet to be addressed.

Parameter estimation becomes a real computational challenge when the number of unknown parameters is large, the search space is large, and the error surface contains many local minima. A natural first attempt appears to be to try to decompose a large pathway model into small, independent components and estimate the parameters for each component separately. This idea of model decomposition for parameter estimation has been successfully applied in many areas, such as Bayesian model learning (Neapolitan 2003), geometric curve fitting (Jiang, Cheng et al. 2005), and the control of large dynamical systems (Williams and Millar 1998). Koh *et al.* (Koh, Teong et al. 2006) recently used model decomposition in the context of HFPN. Here an independent component means an executable sub-graph which can be simulated as a model by itself,

given all the parameters and initial condition relative to the nodes of this sub-graph. The independent components may be identified by either of the following methods which can be actualized automatically by an algorithm: A) If a place node belongs to a given component, then all its incoming transitions (via normal arcs, instead of inhibitory or testing arcs) must also belong to this component. B) If a transition is present in a component, then all of its input places must also be in this component. This type of decomposition method is most effective when the flow of information is unidirectional and feedback loops are short. If the pathway components are tightly coupled or if there are long feedback loops, the entire pathway could be returned as a single component. Thus it needs to be explored in which situations it is feasible to find pathways that can be decomposed into a reasonable number of independent, smaller components.

Challenge 3: Computational efficiency of hybrid modeling.

Our case studies here and in (Wu and Voit, 2009) indicate that the time to compute HFPN models with Cell Illustrator is many times longer than that of a regular ODE solver. Moreover, the computation time is not directly related to whether the models are deterministic or stochastic, continuous or discrete, but rather by the number of transitions and the computational burden associated with them. Thus, it is necessary to characterize the determinants of computational speed and to improve on the slowest processes.

Challenge 4: Discovery of design principles.

The special structure of the equations in BST system offers an elegant way for the discovery of design principles in biological models, called the method of controlled mathematical comparison (MCMC): the investigated pathway is compared with an alternative, hypothetical pathway that differs in just one particular regulatory or operational feature, so that the difference in responses can be contributed to that feature of interest (*e.g.*, (Alves and Savageau 2000)). Because the proposed hybrid models

constitute a BST extension with some discrete and possibly stochastic components, it seems feasible to apply MCMC to the hybrid system in order to evaluate the effects of a particular feature in comparison to systems without this feature. For instance, the importance of stochasticity may be assessed in comparison to the corresponding deterministic model.

Acknowledgements

This work was supported in part by a Molecular and Cellular Biosciences Grant (MCB-0517135; E.O. Voit, PI) from the National Science Foundation. Any opinions, findings, and conclusions or recommendations expressed in this material are those of the authors and do not necessarily reflect the views of the sponsoring institutions.

References

Alves, R. and M. A. Savageau (2000). "Extending the method of mathematically controlled comparison to include numerical comparisons." Bioinformatics 16(9): 786-798.

Blake, W. J., M. Kaern, et al. (2003). "Noise in eukaryotic gene expression." Nature 422(6932): 633-637.

Clarke, E. M., O. Grumberg, et al. (1999). Model Checking, MIT Press.

Clegg, J. S. (1984). "Properties and metabolism of the aqueous cytoplasm and its boundaries." Am. J. Physiol. 246: R133-R151.

D'Argenio, P. R. and J.-P. Katoen (2005). "A theory of stochastic systems part I: Stochastic automata." Information and Computation 203 (1): 1-38.

Elowitz, M. B., A. J. Levine, et al. (2002). "Stochastic Gene Expression in a Single Cell." Science 297(5584): 1183-1186.

Fell, D. A. (1997). Understanding the Control of Metabolism, Portland Press, London.

Gardner, T. S., C. R. Cantor, et al. (2000). "Construction of a genetic toggle switch in Escherichiacoli." Nature 403: 339-342.

Gillespie, D. T. (1976). "A general method for numerically simulating the stochastic time evolution of coupled chemical reactions." J. Comput. Phys. 22: 403.

Gillespie, D. T. (1992). "A rigorous derivation of the chemical master equation." Physica A 188: 404.

Gillespie, D. T. (2007). "Stochastic Simulation of Chemical Kinetics." Annual Review of Physical Chemistry 58(1): 35-55.

Goss, P. J. E. and J. Peccoud (1998). "Quantitative modeling of stochastic systems in molecular biology by using stochastic Petri nets." Proceedings of the National Academy of Sciences 95: 6750-6755.

Haas, P. J. (2002). Stochastic Petri Nets. New York, Springer Verlag.

Hatzimanikatis, V. and J. Bailey (1996). "MCA has more to say." J. Theor. Biol. 182: 233-242.

Heinrich, R. and T. A. Rapoport (1974). "A linear steady-state treatment of enzymatic chains: General properties, control and effector strength." Eur. J. Biochem. 42: 89-95.

Hirata, H., S. Yoshiura, et al. (2002). "Oscillatory Expression of the bHLH Factor Hes1 Regulated by a Negative Feedback Loop." Science 298(5594): 840-843.

Jiang, X., D. C. Cheng, et al. (2005). A Novel Parameter Decomposition Approach to Faithful Fitting of Quadric Surfaces. Pattern Recognition: 27th DAGM Symposium, Lecture Notes in Computer Science 3663 168-175.

Kacser, H. and J. A. Burns (1973). " The control of flux " Symp. Soc. Exp. Biol. 27: 65-104.

Kiehl, T. R., R. M. Mattheyses, et al. (2004). "Hybrid simulation of cellular behavior." Bioinformatics 20(3): 316-322.

Koh, G., H. Teong, et al. (2006). "A decompositional approach to parameter estimation in pathway modeling: a case study of the Akt and MAPK pathways and their crosstalk." Bioinformatics 22(14): e271-280.

Kuthan, H. (2001). "Self-organisation and orderly processes by individual protein complexes in the bacterial cell." Prog. Biophys. Mol. Biol. 75: 1-17.

Luby-Phelps, K., P. E. Castle, et al. (1987). "Hindered diffusion of inert tracer particles in the cytoplasm of mouse 3T3 cells." Proc. Natl. Acad. Sci. U.S.A. 84,: 4910–4913.

Matsuno, H., Y. Tanaka, et al. (2003). "Biopathways representation and simulation on hybrid functional Petri net." In Silico Biol 3: 389-404.

McAdams, H. H. and A. P. Arkin (1997). "Stochastic mechanisms in gene expression." Proc. Natl. Acad. Sci. USA 94: 814.

Minton, A. P. (1993). "Molecular crowding and molecular recognition." J. Mol. Recognit. 6: 211–214.

Minton, A. P. (1998). "Molecular crowding: analysis of effects of high concentrations of inert cosolutes on biochemical equilibria and rates in terms of volume exclusion." Methods Enzymol. 295: 127-149.

Miyano, S. (2008). "Cell Illustrator website." http://www.cellillustrator.com/.

Mocek, W. T., R. Rudnicki, et al. (2005). "Approximation of delays in biochemical systems." Mathematical Biosciences 198(2): 190-216.

Monk, N. A. (2003). "Oscillatory expression of Hes1, p53, and NF-kappaB driven by transcriptional time delays." Current Biology 13(16): 1409-13.

Nagasaki, M., R. Yamaguchi, et al. (2006). "Genomic data assimilation for estimating hybrid functional Petri net from time-course gene expression data." Genome Informatics 17(1): 46-61.

Neapolitan, R. E. (2003). Learning Bayesian Networks. (1st Ed) Prentice Hall.

Qian, H. and E. L. Elson (2002). "Single-molecule enzymology: stochastic Michaelis-Menten kinetics." Biophys. Chem. 101-102: 565-576.

Savageau, M. A. (1969). "Biochemical systems analysis. I. Some mathematical properties of the rate law for the component enzymatic reactions." Journal of Theoretical Biology 25(3): 365-9.

Savageau, M. A. (1969). "Biochemical systems analysis. II. The steady-state solutions for an n-pool system using a power-law approximation." Journal of Theoretical Biology 25(3): 370-9.

Savageau, M. A. (1976). Biochemical systems analysis. A study of function and design in molecular biology, Addison-Wesley.

Savageau, M. A. and E. O. Voit (1987). "Recasting nonlinear differential equations as S-systems: a canonical nonlinear form." Mathematical Biosciences 87(1): 31-113.

Scalettar, B. A., J. R. Abney, et al. (1991). "Dynamics, structure, and functions are coupled in the mitrocondrial matrix." Proc. Natl. Acad. Sci. U.S.A. 88: 8057–8061.

Schnell, S. and T. E. Turner (2004). "Reaction kinetics in intracellular environments with macromolecular crowding: simulations and rate laws." Prog. Biophys. Mol. Biol. 85: 235.

Srere, P., Jones, M.E. and C.K. Matthews (Eds) (1989). Structural and Organizational Aspects of Metabolic Regulation, Alan R. Liss, New York.

Tian, T. and K. Burrage (2006). "Stochastic models for regulatory networks of the genetic toggle switch." Proceedings of the National Academy of Sciences 103(22): 8372-7.

Tian, T., K. Burrage, et al. (2007). "Stochastic delay differential equations for genetic regulatory networks." The Journal of Computational and Applied Mathematics 205(2): 696-707.

Torres, N. V. and E. O. Voit (2002). Pathway Analysis and Optimization in Metabolic Engineering, Cambridge University Press, Cambridge, U.K. .

Verkman, A. S. (2002). "Solute and macromolecule diffusion in cellular aqueous compartments." Trends Biochem. Sci. 27: 27.

Visser, D. and J. J. Heijnen (2002). "The mathematics of metabolic control analysis revisited." Metab Eng 4(2): 114-23.

Voit, E. O. (2000). Computational analysis of biochemical systems: a practical guide for biochemists and molecular biologists, Cambridge University Press.

Voit, E. O. (2005). "Smooth bistable S-systems." IEE Proc. Systems Biol 152: 207-213.

Wang, F.-S., C.-L. Ko, et al. (2007). "Kinetic Modeling Using S-systems and Lin-log Approaches." Biochem. Eng. J. 33: 238-247.

Williams, B. C. and W. Millar (1998). Decompositional, Model-based learning and its Analogy to Diagnosis, AAAI/IAAI.

Wu, J. and E.O. Voit (2009). "Hybrid Modeling In Biochemical Systems Theory by Means of Functional Petri nets " Journal of Bioinformatics and Computational Biology (in press).

PAPER 3

CHAPTER 4

Impact of Delays and Noise on Dopamine Signal Transduction

Jialiang Wu, Zhen Qi, Eberhard O. Voit

In Silico Biology 10(0005)

Impact of Delays and Noise on Dopamine Signal Transduction

Jialiang Wu[1], Zhen Qi[2], Eberhard O. Voit[2*]

1. School of Mathematics, Georgia Institute of Technology, Atlanta, Georgia, United States of America

2. Department of Biomedical Engineering, Georgia Institute of Technology and Emory University Medical School, Atlanta, Georgia, United States of America

*Corresponding Author

Key Words: Amphetamine, Biochemical System Theory (BST), delay, dopamine signaling, HFPN, hybrid modeling, Parkinson's disease, Petri nets, schizophrenia, stochasticity

Original Submission: October 2009

Revised: December 2009

Abstract

Dopamine is a critical neurotransmitter for the normal functioning of the central nervous system. Abnormal dopamine signal transmission in the brain has been implicated in diseases such as Parkinson's disease (PD) and schizophrenia, as well as in various types of drug addition. It is therefore important to understand the dopamine signaling dynamics in the presynaptic neuron of the striatum and the synaptic cleft, where dopamine synthesis, degradation, compartmentalization, release, reuptake, and numerous regulatory processes occur. The biochemical and biological processes governing this dynamics consist of interacting discrete and continuous components, operate at different time scales, and must function effectively in spite of intrinsic stochasticity and external perturbations. Not fitting into the realm of purely deterministic phenomena, the hybrid nature of the system requires special means of mathematical modeling, simulation and analysis. We show here how hybrid functional Petri-nets (HFPNs) and the software Cell Illustrator® facilitate computational analyses of systems that simultaneously contain deterministic, stochastic, and delay components. We evaluate the robustness of dopamine signaling in the presence of delays and noise and discuss implications for normal and abnormal states of the system.

1. Introduction

Dopamine is a neurotransmitter of enormous physiological, pathological, and pharmacological importance. It is a crucial contributor to several diseases, such as Parkinson's disease (PD) and schizophrenia. Dopamine is furthermore associated with addiction to a variety of drugs, because it has a direct effect on the body's reward system. PD is the most common neurodegenerative movement disorder, affecting more than 1% of the world population of age 65 or higher (Olanow and Tatton 1999; von

Campenhausen, Bornschein et al. 2005). Because loss of dopaminergic neurons is responsible for the majority of the motor symptoms of Parkinson's disease, treatment options have mostly targeted the restoration of dopamine function by replacement of dopamine precursors, administration of dopamine agonists, or inhibition of its degradative enzymes.

Schizophrenia is a mental disorder with a worldwide lifetime prevalence of about 0.7%. As with PD, the large number of schizophrenia cases translates into enormous economical and societal losses (MacDonald and Schulz 2009). While the root causes of schizophrenia are still obscure, the so-called *dopamine hypothesis* suggests that dopamine imbalance is the underlying mechanism for symptoms of the disease. Accordingly, the main medication has been the administration of antipsychotics that reduce dopaminergic activity through blockade of the dopamine D2 receptor. Finally, the dopamine signaling system is compromised in many types of drug addiction, for instance to cocaine or methamphetamine, either through competition between the drug and dopamine in the presynaptic neuron or by competition for receptors exposed to the synaptic cleft.

The abnormal activity of dopamine signaling in PD, schizophrenia, and drug addiction demonstrates the important role of dopamine dynamics in the presynaptic neuron of the striatum and the synaptic cleft, where dopamine synthesis, degradation, compartmentalization, release, reuptake, and numerous regulatory processes occur (Figure 1). On the presynaptic side, the biosynthetic dopamine pathway begins with the precursor tyrosine, which is converted into L-DOPA and subsequently into the key neurotransmitter dopamine. Dopamine is packed into intracellular vesicles by the vesicular monoamine transporter. The packed dopamine is released into the synaptic cleft, where it can bind to dopamine receptors on the postsynaptic membrane. Some of the dopamine in the cleft also diffuses out of the cleft, or is transported back into the cytosol of the presynaptic neuron by the dopamine transporter. In addition to this cycle,

dopamine can be degraded by the enzymes catechol O-methyltransferase and monoamine oxidase.

Under normal, unstimulated conditions, relatively small amounts of dopamine cycle between the presynaptic cytosol, vesicle, and synaptic cleft. However, if there is a stimulus, an action potential is produced at the dopaminergic terminal and induces calcium influx into the cytosol. The calcium influx spikes dopamine release into the cleft, where the neurotransmitter binds to its receptor on the postsynaptic membrane. Inside the postsynapse, various downstream signaling cascades are triggered, and the signal is successfully transduced.

The functionality of dopaminergic neurons is altered when these are exposed to certain drugs like amphetamine and methamphetamine. According to current observations, amphetamine and methamphetamine cause dopamine to leak from the vesicles into the cytosol, resulting in significant increases in the cytosolic dopamine level. This excess consequently produces an efflux of dopamine into the synaptic cleft through dopamine transporters instead of the reverse flux that is typical for intact neuron (Sulzer, Chen et al. 1995; McCann, Wong et al. 1998; Schmitz, Lee et al. 2001; Hanson, Sandoval et al. 2004). At the same time, amphetamine and methamphetamine regulate the generation and degradation of dopamine (Costa, Groppetti et al. 1972; Sulzer, Sonders et al. 2005). Through these mechanisms, the drugs substantially alter the neurotransmission characteristics of the dopaminergic synapse.

The dopamine recycling process involves neurotransmitter packaging, release, binding, disassociation, and reuptake. Some of the biological steps associated with these processes take an appreciable amount of time to perform, thereby in effect causing delays. Since these delays must be expected to affect the dynamics of dopamine transmission, and since such effects might be different between intact and diseased systems, it is important to study the consequences of delays on dopamine transmission systematically. Moreover, like most every biological process, dopamine signaling is

subject to germane stochasticity and external perturbations. For example, the rate of an enzymatic or transport process is typically considered constant, leading to a deterministic kinetic description. However, in reality the dynamics of the reaction is a random process, which is strongly exacerbated if only small numbers of reactants are involved (*e.g.*, (Goutsias 2007)). Accounting for stochasticity in a dynamic system requires specialized software, and if the system also contains delays, it is difficult to find a suitable modeling framework, along with supporting software. We show here how *Hybrid Functional Petri Nets* (HFPNs) and the software Cell Illustrator® facilitate the computational analysis of systems that contain deterministic, stochastic, and delay components and demonstrate their utility with an analysis of dopamine signaling. The model describing these aspects has been submitted to a publically accessible model database (see (Wu, Qi et al. 2009)).

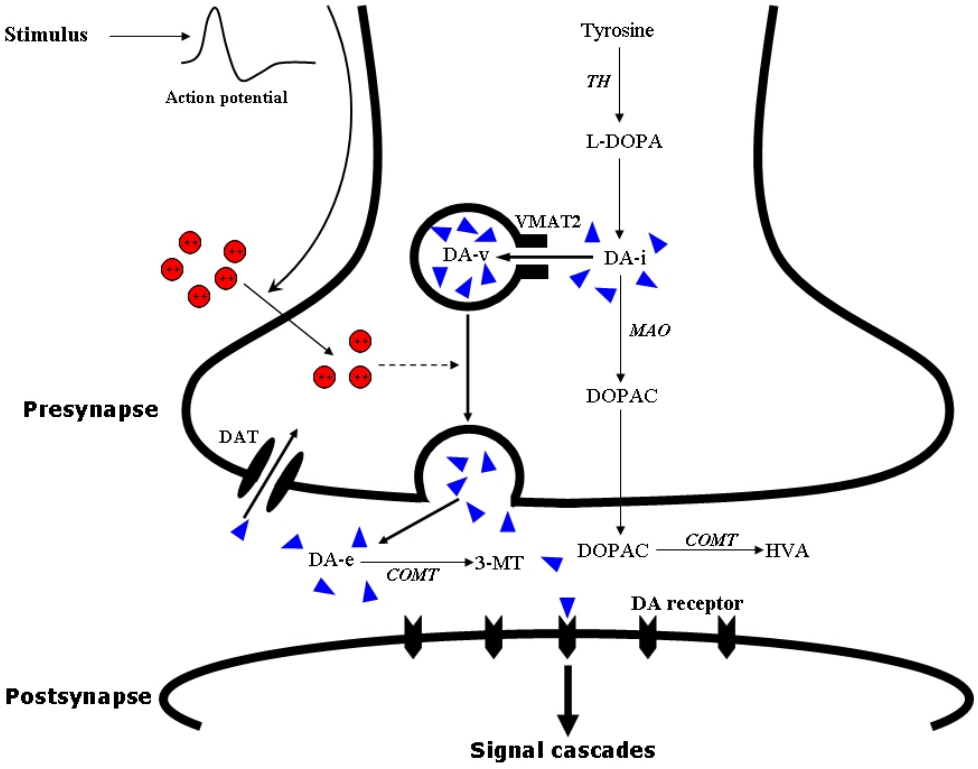

Figure 4.1 The chemical synapse of a dopaminergic neuron and its role in signal transduction.

The top part of the diagram schematically shows key features of the dopamine pathway in the presynapse and, below, in the synaptic cleft of the dopaminergic neuron. Blue triangles represent the neurotransmitter dopamine, while red circles indicate calcium (Ca^{++}) ions. An external stimulus triggers an action potential at the dopaminergic terminal and induces calcium influx into the cytosol. The calcium influx spikes dopamine release into the cleft, where the neurotransmitter binds to its receptor on the postsynaptic membrane. Inside the postsynapse, various downstream signaling cascades are triggered, and the signal is successfully transduced.

2. Methods

The dopamine signaling system as described above consists of interacting discrete and continuous components and processes that operate at different time scales. The hybrid nature of this system requires special means of analysis, because it does not fit neatly into the realm of deterministic models, where sets of ordinary differential equations (ODEs) are used to represent the continuous changes of the participating system components over time. Furthermore, the system is too complicated to permit comprehensive stochastic models and simulations that are based on the Chemical Master Equation, even if these are implemented as stochastic kinetic systems in advanced versions of the Gillespie algorithm (Gillespie 2007). Instead, it is necessary to develop a hybrid modeling methodology that allows us to merge seamlessly the deterministic and stochastic aspects of the system into a unifying framework for integrative systems analyses. A good candidate for this task is a *Hybrid Functional Petri Net* (HFPN, (Nagasaki, Doi et al. 2003)). In previous work, we showed that HFPNs can be combined effectively with methods of *Biochemical Systems Theory* (BST; (Voit 2000)) for the analysis of largely continuous systems, which however are affected significantly by delays and stochastic noise (Wu and Voit 2009 a; Wu and Voit 2009 b). We show here how this hybrid methodology can be used to explore the performance of the dopamine signaling system

under typical perturbations as well as under disturbances from noise and delays. The starting point for the analysis is an entirely deterministic model (Qi, Miller et al. 2008) that captured the dopamine dynamics quite well, but did not account for stochastic perturbations.

2.1 Biochemical Systems Theory

Biochemical Systems Theory (BST) is a firmly established mathematical modeling framework for the analysis of biological systems. BST is based on ordinary differential equations in which all dynamical processes are represented with products of power-law functions. Each of these functions consists of a non-negative *rate constant*, as a multiplicative coefficient, and of all contributing substrates, enzymes, and modifiers as variables. Each variable is raised to a real-valued *kinetic order* that quantifies the effect of the variable on a given reaction. A positive kinetic order signifies activation, while a negative value signifies inhibition and a value of zero corresponds to no contribution at all. BST permits several variants, among which the format of a Generalized Mass Action (GMA) system is most intuitive. In this format, each process is separately represented by a power-law term, while the alternative S-system format first groups all influxes and all effluxes into one term each (Shiraishi and Savageau 1992). The GMA format directly reflects the stoichiometric connectivity of the system and also indicates in its kinetic orders the strengths of interactions among the system variables. Its generic format is thus

$$\dot{X}_i = \sum_{p=1}^{P_i}\left(a_{ip}\prod_{j=1}^{n} X_j^{f_{ijp}} \right) - \sum_{q=1}^{Q_i}\left(b_{iq}\prod_{j=1}^{n} X_j^{g_{ijq}} \right), \qquad i = 1,...,n, \tag{1}$$

where variable X_i is affected by P_i production and Q_i degradation processes; a_{ip} and b_{iq} are rate constants, while f_{ipj} and g_{iqj} are kinetic orders.

While models within BST consist entirely of ODEs, Mocek *et al*. showed that processes with a constant delay can be approximated with arbitrary accuracy within the BST format (Mocek, Rudnicki et al. 2005). This approximation is accomplished through the introduction of auxiliary variables and equations, which however do not require additional biological parameters. Wu and Voit further extended Mocek's method to allow for multiple delays of different types, including discrete, distributed, time dependent, and random delays (Wu and Voit 2009 a).

2.2 Implementation of a GMA model as a Hybrid Functional Petri Net

A Petri net is a mathematical modeling tool for the representation of systems with concurrent processes. One appealing feature is the graphical depiction of all system components and processes, which facilitates intuitive, targeted manipulations and simulations. Originally designed for discrete systems, Petri nets have recently been extended to account for hybrid systems combining both discrete and continuous events. These Hybrid Functional Petri Nets (HFPN) (Nagasaki, Doi et al. 2003) can be simulated conveniently with the software package *Cell Illustrator* (Miyano 2008).

As indicated in Figure 2, it is straightforward to implement a GMA model in the HFPN framework: each time dependent variable X_i is represented in the HFPN as a *continuous place* with the name of the molecular species, whereas every time independent variable is coded either as a *discrete* or *continuous place*, depending on its value type. Every production term $a_{ip}\prod_{j=1}^{n} X_j^{f_{ijp}}$ associated with variable X_i is regarded as the *speed* of an *input transition* for X_i and every degradation term $b_{iq}\prod_{j=1}^{n} X_j^{g_{ijq}}$ is regarded as the *speed* of an *output transition*. According to Petri Net philosophy, direct connectivity exclusively reflects mass flow between places. A continuous place is

graphically represented by a double-lined circle, and a continuous transition by an open rectangle. By contrast, a discrete place is depicted by a single-lined circle and a discrete transition by a solid rectangle.

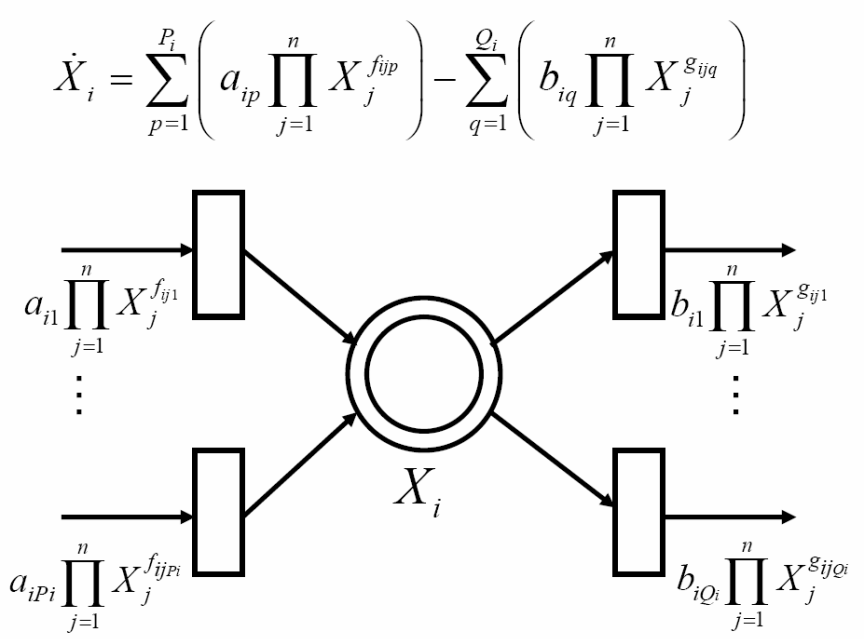

Fig. 4.2 Generic GMA system and its HFPN representation.
Each continuous variable X_i is represented by a double-lined circle, while the continuous transitions are given as open rectangles.

2.3 Representation of delays and noise in the model of dopamine dynamics

In previous work (Wu and Voit 2009 a; Wu and Voit 2009 b) we developed a hybrid approach combining BST and HFPN that facilitates simulations of biological systems containing different effects, including feedback regulations, switches, randomness, and various delays. This modeling strategy can be applied directly to the dopamine signaling system of interest here.

The main delay in the dopamine system is due to the fact that the transport of vesicular dopamine to the synaptic cleft is slower than the biochemical reactions that are governing dopamine biosynthesis and degradation (Qi, Miller et al. 2008). Specifically, an appropriate signal received by the presynapse causes vesicle movement and an

upsurge in dopamine release from the vesicle (modeled as the DA-v pool) into the extracellular, synaptic pool (modeled as DA-e), where it serves as a signaling molecule that binds to specific receptors on the postsynaptic membrane (see Fig. 1). Figure 3 shows the HFPN implementation of the delay due to dopamine translocation, as well as the representation of stochastic variations in the dopamine flux. Because the exact extent of the delay and the magnitude of stochastic noise are not known, we will explore several scenarios that appear to be most relevant. The HFPN implementation of the dopamine signaling model with noise and delays has been submitted to a publically accessible database of models (see (Wu, Qi et al. 2009)).

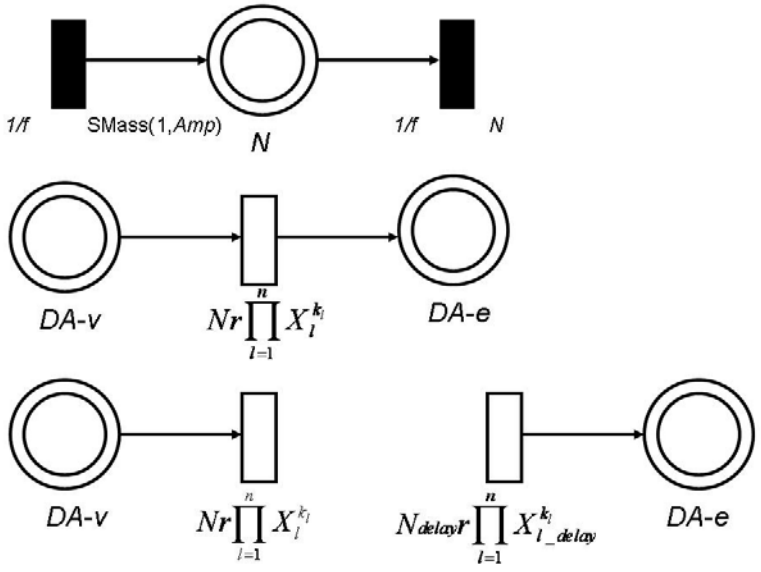

Figure 4.3 Implementation of noisy and delayed processes in a hybrid GMA-HFPN model.

Top panel: The diagram indicates a mechanism with which we simulate random perturbations. The procedure generates a sequence of random numbers, representing noise *N* of frequency *f* and amplitude *Amp*. SMass(1, *Amp*) is a Cell Illustrator function producing Gaussian distributed random numbers with mean 1 and standard deviation *Amp*. Center panel: The diagram indicates how a non-delayed flux with rate constant *r* is affected by noise *N*. Bottom panel: On the left, noise is applied to dopamine release. On the right, delay is assumed to have happened during dopamine translocation, and N_{delay} and X_{l_delay} are the delayed values of *N* and X_l, respectively. Due to space limitations, the specific implementation of delays is

not shown here; however, it follows directly the principles discussed in (Wu and Voit 2009 a; Wu and Voit 2009 b). It is noted that the creation of noise can also be accomplished with generic elements in the more flexible HFPNe variant of hybrid Petri nets.

2.4 Simulation of dopamine flux in response to calcium signals

As indicated in Figure 1, the presynaptic neuron receives signals from other neurons in the form of action potentials, which in turn lead to a rapid calcium influx that ultimately causes a release of dopamine from the presynaptic vesicle pool (DA-v) into the extracellular pool (DA-e). The mechanistic details of this Hodgkin-Huxley type activation are immaterial here, and only the overall effect needs to be modeled. Typically, the dopamine response follows a regular train of signals, which is often described as a spiking pattern. To represent this repeated triggering effect in our model, we multiply dopamine efflux (from DA-v to DA-e) with the following function:

$$signal(t) = \begin{cases} bolus \quad \sin\left(\dfrac{\pi(t-t_0)}{w_1}\right) + 1, & t \in [t_0, t_0 + w_1] \\ 1, & else \end{cases} \tag{2}$$

The function has a baseline level of 1, which represents the resting state of the signaling system. A true signal appears during the time window $[t_0, t_0 + w_1]$, where it rises and falls according to the positive portion of the sine function and up to a maximum height of (1+*bolus*). For a train of n signals, we assume the distance between two subsequent signals to be w_2. According to (Sun, Wu et al. 2002), realistic values for w_1 and w_2 are at the order of tens or hundreds of milliseconds (ms) and a suitable bolus value is between 20 and 40.

3. Results

3.1 Effects of different delays

Most steps in the dopamine signaling system are biochemical reactions, and therefore fast. In comparison, the movement of vesicles, their attachment to the presynaptic membrane, and the subsequent release of dopamine into the synaptic cleft are slower. As detailed in the *Methods* Section, we model this relatively slow process with a time delay (Ryan, Smith et al. 1996). Zhang and coworkers (Zhang, Li et al. 2009) suggested that the most relevant range for this delay is between tens and a few hundred milliseconds. We investigated the effects of different delays within this range in two typical signaling scenarios, as shown in Figures 4 and 5.

When the distance between subsequent signals and the signal width are equal or similar (*e.g.*, w_1=0.01s and w_2=0.01s in Fig. 4), the extracellular dopamine accumulates in the form of a single extended peak, consisting of a fast rise and a relatively slow return to the baseline.

If the distance between two consecutive signals is much greater than the signal width (*e.g.*, w_1=0.01s and w_2=0.2s in Fig. 5), the dopamine responses consist of individual, separated peaks.

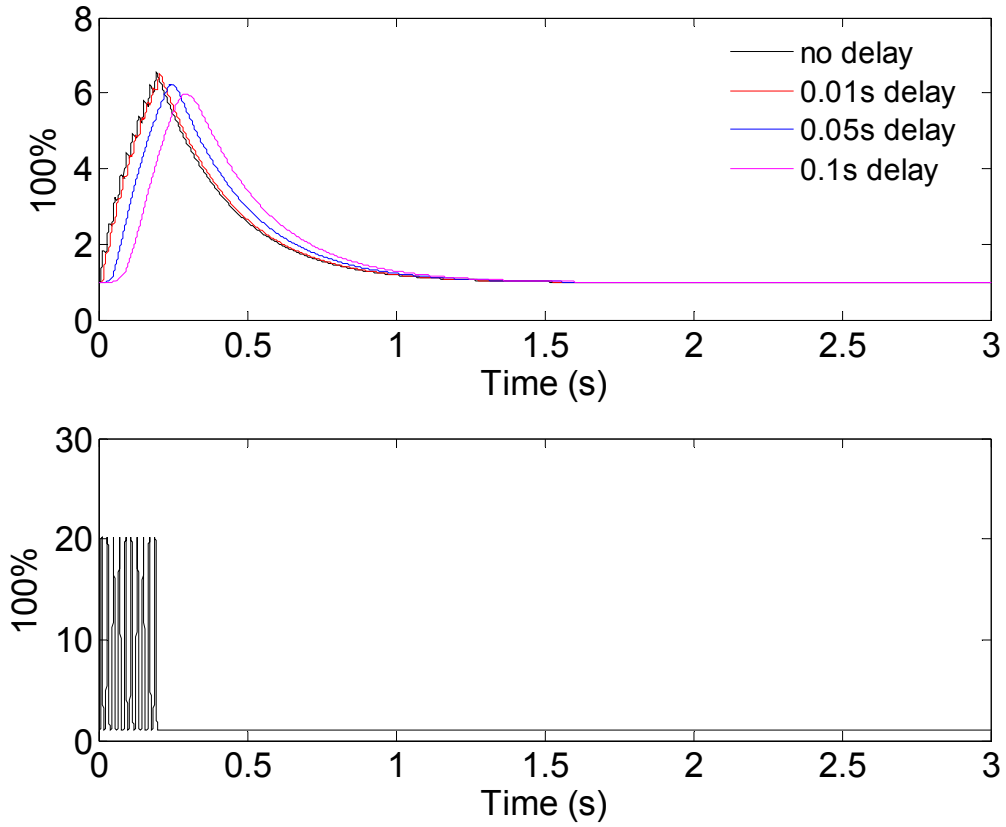

Figure 4.4 Effects of different delays on dopamine signaling.

Lower panel: Train of 10 signals with w_1=0.01s w_2=0.01s, and *bolus*=20. Upper panel: The response to the signal train is a single, extended peak of extracellular dopamine (DA-e). The peak is ragged for no or small delays, but essentially smooth for longer delays.

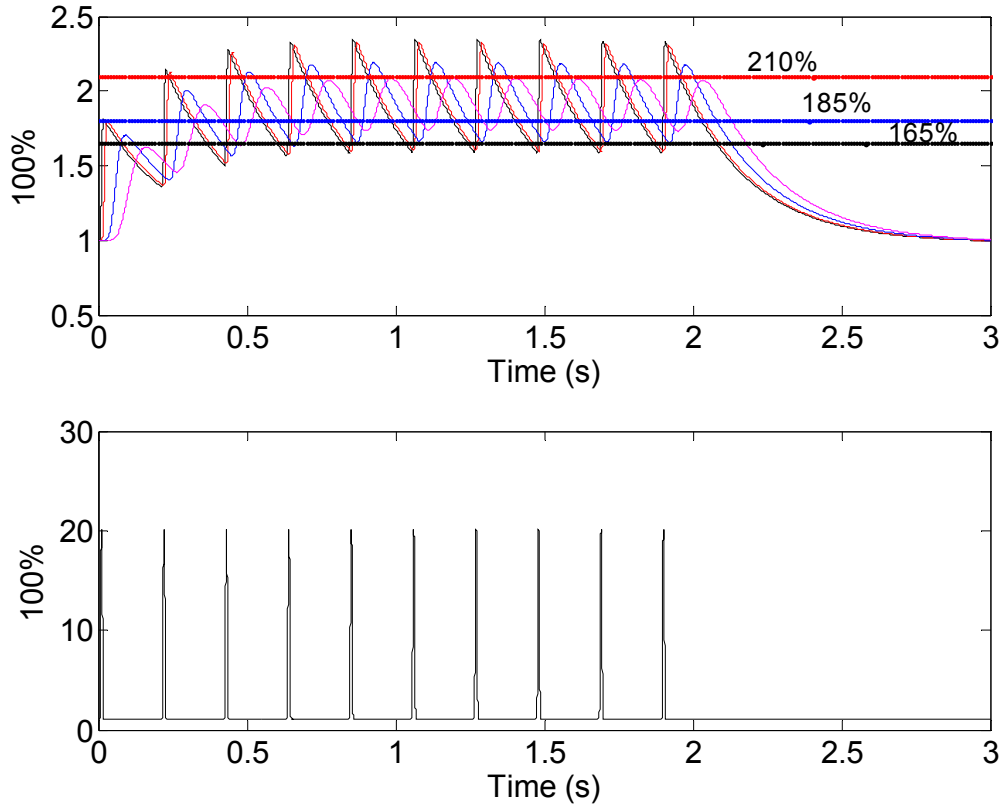

Figure 4.5 Effects of delays when signals are sparse.

Lower panel: Train of 10 signals with w_1=0.01s, w_2=0.2s and *bolus*=20. Upper panel: DA-e responds in the form of 10 separated peaks. Different delays (line colors as in Figure 4) result in some smoothing in the responses, but the peaks remain separated.

As demonstrated in Figures 4 and 5, the dopamine system with realistic delays has the following features:

1. The larger the delay is, the more the peaks of response are reduced in height.
2. The larger the delay is, the less the valleys between peaks are pronounced.

These two features imply that large delays may lead to impairments in the efficiency of the signaling system and that it is possible that signals are lost in the process. Although the delayed responses may have a similar appearance as the responses in the non-delayed system, it is possible that the delayed responses no longer exceed the necessary threshold that is typical for signal transduction in all-or-nothing responses of neurons. For instance, if the threshold in Fig. 5 is 165% of the baseline value, the non-delayed system has ten effective responses (as seen in separable peaks above the threshold line), among which one lasts for 0.07s and the other nine between 0.15s to 0.2s. By contrast, when the dopamine release is delayed by 0.1s, the system only fires twice: once for 0.17s and once for 1.7s. The abnormally long second peak is the result of merging peaks and the fact that the last eight responses do not fall below the threshold.

As a second scenario, suppose that the threshold is 210% of the baseline. In this case, the non-delayed system fires nine signals, lasting from 0.02s to 0.04s, whereas there is no effective response at all when delay is 0.1s. Some representative results are summarized in Table 1. While these results show that delays may affect signaling accuracy, one should also note that the system does retain its signaling capacity if the delay is relatively short (such as 0.01s in our simulations) and if the threshold is positioned differently, for instance, at 185% of the baseline value.

Table 4.1 The number of effective responses changes with different delays

	Non-delayed	0.01s delay	0.05s delay	0.100 s delay
165% baseline	10	10	3	2
185% baseline	9	9	9	9
210% baseline	9	9	8	0

3.2 Effects of stochastic noise

Signal transduction in the dopamine system depends on the attachment of vesicles to the presynaptic membrane and their subsequent release of dopamine into the synaptic cleft (Fernández-Alfonso and Ryan 2006). Of course, the intracellular environment is heterogeneous, and changes in metabolic state, temperature, and pH, as well as various crowding effects must be expected to create stochasticity that cannot be ignored in the context of vesicle dynamics and dopamine release. Because the details of stochasticity in the cytosol cannot be characterized in mechanistic detail, it seems reasonable to let the simulations account for randomness in the dopamine flux from the vesicle pool to the synaptic cleft. This section addresses the effects of this stochasticity with an exploration of noise of different frequencies and amplitudes.

Most processes in dopamine signal transduction are fast, with events such as biochemical reactions and ion flux transduction lasting from several milliseconds to tens of milliseconds. The randomness of such fast events results in noise of high frequency which is at the order of about one hundred Hertz. At the same time, there are also much slower events such as vesicle exocytosis, which may last for one hundred or more milliseconds and whose stochasticity corresponds to noise of several Hertz in frequency. Therefore, the frequency of realistic random perturbations ranges from several to hundreds of events per second (Hz), and it seems that an appropriate amplitude may be up to $\pm$50% of the baseline. As was shown in the *Methods* Section, we model the noise by imposing a sequence of discrete Gaussian random numbers on the rate of dopamine flux. To evaluate the impact of this noise on signaling, we assume again, for illustration purposes, a threshold of 185% of the DA-e concentration level in comparison to the baseline (see Fig. 5) and record a response as effective if the actual DA-e level surpasses this threshold.

As an example, we use the dopamine model again under a train of 10 signals characterized by w_1=0.01s, w_2=0.2s and *bolus*=20. When the signaling system is not

subjected to noise, it always yields nine effective responses. The first response does not reach the threshold and is therefore not deemed effective. This "omission" may serve in the system as a filter that effectively ignores spurious firing. If the system is corrupted by noise, signal responses may be amplified or diminished, or they may merge with one another, resulting in a suboptimal number of effective responses. As indicated by the results in Figures 6 and 7, noise may have the following effects:

1. Not surprisingly, for a fixed noise frequency, noise with larger amplitude imposes more serious distortions on signal transduction than small amplitude noise. Specifically, it results in a significantly reduced number of effective responses.
2. For fixed amplitude, decreased noise frequency of the type tested here leads to reductions in effective responses.
3. In the absence of a signal, noise alone does not significantly change the system dynamics for wide ranges of frequencies and amplitudes (Figure 7).

These results indicate that the signaling system is very robust to noise of high frequency, such as 100 Hz, while it is much more vulnerable to perturbations with frequencies lower than 10Hz.

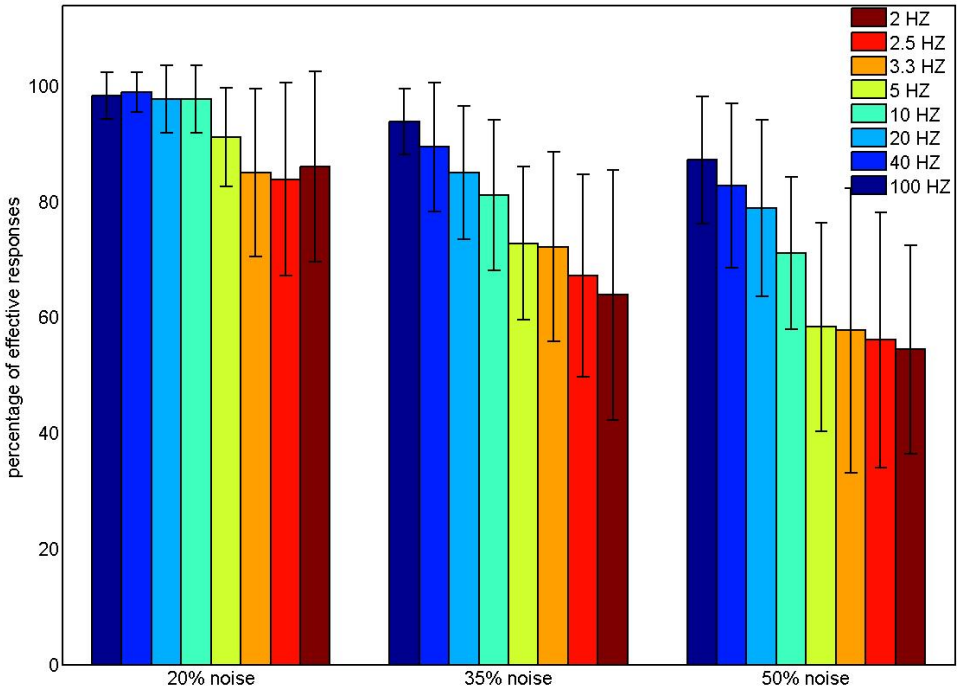

Figure 4.6 Statistics of effective responses in dopamine signaling systems subjected to noise of various amplitudes and frequencies.

Bar color represents noise frequency. The statistics for each bar was calculated from 20 simulation samples.

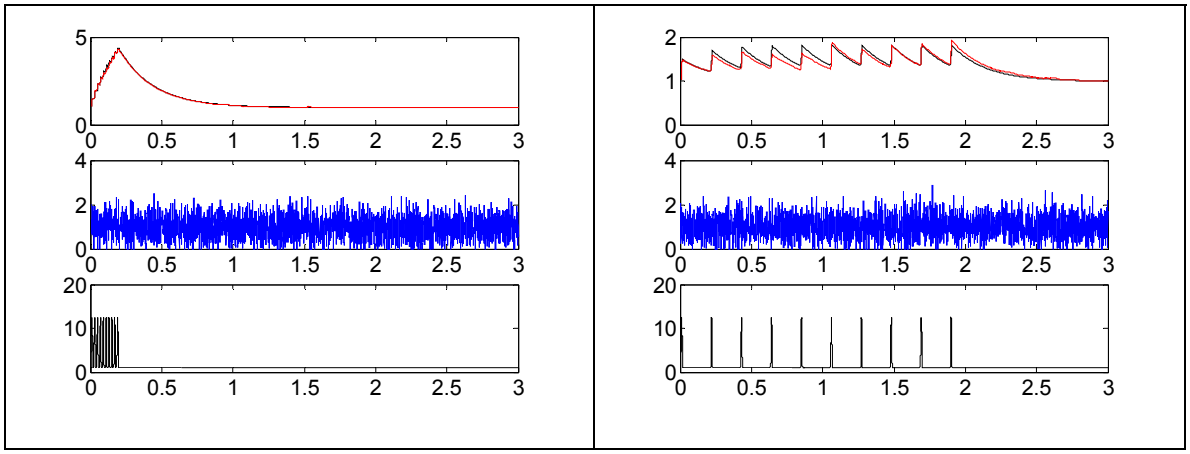

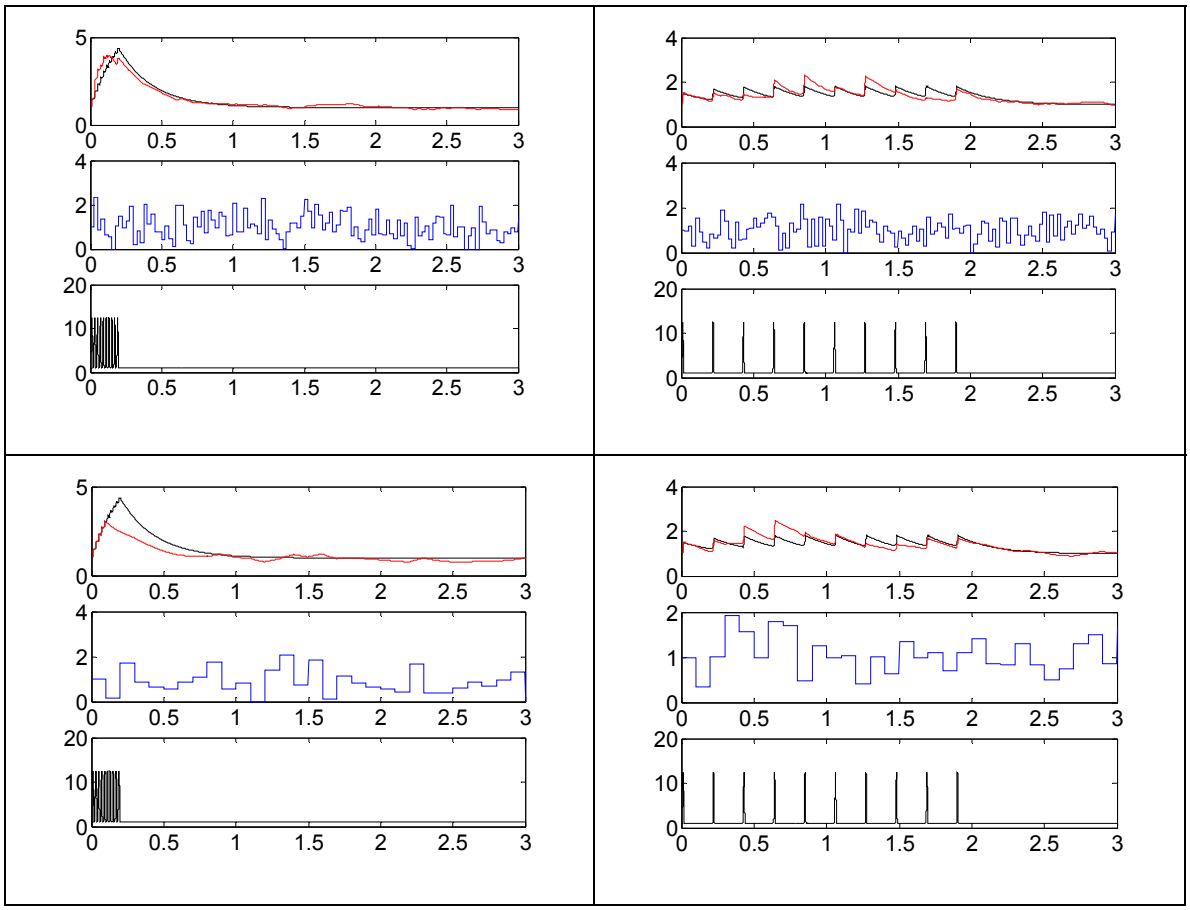

Figure 4.7 Signaling dynamics of dopamine systems subjected to noise.

Noise frequencies are 100Hz, 40Hz and 10Hz in rows 1, 2, and 3, respectively. Left column: w_1=0.01s; w_2=0.01s; right column: w_1=0.01s; w_2=0.2s. The lowest sub-panel for each example shows a train of 10 signals; the center sub-panel visualizes the discrete Gaussian noise applied to the system, while the upper sub-panel shows the system response (DA-e level) to the signal train. Black lines in upper sub-panels show results for the unperturbed system, while red lines show results for systems exposed to noise. Unit for *x*-axes: seconds (s); units for *y*-axes, from bottom to top: signal strength; percentage of noise to baseline; DA-e ratio to baseline.

3.3 Combined effects of delays and noise

The discussions in the previous sections have demonstrated that both noise and delay, when separately in effect, have the tendency to distort signal transduction. These findings raise the question of whether the combination of delay and noise would make the

situation even worse. This answer is very difficult to obtain with intuition and hard thinking alone. Thus, we systematically investigated combined effects of various delays and noise using representative signals with w_1=0.01s, w_2=0.2s. As before, a response was counted as effective when the DA-e level surpassed the threshold of 185% of the baseline.

Figure 8 shows that the two effects may counteract each other and that, surprisingly, the signaling system is more effective in its responses when noise is accompanied by short delays. For instance, the influence of 100Hz noise is best reduced in a system with 0.05s delay, while 40 Hz and 20 Hz noise is well counteracted by a 0.1s delay. However, if the delay is very long, such as 0.2s, noise and delay exacerbate each other's effects and lead to misfiring that appears to be quite unreliable.

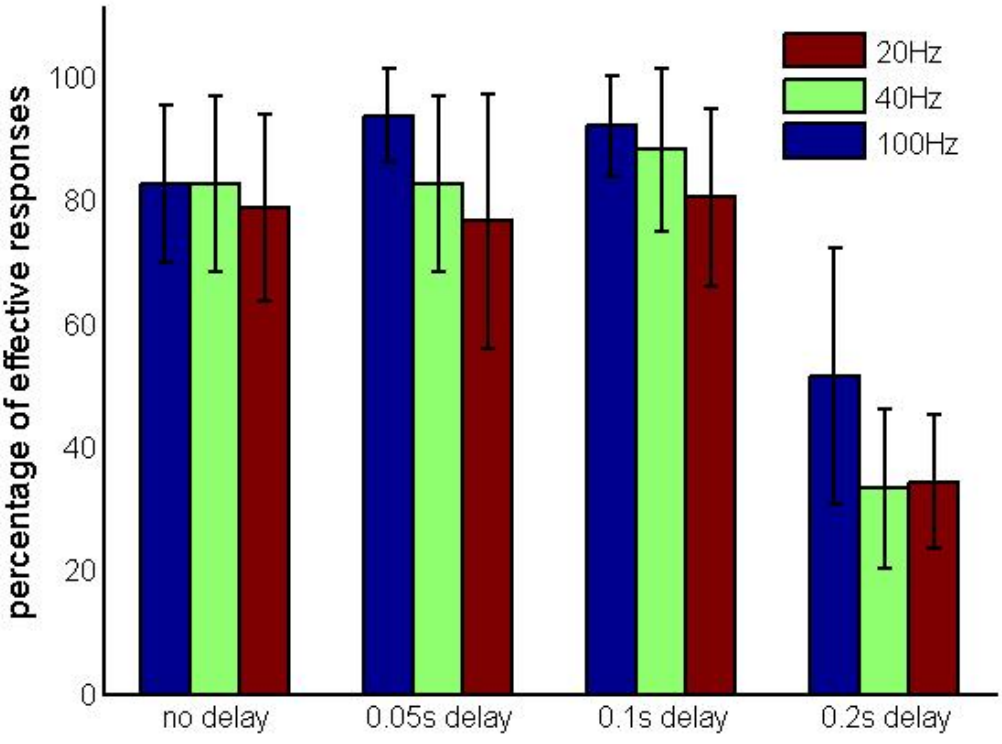

Figure 4.8 Combined effects of different delays and noise.

For short—but not for long—delays, the system is able to counteract high-frequency noise.

4. Discussion

Every signal transduction process starts with an initial stimulus that triggers one or more signaling cascades. The final component of the signaling cascade has a direct effect on gene expression or on the activation of relevant metabolic pathways. In the case of dopamine signaling, the initial stimulus is an action potential that is converted into a rapid influx of calcium into the presynaptic neuron. This influx triggers the release of dopamine into the synaptic cleft, binding to receptors on the postsynaptic membrane, and signal processing by the postsynaptic DARPP-32 protein, which ultimately leads to genomic, metabolic or neurophysiological responses. Predicting the functioning of the dopamine signaling system is difficult, because many molecular components are involved and because dopamine itself is subject to biosynthesis, degradation, diffusion out of the synaptic cleft, and other processes that change over time and are adaptive in nature. For instance, dopamine may affect the proper functioning of dopamine receptors on the postsynaptic cell membrane. These receptors are normally stable, but exhibit greatly diminished receptor activity in response to sharp or prolonged increases in dopamine concentration. In cases of amphetamine and cocaine abuse, this type of down-regulation of dopamine receptors has been associated with a shortened attention span, further drug craving, and loss of interest in social activities even if they are otherwise considered pleasant.

Biological and clinical experiments have shown that different behavioral stimuli can induce various patterns of dopamine release (*e.g.*, (Grace 1991)). These patterns of neurotransmission can be simulated with mathematical models that demonstrate the

induction of different biochemical, cellular, and physiological effects (Qi *et al.*, submitted). Computational models of this type have so far not accounted for stochastic noise, which must be expected to affect the dopamine signaling system on a regular basis. The consideration of noise is not trivial, because the system is highly nonlinear, contains a fair number of molecular components and in addition spans different time scales, which require the inclusion of time delays. The resulting hybrid nature of the system is notoriously difficult to implement and analyze.

We have shown here that the combination of Biochemical Systems Theory (BST) with Hybrid Functional Petri Nets (HFPN) affords us with a powerful method for exploring ill-defined hybrid systems. BST requires only a minimum of assumptions for the representation of a biological system and offers strong guidance for default settings and for the selection of parameter values (Voit 2000). These features are crucial for designing models of a phenomenon like dopamine signaling that occurs deep within the mammalian or human brain, where precise measurements are very difficult to obtain. While BST does not *per se* allow delays and noise, BST models can be implemented with relative ease as HFPNs, which subsequently permit the seamless integration of deterministic methods of systems analysis with delays, switches, and stochastic effects (Wu and Voit 2009 a; Wu and Voit 2009 b).

Our HFPN simulations show that noise and delays can affect the signaling function of the dopamine system in a significant manner. For instance, in situations of low-frequency noise and large delays at the order of hundreds of milliseconds, the dopamine responses to signal trains may degrade into one abnormally long response, thus impairing the normal functioning of the dopamine signaling system.

While the simulations show that noise and delays can corrupt a true signal, our results also show that the signaling system is surprisingly robust. Most processes involved in the dopamine dynamics are fast events such as biochemical reactions and ion fluxes, which occur at the order of a few or tens of milliseconds, while the important

transport and release of dopamine into the cleft is somewhat slower. Much of the noise associated with small numbers of molecules contributing to the governing reactions can be expected to be at the order of maybe tens to one hundred Hertz. As demonstrated in the *Results* section, the dopamine signaling system can successfully tolerate noise of such frequencies even if the noise amplitude is large (the simulations allowed for noise corresponding to 50% of the baseline).

As a natural system in an ever-changing environment, the dopamine system will always be exposed to noise of various frequencies. There is not much that an organism can do to avoid these perturbations. Interestingly, the results of our combined noise-delay analysis show that unavoidable delays in the system, which are due to the relatively slow physical processes of vesicle dynamics and dopamine release, are not always detrimental and may even be advantageous, but only if they are short. Specifically, we found that small delays, at the order of 10 milliseconds, effectively remove the negative effects of fast noise, whereas much longer delays exaggerate the problems caused by noise, up to a point where the signal is no longer reliably transduced. Thus, the cell must assure that delays are not overly long. Indeed, it has been observed that vesicles filled with dopamine are primarily located close to the presynaptic membrane (Südhof 2004), thereby minimizing unavoidable delays, and that vesicles elsewhere in the presynapse primarily serve as back-up dopamine pools that move to the membrane when needed.

Like all mathematical models, the model proposed here is rather simplistic, and it remains to be seen whether the investigated delays and noise frequencies constitute the most relevant combinations. With the advent of *in vivo* imaging and measuring technologies (Gaffield, Rizzoli et al. 2006; Zhang, Li et al. 2009), the near future will reveal more biological details concerning noise and delays, and these will allow us to elucidate with greater accuracy the types and features of perturbations that the dopamine signaling system is facing on a daily basis.

In spite of these uncertainties, the article demonstrates that the effects of combined noise and delays are not easy to predict and may even lead to counterintuitive outcomes. Secondly, the article shows that the embedding of a canonical formalism like BST in a hybrid framework like HFPN can substantially and beneficially expand the repertoire of analytical tools for systems biology.

Acknowledgments

This work was supported by a grant from the National Institutes of Health (P01-ES016731, G.W.M. PI) and an endowment from the Georgia Research Alliance (E.O.V). Any opinions, findings, and conclusions or recommendations expressed in this material are those of the authors and do not necessarily reflect the views of the sponsoring institutions.

References

Aittokallio, T. and B. Schwikowski (2006). "Graph-based methods for analysing networks in cell biology." Brief Bioinform **7**(3): 243-255.

Albert, S., H.-B. Benito, et al. (2007). "Cooperativity and saturation in biochemical networks: A saturable formalism using Taylor series approximations." Biotechnology and Bioengineering **97**(5): 1259-1277.

Alves, R. and M. A. Savageau (2000). "Extending the method of mathematically controlled comparison to include numerical comparisons." Bioinformatics **16**(9): 786-798.

Alves, R. and M. A. Savageau (2000). "Effect of overall feedback inhibition in unbranched biosynthetic pathways." Biophysical Journal **79** 2290-2304.

Bajzer, Z., M. Huzak, et al. (2008). "Mathematical analysis of models for reaction kinetics in intracellular environments." Mathematical Biosciences **215**(1): 35-47.

Bankes, S. C. (2002). "Agent-based modeling: A revolution?" Proceedings of the National Academy of Sciences of the United States of America **99**(Suppl 3): 7199-7200.

Bennett, M. R., D. Volfson, et al. (2007). "Transient Dynamics of Genetic Regulatory Networks." Biophysical journal **92**(10): 3501-3512.

Berg, O. G., J. Paulsson, et al. (2000). "Fluctuations and quality of control in biological cells:
zero-order ultrasensitivity reinvestigated.". Biophys J **79**: 1228-1236.
Blake, W. J., M. Kaern, et al. (2003). "Noise in eukaryotic gene expression." Nature **422**(6932): 633-637.
Bonabeau, E. (2002). "Agent-based modeling: Methods and techniques for simulating human systems." Proceedings of the National Academy of Sciences of the United States of America **99**(Suppl 3): 7280-7287.
Cao, Y., D. T. Gillespie, et al. (2005). "Multiscale stochastic simulation algorithm with stochastic partial equilibrium assumption for chemically reacting systems." J. Comput. Phys. **206**: 395.
Chaouiya, C. (2007). "Petri net modelling of biological networks." Brief Bioinform: bbm029.
Chevalier, M. W. and H. El-Samad (2009). "A rigorous framework for multiscale simulation of stochastic cellular networks." The Journal of chemical physics **131**(5): 054102-054117.
Chou, I.-C. and E. O. Voit (2009). "Recent developments in parameter estimation and structure identification of biochemical and genomic systems." Math. Biosc. **219**: 57-83.
Clarke, E. M., O. Grumberg, et al. (1999). Model Checking, MIT Press.
Costa, E., A. Groppetti, et al. (1972). "Effects of amphetamine on the turnover rate of brain catecholamines and motor activity." Br J Pharmacol **44**(4): 742-751.
D'Argenio, P. R. and J.-P. Katoen (2005). "A theory of stochastic systems part I: Stochastic automata." Information and Computation **203** (1): 1-38.
Dogterom, M. and S. Leibler (1993). "Physical aspects of the growth and regulation of microtubule
structures." Physical Review Letters **70**: 1347-1350.
Elf, J., J. Paulsson, et al. (2003). "Near-critical phenomena in intracellular
metabolite pools." Biophys J **84**: 154-170.
Elowitz, M. B. and S. Leibler (2000). "A synthetic oscillatory network of transcriptional regulators." Nature **403**(6767): 335-338.
Elowitz, M. B., A. J. Levine, et al. (2002). "Stochastic Gene Expression in a Single Cell." Science **297**(5584): 1183-1186.
Fell, D. A. (1997). Understanding the Control of Metabolism, Portland Press, London.
Fernández-Alfonso, T. and T. A. Ryan (2006). "The efficiency of the synaptic vesicle cycle at central nervous system synapses." Trends in cell biology **16**(8): 413-420.
Gaffield, M., S. Rizzoli, et al. (2006). "Mobility of synaptic vesicles in different pools in resting and stimulated frog motor nerve terminals." Neuron **51**: 317–325.
Gardner, T. S., C. R. Cantor, et al. (2000). "Construction of a genetic toggle switch in Escherichiacoli." Nature **403**: 339-342.
Gillespie, D. (1977). "Exact Stochastic Simulation of Coupled Chemical Reactions." J Phys Chem **81**(25): 2340 - 2361.
Gillespie, D. and L. Petzold (2006). Numerical Simulation for Biochemical Kinetics. In System Modelling in Cellular Biology. Z. Szallasi, J. Stelling and V. Periwal, MIT Press.

Gillespie, D. T. (1976). "A general method for numerically simulating the stochastic time evolution of coupled chemical reactions." J. Comput. Phys. **22**: 403.
Gillespie, D. T. (1977). "Exact stochastic simulation of coupled chemical reactions " Journal of Physical Chemistry **81**(25): 2340-2361.
Gillespie, D. T. (1992). "A rigorous derivation of the chemical master equation." Physica A **188**: 404.
Gillespie, D. T. (2000). "The chemical Langevin equation." The Journal of Chemical Physics **113**(1): 297-306.
Gillespie, D. T. (2001). "Approximate accelerated stochastic simulation of chemically reacting systems." Journal of Chemical Physics **115**: 1716.
Gillespie, D. T. (2001). "Approximate accelerated stochastic simulation of chemically reacting systems." J. Chem. Phys. **115**: 1716.
Gillespie, D. T. (2001). "Approximate accelerated stochastic simulation of chemically reacting systems." Journal of chemical physics **115**: 1716-1733.
Gillespie, D. T. (2002). "The chemical Langevin and Fokker-Planck equations for the reversible isomerization reaction." Journal of Physical Chemistry A **106**: 5063.
Gillespie, D. T. (2007). "Stochastic Simulation of Chemical Kinetics." Annual Review of Physical Chemistry **58**(1): 35-55.
Gillespie, D. T. (2007). "Stochastic simulation of chemical kinetics." Annual Review of Physical Chemistry **58**: 35-55.
Gomez-Uribe, C. A. and G. C. Verghese (2007). "Mass fluctuation kinetics: Capturing stochastic effects in systems of chemical reactions through coupled mean-variance computations." The Journal of chemical physics **126**(2): 024109-024112.
Goss, P. J. E. and J. Peccoud (1998). "Quantitative modeling of stochastic systems in molecular biology by using stochastic Petri nets." Proceedings of the National Academy of Sciences **95**: 6750-6755.
Goutsias, J. (2007). "Classical versus stochastic kinetics modeling of biochemical reaction systems." Biophys J **92**(7): 2350-2365.
Grace, A. A. (1991). "Phasic versus tonic dopamine release and the modulation of dopamine system responsivity: a hypothesis for the etiology of schizophrenia." Neuroscience **41**(1): 1-24.
Grimm, V., E. Revilla, et al. (2005). "Pattern-Oriented Modeling of Agent-Based Complex Systems: Lessons from Ecology." Science **310**(5750): 987-991.
Guo, Z., P. M. A. Sloot, et al. (2008). "A hybrid agent-based approach for modeling microbiological systems." Journal of Theoretical Biology **255**(2): 163-175.
Haas, P. J. (2002). Stochastic Petri Nets. New York, Springer Verlag.
Hale, J. and S. Lunel (1993). Introduction to Functional Differential Equations. 1st ed: . New York, Springer-Verlag.
Hale, J. and S. M. V. Lunel Introduction to Functional Differential Equations, Springer.
Hanson, G. R., V. Sandoval, et al. (2004). "Psychostimulants and vesicle trafficking: a novel mechanism and therapeutic implications." Ann N Y Acad Sci **1025**: 146-150.
Hardy, S. and P. N. Robillard (2004). "Modeling and simulation of molecular biology systems using Petri nets: Modeling goals of various approaches." Journal of Bioinformatics and Computational Biology **2**(4): 619-637.

Hatzimanikatis, V. and J. Bailey (1996). "MCA has more to say." Journal of Theorectical Biology **182**: 233-242.
Hatzimanikatis, V. and J. Bailey (1996). "MCA has more to say." J. Theor. Biol. **182**: 233-242.
Hatzimanikatis, V. and J. E. Bailey (1996). "MCA Has More to Say." Journal of Theoretical Biology **182**(3): 233-242.
Heinrich, R. and T. A. Rapoport (1974). "A linear steady-state treatment of enzymatic chains: General properties, control and effector strength." Eur. J. Biochem. **42**: 89-95.
Henri, M. V. (1903). "Lois générales de l'action des diastases." Paris, Hermann.
Hirata, H., S. Yoshiura, et al. (2002). "Oscillatory Expression of the bHLH Factor Hes1 Regulated by a Negative Feedback Loop." Science **298**(5594): 840-843.
Hlavacek, W. S. and M. A. Savageau (1996). "Rules for coupled expression of regulator and effector genes in inducible circuits." J Mol Biol **255** 121-139.
Irvine, D. H. and M. A. Savageau (1985). "Network regulation of the immune response: alternative control points for suppressor modulation of effector lymphocytes." Journal of Immunology **134** 2100-2116.
Ishii, N., K. Nakahigashi, et al. (2007). "Multiple high-throughput analyses monitor the response of E. coli to perturbations." Science **316**(5824): 593-597.
Jiang, X., D. C. Cheng, et al. (2005). A Novel Parameter Decomposition Approach to Faithful Fitting of Quadric Surfaces. Pattern Recognition: 27th DAGM Symposium, Lecture Notes in Computer Science,
. **3663** 168-175.
Kacser, H. and J. A. Burns (1973). " The control of flux " Symp. Soc. Exp. Biol. **27**: 65-104.
Kauffman, S., C. Peterson, et al. (2003). "Random Boolean network models and the yeast transcriptional network." Proceedings of the National Academy of Sciences of the United States of America **100**(25): 14796-14799.
Kiehl, T. R., R. M. Mattheyses, et al. (2004). "Hybrid simulation of cellular behavior." Bioinformatics **20**(3): 316-322.
Koch, A. L. (1966). "The logarithm in biology 1. Mechanisms generating the log-normal distribution exactly." Journal of Theoretical Biology **12**(2): 276-290.
Koh, G., H. Teong, et al. (2006). "A decompositional approach to parameter estimation in pathway modeling: a case study of the Akt and MAPK pathways and their crosstalk." Bioinformatics **22**(14): e271-280.
Kuthan, H. (2001). "Self-organisation and orderly processes by individual protein complexes in the bacterial cell." Prog. Biophys. Mol. Biol. **75**: 1-17.
Law, A. M. and W. D. Kelton (2000). Simulation Modeling and Analysis. Boston, Mc.Graw Hill.
Lee, C. H., K.-H. Kim, et al. (2009). "A moment closure method for stochastic reaction networks." The Journal of chemical physics **130**(13): 134107-134115.
Limpert, E., W. A. Stahel, et al. (2001). "Log-normal Distributions across the Sciences: Keys and Clues." BioScience **51**(5): 341.
Lipniacki, T., P. Paszek, et al. (2006). "Transcriptional stochasticity in gene expression." Journal of Theorectical Biology **238**(2): 348-367.

Longo, D. and J. Hasty (2006). "Dynamics of single-cell gene expression." Molecular Systems Biology **2**.
Lotka, A. (1924). Elements of Physical Biology. Baltimore, Williams and Wilkins
Luby-Phelps, K., P. E. Castle, et al. (1987). "Hindered diffusion of inert tracer particles in the cytoplasm of mouse 3T3 cells." Proc. Natl. Acad. Sci. U.S.A. **84,**: 4910–4913.
MacDonald, A. W. and S. C. Schulz (2009). "What we know: findings that every theory of schizophrenia should explain." Schizophr Bull **35**(3): 493-508.
Maheshri, N. and E. K. O Shea (2007). "Living with Noisy Genes: How Cells Function Reliably with Inherent Variability in Gene Expression." Annual Review of Biophysics and Biomolecular Structure **36**(1): 413-434.
Matsuno, H., Y. Tanaka, et al. (2003). "Biopathways representation and simulation on hybrid functional Petri net." In Silico Biol **3**: 389-404.
May, R. E. (1976). Theoretical Ecology: Principles and Applications. Oxford, Blackwell.
McAdams, H. H. and A. P. Arkin (1997). "Stochastic mechanisms in gene expression." Proc. Natl. Acad. Sci. USA **94**: 814.
McCann, U. D., D. F. Wong, et al. (1998). "Reduced striatal dopamine transporter density in abstinent methamphetamine and methcathinone users: evidence from positron emission tomography studies with [11C]WIN-35,428." J Neurosci **18**(20): 8417-8422.
Michaelis, L. and M. L. Menten (1913). "Die Kinetik der Invertinwirkung." Biochem. Zeitschrift **49**: 333-369.
Milner, P., C. S. Gillespie, et al. (2011). "Moment closure approximations for stochastic kinetic models with rational rate laws." Mathematical Biosciences **231**(2): 99-104.
Minton, A. P. (1993). "Molecular crowding and molecular recognition." J. Mol. Recognit. **6**: 211–214.
Minton, A. P. (1998). "Molecular crowding: analysis of effects of high concentrations of inert cosolutes on biochemical equilibria and rates in terms of volume exclusion." Methods Enzymol. **295**: 127-149.
Miyano, S. (2008). Cell Illustrator.
Miyano, S. (2008). "Cell Illustrator website." http://www.cellillustrator.com/.
Mocek, W. T., R. Rudnicki, et al. (2005). "Approximation of delays in biochemical systems." Math Biosci **198**(2): 190-216.
Mocek, W. T., R. Rudnicki, et al. (2005). "Approximation of delays in biochemical systems." Mathematical Biosciences **198**(2): 190-216.
Monk, N. A. (2003). "Oscillatory expression of Hes1, p53, and NF-kappaB driven by transcriptional time delays." Current Biology **13**(16): 1409-1413.
Monk, N. A. M. (2003). "Oscillatory expression of Hes1, p53, and NF-kappaB driven by transcriptional time delays." Curr. Biol. **13**: 1409.
Nagasaki, M., A. Doi, et al. (2003). "Genomic Object Net: I. A platform for modeling and simulating biopathways." Appl Bioinform **2**(3): 181-184.
Nagasaki, M., R. Yamaguchi, et al. (2006). "Genomic data assimilation for estimating hybrid functional Petri net from time-course gene expression data." Genome Informatics **17**(1): 46-61.
Neapolitan, R. E. (2003). Learning Bayesian Networks. (1st Ed) Prentice Hall.

Neff, K. L. (2010). Biochemical reaction kinetics in dilute and crowded solutions: Predictions of macroscopic and mesoscopic models and experimental observations. Rochester, MN, Mayo Clinic.
Neff, Kevin L., Chetan P. Offord, et al. (2011). "Validation of Fractal-Like Kinetic Models by Time-Resolved Binding Kinetics of Dansylamide and Carbonic Anhydrase in Crowded Media." Biophysical journal **100**(10): 2495-2503.
Olanow, C. W. and W. G. Tatton (1999). "Etiology and pathogenesis of Parkinson's disease." Annu Rev Neurosci **22**: 123-144.
Paulsson, J., O. G. Berg, et al. (2000). "Stochastic focusing: Fluctuation-enhanced sensitivity of intracellular regulation." Proceedings of the National Academy of Sciences **97**(13): 7148-7153.
Paulsson, J. and M. Ehrenberg (2001). "Noise in a minimal regulatory network: plasmid copy number
control. ." Q Rev Biophys **34**: 1-59
Qi, Z., G. W. Miller, et al. (2008). "Computational systems analysis of dopamine metabolism." PLoS ONE **3**(6): e2444.
Qian, H. and E. L. Elson (2002). "Single-molecule enzymology: stochastic Michaelis-Menten kinetics." Biophys. Chem. **101-102**: 565-576.
Rao, C. V. and A. P. Arkin (2003). "Stochastic chemical kinetics and the quasi-steady-state assumption: Application to the Gillespie algorithm." The Journal of chemical physics **118**(11): 4999-5010.
Reddy, V. N., M. L. Mavrovouniotis, et al. (1993). "Petri net representations in metabolic pathways." Proc. Int. Conf. Intell. Syst. Mol. Biol.: 328-336.
Reisig, W. (1985). Petri Nets: An Introduction, Springer Verlag.
Ryan, T., S. Smith, et al. (1996). " The timing of synaptic vesicle endocytosis." Proc Natl Acad Sci USA **93**: 5567-5571.
Savageau, M. (1995). "Michaelis-Menten mechanism reconsidered: implications of fractal kinetics." Journal of Theoretical Biology **176**(1): 115-124.
Savageau, M. A. (1969). "Biochemical systems analysis. I. Some mathematical properties of the rate law for the component enzymatic reactions." Journal of Theoretical Biology **25**(3): 365-369.
Savageau, M. A. (1969). "Biochemical systems analysis. II. The steady-state solutions for an n-pool system using a power-law approximation." Journal of Theoretical Biology **25**(3): 370-379.
Savageau, M. A. (1969 a). "Biochemical systems analysis. I. Some mathematical properties of the rate law for the component enzymatic reactions." Journal of Theorectical Biology **25**(3): 365-369.
Savageau, M. A. (1969 b). "Biochemical systems analysis. II. The steady-state solutions for an n-pool system using a power-law approximation." Journal of Theorectical Biology **25**(3): 370-379.
Savageau, M. A. (1976). Biochemical systems analysis. A study of function and design in molecular biology, Addison-Wesley.
Savageau, M. A. (1985). "A theory of alternative designs for biochemical control systems." Biomed Biochim Acta **44**(6): 875-880.
Savageau, M. A. (1993). "Influence of fractal kinetics on molecular recognition." Journal of Molecular Recognition **6**(4): 149-157.

Savageau, M. A. (2001). "Design principles for elementary gene circuits: Elements, methods, and examples." Chaos **11**: 142-159.
Savageau, M. A. and E. O. Voit (1987). "Recasting Nonlinear Differential-Equations As S-Systems - A Canonical Nonlinear Form." Mathematical Bioscience **87**: 83-115.
Savageau, M. A. and E. O. Voit (1987). "Recasting nonlinear differential equations as S-systems: a canonical nonlinear form." Mathematical Biosciences **87**(1): 31-113.
Scalettar, B. A., J. R. Abney, et al. (1991). "Dynamics, structure, and functions are coupled in the mitrocondrial matrix." Proc. Natl. Acad. Sci. U.S.A. **88**: 8057–8061.
Schmitz, Y., C. J. Lee, et al. (2001). "Amphetamine distorts stimulation-dependent dopamine overflow: effects on D2 autoreceptors, transporters, and synaptic vesicle stores." J Neurosci **21**(16): 5916-5924.
Schnell, S. and T. E. Turner (2004). "Reaction kinetics in intracellular environments with macromolecular crowding: simulations and rate laws." Prog. Biophys. Mol. Biol. **85**: 235.
Segel, L. A. (1988). "On the validity of the steady state assumption of enzyme kinetics." Bull. Math. Biol. **50**: 579-593.
Shiraishi, F. and M. A. Savageau (1992). "The tricarboxylic acid cycle in Dictyostelium discoideum. I. Formulation of alternative kinetic representations." J. Biol. Chem. **267**: 22912-22918.
Singh, A. and J. Hespanha (2006). LogNormal Moment Closures for Biochemical Reactions. In Proc. of the 45th Conf. on Decision and Contr.
Südhof, T. C. (2004). "The Synaptic Vesicle Cycle." Annual Review of Neuroscience **27**(1): 509-547.
Sulzer, D., T. K. Chen, et al. (1995). "Amphetamine redistributes dopamine from synaptic vesicles to the cytosol and promotes reverse transport." J Neurosci **15**(5 Pt 2): 4102-4108.
Sulzer, D., M. S. Sonders, et al. (2005). "Mechanisms of neurotransmitter release by amphetamines: a review." Prog Neurobiol **75**(6): 406-433.
Sun, J. Y., X. S. Wu, et al. (2002). "Single and multiple vesicle fusion induce different rates of endocytosis at a central synapse." Nature **417**(6888): 555-559.
Tian, T. and K. Burrage (2006). "Stochastic models for regulatory networks of the genetic toggle switch." Proc Natl Acad Sci U S A **103**(22): 8372-8377.
Tian, T. and K. Burrage (2006). "Stochastic models for regulatory networks of the genetic toggle switch." Proceedings of the National Academy of Sciences **103**(22): 8372-8377.
Tian, T., K. Burrage, et al. (2007). "Stochastic delay differential equations for genetic regulatory networks." The Journal of Computational and Applied Mathematics **205**(2): 696-707.
Torres, N. V. and E. O. Voit (2002). Pathway Analysis and Optimization in Metabolic Engineering, Cambridge University Press, Cambridge, U.K. .
Twomey, A. (2007). On the Stochastic Modelling of Reaction-Diffusion Processes, University of Oxford. **Master of Science**.
Verkman, A. S. (2002). "Solute and macromolecule diffusion in cellular aqueous compartments." Trends Biochem. Sci. **27**: 27.
Vilar, J. M., H. Y. Kueh, et al. (2002). "Mechanisms of noise-resistance in genetic

oscillators." Proc Natl Acad Sci U S A **99**: 5988-5992.
Visser, D. and J. J. Heijnen (2002). "The mathematics of metabolic control analysis revisited." Metab Eng **4**(2): 114-123.
Visser, D. and J. J. Heijnen (2002). "The Mathematics of Metabolic Control Analysis Revisited." Metabolic Engineering **4**(2): 114-123.
Voit, E. (2005). "Smooth bistable S-systems." IEE Proc Systems Biol **152**: 207-213.
Voit, E. O. (1993). "S-system modeling of complex systems with chaotic input." Environmetrics **4**(2): 153-186.
Voit, E. O. (2000). Computational analysis of biochemical systems: a practical guide for biochemists and molecular biologists, Cambridge University Press.
Voit, E. O. (2005). "Smooth bistable S-systems." IEE Proc. Systems Biol **152**: 207-213.
Volterra, V. (1926). "Variazioni e fluttuazioni del numero d'individui in specie animali conviventi." Mem. R. Accad. dei Lincei. **2**.
von Campenhausen, S., B. Bornschein, et al. (2005). "Prevalence and incidence of Parkinson's disease in Europe." Eur Neuropsychopharmacol **15**(4): 473-490.
Walton, R. J., C. J. Preston, et al. (1977). "Biochemical measurements in Paget's disease of bone." European Journal of Clinical Investigation **7**(1): 37-39.
Wang, F.-S., C.-L. Ko, et al. (2007). "Kinetic Modeling Using S-systems and Lin-log Approaches." Biochem. Eng. J. **33**: 238-247.
Wilensky, U. (1999). NetLogo, Center for Connected Learning and Computer-Based Modeling, Northwestern University. Evanston, IL.
Williams, B. C. and W. Millar (1998). Decompositional, Model-based learning and its Analogy to Diagnosis, AAAI/IAAI.
Wolkenhauer, O., M. Ullah, et al. (2004). "Modelling and Simulation of IntraCellular Dynamics: Choosing an Appropriate Framework " IEEE Transactions on NanoBioscience **3**: 200-207.
Wu, J., Z. Qi, et al. (2009). "dopamine signaling with noise and delays ", from https://cionline.hgc.jp/cifileserver/launchCIOPlayer?model=http://www.csml.org/download/model/csml30/dopamine signaling with noise and delays.csml.gz.
Wu, J. and E. Voit (2009 a). "Hybrid modeling in biochemical systems theory by means of functional petri nets." Journal of bioinformatics and computational biology **7**(1): 107-134.
Wu, J. and E. Voit (2009 b). "Integrative biological systems modeling: challenges and opportunities." Frontiers of Computer Science in China **3**(1): 92-100.
Zhang, Q., Y. Li, et al. (2009). "The Dynamic Control of Kiss-And-Run and Vesicular Reuse Probed with Single Nanoparticles." Science **323**(5920): 1448-1453.

PAPER 4

CHAPTER 5

Constructing Stochastic Models from Deterministic Process Equations by Propensity Adjustment

Jialiang Wu, Brani Vidakovic, Eberhard O. Voit

BMC Systems Biology, 2011. **5**(1): p. 187.

CHAPTER 5

Constructing Stochastic Models from Deterministic Process Equations by Propensity Adjustment

Jialiang Wu[1], Brani Vidakovic [2], Eberhard Voit[2,3§]

[1]Deparment of Mathematics, Bioinformatics Program, Georgia Institute of Technology, Atlanta, GA30332, USA

[2] The Wallace H. Coulter Department of Biomedical Engineering, Georgia Institute of Technology, Atlanta, GA30332, USA

[3]Integrative BioSystems Institute and The Wallace H. Coulter Department of Biomedical Engineering, Georgia Institute of Technology, Atlanta, GA30332, USA

[§]Corresponding author

Email addresses:

JW: wjl@gatech.edu

BV: brani@bme.gatech.edu

EV: eberhard.voit@bme.gatech.edu

October **2011**

Abstract

Background

Gillespie's stochastic simulation algorithm (SSA) for chemical reactions admits three kinds of elementary processes, namely, mass action reactions of 0^{th}, 1^{st} or 2^{nd} order. All other types of reaction processes, for instance those containing non-integer kinetic orders or following other types of kinetic laws, are assumed to be convertible to one of the three elementary kinds, so that SSA can validly be applied. However, the conversion to elementary reactions is often difficult, if not impossible. Within deterministic contexts, a strategy of model reduction is often used. Such a reduction simplifies the actual system of reactions by merging or approximating intermediate steps and omitting reactants such as transient complexes. It would be valuable to adopt a similar reduction strategy to stochastic modelling. Indeed, efforts have been devoted to manipulating the chemical master equation (CME) in order to achieve a proper propensity function for a reduced stochastic system. However, manipulations of CME are almost always complicated, and successes have been limited to relative simple cases.

Results

We propose a rather general strategy for converting a deterministic process model into a corresponding stochastic model and characterize the mathematical connections between the two. The deterministic framework is assumed to be a generalized mass action system and the stochastic analogue is in the format of the chemical master equation. The analysis identifies situations: where a direct conversion is valid; where internal noise affecting the system needs to be taken into account; and where the propensity function must be mathematically adjusted. The conversion from deterministic to stochastic models is illustrated with several representative examples, including reversible reactions with feedback controls, Michaelis-Menten enzyme kinetics, a genetic regulatory motif, and stochastic focusing.

Conclusions

The construction of a stochastic model for a biochemical network requires the utilization of information associated with an equation-based model. The conversion strategy proposed here guides a model design process that ensures a valid transition between deterministic and stochastic models.

Background

Most stochastic models of biochemical reactions are based on the fundamental assumption that no more than one reaction can occur at the exact same time. A consequence of this assumption is that only elementary chemical reactions can be converted directly into stochastic analogues (Gillespie 1977). These include: 1) zero-order reactions, such as the generation of molecules at a constant rate; 2) first-order reactions, with examples including elemental chemical reactions as well as transport and decay processes; and 3) second-order reactions, which include heterogeneous and homogeneous bimolecular reactions (dimerization). Reactions with integer kinetic orders other than 0, 1 and 2 are to be treated as combinations of sequential elementary reactions. The advantage of the premise of non-simultaneous reaction steps is that the stochastic reaction rate can be calculated from a deterministic, equation-based model with some degree of rigor, even though the derivation is usually not based on first physical principles but instead depends on other assumptions and on macroscopic information, such as a fixed rate constant in the equation-based model. The severe disadvantage is that this rigorous treatment is not practical for modelling larger biochemical reaction systems. The reasons include the following. First, in many cases, elementary reaction rates are not available. Secondly, even in the case that all reaction parameters are available, the computational expense is very significant when the system involves many species and reactions, and this fact ultimately leads to a combinatorial explosion of required computations. Within a deterministic modelling framework, the common practice in this

situation is to fit the transient and steady-state experimental data with a phenomenological, (differential) equation-based model, which explicitly or implicitly eliminates or merges some intermediate species and reactions. The best-known examples are probably Michaelis-Menten and Hill rate laws, which are ultimately explicit, but in truth approximate a multivariate system of underlying chemical processes.

Similar model reduction efforts have been carried out for stochastic modelling. For instance, the use of a complex-order function (which corresponds to a reduced equation-based model) was shown to be justified for some types of stochastic simulations. A prominent example is again the Michaelis-Menten rate law, which can be reduced from a system of elementary reactions to an explicit function by means of the *quasi-steady-state assumption* (see Result section and (Rao and Arkin 2003; Cao, Gillespie et al. 2005)). However, model reduction within the stochastic framework has proven to be far more difficult than in the deterministic counterpart. The difficulties are mainly due to the fact that the reduction must be carried out on the chemical master equation (CME). This process is nontrivial and has succeeded only in simple cases.

In general, the construction of a stochastic model for a large biochemical network requires the use of information available from an equation-based model. In the past, several strategies have been proposed for this purpose and within the context of Gillespie's exact stochastic simulation algorithm (SSA; (Gillespie 1977)) and its variants (Gillespie 2007). For example, Tian and Burrage (Tian and Burrage 2006) proposed that a stochastic model could be directly formulated from the deterministic model through a Poisson leaping procedure. However, a rigorous mathematical justification for such a conversion is lacking. Typical moment-based approaches (Singh and Hespanha 2006; Gomez-Uribe and Verghese 2007; Lee, Kim et al. 2009) derive ODEs for the statistical moments of the stochastic model from an equation-based model where the 0^{th}, 1^{st} and 2^{nd}

order reactions follow mass action rate laws. More recently the moment method was extended to cover models consisting of rational rate laws (Milner, Gillespie et al. 2011). Moreover, it was realized that the moment method is complementary to, but cannot fully replace, stochastic simulations, because it does not cover situations like genetic switches (Gomez-Uribe and Verghese 2007; Chevalier and El-Samad 2009).

In this article, we explore the mathematical connection between deterministic and stochastic frameworks for the pertinent case of Generalized Mass Action (GMA) systems, which are frequently used in Biochemical Systems Theory (BST; (Savageau 1969 a; Savageau 1976; Voit 2000)). Specifically, we address two questions: First, under what conditions can a deterministic, equation-based model be converted directly into a stochastic simulation model? And second, what is a proper way of implementing this conversion? We will develop a method to answer these questions and demonstrate it for functions in the canonical power-law format of.GMA systems. However, the results are applicable to other functions and formats as well, as we will demonstrate with several examples.

1.1 Representations of systems of biochemical reactions

Consider a well-stirred biochemical reaction system with constant volume and temperature, where N_s different chemical species $\{S_s\}_{s=1}^{N_s}$, interact through N_r unidirectional reaction channels $\{R_r\}_{r=1}^{N_r}$. Each reaction channel can be characterized as

$$R_r : \underline{v}_{r1}S_1 + \ldots + \underline{v}_{rN_s}S_{N_s} \xrightarrow{k_r} \bar{v}_{r1}S_1 + \ldots + \bar{v}_{rN_s}S_{N_s},$$

where $\underline{v}_{rs}$ and $\bar{v}_{rs}$ are the counts of molecular species S_s consumed and produced due to reaction R_r, respectively, and k_r is the rate constant. The changed amount of S_s $v_{rs} = \bar{v}_{rs} - \underline{v}_{rs}$, which is due to the firing of reaction R_r, defines the stoichiometric

coefficient of S_s in R_r. The stoichiometric coefficients of all species can be summarized according to each reaction R_r in the stoichiometric vector

$$\mathbf{v}_r \triangleq \begin{bmatrix} v_{r1} \\ \vdots \\ v_{rN_s} \end{bmatrix} \in \mathbb{Z}^{N_s}.$$

The stoichiometric vectors of all reactions can further be arranged as the stoichiometric matrix of the system

$$V \triangleq \left[\mathbf{v}_1, \ldots, \mathbf{v}_{N_r} \right] \in \mathbb{Z}^{N_s \times N_r}.$$

The size of the system is defined as $\Phi = AU$, where A is the Avogadro number and U is the reaction volume.

The modelling of biochemical reaction networks typically uses one of two conceptual frameworks: deterministic or stochastic. In a deterministic framework, the state of the system is given by the a non-negative vector $\left[\mathbf{X}(t)\right] = \left[\left[X_1(t)\right], \ldots, \left[X_{N_s}(t)\right] \right]^T \in \mathbb{R}^{N_s}$, where component $\left[X_s(t)\right]$ represents the concentration of species S_s, measured in moles per unit volume. The temporal evolution of the state of the system is modelled by a set of ordinary differential equations, which in our case are assumed to follow a generalized mass action (GMA) kinetic law. By contrast, in a stochastic framework, the state of the systems is characterized by a vector $\mathbf{x}(t) = \left[x_1(t), \ldots, x_{N_s}(t) \right]^T \in \mathbb{Z}^{N_s}$, whose values are non-negative integers. Specifically, $x_s(t) = \Phi\left[X_s(t)\right]$ is the count of S_s molecules, which is a sample value of the random variable $X_s(t)$. The system dynamics of this process is

typically described with the chemical master equation (CME). Both GMA and CME will be discussed in detail in the following sections.

1.2 Motivation for the power-law formalism: reactions in crowded media

Power-law functions with non-integer kinetics have proven very useful in biochemical systems analysis, and forty years of research have demonstrated their wide applicability (*e.g.*, see (Savageau 1969 a; Savageau 1976; Voit 2000)). Generically, this type of description of a biochemical reaction can be seen either as a Taylor approximation in logarithmic space or as a heuristic or phenomenological model that has been applied successfully hundreds of times and in different contexts, even though it is difficult or impossible in many situations to trace it back to first mechanistic principles. A particularly interesting line of support for the power-law format can be seen in the example of a bimolecular reaction occurring in a spatially restricted environment. Savageau demonstrated that the kinetics of such a reaction can be validly formulated as a generalization of the law of mass action, where non-integer kinetic orders are allowed (Savageau 1993; Savageau 1995). Neff and colleagues (Bajzer, Huzak et al. 2008; Neff 2010; Neff, Offord et al. 2011) showed with careful experiments that this formulation is actually more accurate than alternative approaches.

Within the conceptual framework of power-law representations, the rate of the association reaction between molecules of species S_1 and S_2 is given as $k\left[X_1(t)\right]^{f_1}\left[X_2(t)\right]^{f_2}$. Here, k is the *rate constant* and f_1 and f_2 are real-valued *kinetic orders*, which are no longer necessarily positive integers as it is assumed in a mass action law. As an example, consider the reversible bimolecular reaction $S_1 + S_2 \underset{k_b}{\overset{k_f}{\rightleftharpoons}} S_3$. Like Neff

and colleagues (Neff 2010), we begin by formulating a discrete update function for the population of S_3 molecules as

$$x_3(t+\Delta t) - x_3(t) = f\left([X_1],[X_2]\right)\Delta t\ x_1x_2\ -\ g\left([X_3]\right)\Delta t x_3. \qquad (1)$$

The first term on the right-hand side of this equation, $f\left([X_1],[X_2]\right)\Delta t\ x_1x_2$, describes the production of S_3: it depends on the totality of possible collisions x_1x_2 and also on some fraction $f\left([X_1],[X_2]\right)\Delta t$ that actually reacts and forms the product. In a dilute environment, $f\left([X_1],[X_2]\right)$ equals a traditional rate constant, and the reaction obeys the law of mass action, while in a spatially restricted environment, such as the cytoplasm, one needs to take crowding effects into account. As shown in Savageau (Savageau 1993; Savageau 1995), the desired fraction of a reaction in a crowded environment becomes a *rate function* that depends on the current concentrations of S_1 and S_2. The second term, $g\left([X_3]\right)\Delta t x_3$, describes the fraction $g\left([X_3]\right)\Delta t$ of species S_3 that dissociates back into S_1 and S_2. This fraction may depend on some functional form of $[X_3]$ because in a crowded environment the complex may not be able to dissociate effectively. Thus, rate constants in the generalized mass action setting become rate functions (*cf.* (Neff 2010)).

By taking the limit $\Delta t \to 0$, one obtains the differential equation

$$\frac{dx_3}{dt} = f\left([X_1],[X_2]\right)x_1x_2\ -\ g\left([X_3]\right)x_3. \qquad (2)$$

Savageau used Taylor series expansion to approximate the functions f and g in the logarithmic space $\left(\log[X_1],\log[X_2]\right)$ around some operating point (a,b). The result for f is

$$
\begin{aligned}
&\log f\left(\left[X_1\right],\left[X_2\right]\right) \triangleq F\left(\log\left[X_1\right],\log\left[X_2\right]\right) \\
&= F(a,b) + \left.\frac{\partial f\left(\left[X_1\right],\left[X_2\right]\right)}{\partial\left[X_1\right]}\right|_{(a,b)} (\log\left[X_1\right]-a) \\
&+ \left.\frac{\partial f\left(\left[X_1\right],\left[X_2\right]\right)}{\partial\left[X_2\right]}\right|_{(a,b)} (\log\left[X_2\right]-b) + \mathrm{HOT} \\
&\approx k_f + \alpha\log\left[X_1\right] + \beta\log\left[X_2\right],
\end{aligned}
\tag{3}
$$

where $k_f, \alpha,$ and β are constants related to the chosen operating point (a, b). The final step is achieved by ignoring all higher order terms (HOT) beyond the constant and linear terms. Transformation back to the Cartesian space yields

$$
f\left(\left[X_1\right],\left[X_2\right]\right) \approx k_a\left[X_1\right]^{\alpha}\left[X_2\right]^{\beta}, k_a = e^{k_f}. \tag{4}
$$

The same procedure leads to the power-law expression for the degradation term: $g\left(\left[X_3\right]\right) \approx k_d\left[X_3\right]^{\gamma}$. By combining constants we arrive at a power-law representation for the dynamics of species S_3 as

$$
\begin{aligned}
\frac{d\left[X_3\right]}{dt} &= k_a\left[X_1\right]^{\alpha}\left[X_2\right]^{\beta}\left[X_1\right]\left[X_2\right] - k_d\left[X_3\right]^{\gamma}\left[X_3\right] \\
&= k_a\left[X_1\right]^{a}\left[X_2\right]^{b} - k_d\left[X_3\right]^{c},
\end{aligned}
\tag{5}
$$

where $a = \alpha + 1, b = \beta + 1,$ and $c = \gamma + 1$. As long as k_f, k_d, a, b and c remain more or less constant throughout a relevant range, the power-law model is mathematically well justified. In actual applications, the values of rate constants and kinetic orders can be estimated from experimental data (Chou and Voit 2009). When the functions f and g are originally not in power-law format, they can be locally approximated by power-law functions with a procedure similar to the one shown above (Equations (3) to (5)). An illustration will be given in the example section.

1.3 The Generalized Mass Action (GMA) format

In the GMA format within Biochemical Systems Theory, each process is represented as univariate or multivariate power-law representation. GMA models may be developed *de novo* or as an approximation of some other nonlinear rate laws. GMA models characterize the time evolution of the system state given that the system was in the state $X(t_0)$ at some initial time t_0. Generically, the state of the system is changed within a sufficiently small time interval by one out of the N_r possible reactions that can occur in the system. The reaction velocity through reaction channel R_r is:

$$\left[\frac{[X_1(t)]'}{v_{r1}} = \ldots = \frac{[X_{N_s}(t)]'}{v_{rN_s}}\right] = k_r \prod_{s=1}^{N_s} [X_s(t)]^{f_{rs}} \qquad (6)$$

for those $v_{rs} = \bar{v}_{rs} - \underline{v}_{rs} \neq 0, s = 1, \ldots, N_s$. As shown in the example of a bimolecular reaction, the kinetic order f_{rs} associated with species S_s captures the effects of both reactant properties (such as the stoichiometric coefficient $\underline{v}_{rs}$) and environmental influences (such as temperature, pressure, molecular crowding effects, etc.). Therefore f_{rs} does not necessary equal an integer $\underline{v}_{rs}$, which is assumed to be the case in mass action kinetics, but is possibly real-valued and may be negative. Summing up the contributions of all reactions, one obtains a GMA model describing the dynamics of S_s as

$$\frac{d}{dt}[X_s(t)] = \sum_{r=1}^{N_r} v_{rs} k_r \prod_{s=1}^{N_s} [X_s(t)]^{f_{rs}} \qquad (7)$$

for every $s = 1, \ldots, N_s$. Each reaction contributes either a production flux or a degradation flux to the dynamics of a certain species. Positive terms ($v_{rs} > 0$) represent the production of S_s, while negative terms ($v_{rs} < 0$) describe degradation. If f_{rs} is positive, then S_s accelerates the reaction R_r; a negative value represents that S_s inhibits the reaction, and

f_{rs}=0 implies that S_s has no influence on the reaction. The rate constant k_r for reaction R_r, is either positive or zero. Both, the rate constant and the kinetic order, are to be estimated from data.

1.4 Proper use of equation-based functions for stochastic simulations

The fundamental concept of a stochastic simulation is the propensity function $\alpha(\mathbf{X})$, and $\alpha(\mathbf{X})dt$ describes the probability that a reaction will change the value of a system variable within the next (infinitesimal) time interval $(t, t+dt)$. While a formal definition will be given later (Equation 18), it is easy to intuit that the propensity function is in some sense analogous to the rate in the corresponding deterministic model. In fact, the propensity function is traditionally assumed to be $\alpha(\mathbf{X}) = f_s(\mathbf{X})$, if the deterministic model is $X_s' = f_s(\mathbf{X}, t), s = 1, \ldots, N_s$. However, a proper justification for this common practice is by and large missing. Indeed, we will show that the direct use of a rate function as the propensity function in a stochastic simulation algorithm requires that at least one of the following assumptions be true:

1) *f* is a linear function;

2) the reaction is monomolecular;

3) all X_i in the system are noise-free variables, *i.e.*, without (or with ignorable) fluctuations, which implies that the covariance of any two participating reactants is zero (or close to zero).

Each of these assumptions constitutes a sufficient condition for the direct use of a rate function as the propensity function and applies, in principle, to GMA as well as other systems. The validity of these conditions will be discussed later. Specifically, the first condition will be addressed in the Results section under the titles "0^{th}-order reaction

kinetics" and "1st-order reaction kinetics," while the second condition will be discussed under the title "Real-valued order monomolecular reaction kinetics." The third condition will be the focus of Equations (29-36) and their associated explanations.

In reality, the rates of reactions in biochemical systems are commonly nonlinear functions of the reactant species, and fluctuations within each species are not necessarily ignorable. Therefore, to the valid use of an equation-based model in a stochastic simulation mandates that we know how to define a proper propensity function. The following section addresses this issue. It uses statistical techniques to characterize estimates for both the mean and variance of the propensity function, and these features will allow an assessment of the validity of the assumption $\alpha(\mathbf{X}) = f_s(\mathbf{X})$ and prescribe adjustments if the assumption is not valid.

Methods

2.1. Deriving the mean and variance of a power-law function of random variables

Consider a generic power-law function of random variables X_s with the format $PL(\mathbf{X}) = k\prod_{s=1}^{N_s} {X_s}^{f_s}$. Estimates of its mean μ_{PL} and variance σ_{PL} are given as

$$\mu_{PL} \approx k\prod_{s=1}^{N_s} {\mu_s}^{f_s} \exp\left(\sum_{i<j}^{N_s} f_i f_j \operatorname{cov}\left[\log X_i, \log X_j\right]\right) \tag{8}$$

$${\sigma_{PL}}^2 \approx {\mu_{PL}}^2 \Omega \tag{9}$$

(for details, see Additional file 1). Here,

$$\Omega = \sum_{s=1}^{N_s} f_s \mu_s^{-2} \sigma_s^{\,2} + 2 \sum_{i<j}^{N_s} f_i f_j \operatorname{cov}\left[\log X_i, \log X_j\right] \tag{10}$$

and $\mu_s = \mathrm{E}\left[X_s\right]$ and $\sigma_s^{\,2} = \mathrm{E}\left[(X_s - \mu_s)^2\right]$ are the mean and variance of random variable X_s, respectively. If we choose to express $\operatorname{cov}\left[\log X_i, \log X_j\right]$ as a function of μ_s, $\sigma_s^{\,2}$ and covariance $\sigma_{ij} = \operatorname{cov}\left[X_i, X_j\right]$, using a Taylor approximation, we obtain

$$\mu_{PL} \approx k \prod_{s=1}^{N_s} \mu_s^{\,f_s} \exp\left(-\frac{1}{2} \sum_{s=1}^{N_s} f_s \sigma_s^{\,2} / \mu_s^{\,2} + \frac{1}{2}\Omega\right) \tag{11}$$

$$\sigma_{PL}^{\,2} \approx \mu_{PL}^{\,2} \Omega, \tag{12}$$

where

$$\begin{aligned} \Omega \approx & \sum_{s=1}^{N_s} f_s \left(\sigma_s / \mu_s\right)^2 + 2 \sum_{i<j}^{N_s} f_i f_j \{\sigma_{ij} / (\mu_i \mu_j) + \frac{1}{2} \log(\mu_i) \left(\sigma_j / \mu_j\right)^2 \\ & + \frac{1}{2} \log(\mu_j) \left(\sigma_i / \mu_i\right)^2 - \frac{1}{4} \left(\sigma_i / \mu_i\right)^2 \left(\sigma_j / \mu_j\right)^2 \}. \end{aligned} \tag{13}$$

Since many biochemical variables approximately follow a log-normal distribution (Koch 1966; Walton, Preston et al. 1977; Limpert, Stahel et al. 2001), it is valuable to consider the special situation where $\left(X_1, \ldots, X_s\right)$ is log-normally distributed (*i.e.*, $\left(\log X_1, \ldots, \log X_s\right)$ is normally distributed). In such a case, a simpler alternative way to calculate $\operatorname{cov}\left[\log X_i, \log X_j\right]$ is

$$\operatorname{cov}\left[\log X_i, \log X_j\right] = \log\left(1 + \frac{\sigma_{ij}}{\mu_i \mu_j}\right). \tag{14}$$

(Law and Kelton 2000). By substituting this result into (8)-(10), one obtains

$$\mu_{PL} \approx k \prod_{s=1}^{N_s} \mu_s^{f_s} \prod_{i<j}^{N_s} \left(1 + \frac{\sigma_{ij}}{\mu_i \mu_j} \right)^{f_i f_j} \tag{15}$$

$$\sigma_{PL}{}^2 \approx \mu_{PL}{}^2 \Omega, \tag{16}$$

where

$$\Omega = \sum_{s=1}^{N_s} f_s \left(\frac{\sigma_s}{\mu_s} \right)^2 + 2 \sum_{i<j}^{N_s} f_i f_j \log \left(1 + \frac{\sigma_{ij}}{\mu_i \mu_j} \right). \tag{17}$$

The approximation formulae for μ_{PL} and $\sigma_{PL}{}^2$ in eqns. (8)-(10) provide an easy numerical implementation if observation data are available to estimate $\mathrm{cov}\left[\log X_i, \log X_j \right]$. Furthermore, Equations (11)-(13) demonstrate how μ_{PL} and $\sigma_{PL}{}^2$ are related to μ_s, $\sigma_s{}^2$ and σ_{ij}; however, the price of this insight is paid by the possible inaccuracy introduced through the Taylor approximation. Equations (15)-(17) also provide a functional dependence of μ_{PL} and $\sigma_{PL}{}^2$ on $(\mu_s, \sigma_s{}^2, \sigma_{ij})$, but it is only valid if the additional assumption of log-normality is acceptable.

2.2 Deriving proper propensity functions for stochastic simulations from differential equation-based models

Assuming that the GMA model faithfully captures the average behaviour of a biochemical reaction system and recalling $\left[\mathbf{X}(t) \right] = \left([X_1(t)], \ldots, [X_{N_s}(t)] \right)^T$, the expected metabolite numbers are defined as the expectation

$$E\left[\mathbf{X} \right] = \left[\mathbf{X} \right] \Phi, \tag{18}$$

where Φ is the system size as defined above.

To describe the reaction channel R_r stochastically, one needs the state update vector $\mathbf{v}_r$ and must characterize the quantity of molecules flowing through of reaction channel R_r during a small time interval. The key concept of this type of description is the propensity function $\alpha_r(\mathbf{x})$, which is defined as

$\alpha_r(\mathbf{x})dt$ = the probability that exactly one reaction R_r will occur somewhere inside U within infinitesmal interval $(t, t+dt)$, given current state $\mathbf{X}(t) = \mathbf{x}$. (19)

(Gillespie 1977). Because of the probabilistic nature of the propensity function, **X**(t) is no longer deterministic, and the result is instead stochastic and based on the transition probability

$$P(\mathbf{x}, t \mid \mathbf{x}_0, t_0) = \text{Prob}\{\mathbf{X}(t) = \mathbf{x}, \text{ given } \mathbf{X}(t_0) = \mathbf{x}_0\}, \tag{20}$$

which follows the chemical master equation (CME)

$$\frac{\partial P(\mathbf{x}, t \mid \mathbf{x}_0, t_0)}{\partial t} = \sum_{r=1}^{N_r} \left[\alpha_r(\mathbf{x} + \mathbf{v}_r) P(\mathbf{x} + \mathbf{v}_r, t \mid \mathbf{x}_0, t_0) - \alpha_r(\mathbf{x}) P(\mathbf{x}, t \mid \mathbf{x}_0, t_0)\right]. \tag{21}$$

Updating CME requires knowledge of every possible combination of all species counts within the population, which immediately implies that it can be solved analytically for only a few very simple systems and that numerical solutions are usually prohibitively expensive (Gillespie and Petzold 2006). To address the inherent intractability of CME, Gillespie developed an algorithm, called the *Stochastic Simulation Algorithm* (SSA), to simulate CME models (Gillespie 1977). SSA is an exact procedure for numerically simulating the time evolution of a well-stirred reaction system. It is rigorously based on the same microphysical premise that underlies CME and gives a more realistic representation of a system's evolution than a deterministic reaction rate equation represented by ODEs. SSA requires knowledge of the propensity function, which

however is truly available only for elementary reactions. These reactions include: 1) 0^{th} order reactions, exemplified with the generation of a molecule at a constant rate; 2) 1^{st} order monomolecular reactions, such as an elemental chemical conversion or decay of a single molecule; 3) 2^{nd} order bimolecular reactions, including reactive collisions between two molecules of the same or different species. The reactive collision of more than two molecules at exactly the same time is considered highly unlikely and modelled as two or more sequential bimolecular reactions.

For elementary reactions, the propensity function of reaction R_r is computed as the product of a stochastic rate constant c_r and the number h_r of distinct combinations of reactant molecules, i.e.

$$\alpha_r(\mathbf{x}) = c_r h_r(\mathbf{x}), \quad r = 1,\ldots,N_r. \tag{22}$$

Here $h_r(\mathbf{x}) = \begin{cases} \prod_{s=1}^{N_s} \binom{x_s}{\underline{\nu}_{rs}} \approx \dfrac{\prod_{s=1}^{N_s} x_s^{\underline{\nu}_{rs}}}{\prod_{s=1}^{N_s} \underline{\nu}_{rs}!}, & \text{for } x_s \geq \underline{\nu}_{rs} > 0 \\ 0, \quad \text{otherwise} \end{cases}$, where x_s is the sample value of random variable X_s. The approximation is invoked when x_s is large and $(x_s - 1),\ldots,(x_s - \underline{\nu}_{rs} + 1)$ are approximately equal to x_s.

In Gillespie's original formulation (Gillespie 1977) c_r is a constant that only depends on the physical properties of the reactant molecules and the temperature of the system, and $c_r dt$ is the probability that a particular combination of reactant molecules will react within the next infinitesimally small time interval $(t, t+dt)$. The constant c_r can be calculated from the corresponding deterministic rate constants, if they are known.

Since the assumption of mass action kinetics is not valid generally, especially in spatially restricted environments and in situations dominated by macromolecular crowding, we address the broader scenario where c_r is not a constant but a function of the reactant concentrations. Thus, we denote c_r as a *stochastic rate function*, while retaining the definition of h_r as above. Knowing that any positive-valued differentiable function can be approximated locally by a power-law function, we assume the functional form of the stochastic rate function as

$$c_r(\mathbf{x}) = \kappa_r \prod_{s=1}^{N_s} x_s(t)^{\varepsilon_{rs}}. \tag{23}$$

Here, κ_r and ε_{rs} are constants that will be specified in the next section, and $r = 1,\ldots,N_r$. Note that ε_{rs} are now real-valued. Once the stochastic rate function is determined (see below), the propensity function can be calculated as

$$\alpha_r(\mathbf{x}) = c_r(\mathbf{x})h_r(\mathbf{x}) = \frac{\kappa_r}{\prod_{s=1}^{N_s} \underline{\nu}_{rs}!} \prod_{s=1}^{N_s} x_s^{\underline{\nu}_{rs}+\varepsilon_{rs}}. \tag{24}$$

In order to identify the functional expression for a stochastic rate function, and thus the propensity function, we consider the connection between the stochastic and the deterministic equation models. By multiplying CME with **x** and summing over all **x**, we obtain

$$\frac{d}{dt}E\left[\mathbf{X}(t)\right] = \sum_{r=1}^{N_r} \mathbf{v}_r E\left[\alpha_r(\mathbf{X}(t))\right]. \tag{25}$$

Similarly, the expectation for any species $X_s(t)$ is given as

$$\frac{d}{dt}E\left[X_s(t)\right] = \sum_{r=1}^{N_r} \nu_{rs} E\left[\alpha_r(\mathbf{X}(t))\right], \quad s = 1,\ldots,N_s. \tag{26}$$

The details of these derivations are shown in Additional file 1.

We can use these results directly to compute the propensity function for a stochastic GMA model, assuming that its deterministic counterpart is well defined. Specifically, we start with the deterministic GMA equation for X_s,

$$\frac{d}{dt}[X_s(t)] = \sum_{r=1}^{N_r} v_{rs} k_r \prod_{s'=1}^{N_s} [X_{s'}(t)]^{f_{rs'}}, \quad s = 1, \ldots, N_s, \tag{27}$$

where v_{rs}, k_r and $f_{rs'}$ are again the stoichiometric coefficients, rate constants, and kinetic orders, respectively. By substituting $[X_s] = \frac{E[X_s]}{\Phi}$ from Equation (18) into this GMA model, we obtain a "particle-based" equation of the format

$$\frac{d}{dt}\left(\frac{E[X_s]}{\Phi}\right) = \sum_{r=1}^{N_r} v_{rs} k_r \prod_{s'=1}^{N_s} \left(\frac{E[X_{s'}]}{\Phi}\right)^{f_{rs'}}, s = 1, \ldots, N_s .$$

Elementary operations allow us to rewrite this equation as

$$\frac{d}{dt}\left(E[X_s]\right) = \sum_{r=1}^{N_r} v_{rs} k_r \Phi^{1-F_r} \prod_{s'=1}^{N_s} E[X_{s'}]^{f_{rs'}}, \quad s = 1, \ldots, N_s, \tag{28}$$

where $F_r = \sum_{s'=1}^{N_s} f_{rs'}$. In this formulation, the differential operator is justified only when large numbers of molecules are involved. The assumption that the deterministic equations precisely capture the average behaviour of the biochemical reaction system directly equates the stochastic CME (25) to the deterministic equation based model (28)

$$E[\alpha_r(\mathbf{X}(t))] = k_r \Phi^{1-F_r} \prod_{s'=1}^{N_s} E[X_{s'}]^{f_{rs'}}. \tag{29}$$

Now we have two choices for approximating the expectation of the propensity function on left-hand side of equation (29):

1) adopt a zero-covariance assumption as was done in (Wolkenhauer, Ullah et al. 2004), which implies ignoring random fluctuations within every species as well as their correlations. This assumption is only justified for some special cases such as monomolecular and bimolecular reactions under the thermodynamic limit (cf. (Gillespie 2007; Gomez-Uribe and Verghese 2007)), but is not necessary valid in generality. Here the thermodynamic limit is defined as a finite concentration limit which the system reaches when both population and volume approach infinity. Under this assumption, the left hand side of (29) becomes

$$E\left[\alpha_r(\mathbf{x})\right] = E\left[\frac{\kappa_r}{\prod_{s=1}^{N_s} \underline{\nu}_{rs}!} \prod_{s=1}^{N_s} x_s^{\underline{\nu}_{rs}+\varepsilon_{rs}}\right] = \frac{\kappa_r}{\prod_{s=1}^{N_s} \underline{\nu}_{rs}!} \prod_{s=1}^{N_s} E\left[X_s\right]^{\underline{\nu}_{rs}+\varepsilon_{rs}} \tag{30}$$

for every $r = 1,\ldots,N_r$, and Equation (24) yields

$$\varepsilon_{rs} = f_{rs} - \underline{\nu}_{rs}$$

$$\kappa_r = k_r \Phi^{1-F_r} \prod_{s=1}^{N_s} \underline{\nu}_{rs}!$$

$$c_r(\mathbf{x}) = k_r \Phi^{1-F_r} \prod_{s=1}^{N_s} \underline{\nu}_{rs}! x_s^{\varepsilon_{rs}} \tag{31}$$

and

$$\alpha_{r\_0}(\mathbf{x}) = k_r \Phi^{1-F_r} \prod_{s=1}^{N_s} x_s^{f_{rs}}. \tag{32}$$

Here, the index *r*_0 is used to distinguish this 0-covariance propensity function from a second type of propensity in the next section.

With the zero-covariance assumption, one can substitute (32) back into the equation for the expectation for each species, which yields

$$\frac{d}{dt}E\left[X_s(t)\right]=\sum_{r=1}^{N_r}v_{rs}k_r\Phi^{1-F_s}\prod_{s=1}^{N_s}\mu_s^{\,f_{rs}} \tag{33}$$

for every $s=1,\ldots,N_s$.. Note that this result is exactly equivalent to the equation-based model (27).

Equation (33) is based on assumption that both the fluctuations within species and their correlations are ignorable, which is not necessarily true in reality. If one uses it in simulations where the assumptions are not satisfied, it is possible that the means for the molecular species are significantly different from the corresponding equation-based model values. This discrepancy arises because the evolution of each species in the stochastic simulation is in truth affected by the covariance which is not necessarily zero, as it was assumed. This phenomenon was observed by Paulsson and collaborators (Paulsson, Berg et al. 2000) and further discussed in different moment-based approaches (Gomez-Uribe and Verghese 2007; Lee, Kim et al. 2009). To assess the applicability limit of the propensity defined by (32), we can apply approximation techniques as shown in eqns. (8)-(10) on the functional expression of α_{r_0} and obtain mean and variance as

$$\mu_{\alpha_{r\_0}}=E\left[\alpha_{r\_0}(\mathbf{X}(t))\right]\approx k_r\Phi^{1-F_r}\prod_{s'=1}^{N_s}E\left[X_{s'}\right]^{f_{rs'}}\exp\left(\sum_{i<j}^{N_s}f_{ri}f_{rj}\,\mathrm{cov}\left[\log X_i,\log X_j\right]\right) \tag{34}$$

$$\sigma_{\alpha_{r\_0}}{}^2\approx\mu_{\alpha_{r\_0}}{}^2\Omega_r, \tag{35}$$

where

$$\Omega_r=\sum_{s=1}^{N_s}f_{rs}\mu_s^{-2}\sigma_s{}^2+2\sum_{i<j}^{N_s}f_{ri}f_{rj}\,\mathrm{cov}\left[\log X_i,\log X_j\right], \tag{36}$$

for every $s = 1, \ldots, N_s$. These expressions demonstrate that even with large numbers of molecules the mean of CME does not always converge to the GMA model. Indeed, the convergence is only guaranteed in one of the following special situations: 1) the reaction is of 0^{th} order; 2) the reaction is a real value-order monomolecular reaction, with 1^{st} order reaction as a special case; 3) the covariance contribution in (34) is sufficiently small to be ignored for all participating reactant species of a particular reaction channel. Except for these three special situations, the covariance as shown in (34) significantly affects the mean dynamics. Therefore, stochastic simulations using zero-covariance propensity functions will in general yield means different from what the deterministic GMA model produces. How large these differences are cannot be said in generality. Under the assumption that the GMA model correctly captures the mean dynamics of every species, this conclusion means that α_{r_0} is not necessarily an accurate propensity function for stochastic simulations, and the direct conversion of the equation-based model into a propensity function must be considered with caution.

Moreover, there is no theoretical basis to assume that there are no fluctuations in the molecular species or that these are independent. Therefore, we need to consider the second treatment of the expectation of the propensity function and study the possible effects of a non-zero covariance.

2) We again assume that the GMA model is well defined, which implies that information regarding the species correlations and fluctuations has been captured in the parameters of the GMA model on the left hand size of Equations (7) and (28). To gain information regarding correlations, we use Taylor expansion to approximate the propensity function (see Additional file 1 for details):

$$E\left[\alpha_r(\mathbf{X}(t))\right] = E\left[\frac{\kappa_r}{\prod_{s=1}^{N_s}\underline{\nu}_{rs}!}\prod_{s=1}^{N_s}X_s^{\underline{\nu}_{rs}+\varepsilon_{rs}}\right] \approx \frac{\kappa_r}{\prod_{s=1}^{N_s}\underline{\nu}_{rs}!}\prod_{s=1}^{N_s}E\left[X_s\right]^{\underline{\nu}_{rs}+\varepsilon_{rs}}\exp\left(\sum_{i<j}^{N_s}\left(\underline{\nu}_{ri}+\varepsilon_{ri}\right)\left(\underline{\nu}_{rj}+\varepsilon_{rj}\right)\mathrm{cov}\left[\log X_i,\log X_j\right]\right). \tag{37}$$

After substitution of (37) in (29), one obtains

$$\kappa_r = k_r\Phi^{1-F_r}\prod_{s=1}^{N_s}\underline{\nu}_{rs}!\exp\left(-\sum_{i<j}^{N_s}f_{ri}f_{rj}\,\mathrm{cov}\left[\log X_i,\log X_j\right]\right)$$

$$\varepsilon_{rs} = f_{rs}-\underline{\nu}_{rs}.$$

Given the state **x** of the system at time *t***,** the stochastic rate function of reaction R_r is

$$c_r(\mathbf{x}) = \kappa_r\prod_{s=1}^{N_s}x_s^{\varepsilon_{rs}} = k_r\Phi^{1-F_r}\prod_{s=1}^{N_s}\underline{\nu}_{rs}!\exp\left(-\sum_{i<j}^{N_s}f_{ri}f_{rj}\,\mathrm{cov}\left[\log X_i(t),\log X_j(t)\right]\right)\prod_{s=1}^{N_s}x_s^{f_{rs}-\underline{\nu}_{rs}}. \tag{38}$$

Here it is important to understand that although the random variables $\{X_s\}_{s\in S}$ appear in the expression $c_r(\mathbf{x})$, $c_r(\mathbf{x})$ is not a function of random variables but a deterministic function. The reason is that the $\mathrm{cov}\left[\log X_i(t),\log X_j(t)\right]$ in the composition of $c_r(\mathbf{x})$, which as the numerical characteristic of the random variables $\{X_s\}_{s\in S}$, is deterministic. Therefore, the stochastic rate function $c_r(\mathbf{x})$ is a well-justified deterministic function that is affected by both the state of the system $[x_1,\ldots,x_{N_s}]$ and $\mathrm{cov}\left[\log X_i(t),\log X_j(t)\right]$, the numerical characteristic of fluctuations in the random variables $\{X_s\}_{s\in S}$.

Given the expression $c_r(\mathbf{x})$, the propensity function is

$$\begin{aligned}\alpha_r(\mathbf{x}) &= c_r(\mathbf{x})h_r(\mathbf{x}) \\ &= \frac{k_r\Phi^{1-F_r}\prod_{s=1}^{N_s}\underline{\nu}_{rs}!\exp\left(-\sum_{i<j}^{N_s} f_{ri}f_{rj}\,\mathrm{cov}\left[\log X_i(t),\log X_j(t)\right]\right)\prod_{s=1}^{N_s} x_s^{\,f_{rs}-\underline{\nu}_{rs}}}{\prod_{s=1}^{N_s}\underline{\nu}_{rs}!}\prod_{s=1}^{N_s} \\ &= k_r\Phi^{1-F_r}\prod_{s=1}^{N_s} x_s^{\,f_{rs}}\exp\left(-\sum_{i<j}^{N_s} f_{ri}f_{rj}\,\mathrm{cov}\left[\log X_i(t),\log X_j(t)\right]\right).\end{aligned} \tag{39}$$

These results are based on the assumption that there are large numbers of molecules for all reactant species participating in reaction R_r. For simplicity of discussion, we define the *propensity adjustment factor* (paf) of reaction R_r as

$$paf(t) \triangleq \exp\left(-\sum_{i<j}^{N_s} f_{ri}f_{rj}\,\mathrm{cov}\left[\log X_i(t),\log X_j(t)\right]\right). \tag{40}$$

paf is a function of time *t* and represents the contribution of the reactants to correlations among species in the calculation of the propensity function for reaction R_r. We denote the propensity function in (39), which accounts for the contribution of the covariance, as α_{r_cov}, in order to distinguish it from the propensity function α_{r_0} (32), which is based on the assumption of zero-covariance, *i.e.*,

$$\alpha_{r\_\mathrm{cov}}(\mathbf{x}) = paf(t)k_r\Phi^{1-F_r}\prod_{s=1}^{N_s} x_s^{\,f_{rs}}. \tag{41}$$

Remembering that $\mathrm{cov}\left[\log X_i(t),\log X_j(t)\right]$, which is a component in both the stochastic rate function $c_r(\mathbf{x})$ and now in the function *paf*(*t*), is a deterministic function rather than a function of random variables, *paf*(*t*) is a deterministic correction to the kinetic constant

k_r in the construction of α_{r_cov} in (41), which corrects the stochastic simulation toward the correct average.

In contrast to the propensity function α_{r_0}, α_{r_cov} leads to accurate stochastic simulations. To illustrate this difference, we analyze $\frac{d}{dt}E\left[X_s(t)\right]$ as follows: We apply the approximation techniques in eqns. (9)-(11) in order to obtain the mean and variance of the propensity function α_{r_cov}:

$$\mu_{\alpha_{r\_\mathrm{cov}}} = E\left[\alpha_{r\_\mathrm{cov}}(\mathbf{X}(t))\right] \approx k_r \Phi^{1-F_r} \prod_{s'=1}^{N_s} E\left[X_{s'}\right]^{f_{rs'}} \tag{42}$$

$$\sigma_{\alpha_{r\_\mathrm{cov}}}{}^2 \approx \mu_{\alpha_{r\_\mathrm{cov}}}{}^2 \Omega_r. \tag{43}$$

Here

$$\Omega_r = \sum_{s=1}^{N_s} f_{rs} \mu_s{}^{-2} \sigma_s{}^2 + 2 \sum_{i<j}^{N_s} f_{ri} f_{rj} \operatorname{cov}\left[\log X_i, \log X_j\right]. \tag{44}$$

By substituting (42) back into the derivation of CME (26), one obtains

$$\begin{aligned} &\frac{d}{dt}E\left[X_s(t)\right] \\ &= \sum_{r=1}^{N_r} v_{rs} E\left[\alpha_{r\_\mathrm{cov}}(\mathbf{X}(t))\right] \\ &\approx \sum_{r=1}^{N_r} v_{rs} k_r \Phi^{1-F_r} \prod_{s'=1}^{N_s} \mu_{s'}{}^{f_{rs'}} \end{aligned} \tag{45}$$

for every $s = 1, \ldots, N_s$, which is equivalent in approximation to the GMA model (28). In the other words, the mean of every molecular species obtained by using α_{r_cov} in the

CME derived equation (27) is approximately identical to the corresponding macroscopic variable in the GMA model.

1.3 Calculation of $\mathrm{cov}\left[\log X_i(t), \log X_j(t)\right]$

When data in the form of multiple time series for all the reactants are available, it is possible to compute $\mathrm{cov}\left[\log X_i(t), \log X_j(t)\right]$ directly from these data. Once this covariance is known, the function *paf*, α_{r_cov} and the mean dynamics can all be assessed. Alas, the availability of several time series data for all reactants under comparable conditions is rare, so that $\mathrm{cov}\left[\log X_i(t), \log X_j(t)\right]$ must be estimated in a different manner.

If one can validly assume that the covariance based on α_{r_0} does not differ significantly from the covariance based on α_{r_cov}, one may calculate $\mathrm{cov}\left[\log X_i(t), \log X_j(t)\right]$ by one of following methods.

Method 1:

One uses α_{r_0} to generate multiple sets of time series data of all reactants and then computes $\mathrm{cov}\left[\log X_i(t), \log X_j(t)\right]$.

Method 2:

First, $\mathrm{cov}\left[\log X_i(t), \log X_j(t)\right]$ is expressed as a function of mean and covariance in one of the following ways; either as

$$\begin{aligned}\mathrm{cov}\left[\log X_i, \log X_j\right] &\approx \sigma_{ij}/(\mu_i\mu_j) + \frac{1}{2}\log(\mu_i)\left(\sigma_j/\mu_j\right)^2 \\ &+ \frac{1}{2}\log(\mu_j)\left(\sigma_i/\mu_i\right)^2 - \frac{1}{4}\left(\sigma_i/\mu_i\right)^2\left(\sigma_j/\mu_j\right)^2\end{aligned} \tag{46}$$

or as Equation (14):

$$\mathrm{cov}\left[\log X_i, \log X_j\right] = \log\left(1 + \frac{\sigma_{ij}}{\mu_i\mu_j}\right).$$

The first functional expression of $\mathrm{cov}\left[\log X_i(t), \log X_j(t)\right]$ is achieved by Taylor approximation, whereas the second expression is obtained by the additional assumption that the concentrations $\left(X_1, \ldots, X_s\right)$ are log-normally distributed (Law and Kelton 2000; Singh and Hespanha 2006). The consideration of a log-normal distribution is often justified by the fact that many biochemical data have indeed been observed to be log-normally distributed (*e.g.*, (Koch 1966; Walton, Preston et al. 1977; Limpert, Stahel et al. 2001)).

Second, one uses α_{r_0} to approximate the mean and covariance either by direct simulation, as shown in method 1, or by a moment-based approach, which is explained in Additional file 2, and which yields the differential equations

$$\frac{\partial \mu_s}{\partial t} \approx \sum_{r=1}^{N_r} v_{r,s} \left\{ \alpha_{r\_0}(\boldsymbol{\mu}) + \frac{1}{2} \sum_{m,n=1}^{N_s} \frac{\partial^2 \alpha_{r\_0}(\boldsymbol{\mu})}{\partial X_m \partial X_n} \sigma_{mn} \right\}$$

$$\frac{\partial \sigma_{ij}}{\partial t} \approx \sum_{r=1}^{N_r} \left\{ v_{r,i} \sum_{s=1}^{N_s} \frac{\partial \alpha_{r\_0}(\boldsymbol{\mu})}{\partial X_s} \sigma_{js} + v_{r,j} \sum_{s=1}^{N_s} \frac{\partial \alpha_{r\_0}(\boldsymbol{\mu})}{\partial X_s} \sigma_{is} + v_{r,i} v_{r,j} \left[\alpha_{r\_0}(\boldsymbol{\mu}) + \frac{1}{2} \sum_{m,n=1}^{N_s} \frac{\partial^2 \alpha_{r\_0}(\boldsymbol{\mu})}{\partial X_m \partial X_n} \sigma_{mn} \right] \right\}.$$

For convenience of computational implementation, the above equations can be written in matrix format

$$\frac{\partial \mu}{\partial t} \approx V^T \left(\alpha + \frac{1}{2} \alpha'' \odot \sigma \right)$$

$$\frac{\partial \sigma}{\partial t} \approx \left(\sigma \left(\alpha' V \right) \right)^T + \sigma \left(\alpha' V \right) + V^T \Lambda V.$$

Here for $r = 1, \ldots, N_r$, and $s, m, n = 1, \ldots, N_s$, $\mu = \left(\mu_1, \ldots, \mu_{N_s} \right)^T$, $\left(V \right)_{rs} = v_{rs}$, $\alpha = \left(\alpha_1, \ldots, \alpha_{N_r} \right)^T$,

$\alpha'' = \left(\alpha_1'', \ldots, \alpha_{N_r}'' \right)^T$, $\left(\alpha_r'' \right)_{mn} = \frac{\partial^2 \alpha_r(\mathbf{X})}{\partial X_m \partial X_n}$, $\alpha_r'' \odot \sigma = \sum_{m,n=1}^{N_s} \frac{\partial^2 \alpha_r(\mathbf{X})}{\partial X_m \partial X_n} |_{\mathbf{X}=\boldsymbol{\mu}} \sigma_{mn}$,

$\alpha'' \odot \sigma \triangleq \left(\alpha_1'' \odot \sigma, \ldots, \alpha_{N_r}'' \odot \sigma \right)^T$, $\alpha' = (\alpha_1', \ldots, \alpha_{N_r}')$, $\alpha_r' = \left(\frac{\partial \alpha_r(\boldsymbol{\mu})}{\partial X_1}, \ldots, \frac{\partial \alpha_r(\boldsymbol{\mu})}{\partial X_{N_s}} \right)^T$,

and Λ is a diagonal matrix with $\left(\Lambda \right)_{rr} = \alpha_r(\boldsymbol{\mu}) + \frac{1}{2} \sum_{m,n=1}^{N_s} \frac{\partial^2 \alpha_r(\boldsymbol{\mu})}{\partial X_m \partial X_n} \sigma_{mn}$.

1.4 Statistic criteria for propensity adjustment

Assuming that an equation-based model captures the average behaviour and one intend to find propensity function for stochastic simulation that will reproduce that means. One can use the 95% confidence interval to evaluate the need of propensity adjustment. Specifically, for stable systems that will reach a steady state, if the steady state of the ODEs x_{st} is within the 95% confidence interval *n* runs of stochastic simulations, i.e.

$x_{st} \in \left[\mu_{st} - 1.96\frac{\delta_{st}}{\sqrt{n}}, \mu_{st} + 1.96\frac{\delta_{st}}{\sqrt{n}} \right]$, then the rate function in the equation-based model can be used as the propensity without adjustment; otherwise propensity adjustment is needed. Here μ_{st} and δ_{st} can be attained from either moment-base method or n independent runs of stochastic simulation using propensity without adjustment. An example can be found at the result section: reversible reaction with feedback controls.

For other systems that do not reach steady state but certain features of transient behavior are of the highest interest, one can judge the need of propensity adjustment by whether the features of the equation-based model lay within the 95% confidence interval of the corresponding characteristic given by moment-base prediction or n runs of stochastic simulations. The repressilator example in the result section will be a demonstration.

3.Results

3.1. Generic special cases

It is generally not valid to translate a rate from a deterministic biochemical model into a propensity function of the corresponding stochastic simulation without adjustment (see Equations. (34)-(36)). However, in some situations, the propensity adjustment (*e.g.*, Equations (40)-(44)) is not needed, and in some other cases it becomes relatively simple.

1) 0^{th}-order reaction kinetics

Consider a very simple equation-based model of the type

$$\frac{d\left[X_s(t)\right]}{dt} = k_r \text{ or } \frac{dE\left[X_s(t)\right]}{dt} = k_r \Phi, \tag{47}$$

for all $s = 1, \ldots, N_s$, $f_{rs} = 0$. According to Equations (40)-(44), one obtains

$\Omega_r = 0$

$\sigma_{\alpha_r}{}^2 \approx 0$

$\mu_{\alpha_r} \approx \exp\left(\log\left(k_r \Phi\right)\right) = k_r \Phi$ i.e. $E\left[\alpha_r(\mathbf{X})\right] \approx \alpha_r\left(E\left[\mathbf{X}\right]\right)$

$\alpha_{r\_\mathrm{cov}} \approx k_r \Phi = \alpha_{r\_0}$.

Thus, for a 0^{th}-order reaction, its rate equation can be taken directly as the propensity function in stochastic simulations.

2) 1^{st}-order reaction kinetics

Direct application of Eqs. (40)-(44) yields

$$\frac{d\left[X_i(t)\right]}{dt} = k_r\left[X_j(t)\right] \text{ or } \frac{dE\left[X_i(t)\right]}{dt} = k_r E\left[X_j(t)\right], \tag{48}$$

$f_{rs} = \delta_{sj}$, $i, j = 1, \ldots, N_s$. Therefore, according to Equations (40)-(44)

$\Omega_r = \left(\sigma_j / \mu_j\right)^2$

$\left(\sigma_{\alpha_r} / \mu_{\alpha_r}\right)^2 = \left(\sigma_j / \mu_j\right)^2$

$\mu_{\alpha_r} \approx \exp\left(\log\left(k_r \mu_j\right)\right) = k_r \mu_j$ i.e. $E\left[\alpha_r(\mathbf{X})\right] \approx \alpha_r\left(E\left[\mathbf{X}\right]\right)$

$\alpha_{r\_\mathrm{cov}}(\mathbf{X}) \approx k_r X_j = \alpha_{r\_0}(\mathbf{X})$.

Thus, for 1^{st}-order reactions, the rate equation can again be taken directly as the propensity function in stochastic simulations.

3) Real-valued order monomolecular reaction kinetics

Consider a reaction with kinetics of the type

$$\frac{d\left[X_i(t)\right]}{dt} = k_r\left[X_j(t)\right]^{f_{rj}} \text{ or } \frac{dE\left[X_i(t)\right]}{dt} = k_r\Phi^{1-f_{rj}}E\left[X_j(t)\right]^{f_{rj}}, \qquad (49)$$

$f_{rj} \neq 0, f_{rs} = 0$, for any $s \neq j, s = 1,\ldots,N_s$. Equations (40)-(44) lead to

$$\Omega_r = \left(\sigma_j/\mu_j\right)^2$$
$$\left(\sigma_{\alpha_r}/\mu_{\alpha_r}\right)^2 = \left(\sigma_j/\mu_j\right)^2$$
$$\mu_{\alpha_r} \approx k_r\Phi^{1-f_{rj}}\mu_j^{f_{rj}} \text{ i.e. } E\left[\alpha_r(\mathbf{X})\right] \approx \alpha_r\left(E\left[\mathbf{X}\right]\right)$$
$$\alpha_{r\_\mathrm{cov}}\left(\mathbf{X}\right) \approx k_r\Phi^{1-f_{rj}}X_j^{f_{rj}} = \alpha_{r\_0}\left(\mathbf{X}\right).$$

Thus, for reaction kinetics involving a single variable and a real-valued order, the rate equation can again be taken as the propensity function in stochastic simulations.

4) 2nd-order reaction kinetics

This type of reaction can be expressed as

$$\frac{d}{dt}\left[X_s(t)\right] = k_r\left[X_i(t)\right]\left[X_j(t)\right] \text{ or } \frac{dE\left[X_s(t)\right]}{dt} = k_r\Phi^{-1}E\left[X_i(t)\right]E\left[X_j(t)\right], \quad (50)$$

$i, j \in \{1,\ldots,N_s\}, i \neq j, f_{ri} = f_{rj} = 1,$ and $f_{rs} = 0,$ for all $s \neq i, j.$ Therefore, according to Equations (40)-(44)

$$\Omega_r = \left(\sigma_i/\mu_i\right)^2 + \left(\sigma_j/\mu_j\right)^2 + 2\,\mathrm{cov}\left[\log X_i, \log X_j\right]$$
$$= \left(\sigma_i/\mu_i\right)^2 + \left(\sigma_s/\mu_s\right)^2 + 2\{\mathrm{cov}\left[X_i/\mu_i, X_j/\mu_j\right]$$
$$+\frac{1}{2}\log(\mu_i)\left(\sigma_j/\mu_j\right)^2 + \frac{1}{2}\log(\mu_j)\left(\sigma_i/\mu_i\right)^2 - \frac{1}{4}\left(\sigma_i/\mu_i\right)^2\left(\sigma_j/\mu_j\right)^2\}$$

$$\left(\sigma_{\alpha_r}/\mu_{\alpha_r}\right)^2 = \Omega_r = \left(\sigma_i/\mu_i\right)^2 + \left(\sigma_j/\mu_j\right)^2 + 2\,\mathrm{cov}\left[\log X_i, \log X_j\right]$$
$$\mu_{\alpha_r} \approx k_r(N_AV)^{-1}\mu_i\mu_j$$
$$\alpha_{r\_\mathrm{cov}}(\mathbf{X}) = k_r\Phi^{-1}X_iX_j\exp\left(-\mathrm{cov}\left[\log X_i, \log X_j\right]\right) \neq \alpha_{r\_0}(\mathbf{X}).$$

Thus, the proper propensity function for 2nd-order reactions is different from the rate equation. The difference can be ignored only if the contribution from the covariance is

insignificant. In general, the rate equation yields only an approximate propensity function for stochastic simulations, and the approximation quality must be assessed on a case-by-case basis.

5) Bimolecular reaction with real-valued order kinetics

This type of reaction can be formulated as

$$\frac{d\left[X_s(t)\right]}{dt} = k_r \left[X_i(t)\right]^{f_i} \left[X_j(t)\right]^{f_j} \text{ or } \frac{dE\left[X_s(t)\right]}{dt} = k_r \Phi^{1-f_i-f_j} E\left[X_i(t)\right]^{f_i} E\left[X_j(t)\right]^{f_j}, \quad (51)$$

$i, j \in \{1,\ldots,N_s\}, i \neq j, f_{ri}, f_{rj} \neq 0,$ and $f_{rs} = 0,$ for all $s \neq i, j.$ According to Equations (40)-(44) we obtain

$$\Omega_r = \left(\sigma_i/\mu_i\right)^2 + \left(\sigma_j/\mu_j\right)^2 + 2 f_i f_j \operatorname{cov}\left[\log X_i, \log X_j\right]$$
$$= \left(\sigma_i/\mu_i\right)^2 + \left(\sigma_j/\mu_j\right)^2 + 2 f_i f_j \{\operatorname{cov}\left[X_i/\mu_i, X_j/\mu_j\right]$$
$$+ \frac{1}{2}\log(\mu_i)\left(\sigma_j/\mu_j\right)^2 + \frac{1}{2}\log(\mu_j)\left(\sigma_i/\mu_i\right)^2 - \frac{1}{4}\left(\sigma_i/\mu_i\right)^2\left(\sigma_j/\mu_j\right)^2\}$$

$$\left(\sigma_{\alpha_r}/\mu_{\alpha_r}\right)^2 = \Omega_r = \left(\sigma_i/\mu_i\right)^2 + \left(\sigma_j/\mu_j\right)^2 + 2 f_i f_j \operatorname{cov}\left[\log X_i, \log X_j\right]$$
$$\mu_{\alpha_r} \approx k_r \Phi^{f_i+f_j-1} \mu_i^{f_i} \mu_j^{f_j}$$
$$\alpha_{r\_\mathrm{cov}}(\mathbf{X}) = k_r \Phi^{f_i+f_j-1} X_i^{f_i} X_j^{f_j} \exp\left(-f_i f_j \operatorname{cov}\left[\log X_i, \log X_j\right]\right) \neq \alpha_{r\_0}(\mathbf{X}).$$

For bimolecular reactions of complex order, the propensity function is different from the rate equation. The difference can be ignored only if the contribution from the covariance is insignificant.

3.2 Power-law representation of a reversible reaction with feedback controls

We consider a reversible reaction with feedback controls (see Figure 1) whose average behaviour is accurately described by the following GMA model

$$\begin{aligned}&\frac{dx_1}{dt}=\frac{dx_2}{dt}=-\frac{dx_3}{dt}\\&=-k_f\Phi^{1-f_1-f_2-f_3}x_1^{f_1}x_2^{f_2}x_3^{f_3}+k_b\Phi^{1-g_1-g_3}x_1^{g_1}x_3^{g_3}.\end{aligned}\tag{52}$$

Here S_3 feeds back to inhibit the forward reaction and S_1 feeds back on the backward reaction and accelerates it. The task is to develop a stochastic model whose performance converges to that of the deterministic GMA model. We can see from equations (52) that three variables x_1, x_2 and x_3 contribute to the forward flux $k_f\Phi^{1-f_1-f_2-f_3}x_1^{f_1}x_2^{f_2}x_3^{f_3}$ and two variables x_1 and x_3 contribute to the backward flux $k_b\Phi^{1-g_1-g_3}x_1^{g_1}x_3^{g_3}$. Because several variables are involved, their covariance has the potential of affecting the forward and the backward propensity functions in a stochastic simulation. To obtain the covariance information, we formulate the moment equations (53) from the ODE model (52).

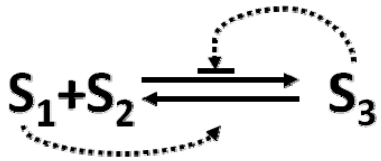

Figure 5.1 Scheme of reversible reaction with feedback controls

To simplify the calculation, as explained in detail in Additional file 2, we set the third central moment to zero and obtain a closed-form set of ODEs. Expressed differently, the rate of change in mean and covariance depends only on the functions of mean and covariance themselves, but not on higher-order moments. Thus,

$$\begin{aligned}&\frac{\partial\mu}{\partial t}\approx V^T\left(\alpha+\frac{1}{2}\alpha''\odot\sigma\right)\\&\frac{\partial\sigma}{\partial t}\approx\left(\sigma\left(\alpha' V\right)\right)^T+\sigma\left(\alpha' V\right)+V^T\Lambda V.\end{aligned}\tag{53}$$

Here $\mu = (\mu_1, \mu_2, \mu_3)^T, V = \begin{bmatrix} -1 & -1 & 1 \\ 1 & 1 & -1 \end{bmatrix}, \alpha = (\alpha_1, \alpha_2)^T = \begin{bmatrix} k_f \Phi^{1-f_1-f_2-f_3} x_1^{f_1} x_2^{f_2} x_3^{f_3} \\ k_b \Phi^{1-g_1-g_3} x_1^{g_1} x_3^{g_3} \end{bmatrix}$.

Moreover, for $r = 1, 2$ and $m, n = 1, 2, 3, (\alpha_r")_{mn} = \dfrac{\partial^2 \alpha_r(\mathbf{X})}{\partial x_m \partial x_n}, \alpha" = (\alpha_1", \alpha_2")^T$,

$\sigma = \begin{bmatrix} \sigma_{11} & \sigma_{12} & \sigma_{13} \\ \sigma_{21} & \sigma_{22} & \sigma_{23} \\ \sigma_{31} & \sigma_{32} & \sigma_{33} \end{bmatrix}, \alpha_r" \odot \sigma \triangleq \sum_{m,n=1}^{3} \dfrac{\partial^2 \alpha_r(\mathbf{X})}{\partial x_m \partial x_n}|_{\mathbf{X}=\boldsymbol{\mu}} \sigma_{mn}$, $\alpha" \odot \sigma \triangleq (\alpha_1" \odot \sigma, \alpha_2" \odot \sigma)^T$,

$\alpha' = (\alpha_1', \alpha_2'), \alpha_r' = \left(\dfrac{\partial \alpha_r(\boldsymbol{\mu})}{\partial x_1}, \dfrac{\partial \alpha_r(\boldsymbol{\mu})}{\partial x_2}, \dfrac{\partial \alpha_r(\boldsymbol{\mu})}{\partial x_3} \right)^T$, and

$$\Lambda = \begin{bmatrix} \alpha_1(\boldsymbol{\mu}) + \dfrac{1}{2} \sum_{m,n=1}^{3} \dfrac{\partial^2 \alpha_1(\boldsymbol{\mu})}{\partial x_m \partial x_n} \sigma_{mn} & 0 \\ 0 & \alpha_2(\boldsymbol{\mu}) + \dfrac{1}{2} \sum_{m,n=1}^{3} \dfrac{\partial^2 \alpha_2(\boldsymbol{\mu})}{\partial x_m \partial x_n} \sigma_{mn} \end{bmatrix}.$$

Two initial conditions are chosen for representative simulations; they differ by a factor of 20 in species populations and reaction volume between the upper and lower panels of Figure 2. The purpose is to observe the thermodynamic limit of the systems: both scenarios have the same initial concentrations, but the system in the lower panel case has a larger species populations and reaction volume and can thus be regarded as the thermodynamic limit sample of system in the upper panel. As demonstrated by the figures in the first column, the moment approach predicts that for both population sizes the average trajectories of the stochastic model (without propensity adjustment) dynamics is lower than that of the equation-based model: the differences are about 10% of steady state value of the equation-based model in the upper figure and 1% in the lower figure; for 100 runs of stochastic simulation, the steady state value of the equation-based model lays outside of the 95% confidence interval in the upper figure while it is inside in the lower figure. Therefore, we can expect that the propensity adjustment will significantly contribute to the stochastic simulation for the upper case while not for the lower case. This expectation is confirmed by the simulation results in the third and fourth columns.

With the common assumption that the deterministic equations precisely capture the system's average behaviour, the case in the upper panel represents the situation where propensity adjustment is needed, while the lower panel represents the situation that a propensity without adjustment is sufficient when the system approaches its thermodynamics limit. This example furthermore demonstrates that either the moment approach or the stochastic simulations without propensity adjustment can be used to estimate whether there is a need to construct a propensity adjustment function for stochastic simulations.

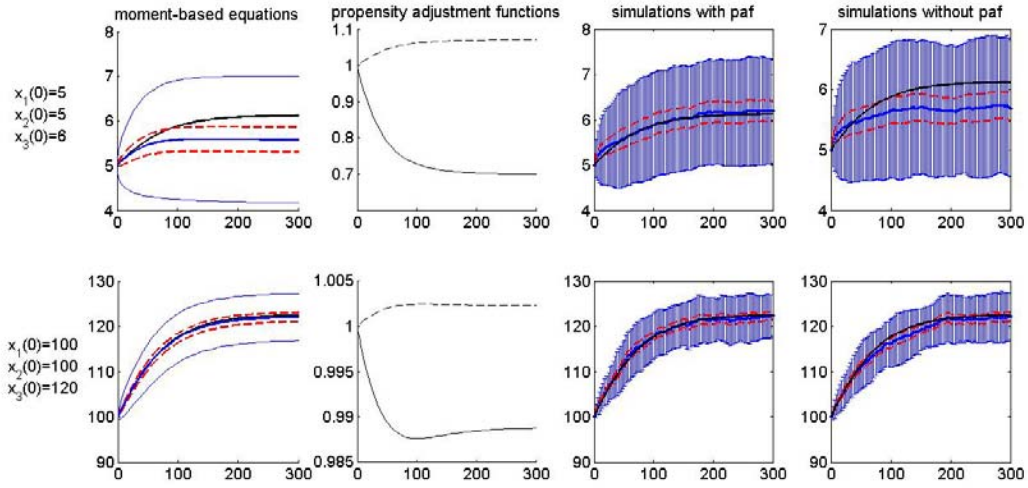

Figure 5.2 Reversible reaction with feedback controls

In all panels, the *y*-axis represents the copy number of a species and the *x*-axis denotes time in seconds. The upper panels and the lower panels use two different sets of initial conditions: $\left(x_1(0), x_2(0), x_3(0), U\right) = \left(5, 5, 6, 1\mu m^3\right)$ and $\left(x_1(0), x_2(0), x_3(0), U\right) = \left(100, 100, 120, 20\mu m^3\right)$, respectively. Other simulation parameters are $\left(f_1, f_{2,} f_3, g_1, g_3, k_f, k_g\right) = \left(1.3, 1.8, -1, 1, 1, 0.5, 0.5\right)$. In both the upper and lower panels, the first column compares the time evolution of S_1 molecules by different ODEs methods: the black line shows the solution of Equation (52) for x_1; the blue lines are the solutions of Equation (53) for μ_1 and $\mu_1 \pm \sigma_1$, respectively. The second column shows the propensity adjustment functions for the forward reaction (solid line) and the backward reaction (dashed line). The third column shows 100 independent stochastic

simulations with propensity adjustment (blue error bars), in comparison with the ODE (Equation (52)) prediction (black line). Fourth column: a second set of 100 independent stochastic simulations without propensity adjustment (blue error bars), in comparison with the ODE (Equation (52)) prediction (black line). The red dotted lines framing around mean by either moment-based method or stochastic simulation indicate the 95% confidence interval.

3.3 Repressilator

Interestingly, a propensity function may even be obtained through power-law approximation of some function that describes complex transient behaviours of a reaction network. As an example, consider the so-called *repressilator* (Elowitz and Leibler 2000), which is a three-component genetic circuit where each component represses its downstream neighbour. More specifically (as shown in Figure 3), gene G_1 codes for protein x_1, whose dimer y_1 subsequently represses the transcription of the gene G_2. Similarly, y_2, the dimer of gene G_2's protein product x_2, represses the transcription of gene G_3, and y_3, the dimer of gene G_3's protein product x_3, represses the transcription of gene G_1. The corresponding differential equation model following mass action kinetics is given by (Bennett, Volfson et al. 2007)

$$\begin{aligned}
x_i' &= -2\kappa_+ x_i^2 + 2\kappa_- y_i + \sigma m_i - \gamma_p x_i \\
y_i' &= \kappa_+ x_i^2 - \kappa_- y_i - k_+ y_i d_{0,j} + k_- d_{r,j} \\
d_{0,i}' &= -k_+ y_k d_{0,i} + k_- d_{r,i} \\
d_{r,i}' &= k_+ y_k d_{0,i} - k_- d_{r,i} \\
m_i' &= d_{0,i} - \gamma_m m_i,
\end{aligned} \tag{54}$$

where $i = 1,2,3;\ j = 2,3,1;\ k = 3,1,2;$ the rate constants are explained in the diagram below

$$x_i + x_i \underset{\kappa_-}{\overset{\kappa_+}{\rightleftharpoons}} y_i$$

$$d_{0,i} + y_k \underset{k_-}{\overset{k_+}{\rightleftharpoons}} d_{r,i}$$

$$d_{0,i} \xrightarrow{\alpha} d_{0,i} + m_i$$

$$m_i \xrightarrow{\sigma} m_i + x_i$$

$$x_i \xrightarrow{\gamma_p} \phi$$

$$m_i \xrightarrow{\gamma_m} \phi$$

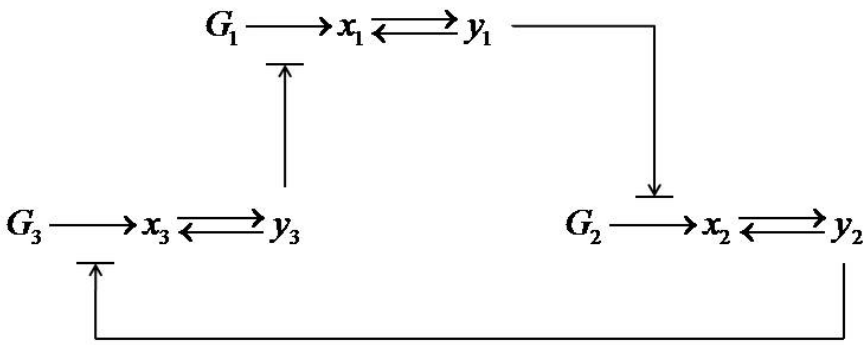

Figure 5.3 Reaction scheme of the *repressilator*

Gene G_1 codes for protein x_1, whose dimer y_1 subsequently represses the transcription of the gene G_2. Similarly, y_2, the dimer of gene G_2's protein product x_2, represses the transcription of gene G_3, and y_3, the dimer of gene G_3's protein product x_3, represses the transcription of gene G_1.

Assuming that the reversible dimerization and the dissociation/association of a protein dimer from/to the promoter are much faster than other processes, the full systems can be reduced to

$$x_i' = \sigma p(x_i)^{-1} m_i - \gamma_p p(x_i)^{-1} x_i$$
$$m_i' = \frac{\alpha d}{1 + c_d c_p x_k^{\,2}} - \gamma_m m_i \qquad (55)$$

(Bennett, Volfson et al. 2007).

Here $\Phi = 1, p(x_i) = 1 + 4c_p x_i + \frac{4c_d c_p dx_i}{(1 + c_d c_p x_i^{\,2})^2}, c_p = \kappa_+ / \kappa_-, c_d = k_+ / k_-$ and $d = d_{0,i} + d_{r,i}$ for i=1,2,3. It has been shown that the simplified ODEs rather accurately approximate the transient dynamics of the full system by retaining the original oscillation period and amplitude.

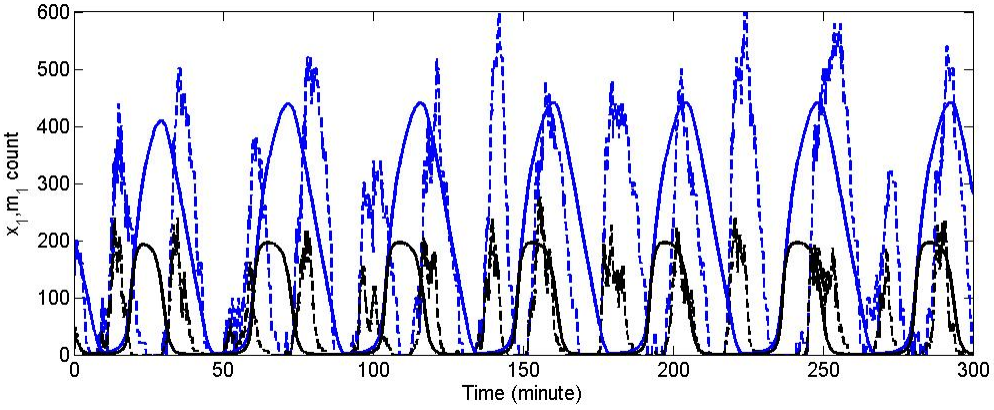

Figure 5.4 Scaling of the repressilator equations changes the oscillation period in the stochastic simulation

Solid lines represent solutions of ODEs (56), while dotted lines are trajectories of a stochastic simulation; blue lines represent x_1 and black lines represent m_1.

In (Bennett, Volfson et al. 2007), the system (55) is further rescaled by setting $\tilde{t} = \gamma_m t, \tilde{x}_i = \sqrt{c_d c_p}\, x_i$ and $\tilde{m}_i = \left(\sigma \sqrt{c_d c_p}\, m_i\right) \Big/ \left(\gamma_m \beta\right)$, which yields

$$\frac{d\tilde{x}_i}{d\tilde{t}} = \beta p(\tilde{x}_i)^{-1}\tilde{m}_i - \beta p(\tilde{x}_i)^{-1}\tilde{x}_i$$
$$\frac{d\tilde{m}_i}{d\tilde{t}} = \frac{\kappa d'}{1+\tilde{x}_k^{\ 2}} - \tilde{m}_i. \qquad (56)$$

Intriguingly, one makes the following observation. The scaled ODE system (56) is consistent with the original system (55) in oscillation amplitude and period. However, its corresponding stochastic model produces results that deviate substantially from the average responses. To see the effects of the transition from a deterministic to a stochastic model, we apply SSA to the scaled system (56). The main result is that the oscillation periods of both x_i and m_i are reduced to half (Figure 4). The reason is that, in the stochastic simulation, the oscillation period is very sensitive to the ratio of x_i and m_i, which has been altered by the scaling operation. Therefore, in general one needs to pay attention to how scaling may affect the stochastic performance when the model is generated through the conversion of an ODE model.

We can see from equations (55) that two variables x_i and m_i contribute to the production of x_i; hence, their covariance could affect the propensity function of x_i in the production reaction of a stochastic simulation. Similar to the example of a reversible reaction (Equation 52), it is therefore necessary to evaluate covariance effects and to judge whether the propensity function needs adjusting. Thus, we need to compare the difference between the dynamics of the phenomenological model (55) and the dynamics under the influence of covariance, which can be produced by either stochastic simulation or the moment approach.

Obtaining the covariance-influenced dynamics with the moment-based approach is complicated, and we need to discuss some implementation issues.

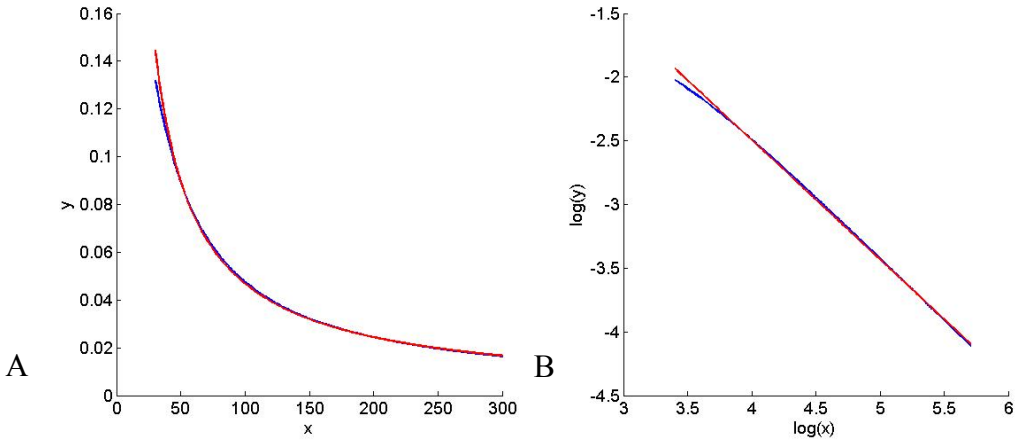

Figure 5.5 Power-law approximation of $p(x_i)^{-1}$

A: Approximation of $y_i = p(x_i)^{-1}$ by two straight lines in log-log space. B: Corresponding two-piecewise power-law function in Cartesian space. Both axes are unitless.

First, the moment-based approach requires information regarding the first and the second derivatives of $p(x_i)^{-1}$, which have rather complicated functional forms. To simplify the calculation, we replace the function $p(x_i)^{-1}$ with an approximating power-law function. Specifically, suppose the original parameter values are $\kappa_+ = k_+ = 5$, $\kappa_- = k_- = 100$ and $d = 20$. Plotting the data $\left(x_i, p(x_i)^{-1}\right)$ in log-log space (Figure 5.A) indicates that the original function is represented well by a straight line:

$$\log y_i = \log 3.5188 - 0.9384 \log x_i, \quad .$$

at $x_i \in [30, 300]$ In Cartesian space, this line corresponds to the power-law function

$$y_i = 3.5188 x_i^{-0.9384},$$

which models the original function very well (see Figure 5.B). For $x_i \in [1, 30]$, this power law function does not fit the original function precisely; the effect of this imprecision can be evaluated latter at after we use this power law function in the moment-based method.

Moreover, using the truncated moment equations to estimate the mean and variance involves multiple approximations: First, the function $p(x_i)^{-1}$ on the right-hand side of (55) is replaced by a power-law function (see Figure 5). Second, the result is approximated by Taylor expansion to the second order. Third, similar to the example of a reversible reaction, the central moment of the third degree is assumed to be zero, which leads to a closed-form ODE for the first two moments.

Solving the technical issues as described, one obtains the corresponding moment-based model of (55) (not shown) with results shown in the Figure 6. We assume that one's concerns are the period and amplitude of oscillation within of the time interval between 0 and 400 seconds. As show in Figure 6, the GMA approximation (black dashed line) fits the original ODEs (bold black solid line) very well at the beginning but as time goes on and the approximation error is accumulated. As seem at the time interval of [350, 400] the GMA approximation deviate from the original ODEs significantly. However, it does not mean that this GMA approximation can not be used as propensity function for stochastic simulation; the moment-base method based on the GMA approximation shows that when the GMA approximation is used as propensity function (without adjustment) for stochastic simulation, the resulted mean (red solid line) consistently fit the trajectory of the original ODEs (bold solid black line) very well up to T=400 second. The oscillation period and amplitude by the stochastic simulation based on the GMA approximation (without adjustment) are almost identical to those of the original ODEs. Therefore propensity adjustment for the GMA approximation is not needed; this GMA approximation can be use as propensity function for stochastic simulation

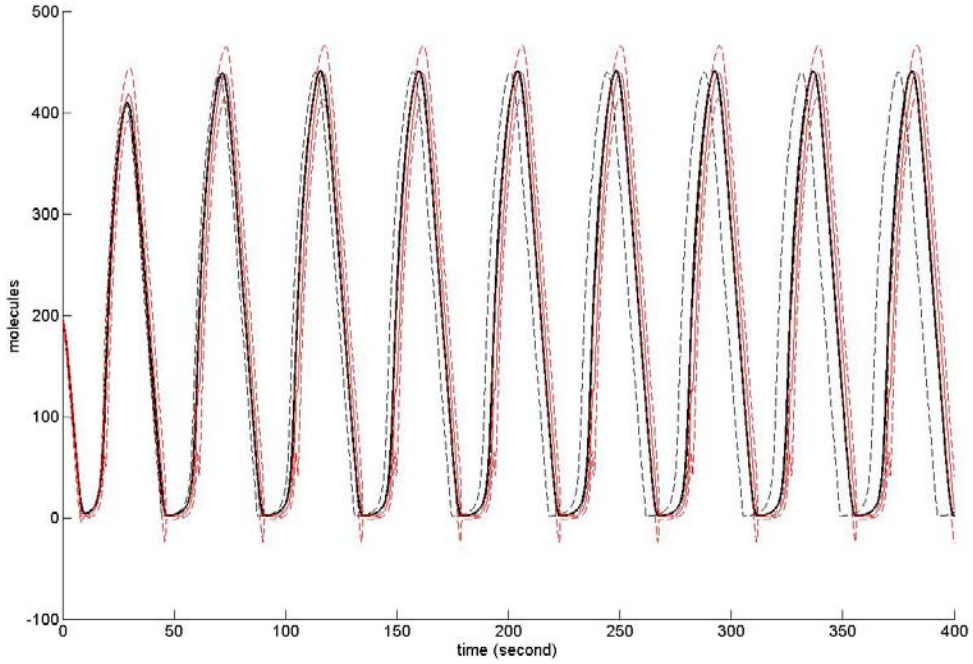

Figure 5.6 A comparison of the dynamics of repressilator using the original ODEs, GMA approximation and its corresponding moment-based ODEs. The mean of the moment-based ODEs based on the GMA approximation fits the original ODEs very well up to T=400s. Black bold line: original ODEs; black dashed line: the GMA approximation; Red line: mean of the moment-based ODEs based on the GMA approximation; red dashed line framing around the red line: standard deviations around the mean by moment-based ODEs. X-axis is time in second, Y-axis is the number of x_1 molecules without unit.

Therefore, a stochastic model for the repressilator system can be generated by using the scheme in (32) without propensity adjustment. Moreover, the imprecision caused by power law approximation can be tolerated when its corresponding moment-based mean matches well the original ODEs in the sense of the most interested features.

3.4 Enzymatic reaction using a quasi-steady state assumption (QSSA)

We consider an enzymatic reaction following the Michaelis-Menten mechanism:

$$E + S \underset{k_{-1}}{\overset{k_1}{\rightleftharpoons}} ES \xrightarrow{k_2} P + E.$$

Here enzyme E reacts with substrate S through a reversible reaction to form complex ES, which can proceed to yield product P and to release the enzyme E. By assuming the law of mass action for the reaction kinetics we obtain a set of differential equations for the system dynamics:

$$\begin{aligned}\frac{d[S]}{dt} &= k_{-1}[ES] - k_1[S]\left([E]_0 - [ES]\right)\\ \frac{d[ES]}{dt} &= k_1[S]\left([E]_0 - [ES]\right) - \left(k_1 + k_2\right)[ES]\\ \frac{d[P]}{dt} &= k_2[ES],\end{aligned} \tag{57}$$

where the total amount of enzyme in the form of free enzyme and complex $[E]_0 \triangleq [E] + [ES]$ is assumed to be constant. In addiction, by making the so-called *quasi steady state assumption* (QSSA) (Michaelis and Menten 1913; Segel 1988), assuming that the complex ES is essentially in steady state, we can assert $\frac{d[ES]}{dt} \approx 0$. As it has been discussed many times in the literature, QSSA reduces the system and leads to the approximate form

$$\begin{aligned}\frac{d[S]}{dt} &= -\frac{V_{\max}[S]}{K_m + [S]}\\ \frac{d[P]}{dt} &= \frac{V_{\max}[S]}{K_m + [S]},\end{aligned} \tag{58}$$

which is known as *Michaelis-Menten kinetics* (Michaelis and Menten 1913). The characterizing parameters are $V_{\max} = k_2[E]_0$ and $K_m = (k_{-1} + k_2)/k_1$.

Applying QSSA, Rao and Arkin (Rao and Arkin 2003) were able to reduce the CME of S and ES to a CME only containing S. For the reduced CME, the propensity function for the overall reaction $S \to P$ is

$$\alpha(s) = \frac{V_{\max} s}{K_m + s}, \tag{59}$$

where the volume was scaled so that $\Phi = 1$ and the lower-case letter s denotes the molecule count of species S. Instead of reviewing the relatively complicated manipulations with CME, we show in the following that the techniques described above lead directly from the equation-based model to the propensity function for the reduced system.

First, we recast the equation-based model into the GMA format (Savageau and Voit 1987), by introducing an auxiliary variable $[T] \triangleq K_m + [S]$. The result,

$$\begin{aligned} \frac{d[S]}{dt} &= -V_{\max}[S][T]^{-1} \\ \frac{d[T]}{dt} &= \frac{d[S]}{dt} = -V_{\max}[S][T]^{-1} \end{aligned} \tag{60}$$

is exactly equivalent to the reduced system in (58) with the initial condition $[S]_0$ and $[T]_0 = K_m + [S]_0$. The corresponding stochastic model has only one reaction channel and the propensity function is

$$\alpha(s,t) = V_{\max} s t^{-1}. \tag{61}$$

The propensity adjustment factor can be set to 1 because T is a function of s and its covariance with s is therefore 1. By applying $t = K_m + s$, the propensity function can be simplified as

$$\alpha(s,t) = V_{\max} s t^{-1} = V_{\max} s (K_m + s)^{-1} = \alpha(s). \tag{62}$$

Thus, we arrive at the propensity function for the reduced system, which is identical to the result of Rao and Arkin obtained through manipulations of CME.

In the above derivation, we used the simplest type of recasting, where a new, auxiliary variable simply consists of an old variable plus a constant. This reformulation of the Michaelis-Menten process as a pair of GMA equations is a special case of a much more general recasting technique that permits the equivalent conversion of any system of ordinary differential equations into a power-law format (Savageau and Voit 1987). However, this equivalence transformation imposes constraints on the variables of the GMA equations, and it is at this point unclear whether there are mathematical warranties ensuring that the proposed transition from differential to stochastic equations indeed preserves these constraints in all cases. This question will require further investigation.

3.5 Stochastic Focusing

Stochastic focusing (Paulsson, Berg et al. 2000) describes the phenomenon that the fluctuations of a chemical species can drive the system to reach a different steady state than what a deterministic ODE model predicts. To demonstrate the utility of propensity adjustment, we derive a stochastic model which produces consistent results with those of the deterministic model.

Following (Twomey 2007), we consider the following reactions system

$$\begin{aligned} &\phi \xrightarrow{k_1} I \xrightarrow{k_2} P \xrightarrow{k_3} \phi \\ &I + S \xrightarrow{k_4} S \\ &S \underset{k_5}{\overset{k_6}{\rightleftharpoons}} \phi \end{aligned} \tag{63}$$

This system can be interpreted as follows: the intermediate species I is produced at constant rate k_1 from some source ϕ and degrades with rate k_4 through the catalysis with signalling molecule S; the end product P is converted from species I at rate k_2 and degrades at rate k_3; the signalling molecule S is produced and degrades at rates k_5 and k_6, respectively. Moreover, the value of k_5 is reduced to half at a certain time point to

achieve a significant divergence effect. In order to capture the average dynamics of the system accurately, we use a power-law model in GMA format instead of the mass action rate law in (Twomey 2007).

$$\begin{aligned}\frac{di}{dt} &= k_1 - k_2 i - k_4 i^{f_I} s^{f_S} \\ \frac{dp}{dt} &= k_2 i - k_3 p \\ \frac{ds}{dt} &= k_5 - k_6 s\end{aligned} \tag{64}$$

The system size is set to 1. We can see from equations (64) that two variables i and s contribute to the degradation of I and that their covariance could therefore affect the propensity function of I in the degradation reaction of a stochastic simulation. To calculate the propensity adjustment function $paf_4(t) = \exp\left(-f_I f_S \operatorname{cov}\left[\log I(t), \log S(t)\right]\right)$ for reaction $R_4 : I + S \xrightarrow{k_4} S$, we formulate equations (*cf.* (60)) for the moments as

$$\begin{aligned}\frac{\partial \mu}{\partial t} &\approx V^T \left(\alpha + \frac{1}{2} \alpha'' \odot \sigma \right) \\ \frac{\partial \sigma}{\partial t} &\approx \left(\sigma\left(\alpha' V\right) \right)^T + \sigma\left(\alpha' V\right) + V^T \Lambda V.\end{aligned} \tag{65}$$

Here $\mu = (\mu_I, \mu_P, \mu_S)^T, V = \begin{bmatrix} 1 & 0 & 0 \\ -1 & 1 & 0 \\ 0 & -1 & 0 \\ -1 & 0 & 0 \\ 0 & 0 & 1 \\ 0 & 0 & -1 \end{bmatrix}, \alpha = \begin{bmatrix} \alpha_1 \\ \alpha_2 \\ \alpha_3 \\ \alpha_4 \\ \alpha_5 \\ \alpha_6 \end{bmatrix} = \begin{bmatrix} k_1 \\ k_2 i \\ k_3 p \\ k_4 i^{f_I} s^{f_S} \\ k_5 \\ k_6 s \end{bmatrix}$.

Moreover, for $r = 1, \ldots, 6$ and $m, n = i, p, s, (\alpha_r'')_{mn} = \dfrac{\partial^2 \alpha_r}{\partial m \partial n}, \alpha'' = (\alpha_1'', \ldots, \alpha_6'')^T$,

$\sigma = \begin{bmatrix} \sigma_{11} & \sigma_{12} & \sigma_{13} \\ \sigma_{21} & \sigma_{22} & \sigma_{23} \\ \sigma_{31} & \sigma_{32} & \sigma_{33} \end{bmatrix}, \alpha_r'' \odot \sigma = \sum_{m,n=i,p,s} \dfrac{\partial^2 \alpha_r(\boldsymbol{\mu})}{\partial m \partial n} \sigma_{mn}$, $\alpha'' \odot \sigma \triangleq (\alpha_1'' \odot \sigma, \ldots, \alpha_6'' \odot \sigma)^T$,

$\alpha' = (\alpha_1', \ldots, \alpha_6'), \alpha_r' = \left(\dfrac{\partial \alpha_r}{\partial i}, \dfrac{\partial \alpha_r}{\partial p}, \dfrac{\partial \alpha_r}{\partial s} \right)^T$, and the diagonal matrix Λ is defined by $(\Lambda)_{rr} = \alpha_r + \dfrac{1}{2} \sum_{m,n=i,p,s} \dfrac{\partial^2 \alpha_r}{\partial m \partial n} \sigma_{mn}$.

The stochastic focusing model without propensity adjustment yields results quite different from those of the deterministic model, as is illustrated in Figure 7. In this figure, the blue lines in the 1st panel are predicted from the moment equations (65) and the blue error bars for μ_P in the 2nd panel are obtained from ten independent stochastic simulations. Both diverge systematically from the black line predicted by ODE model (64). By contrast, the stochastic model with propensity adjustment produces results consistent with the deterministic model, as shown by the 4th panel.

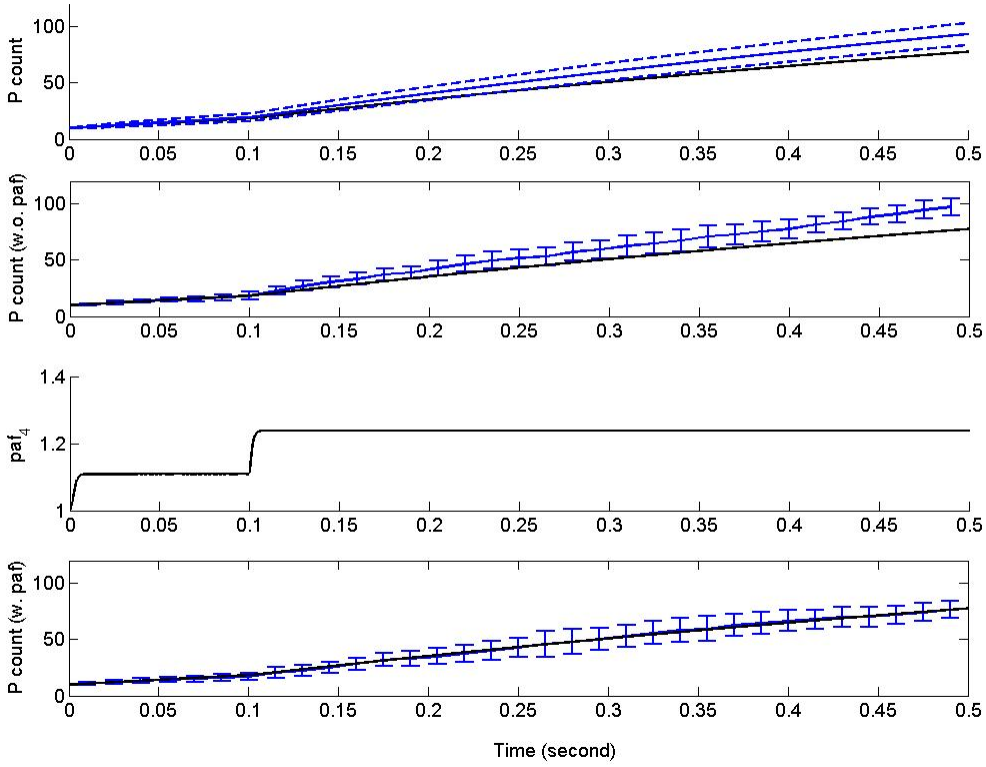

Figure 5.7 Stochastic focusing

The first panel compares the time evolution of product molecules P obtained with different methods: black line represents the solution of ODE model (64) for P; blue solid line and blue dashed lines are the solutions of moment-based model (65) for μ_P and $\mu_P \pm \sigma_P$, respectively. The second panel indicates that the stochastic simulations without propensity adjustment (blue error bar) diverge from the prediction by the ODEs model (64) (black line). The third panel shows the propensity adjustment function $paf_4(t) = \exp\left(-f_I f_S \operatorname{cov}\left[\log I(t), \log S(t)\right]\right)$ for the reaction $R_4 : I + S \xrightarrow{k_4} S$. The fourth panel shows that the propensity adjustment function paf_4 achieves convergence between the stochastic simulation and the ODE model (64) (black line): the blue error bar was computed from 100 independent stochastic simulations with propensity adjustment paf_4. The simulation parameters are $\left(i(0), p(0), s(0), k_1, k_2, k_3, k_4, k_5, k_6, f_I, f_S\right) = \left(0, 10, 100, 10^4, 10^3, 1, 9.9\times10^3, 10^4, 10^3, 1.1, 0.9\right)$; at t=0.1, the value of k_5 changes from 10^4 to 0.5×10^4.

Discussion and Conclusion

Gillespie's stochastic simulation algorithm (SSA), as well as later variants, permits three kinds of elementary reactions to be modelled: 0^{th}, 1^{st} and 2^{nd} order reactions that are assumed to follow the law of mass action. All other types of reactions, containing non-integer kinetic orders and/or following other types of kinetic law, are assumed to be convertible to one of these three kinds, so that SSA can validly be applied. However, the conversion to elementary reactions is often difficult, infeasible, or simply impossible. First, the kinetic parameters of the underlying elementary reactions are in many cases unknown for a complex-order reaction. Second, even when all elementary kinetic parameters are available, the multitude of reaction channels and participating species creates a combinatorial complexity that renders SSA simulations computationally impractical. Within a deterministic framework, model reduction is a possible and often-used strategy to address such challenges. For example, a reduced mechanistic model, such as the Michaelis-Menten rate law, is often proposed to fit the experimental data, at the cost of sacrificing the original mechanistic interpretation. The reduction in these cases simplifies the original formulation by approximating, merging, or omitting intermediate reaction steps and reactants. It would be beneficial to adopt a similar reduction strategy to stochastic modelling. However, we have shown here that caution is necessary.

We have shown that the direct use of a rate constant or a rate function f as the propensity function in a stochastic simulation algorithm requires that at least one of the following assumptions be true:

1) f is a linear function; this assumption has been validated in the Results sections addressing 0^{th}-order and 1^{st}-order reaction kinetics.

2) the reaction is monomolecular; this assumptions was evaluated in the Results section describing real-valued order monomolecular reaction kinetics.

3) all X_i in the system are noise-free variables, *i.e.*, without (or with ignorable) fluctuations; this assumption implies that the covariance of any two participating reactants is zero (or close to zero). This assumption is assessed in equations (29 - 36).

Each of these three conditions is a sufficient condition for the direct use of a rate function *f* as the propensity function. Moreover, these statements are valid for function of general format, not just for GMA. This is so because the functional formats in cases 1 and 2 above are special cases of the GMA format. For the third case, a formal proof is only given for functions in GMA format, because this structured format allows us to give an explicit estimation on how the covariance can affect the average behavior of a stochastic simulation through equation (34). For functions not in GMA format, the conclusion is still holds, although an analogous explicit estimation is lacking. The argument is as follows. The bimolecular reaction $E\left[\alpha_r(\mathbf{X}(t))\right]$ contains at least one quadratic moment of the form $E\left[X_i(t)X_j(t)\right]$ (*cf.* (Gillespie 2007) and page 38). Therefore, by definition of the covariance, $E\left[X_i(t)X_j(t)\right] = E\left[X_i(t)\right]E\left[X_i(t)\right] + \mathrm{cov}\left(X_i(t), X_j(t)\right)$, we obtain

$E\left[X_i(t)X_j(t)\right] = E\left[X_i(t)\right]E\left[X_i(t)\right] \Leftrightarrow \ \mathrm{cov}\left(X_i(t), X_j(t)\right) = 0$.

This result implies the following: If the covariance between every pair of random variables is zero (or ignorable), $E\left[X_i(t)X_j(t)\right] = E\left[X_i(t)\right]E\left[X_i(t)\right]$ and therefore $E\left[\alpha_r(\mathbf{X}(t))\right] = \alpha_r(E\left[\mathbf{X}(t)\right])$. Expressed in words, the expectation of the propensity function on left-hand side of equation (29) equals its rate function, and the rate function can be directly used as propensity function in stochastic simulations.

If at least one of the three assumptions is satisfied, the stochastic simulation algorithm (SSA) is applicable without changes.

In the past, efforts have been made to manipulate the chemical master equation (CME) in order to achieve a proper propensity function for a reduced system (*e.g.*, see (Rao and Arkin 2003)). However, manipulations of CME are usually complicated, and successes have been modest and rare. Here we propose an alternative strategy for converting a reduced dynamical model into a stochastic analogue. To achieve this conversion, we addressed two fundamental issues: First, under what conditions can a deterministic, equation-based model be validly used in stochastic simulations? And second, what is a proper strategy to implement such a conversion?

To address the first question, we showed that the following steps are necessary:

(1) A concentration-based model needs to be converted into a particle-based model by accounting for the size of the system; if the concentration-based model is scaled (as was illustrated with the repressilator example), it may first have to be un-scaled in order to render the conversion valid;

(2) The difference between the mean of a stochastic model without propensity adjustment and the corresponding quantities of the equation-based model should be evaluated. The mean of the stochastic model is obtained either through stochastic simulations or through a moment-based approach. If the difference is significant, then an adjustment of the propensity function for a non-elementary reaction is necessary.

To answer the second question, we need to execute the following steps

(3) Compute a propensity adjustment function, either through simulated or experimental data or through a moment-based approach, in order to achieve the corrected propensity function (41);

(4) Apply SSA or one of its variants using a propensity function with adjustment to obtain valid simulation trajectories.

When the propensity needs adjusting, an accurate propensity adjustment function (*paf*) is essential for obtaining the proper correction of the propensity. It is usually impossible to compute *paf* exactly, which necessitates a suitable approximation. The approximation error in *paf* originates from the following sources:

1) The expression of *paf* in Equation (40) is a function of the mean, variance, and covariance, which are computed with a 2^{nd}-order Taylor expansion in log space.

2) The moment-based approach, from which the functions of mean, variance and covariance are usually derived, is an approximation method that yields a closed ODE system for the moments. In the method used here, the propensity function is approximated by a 2^{nd}-order Taylor expansion, and the moments up to a certain degree (2 in our treatment) are retained, while all higher moments are assumed to be zero. One might expect that a higher-order Taylor expansion would improve the accuracy of *paf*, but it would come with a much higher computational cost. The error control of *paf* and the relative computational issues should be addressed in future studies.

Since computation cost is a major concern with the stochastic simulation of large biochemical reaction networks, another issue has yet to be addressed. Namely, how does the propensity function of a reduced system affect the accuracy and efficiency of various leaping methods that have been proposed to speed up SSA? Moreover, the question of

molecular population sizes requires further analysis. Our derivation assumed large reactant populations, but simulations of a reversible pathway indicated that the method works rather well even for small populations. A more careful investigation of this issue of population size in different scenarios is still needed and should be the subject of further research.

Authors' contribution

JW developed the mathematical derivations, designed and performed the simulation, and drafted the manuscript. BV contributed to the statistical reasoning and revised the manuscript. EV supervised the research and revised the manuscript. All authors read and approved the final manuscript.

Acknowledgements

The authors thank Dr. Yi Jiang for useful comments and for providing seminal references. The authors also appreciate Dr. Mukhtar Ullah's and Dr. Olaf Wolkenhauer's insightful comments and conceptual clarifications. This work was supported in part by a Molecular and Cellular Biosciences Grant (MCB-0946595; E.O. Voit, PI) from the National Science Foundation. Any opinions, findings, and conclusions or recommendations expressed in this material are those of the authors and do not necessarily reflect the views of the sponsoring institutions.

Appendixes

Appendix A–Derivation of the mean and variance of a power-law function of random variables

Appendix B –Computation of approximate mean and covariance for a generic propensity function to be used in stochastic simulations

References

1. Gillespie, D., *Exact Stochastic Simulation of Coupled Chemical Reactions.* J Phys Chem, 1977. 81(25): p. 2340 - 2361.

2. Rao, C.V. and A.P. Arkin, Stochastic chemical kinetics and the quasi-steady-state assumption: Application to the Gillespie algorithm. The Journal of chemical physics, 2003. 118(11): p. 4999-5010.

3. Cao, Y., D.T. Gillespie, and L.R. Petzold, Multiscale stochastic simulation algorithm with stochastic partial equilibrium assumption for chemically reacting systems. J. Comput. Phys., 2005. 206: p. 395.

4. Gillespie, D.T., *Stochastic simulation of chemical kinetics.* Annual Review of Physical Chemistry, 2007. 58: p. 35-55.

5. Tian, T. and K. Burrage, *Stochastic models for regulatory networks of the genetic toggle switch.* Proc Natl Acad Sci U S A, 2006. 103(22): p. 8372-7.

6. Gomez-Uribe, C.A. and G.C. Verghese, Mass fluctuation kinetics: Capturing stochastic effects in systems of chemical reactions through coupled mean-variance computations. The Journal of chemical physics, 2007. 126(2): p. 024109-12.

7. Lee, C.H., K.-H. Kim, and P. Kim, *A moment closure method for stochastic reaction networks.* The Journal of chemical physics, 2009. 130(13): p. 134107-15.

8. Singh, A. and J. Hespanha. LogNormal Moment Closures for Biochemical Reactions. in In Proc. of the 45th Conf. on Decision and Contr. 2006.

9. Milner, P., C.S. Gillespie, and D.J. Wilkinson, *Moment closure approximations for stochastic kinetic models with rational rate laws.* Mathematical Biosciences, 2011. 231(2): p. 99-104.

10. Chevalier, M.W. and H. El-Samad, *A rigorous framework for multiscale simulation of stochastic cellular networks.* The Journal of chemical physics, 2009. 131(5): p. 054102-17.

11. Voit, E.O., Computational analysis of biochemical systems: a practical guide for biochemists and molecular biologists. Vol. xii. 2000: Cambridge University Press.

12. Savageau, M.A., Biochemical systems analysis. I. Some mathematical properties of the rate law for the component enzymatic reactions. Journal of Theorectical Biology, 1969 a. 25(3): p. 365-9.

13. Savageau, M.A., Biochemical systems analysis. A study of function and design in molecular biology. Vol. xvii. 1976: Addison-Wesley.

14. Savageau, M., *Michaelis-Menten mechanism reconsidered: implications of fractal kinetics.* Journal of Theoretical Biology, 1995. 176(1): p. 115-124.

15. Savageau, M.A., *Influence of fractal kinetics on molecular recognition.* Journal of Molecular Recognition, 1993. 6(4): p. 149-157.

16. Bajzer, Z., et al., Mathematical analysis of models for reaction kinetics in intracellular environments. Mathematical Biosciences, 2008. 215(1): p. 35-47.

17. Neff, K.L., Biochemical reaction kinetics in dilute and crowded solutions: Predictions of macroscopic and mesoscopic models and experimental observations. 2010, Mayo Clinic: Rochester, MN.

18. Neff, Kevin L., et al., Validation of Fractal-Like Kinetic Models by Time-Resolved Binding Kinetics of Dansylamide and Carbonic Anhydrase in Crowded Media. Biophysical journal, 2011. 100(10): p. 2495-2503.

19. Chou, I.-C. and E.O. Voit, Recent developments in parameter estimation and structure identification of biochemical and genomic systems. Math. Biosc. , 2009. 219: p. 57-83.

20. Walton, R.J., et al., *Biochemical measurements in Paget's disease of bone.* European Journal of Clinical Investigation, 1977. 7(1): p. 37-39.

21. Koch, A.L., The logarithm in biology 1. Mechanisms generating the log-normal distribution exactly. Journal of Theoretical Biology, 1966. 12(2): p. 276-290.

22. Limpert, E., W.A. Stahel, and M. Abbt, *Log-normal Distributions across the Sciences: Keys and Clues.* BioScience, 2001. 51(5): p. 341.

23. Law, A.M. and W.D. Kelton, *Simulation Modeling and Analysis*. 3 ed. 2000, Boston: Mc.Graw Hill.

24. Gillespie, D. and L. Petzold, *Numerical Simulation for Biochemical Kinetics*, in *In System Modelling in Cellular Biology*, Z. Szallasi, J. Stelling, and V. Periwal, Editors. 2006, MIT Press.

25. Wolkenhauer, O., et al., *Modelling and Simulation of IntraCellular Dynamics: Choosing an Appropriate Framework* IEEE Transactions on NanoBioscience, 2004. 3: p. 200-207.

26. Paulsson, J., O.G. Berg, and M. Ehrenberg, *Stochastic focusing: Fluctuation-enhanced sensitivity of intracellular regulation.* Proceedings of the National Academy of Sciences, 2000. 97(13): p. 7148-7153.

27. Elowitz, M.B. and S. Leibler, *A synthetic oscillatory network of transcriptional regulators.* Nature, 2000. 403(6767): p. 335-338.

28. Bennett, M.R., et al., *Transient Dynamics of Genetic Regulatory Networks.* Biophysical journal, 2007. 92(10): p. 3501-3512.

29. Segel, L.A., On the validity of the steady state assumption of enzyme kinetics. Bull. Math. Biol. , 1988. 50: p. 579-593.

30. Michaelis, L. and M.L. Menten, *Die Kinetik der Invertinwirkung.* Biochem. Zeitschrift 1913. 49: p. 333-369.

31. Savageau, M.A. and E.O. Voit, Recasting Nonlinear Differential-Equations As S-Systems - A Canonical Nonlinear Form. Mathematical Bioscience, 1987. 87: p. 83-115.

32. Twomey, A., On the Stochastic Modelling of Reaction-Diffusion Processes. 2007, University of Oxford.

PAPER 5

CHAPTER 6

Stochastic 3-D Simulation for Diffusion-Controlled Reactions with Concentration-Dependent Kinetic Rates in Crowded Environments

Jialiang Wu, Eberhard O. Voit

(Submitted to *Biophysical Journal*)

Stochastic 3-D Simulations for Diffusion-Controlled Reactions with Concentration-Dependent Kinetic Rates in Crowded Environments

Jialiang Wu[1], Eberhard O. Voit[2,3§]

[1]Department of Mathematics, Bioinformatics Program, Georgia Institute of Technology, Atlanta, GA 30332, USA

[2] The Wallace H. Coulter Department of Biomedical Engineering, Georgia Institute of Technology, Atlanta, GA 30332, USA

[3]Integrative BioSystems Institute, Georgia Institute of Technology, Atlanta, GA 30332, USA

[§]Corresponding author

Email addresses:

JW: wjl@gatech.edu

EV: eberhard.voit@bme.gatech.edu

November 2011

Keywords: Agent-based model, Biochemical Systems Theory, Crowding, Generalized Mass Action kinetics, Stochastic simulation

Abstract

Models based on mass action kinetics are widely used but, in a strict sense, limited to biochemical reactions in dilute solution, where reactants freely diffuse and react in an unobstructed space. Modeling diffusion-reaction kinetics in a crowded environment, such as the cytoplasm, requires fractal-like ordinary differential equation (ODE) models. In particular, generalized mass action systems have been proposed and successfully validated for this purpose. In this paper, we establish two novel, particle-based methods to simulate biochemical diffusion-reaction systems within crowded environments. We distinguish two conceptually different situations. In the first, the ODEs capture a microscopic "reaction-only" mechanism, while diffusion is modeled separately. In the second case, the ODEs model the combined effects of both reaction and diffusion. This distinction consequently leads to two simulation methods that both effectively simulate and quantify crowding effects, including reduced reaction volumes, reduced diffusion rates, and reduced accessibility between potentially reacting particles. The proposed methods account for fractal-like kinetics, where the reaction rate depends on the local concentrations of the molecules undergoing the reaction. Rooted in an agent based modeling framework, this aspect of the methods offers the capacity to address sophisticated intracellular spatial effects, such as macromolecular crowding.

Introduction

It is well known that the cytoplasmic environment is highly structured and crowded, and that it is thus significantly different from the typical biochemical milieu *in vitro*. The intracellular concentration of macromolecules is 50-400 mg/ml, which is much higher than the typical 1-10 mg/ml in an aqueous solution (Fulton 1982). In addition, the fraction of the intracellular volume occupied by macromolecules is estimated to be 0.2-

0.3 for cytoplasm (Ellis 2001); even 0.4 has been reported for *E. coli* (Zimmerman and Trach 1991). The same authors estimate that, when 30% of the volume of a solution is occupied by identical globular molecules, less than 1% of the remaining space is available for additional molecules of the same size, due to an "excluded volume" effect caused by steric repulsion, which results in mutual impenetrability of macromolecular solutes (Zimmerman and Trach 1991). The high concentration of macromolecules inside the cell is commonly known as macromolecular crowding. This crowding is a physically nonspecific effect that affects both the free energy and the mobility of macromolecules, resulting in slower diffusion and altered macromolecular reaction rates and equilibria. For instance, the apparent translational diffusion rate in a crowded environment is 5-20 times slower than in saline solution (Elowitz, Surette et al. 1999). Moreover, the observed diffusion is often anomalous in a sense that it is sub-linear, as opposed to linear *in vitro*, and that it scales with the mean-squared displacement of molecules over time (Weiss, Elsner et al. 2004). While macromolecular crowding tends to impede diffusion, it actually enhances the reaction speed nonspecifically, due to the reduction in total available volume. Possibly enhanced reactions include the formation of macromolecular complexes in solution, binding of macromolecules to surface sites, the formation of insoluble aggregates, and compaction or folding of proteins. However, the magnitude of the effect is strongly determined by the relative sizes and shapes of concentrated crowding species and on the dilution of the macromolecular reactants and products. Thus, macromolecular crowding is generally expected to increase the rate of slow, transition-state-limited association reactions and to decrease the rate of fast, diffusion-limited association reactions (Zhou, Rivas et al. 2008).

Macromolecules of different types and abundances are heterogeneously distributed within the living cell. For a cell with a size at the order of μm, chemical concentrations usually range from nM to μM, corresponding to molecular numbers at the order of a few dozen to thousands (Grima and Schnell 2008; Ishihama, Schmidt et al.

2008). Given that the fluctuation of a collection of N particles is at the order of $N^{1/2}$ (van Kampen 2007), fluctuations in small numbers of reactants are likely to affect the system dynamics. The stochastic effects originating from spatial heterogeneity and small numbers of reactants have been associated with important biological consequences, as it has been demonstrated by numerous examples, including microtubule formation (Dogterom and Leibler 1993), ultrasensitive modification and de-modification reactions (Paulsson, Berg et al. 2000), plasmid copy number control (Paulsson and Ehrenberg 2001), noise-induced oscillations (Vilar, Kueh et al. 2002) and metabolite dynamics (Elf, Paulsson et al. 2003).

Various spatial modeling methods have been developed to simulate intracellular biochemical reactions in crowded environments. According to the level of detail in treating molecular objects, these methods can be divided into three categories: macro-, meso- and microscopic.

Macroscopic methods characterize the state of a system through mean-field approximations. Partial differential equations (PDE) belong to this category (Slepchenko, Schaff et al. 2002; Francke, Postma et al. 2003; Slepchenko, Schaff et al. 2003; Mayawala, Vlachos et al. 2006). Although they are among the most computationally scalable computational methods for spatial phenomena, it is difficult to let them account for stochastic effects that derive from structured environments and small numbers, because they are genuinely deterministic. More importantly in the present context, it is difficult to use PDEs to represent complicated spatial effects such as macromolecular crowding, confinement and absorption, which require details regarding molecular shapes and sizes, as well as the heterogeneity of the reaction space.

Mesoscopic methods treat molecules individually yet do not trace their exact location in subspace. Among them, spatial Gillespie methods usually divide the total reaction space

evenly into identical subvolumes, and Gillespie-type algorithms are applied to simulate each subspace (Stundzia and Lumsden 1996; Elf, Doncic et al. 2003; Rodríguez, Kaandorp et al. 2006; Grima and Schnell 2007). To satisfy the homogeneity requirement of Gillespie's algorithms, the size of each subvolume needs to be chosen small enough so that every reactive species can be regarded as uniformly distributed. This is achieved by ensuring that the frequency of molecular diffusion events between adjacent subvolumes is much higher than the reaction frequency within each subvolume. Thus, at each time step, each molecule, represented as a point particle, either reacts within its current subvolume or diffuses to an adjacent subvolume. The reaction probability is determined by a propensity function, while the diffusion probability is D/l^2, where D is the diffusion rate and l is the side length of the subvolume. To the best of our knowledge, all mesoscopic methods developed so far treat molecules as point particles, and crowding effects on either reaction or diffusion have not been effectively simulated.

Microscopic methods treat every molecule as a distinct computational object and trace its position in a continuous space or on a discrete lattice over time. Focusing on this molecular level of detail, unsurprisingly, these methods are computationally very expensive. Depending on their treatment of space, microscopic methods can be further divided into two groups:

- **Lattice based diffusion-reaction models** discretize the total reaction space into regular polygons (Lee, Dinner et al. 2003; Ander, Beltrao et al. 2004; Hattne, Fange et al. 2005; Eide and Chakraborty 2006; Mayawala, Vlachos et al. 2006; Rodríguez, Kaandorp et al. 2006). Usually, only one or a few particles are allowed within each polygon, depending on the relative shape and size of the molecules and the lattice. Diffusion is modeled as a particle's random walk among available lattice points, and bimolecular reactions occur with some

probability when two reactive particles encounter one another in the same lattice location. Lattice based methods permit a simple treatment of space. However, the artificial nature of the space limits spatial resolution and may introduce biased movements, a phenomenon collectively called *lattice anisotropy*. Moreover, it is difficult for lattice based methods to account for volume exclusion effects with molecular species of different sizes and shapes.

- **Off-lattice diffusion-reaction methods** (Stiles and Bartol 2001; Andrews and Bray 2004; van Zon and Ten Wolde 2005; Grima and Schnell 2006) explicitly track every particle's position in a continuous space over time. Particles have certain probabilities to react when they encounter one another within some fixed reaction radius, which is computed from specified macroscopic reaction rates. Off-lattice particle based methods can account for volume exclusion effects, but only when particles are treated with shape and size instead of being volume-less points.

In this paper we develop two novel, microscopic particle-based methods to simulate a biochemical diffusion-reaction system within a crowded environment, which typically is the cytoplasm. The novel contributions of these methods are the following. First, by its nature, an ODE is deterministic and continuous and does not account for spatial features. However, after embedding the ODE into a method accounting for spatial effects, their combination is applicable in discrete, stochastic, and spatial simulations. This embedding can be implemented in two distinct ways, in which phenomenological ODEs play different roles; we will discuss these later. Second, the two proposed methods effectively simulate and quantify crowding effects, including reduced reaction volumes, reduced diffusion rates, and reduced accessibility between potentially reacting particles. Third, the proposed methods account for fractal-like kinetics, where the kinetic reaction

rate depends on the local concentrations of the molecules undergoing the reaction; this aspect is, to the best of our knowledge, novel in the field of stochastic simulations. Rooted in an agent based modeling framework, this aspect of the methods offers the capacity to address sophisticated intracellular spatial effects, such as macromolecular crowding, active transport along cytoskeleton structures, and reactions on heterogeneous surfaces as well as in porous media.

We first demonstrate the validity of the proposed methods with representative elementary types of biochemical processes in non-crowded spaces: an association reaction ($A + B \xrightarrow{k_f} C$), a dissociation reaction ($C \xrightarrow{k_d} A + B$), and their combination—the reversible reaction $A + B \underset{k_d}{\overset{k_f}{\rightleftharpoons}} C$. These reactions will be modeled with power-law functions, according to the tenets of Biochemical Systems Theory (Savageau 1969 a; Savageau 1976; Voit 2000; Torres and Voit 2002). After this initial validation, we quantify macromolecular crowding effects theoretically and numerically through examples of enzymatic reactions. Finally, we investigate an actual experimental system representative for molecular crowding, namely the binding of dansylamide and carbonic anhydrase in artificial media (Neff, Offord et al. 2011), and discover some surprising results.

Methods

Motivation for power-law representations of reactions in crowded media

Power-law functions with non-integer kinetics have proven very useful in biochemical systems analysis, and forty years of research have demonstrated their wide applicability (*e.g.*, see (Savageau 1969 a; Savageau 1976; Voit 2000; Torres and Voit 2002)). Generically, this type of description of a biochemical reaction can be seen either as a Taylor approximation in logarithmic space or as a heuristic or phenomenological model

that has been applied successfully hundreds of times and in different contexts, even though it is difficult or impossible in many situations to trace it back to first mechanistic principles. A particularly interesting line of support for the power-law format can be seen in the example of a bimolecular reaction occurring in a spatially restricted environment. Savageau demonstrated with theoretical arguments that the kinetics of such a reaction can be validly formulated as a generalization of the law of mass action, where non-integer kinetic orders are allowed (Savageau 1993; Savageau 1995). More recently, Neff and colleagues showed with careful experiments that this formulation is indeed valid and more accurate than alternative approaches (Bajzer, Huzak et al. 2008; Neff 2010; Neff, Offord et al. 2011).

As demonstrated many times in the field of Biochemical Systems Theory, and most recently within the context of stochastic kinetic modeling (*e.g.*, (Wu, Vidakovic et al. 2011)), the rate of the association reaction between molecules of species S_1 and S_2 can be represented as a power-law function of the form $k\left[X_1(t)\right]^{f_1}\left[X_2(t)\right]^{f_2}$. In this formulation, *k* is a *rate constant* and f_1 and f_2 are real-valued *kinetic orders*, which are not necessarily positive integers as in typical mass action laws. A generic example is the bi-directional bimolecular reaction $S_1 + S_2 \underset{k_b}{\overset{k_f}{\rightleftharpoons}} S_3$. Adapting ideas from Neff and colleagues (Neff 2010), we formulate a discrete update function for the population of S_3 molecules within a time interval Δt as

$$x_3(t+\Delta t) - x_3(t) = f\left(\left[X_1\right],\left[X_2\right]\right)\Delta t\ x_1x_2\ -\ g\left(\left[X_3\right]\right)\Delta t x_3. \qquad (1)$$

The right-hand side contains two terms. The first, $f\left(\left[X_1\right],\left[X_2\right]\right)\Delta t\ x_1x_2$, describes the production of S_3 and can be interpreted as the statement "among all possible collisions x_1x_2, some fraction $f\left(\left[X_1\right],\left[X_2\right]\right)\Delta t$ reacts and forms the product." In a dilute and well-

mixed environment, $f\left(\left[X_1\right],\left[X_2\right]\right)$ reduces to a traditional rate constant, and the reaction obeys the law of mass action. However, in a spatially restricted environment, crowding effects need to be taken into account. Savageau (Savageau 1993; Savageau 1995) demonstrated that the appropriate fraction of a reaction in this case is a function that depends on the current concentrations of S_1 and S_2. Similar to the first term, the degradation term $g\left(\left[X_3\right]\right)\Delta t x_3$ represents the fraction $g\left(\left[X_3\right]\right)\Delta t$ of species S_3 that dissociates back into S_1 and S_2 as a fraction that may depend on some functional form of $\left[X_3\right]$, because the complex may not be able to dissociate effectively in a crowded environment.

Taking the limit $\Delta t \to 0$ in Eq. (1) yields the differential equation

$$\frac{dx_3}{dt} = f\left(\left[X_1\right],\left[X_2\right]\right)x_1x_2 \; - \; g\left(\left[X_3\right]\right)x_3. \tag{2}$$

and Taylor series expansion in the logarithmic space $\left(\log\left[X_1\right],\log\left[X_2\right],\log f\right)$ around some operating point $\left(a,b,f(a,b)\right)$ leads to

$$\begin{aligned}
&\log f\left(\left[X_1\right],\left[X_2\right]\right) \triangleq F\left(\log\left[X_1\right],\log\left[X_2\right]\right) \\
&= F(a,b) + \left.\frac{\partial f\left(\left[X_1\right],\left[X_2\right]\right)}{\partial\left[X_1\right]}\right|_{(a,b)} (\log\left[X_1\right]-a) \\
&+ \left.\frac{\partial f\left(\left[X_1\right],\left[X_2\right]\right)}{\partial\left[X_2\right]}\right|_{(a,b)} (\log\left[X_2\right]-b) + \text{HOT} \\
&\approx k_f + \alpha\log\left[X_1\right] + \beta\log\left[X_2\right].
\end{aligned} \tag{3}$$

As is typical, the parameters $k_f, \alpha,$ and β depend on the chosen operating point (a, b). Ignoring all higher order terms (HOT) beyond the constant and linear terms transforms the term in (3) back to the Cartesian space:

$$f\left(\left[X_1\right],\left[X_2\right]\right) \approx k_a \left[X_1\right]^{\alpha} \left[X_2\right]^{\beta}, k_a = e^{k_f}. \tag{4}$$

The same procedure yields a power-law expression for the degradation term: $g\left(\left[X_3\right]\right) \approx k_d \left[X_3\right]^{\gamma}$. Combining constants leads to a power-law representation for the dynamics of species S_3, namely

$$\begin{aligned} \frac{d\left[X_3\right]}{dt} &= \left(k_a \left[X_1\right]^{\alpha} \left[X_2\right]^{\beta}\right)\left[X_1\right]\left[X_2\right] - \left(k_d \left[X_3\right]^{\gamma}\right)\left[X_3\right] \\ &= k_a \left[X_1\right]^{f_1} \left[X_2\right]^{f_2} - k_d \left[X_3\right]^{f_3}, \end{aligned} \tag{5}$$

where $f_1 = \alpha + 1, f_2 = \beta + 1,$ and $f_3 = \gamma + 1.$

One notes that these considerations apply to all formats within Biochemical Systems Theory, so that the results for GMA systems reported below also apply to models in alternative the S-system format (Savageau 1969 a; Savageau 1976; Voit 2000; Torres and Voit 2002).

Extensions of strict ODE representations

The derivation of methods for stochastic simulations in crowded environments is similar in spirit to recent literature reports (Pogson, Smallwood et al. 2006; Klann, Lapin et al. 2011), but entails three important distinctions: First, in addition to the association reaction, as discussed in the earlier work, we also consider the reverse dissociation reaction. Second, the kinetic rates for both association and dissociation reactions are considered to be concentration (and therefore time) dependent, which is a generalization of the constant value discussed in the two references. Finally, we distinguish two situations where a phenomenological ODE plays different roles. In the first method, the ODE is used to characterize only the reaction kinetics, while Brownian random walk is used to implement the diffusion process, so that the resulting reaction-diffusion dynamics

is in general different from the reaction-only ODE prediction. In the second method, the ODE is assumed to characterize a species concentration, which is driven by the combined effect of reaction and diffusion; therefore, it is only applicable to a homogeneous system.

This conceptual distinction has consequences. With the first method we are able to give a theoretical characterization and prediction of how diffusion affects the system dynamics, whereas the second method allows us to characterize the microscopic reaction mechanism with which the two reacting molecules collide. The two methods are first developed and validated in an unobstructed space. Afterwards, crowding agents are added to create a virtual, crowded environment, and the effects of crowding on the reaction-diffusion system will be quantified and demonstrated.

Method 1: Extending a reaction-kinetic ODE to spatial stochastic modeling

i) Association reaction

Consider the bimolecular association reaction $S_1 + S_2 \xrightarrow{k_a} S_3$, which we model with the term $k_a\left[X_1(t)\right]^{f_1}\left[X_2(t)\right]^{f_2}$, as discussed before. Under the idealistic assumption of perfect and instant mixing, the diffusion rate is infinite, and the reaction dynamics follows the equation

$$\frac{d\left[X_1(t)\right]}{dt} = \frac{d\left[X_2(t)\right]}{dt} = -\frac{d\left[X_3(t)\right]}{dt} = -k_a\left[X_1(t)\right]^{f_1}\left[X_2(t)\right]^{f_2}. \qquad (6)$$

To characterize the concentration dependence of the kinetic rate, we introduce the notation $k_{a\_concentration}(t) \triangleq k_a\left[X_1(t)\right]^{f_1-1}\left[X_2(t)\right]^{f_2-1}$ and convert the equation into the mass-action-like format

$$\frac{d[X_1(t)]}{dt} = \frac{d[X_2(t)]}{dt} = -\frac{d[X_3(t)]}{dt} = -k_{a\_concentration}(t)[X_1(t)][X_2(t)], \quad (7)$$

.

where the rate "constant" depends on time. To distinguish this formulation from the case of a traditional mass action representation, $k_{a\_concentration}(t)$ is called a *concentration-dependent kinetic rate function*.

Now consider the dynamics of species S_1. The concentration based equation for S_1 can be converted into the corresponding particle-based equation

$$\frac{dx_1(t)}{dt} = -k_a \left(N_A V\right)^{1-f_1-f_2} x_1(t)^{f_1} x_2(t)^{f_2} \quad (8)$$

by the relationship $[X(t)] = \frac{x(t)}{N_A V}$, where N_A is the Avogadro number and V is the total variable reaction volume. In this conversion, one needs to pay special attention to the appropriate units. In the following, we use μM as concentration unit, μm as the spatial unit, and *s* as the unit for time. With these settings, the unit for the association rate constant k_a is $(\mu M)^{1-f_1-f_2} s^{-1} = \left(10^{-21} mol/\mu m^3\right)^{1-f_1-f_2} s^{-1}$ and the unit for $k_{a\_concentration}(t)$ is $(\mu M)^{-1} s^{-1}$. Thus, $k_a \left(N_A V\right)^{1-f_1-f_2}$, the coefficient in Eq. (8) takes the form

$$\begin{aligned} k_a \left(N_A V\right)^{1-f_1-f_2} &= \bar{k}_a \left(10^{-21} mol/\mu m^3\right)^{1-f_1-f_2} s^{-1} \left(6.023\times 10^{23}/mol \times \bar{V}\,\mu m^3\right)^{1-f_1} \\ &= \bar{k}_a \left(602.3\bar{V}\right)^{1-f_1-f_2} s^{-1}. \end{aligned} \quad (9)$$

Here, k_a and V on the left-hand side are quantities that take the numerical values of $\bar{k}_a$ and $\bar{V}$ on the right-hand side, respectively. Eq. (9) demonstrates that the time unit on the right-hand side of Eq. (8) is s^{-1}, which is consistent with that of the left-hand side.

In a similar manner (see Eq.(11)), we define the *particle-based association kinetic rate function* as

$$k_{a\_particle}(t) \triangleq k_a \left(N_A V\right)^{1-f_1-f_2} x_1(t)^{f_1-1} x_2(t)^{f_2-1}, \tag{10}$$

which can be converted back to the mass action format

$$\begin{aligned} \frac{dx_1(t)}{dt} &= -\left[k_a \left(N_A V\right)^{1-f_1-f_2} x_1(t)^{f_1-1} x_2(t)^{f_2-1}\right] x_1(t) x_2(t) \\ &= -k_{a\_particle}(t) x_1(t) x_2(t) \end{aligned} \tag{11}$$

by using the particle-based GMA Eq.(8). Moreover, $k_{a\_particle}(t)$ is related to $k_{a\_concentration}(t)$ in the following manner:

$$\begin{aligned} k_{a\_particle}(t) &\triangleq k_a \left(N_A V\right)^{1-f_1-f_2} x_1(t)^{f_1-1} x_2(t)^{f_2-1} \\ &= \left(N_A V\right)^{-1} k_a \left(\frac{x_1(t)}{N_A V}\right)^{f_1-1} \left(\frac{x_2(t)}{N_A V}\right)^{f_2-1} \\ &= \left(N_A V\right)^{-1} k_{a\_concentration}, \end{aligned} \tag{12}$$

which, with the assumed units, becomes $k_{a\_particle}(t) = \left(602.3\bar{V}\right)^{-1} k_{a\_concentration}$.

Discretizing Eq. (11) yields

$$\frac{\Delta x_1(t)}{\Delta t} = -k_{a\_particle}(t)x_1(t)x_2(t). \tag{13}$$

Here $\Delta x_1(t)$ is the number of S_1 molecules that were changed due to association reactions fired during the time interval $(t, t+\Delta t)$. Expressed differently, within Δt, the proportion

$$\frac{|\Delta x_1(t)|}{x_1(t)} = \frac{\Delta t k_{a\_particle}(t)Vx_2(t)}{V} \tag{14}$$

of S_1 molecules participating in association reactions corresponds to the ratio between $\Delta t k_{a\_particle}(t)Vx_2(t)$ and V. The numerator $\Delta t k_{a\_particle}(t)Vx_2(t)$ on the right-hand side is the portion of the volume where association reactions occur. This effective reaction volume is occupied by a total of $x_2(t)$ molecules of type S_2 and therefore can be evenly divided and assigned to every S_2 molecule as

$$\begin{aligned} V_{reaction} &\triangleq \Delta t k_{a\_particle}(t)V \\ &= \Delta t k_a \left(N_A V\right)^{1-f_1-f_2} x_1(t)^{f_1-1} x_2(t)^{f_2-1} V. \end{aligned} \tag{15}$$

In other words, when one S_1 molecule enters into the volume $V_{reaction}$ which encloses an S_2 molecule, the two molecules react with probability 1. Moreover, with Eq. (9), it is easy to see that the unit of $V_{reaction}$ is μm^3, confirming that the definition of $V_{reaction}$ is appropriate.

In the special case of a mass action reaction where $f_1 = f_2 = 1$, the reaction volume does not depend on the concentration:

$$V_{reaction} = \Delta t k_a N_A^{-1}. \tag{16}$$

By similar reasoning, one obtains a symmetric result for S_2:

$$\frac{|\Delta x_2(t)|}{x_2(t)} = \frac{\Delta t k_{a\_particle}(t) V x_1(t)}{V} = \frac{V_{reaction} x_1(t)}{V}. \tag{17}$$

Eq. (17) implies that, when one S_2 molecule enters into $V_{reaction}$ enclosing a S_1 molecule, the two molecules react. By assuming a spherical reaction volume, it is useful to introduce the concept of the *reaction radius* as

$$\begin{aligned} r_{reaction} &= \left(\frac{3}{4\pi} V_{reaction} \right)^{1/3} \\ &= \left(\frac{3}{4\pi} \Delta t k_{a\_particle}(t) V \right)^{1/3} \\ &= \left[\frac{3}{4\pi} \Delta t k_a \left(N_A V \right)^{1-f_1-f_2} x_1(t)^{f_1-1} x_2(t)^{f_2-1} V \right]^{1/3}, \end{aligned} \tag{18}$$

i.e., one S_1 molecule and one S_2 molecule react with probability 1 when the distance between them is less than or equal to $r_{reaction}$. For generalized mass action kinetics, the reaction radius is a function of concentrations, while in the special case of standard mass action kinetics, the reaction radius reduces to $r_{reaction} = \left(\frac{3}{4\pi} \Delta V \right)^{1/3} = \left[\frac{3\Delta t k_a}{4\pi N_A} \right]^{1/3}$, which again is concentration independent.

ii) Dissociation reaction

We also consider, within the conceptual framework of power-law representations, the dissociation reaction $S_3 \xrightarrow{k_d} S_1 + S_2$ where the rate of dissociation is given as $k_d \left[X_3(t) \right]^{f_3}$. Here k_d is the *dissociation rate constant* with unit $\left(\mu M \right)^{1-f_3} s^{-1}$ and f_3 is a real-valued *kinetic order*, which is not necessarily 1 as it is assumed in a mass action law. The concentration-based equation for the systems dynamics is

$$\frac{d[X_3(t)]}{dt} = -\frac{d[X_1(t)]}{dt} = -\frac{d[X_2(t)]}{dt} = -k_d[X_3(t)]^{f_3}. \quad (19)$$

The concentration based equation of S_3 can be converted into the corresponding particle-based equation as before, namely

$$\frac{dx_3(t)}{dt} = -k_d(N_A V)^{1-f_3} x_3(t)^{f_3}. \quad (20)$$

In order to characterize how the substrate concentration affects the kinetic rate, one defines the *particle-based dissociation kinetic rate function* as

$$k_{d\_particle}(t) \triangleq k_d(N_A V)^{1-f_3} x_3(t)^{f_3-1}, \quad (21)$$

which transforms (20) back to the apparent mass action format

$$\frac{dx_3(t)}{dt} = -k_{d\_particle}(t)x_3(t), \quad (22)$$

where however $k_{d\_particle}$ is not necessarily constant. Discretizing yields

$$\frac{|\Delta x_3(t)|}{x_3(t)} = \Delta t k_{d\_particle}(t). \quad (23)$$

Here $\frac{|\Delta x_3(t)|}{x_3(t)}$ is the proportion of S_3 molecules participating in dissociation reactions within Δt, which equals the probability for each S_3 molecule to fire a dissociation reaction during Δt, *i.e.*,

$$p_d = \Delta t k_{d\_particle}(t). \tag{24}$$

In the generalized mass reaction framework, the firing probability p_d of a dissociation event is a function of the substrate concentration, which represents the restricting effects of the crowded environment on the dissociation process. By contrast, in the idealized dilute case where the mass action law holds, $f_3 = 1$ implies $p_d = \Delta t k_d$, which means that the dissociation probability becomes concentration independent.

iii) Particle-based diffusion

Suppose that the position of a diffusing particle at time t is $\big(X(t), Y(t), Z(t)\big)$. Within an obstacle-free space, the particle diffuses freely and its position $\big(X(t+\Delta t), Y(t+\Delta t), Z(t+\Delta t)\big)$ at time $t+\Delta t$ is updated by the equations

$$\begin{aligned} X(t+\Delta t) &= X(t) + \sqrt{2D\Delta t}\,\gamma_x, \\ Y(t+\Delta t) &= Y(t) + \sqrt{2D\Delta t}\,\gamma_y, \\ Z(t+\Delta t) &= Z(t) + \sqrt{2D\Delta t}\,\gamma_z, \end{aligned} \tag{25}$$

where D is the diffusion rate constant, and where γ_x, γ_y and γ_z are random numbers that are independently sampled from the normal distribution with zero mean and unit variance (Chandrasekhar 1943).

In simulations, the time step Δt needs to be small enough so that the average diffusion distance of reactants $\sqrt{2(D_1 + D_2)\Delta t}$ within Δt should be less or equal to the reaction radius $r_{reaction}$, i.e.

$$\sqrt{2(D_1+D_2)\Delta t} \le r_{reaction} = \left[\frac{3}{4\pi}\Delta t k_a \left(N_A V\right)^{1-f_1-f_2} x_1(t)^{f_1-1} x_2(t)^{f_2-1} V\right]^{1/3}$$, which implies

$$\Delta t \le \frac{\left[\frac{3}{4\pi} k_a \left(N_A V\right)^{1-f_1-f_2} x_1(t)^{f_1-1} x_2(t)^{f_2-1} V\right]^2}{8(D_1+D_2)^3}. \quad (26)$$

Here D_1 and D_2 are the diffusion rate constants for the potentially reacting particles and therefore $D_1 + D_2$ is the effective diffusion rate.

The dynamics of the reaction system can be assessed with the following algorithm.

Algorithm 1.1

Initiation

1. Choose the size of time step Δt according to Eq. (26) at t=0.

Iteration

While $t \le T_{\max}$, repeat

2. Association reactions: For each S_1 molecule react with any one of the S_2 molecules within the collision radius $r_{reaction}$: replace the S_1 molecule with an S_3 molecule and remove the S_2 molecule.
3. Dissociation reactions: For each molecule of species S_3, generate a random number u which is uniformly distributed in (0, 1). If $u \le p_d$, the S_3 molecule dissociates into one S_1 molecule and one S_2 molecule; the two newly generated molecules are set apart from one another with a distance $r_{reaction}$, and the center of mass remains at the original location of the S_3 molecule.

4. Diffusion: update each molecule's location according to Eq. (25).
5. Update Δt according to Eq.(26).
6. $t = t + \Delta t$.

End while.

Algorithm 1.1 is computationally expensive. For instance, with typical parameters $D_1 = D_2 = 10\mu m^2 s^{-1}, f_1 = f_2 = 1, V = 1\mu m^3$ and $k_a = 1\mu M^{-1} s^{-1}$, Δt is very small ($\Delta t \approx 10^{-7} s$), thus requiring huge numbers of simulation steps for processes within realistic time intervals of seconds and minutes. The situation is even more severe for faster diffusing molecules. To overcome this computational limitation, while reducing the simulation time considerably, we introduce the *collision volume* $V_{collison}$ which has a bigger radius than the reaction volume $V_{reaction}$, so that a larger simulation time step is allowed. Now, the two reacting molecules encounter each other within $V_{collison}$ through diffusion, but only react with reaction probability

$$p_{reaction} \triangleq \frac{V_{reaction}}{V_{collison}}, \tag{27}$$

which is less than 1. By assuming a spherical collision volume, we can define the *collision radius* as

$$r_{collision} = \left(\frac{3}{4\pi} V_{collision} \right)^{1/3}. \tag{28}$$

With either $V_{collison}$ or $r_{collison}$ chosen, the simulation time step can computed as

$$\Delta t = \frac{r_{collision}^{\ 2}}{6D} = \frac{\left(\frac{3}{4\pi} V_{collision} \right)^{2/3}}{6D}. \tag{29}$$

In practice, $V_{collison}$ or $r_{collison}$ are often chosen to be large enough to satisfy $p_{reaction} = \frac{V_{reaction}}{V_{collison}} \ll 1$, which yields the following benefits: 1) A bigger simulation time step Δt is allowed to accelerate the simulation; 2) In the scenario of the bidirectional association-dissociation reaction, the two molecules resulted from a dissociation reaction are placed in the same physical location or next to one another; however, their proximity does not cause them to react right away, because of a small association reaction probability; 3) There could be more than one reacting S_2 molecule within $r_{collison}$ of a S_1 molecule. According to the law of addition for independent events, the probability for the S_1 molecule to react with one of the *n* neighboring S_2 molecules is *np*, and in our case we find $np \le 1$. Instead of generating $O(n)$ random numbers to test whether the S_1 molecule reacts with one of its *n* neighboring S_2 molecules, only one random number is required to account for multiple neighbors, thereby improving the simulation efficiency.

Implementing the above considerations, a particle-based algorithm to simulate concentration-dependent reactions can be summarized as follows.

Algorithm 1.2

Initiation

1. Select $V_{collison}$ or $r_{collison}$.
2. Set the size of time step Δt according to Eq. (29).

Iteration

While $t \le T_{\max}$, repeat

3. Association reactions: For each S_1 molecule denote n as the number of S_2 molecules within its collision radius $r_{collision}$. Sample a uniform random number u from (0, 1). If $u \le np_{reaction} = n\frac{V_{reaction}}{V_{collison}}$, then the S_1 molecule reacts with an arbitrary S_2 molecule, selected from among the n candidates; otherwise, no association reaction occurs to this S_1 molecule within Δt.
4. Dissociation reactions: For each molecule of species S_3, generate a random number u which is uniformly distributed in (0, 1). If $u \le p_d$, the S_3 molecule dissociates into one S_1 molecule and one S_2 molecule; the two newly generated molecules are set next to one another with a distance $r_{collision}$ and with the center of mass remaining at the original S_3 molecule location. If $u > p_d$, no dissociation reaction occurs to this S_3 molecule within Δt.
5. Diffusion: update each molecule's location according to Eq.(25).
6. $t = t + \Delta t$.

End while.

In summary, the diffusion-reaction process is simulated in Method 1 with the following strategies:

1) Bimolecular reaction mechanisms, characterized in terms of reaction volume, reaction radius, and reaction probability upon collision, are constructed solely from $k_a(t)$, with the information defined in the phenomenological reaction Eq. (8), which is formulated as an ODE.
2) The diffusion is implemented as a Brownian process.

3) The combined effects of diffusion and reaction are no longer captured by the phenomenological reaction Eq. (8), which only contributes to the reaction aspect of the simulation. (Note: We will show later that the combined effect can be predicted by Eq. (43), which incorporate both diffusion and reaction effects.)

As an alternative to this Method 1, we present in the next section a different particle-based simulation method that adopts a distinctly different logical starting point: the combined effects of diffusion and reaction are captured by the phenomenological Eq. (8). We will show how to construct the microscopic reaction mechanism upon particle collision, which, as it turns out, depends on diffusion.

Method 2: An ODE for diffusion-controlled reactions in a homogeneous system

Consider the bimolecular association reaction $S_1 + S_2 \xrightarrow{k_a} S_3$. Within the framework of diffusion-controlled reaction theory (Smoluchowski 1917; Berg and von Hippel 1985), the bimolecular reaction process is divided into two steps: first, two reactants come into contact or proximity through diffusion; second, upon encounter, the two molecules react with a certain probability, which is determined by factors such as their relative momentum and orientation. More specifically, in 3D space, the *collision rate* of two spherical molecule *1* and *2* is given by

$$k_D = 4\pi r_{12}(D_1 + D_2). \tag{30}$$

Here r_{12} represents the interaction distance of two molecules. In the case that the two molecules interact through direct contact, $r_{12} = r_1 + r_2$, which is the sum of the radii of the two molecules. In the case that the two molecules come to an interaction under an

electromagnetic field, the effective interaction radius is $r_{12} > r_1 + r_2$. For our assumption regarding units (μM for concentration unit, μm for spatial unit, s for time unit), the unit for the diffusion rate is $\mu m^2 / s$, and the unit for a collision rate constant $k_{D\_concentration}$ is therefore $\mu m^3 / s$. By virtue of the relationship $\mu m^3 s^{-1} = 602.3(\mu M s)^{-1}$, the above formula can be converted into an expression with unit $(\mu M s)^{-1}$,

$$k_{D\_concentration} = 602.3 \times 4\pi r_{12} (D_1 + D_2), \tag{31}$$

which is concentration-based and consistent with the unit of $k_{a\_concentration}(t)$. Furthermore, using reasoning as in the context of Eq. (12), the concentration-based collision rate $k_{D\_concentration}$ can be rewritten as a *particle-based collision rate*:

$$\begin{aligned} k_{D\_particle} &= (N_A V)^{-1} k_{D\_concentration} \\ &= (602.3\bar{V})^{-1} 602.3 \times 4\pi r_{12} (D_1 + D_2) \\ &= \bar{V}^{-1} 4\pi r_{12} (D_1 + D_2). \end{aligned} \tag{32}$$

The collision rate represents the maximal reaction rate in the situation that two colliding molecules react with 100% probability. However, in general, not every encounter between two molecules leads to a reaction. To quantify the percentage of successful reactions upon collision, *the microscopic reaction rate* k_{micro} is defined. The combination of the collision rate and the microscopic reaction rate leads to the *effective reaction rate* $k_{effective}$ (Berg and von Hippel 1985), which is observable at the macroscopic level and corresponds to the reaction rate in ODE models:

$$\frac{1}{k_{effective}} = \frac{1}{k_{micro}} + \frac{1}{k_{D\_concentration}}. \tag{33}$$

Since both $k_{effective}$ and $k_{D\_concentration}$ are either measurable or can be calculated, k_{micro} can be calculated through the above equation, even though it can usually not be measured directly through an experiment.

In dilute milieus where mass action kinetics holds, all these rates are constant in time. By contrast, in crowded media where the generalized mass action rate law is used to characterize the system dynamics phenomenologically, $k_{effective}$ is a function of time and reactant concentrations. In situations of crowding, the diffusion rate is observed to reach a steady value after some initial phase where diffusion with a time-dependent rate, termed *anomalous diffusion* (Bouchaud and Georges 1990; Weiss, Elsner et al. 2004), is observed. The assumption that the reactants' diffusion rates remain constant in time implies that the collision rate is a constant and therefore mandates that the microscopic reaction rate is a function of time and concentrations. Although a time and concentration dependent microscopic reaction rate at first seems to contradict the intuition that the affinity of two reacting molecules is a biophysical property and thus constant in time, it has become an acceptable formulation, because the underlying physical principles are not entirely understood. It is also unclear how environmental crowding agents nonspecifically affect the orientation and affinity of reacting molecules (Zhou, Rivas et al. 2008). As a result, a phenomenological characterization of the microscopic reaction rate may be interpreted as an aggregation of these unknown effects. Therefore, in order to summarize the crowding effects at a microscopic level, by applying $k_{effective} = k_{a\_concentration}$ to Eq. (33), we introduce the *concentration-based microscopic rate function*

$$\begin{aligned} k_{micro\_concentration} &= \frac{k_{D\_concentration} k_{a\_concentration}}{k_{D\_concentration} - k_{a\_concentration}} \\ &= \frac{k_{D\_concentration} k_a \left[X_1\right]^{f_1-1} \left[X_2\right]^{f_1-1}}{k_{D\_concentration} - k_a \left[X_1\right]^{f_1-1} \left[X_2\right]^{f_1-1}}. \end{aligned} \tag{34}$$

The corresponding particle-based analogue is

$$k_{micro\_particle} = \left(N_A V\right)^{-1} k_{micro\_concentration}. \tag{35}$$

By applying $V_{reaction} \triangleq \Delta t k_{a\_particle}(t) V$, as defined in Eq. (15), the reaction volume corresponding to $k_{micro\_particle}$ is

$$\begin{aligned} V_{micro} &= \Delta t k_{micro\_particle} V \\ &= \Delta t N_A^{-1} k_{micro\_concentration}. \end{aligned} \tag{36}$$

Under the assumption of spherical volumes, the microscopic reaction radius can be defined as

$$r_{micro} = \left(\frac{3}{4\pi} V_{micro} \right)^{1/3}. \tag{37}$$

V_{micro} is unlikely to be equivalent with the collision volume $\frac{4\pi r_{12}^{\ 3}}{3}$, but this mismatch can be adjusted by introducing the *reaction probability of association*

$$p_{micro} = \frac{V_{micro}}{4\pi r_{12}^{\ 3} \big/ 3}, \tag{38}$$

which expresses that two molecules react with probability p_{micro} when they come closer to each other than r_{micro}.

With these specifications, the simulation of a diffusion-reaction process can be implemented as the following algorithm.

Algorithm 2

Initiation:

1. Select $r_{12} \geq r_1 + r_2$ and set the size of the time step as $\Delta t = \frac{r_{12}^2}{6D}$.

Iteration

While $t \leq T_{\max}$, repeat

2. Association reactions: For each S_1 molecule denote *n* as the number of S_2 molecules within its collision radius r_{micro}. Sample a uniform random *u* number from (0, 1). If $u \leq np_{micro}$, then the S_1 molecule reacts with an arbitrary S_2 molecule from among the *n* S_2 molecules; otherwise, no association reaction occurs with this S_1 molecule within Δt.
3. Dissociation reactions: For each molecule of species S_3 generate a uniform random number *u* from (0, 1). If $u \leq p_d$, the S_3 molecule dissociates into one S_1 molecule and one S_2 molecule. The two newly generated molecules are set next to one another with a distance r_{micro} and with the center of mass remaining at the original location of the S_3 molecule. If $u > p_d$, no dissociation reaction occurs to this S_3 molecule.
4. Diffusion: update each molecule's location according to Eq.(25).
5. $t = t + \Delta t$.

End while.

It is clear that Algorithm 2 is only different from Algorithm 1 by replacing $r_{reaction}$ by r_{micro} and $p_{reaction}$ by p_{micro}. Though similar in format, these two algorithms are

based on distinctly different concepts and assumptions and will therefore yield different results. The differences will be first discussed theoretically and then demonstrated through numerical examples.

Results

Distinction between Algorithms 1 and 2: theoretical considerations

We first re-exam Algorithm 1 in the context of diffusion-controlled reaction theory and develop a formula to predict how diffusion affects the system dynamics. In Algorithm 1 two reacting particles react with probability $p = \frac{V_{reaction}}{V_{collison}}$ as they come closer than the collision radius $r_{collison}$. This approach can be dissected into two steps: First, the two particles need to encounter one another within the collision volume $V_{collison} = \frac{4\pi r_{collison}^{\ 3}}{3}$; this encounter rate is given by

$$k_D = 4\pi r_{collison}\left(D_1 + D_2\right). \tag{39}$$

Here the unit of k_D is $\mu m^3 s^{-1}$. Using the earlier relationship $\mu m^3 s^{-1} = 602.3\left(\mu M s\right)^{-1}$, the above formula can be converted into an expression with unit $\left(\mu M s\right)^{-1}$,

$$k_{D\_concentration} = 602.3 \times 4\pi r_{collison}\left(D_1 + D_2\right), \tag{40}$$

which is concentration-based and consistent with the unit of $k_{a\_concentration}(t)$. Furthermore, with reasoning similar to Eq. (12), $k_{D\_concentration}$ can be reformulated as a particle-based rate constant:

$$
\begin{aligned}
k_{D\_particle} &= \left(N_A V\right)^{-1} k_{D\_concentration} \\
&= \left(602.3\bar{V}\right)^{-1} k_{D\_concentration} \\
&= \bar{V}^{-1} 4\pi r_{collison}\left(D_1 + D_2\right).
\end{aligned} \tag{41}
$$

Second, upon collision, the two particles react with a probability that is the ratio of reaction volume and collision volume, *i.e.*, $p = \frac{V_{reaction}}{V_{collison}}$.

As a reminder, Algorithm 1.1 uses $k_{a\_particle}(t)$ as the microscopic reaction rate k_{micro}, which gives rise to the reaction volume $V_{reaction} \triangleq \Delta t k_{reaction}(t) V$, within which two molecules react with probability 1. To improve the computational efficiency, a larger size collision volume $V_{collison}$ is used instead of $V_{reaction}$, and the mismatch is adjusted by introducing reaction probability $p_{reaction} = \frac{V_{reaction}}{V_{collison}}$.

The particle-based effective kinetic rate is given by combining the particle-based collision rate and the microscopic reaction rate as

$$
\begin{aligned}
k_{effective\_particle} &= \left(\frac{1}{k_{micro}} + \frac{1}{k_{D\_particle}}\right)^{-1} \\
&= \left(\frac{1}{k_{a\_particle}} + \frac{1}{\bar{V}^{-1} 4\pi r_{collison}\left(D_1 + D_2\right)}\right)^{-1}.
\end{aligned} \tag{42}
$$

Under the condition that reactants are homogeneously distributed, $k_{effective\_particle}(t)$ gives rise to the particle-based, diffusion-controlled reaction ODE

$$\frac{dx_1(t)}{dt} = -k_{effective\_particle}(t)x_1(t)x_2(t)$$
$$= -\left(\frac{1}{k_{a\_particle}(t)} + \frac{1}{\bar{V}^{-1}4\pi r_{collison}\left(D_1 + D_2\right)}\right)^{-1} x_1(t)x_2(t). \quad (43)$$

This diffusion-controlled reaction ODE assesses the effects of diffusion on the system dynamics: in general,

$$k_{effective\_particle} = \frac{k_{a\_particle}}{\frac{k_{a\_particle}}{\bar{V}^{-1}8\pi r_{collison}\left(D_1 + D_2\right)} + 1} < k_{a\_particle}. \quad (44)$$

When $D \longrightarrow \infty$, we obtain $k_{effective\_particle}(t) \longrightarrow k_{a\_particle}(t)$. In words: when the diffusion rate becomes large, the dynamics of the diffusion-controlled reaction system (Eq.(43)) converges to that of the well-stirred system $\frac{dx_1(t)}{dt} = -k_{a\_particle}(t)x_1(t)x_2(t)$, which was given in Eq. (11). Therefore, Algorithm 1 can be used to detect the influence of diffusion on the overall system dynamics, no matter whether the reactants are homogeneously distributed or not.

By contrast, Algorithm 2 starts with the assumption that the phenomenological ODE captures the combined effect of reaction and diffusion, which leads to $k_{effective\_particle}(t) = k_{a\_particle}(t)$. Based on this assumption, the algorithm traces the microscopic reaction rate k_{micro} through the general diffusion-controlled reaction relationship $\frac{1}{k_{effective\_particle}} = \frac{1}{k_{micro}} + \frac{1}{k_{D\_particle}}$, in order to define a particle-based reaction scheme. Therefore, no matter what the diffusion rate is, the simulations of a homogeneous system in Algorithm 2 will always yield the same overall system dynamics, namely

$$\frac{dx_1(t)}{dt} = -k_{a\_particle}(t)x_1(t)x_2(t),$$

which corresponds to Eq. (11).

Numerical Confirmation of Methods 1 and 2

Assessment of association reactions

Consider a reaction-diffusion system with input, where initially the reactants S_1, S_2 and S_3 are homogeneously distributed within a cube and assumed to diffuse with rate *D*. The reaction scheme

$$\phi \xrightarrow{c_1} S_1,$$
$$\phi \xrightarrow{c_2} S_2,$$
$$S_1 + S_2 \xrightarrow{k_a} S_3,$$

can be modeled with the GMA reaction-only equations

$$\begin{cases} \dfrac{d\left[X_1(t)\right]}{dt} = c_1 - k_a\left[X_1(t)\right]^{f_1}\left[X_2(t)\right]^{f_2}, \\ \dfrac{d\left[X_2(t)\right]}{dt} = c_2 - k_a\left[X_1(t)\right]^{f_1}\left[X_2(t)\right]^{f_2}, \\ \dfrac{d\left[X_3(t)\right]}{dt} = k_a\left[X_1(t)\right]^{f_1}\left[X_2(t)\right]^{f_2}. \end{cases}$$

or

$$\begin{cases} \dfrac{dx_1(t)}{dt} = c_1(602.3\bar{V}) - k_{a\_particle}(t)x_1(t)x_2(t), \\ \dfrac{dx_2(t)}{dt} = c_2(602.3\bar{V}) - k_{a\_particle}(t)x_1(t)x_2(t), \\ \dfrac{dx_3(t)}{dt} = k_{a\_particle}(t)x_1(t)x_2(t), \end{cases} \tag{45}$$

where the first system is concentration based and the second particle based.

Using Algorithm 1, the dynamics of a homogeneous system can be assessed by the corresponding diffusion-control reaction ODEs

$$\begin{cases} \dfrac{dx_1(t)}{dt} = c_1(602.3\bar{V}) - k_{effective\_particle}(t)x_1(t)x_2(t), \\ \dfrac{dx_2(t)}{dt} = c_2(602.3\bar{V}) - k_{effective\_particle}(t)x_1(t)x_2(t), \\ \dfrac{dx_3(t)}{dt} = k_{effective\_particle}(t)x_1(t)x_2(t), \end{cases} \tag{46}$$

where $k_{effective\_particle}(t)$ is defined as in Eq. (42). As discussed in the previous section, the dynamics of Eq. (46) converges to that of the Eq.(45) as $D \longrightarrow \infty$.

The upper panel of Fig.1 shows some representative results. When the diffusion rate is low (*e.g.*, D=0.16 or D=0.32) the simulations with Algorithm 1 significantly diverge from the prediction of the reaction-only Eq. (45), which does not account for diffusion. By contrast, the system behavior is very well captured by the diffusion-controlled reaction Eq. (46). As the diffusion rate increases (*e.g.*, D=1.6 or D=3.2), the

trajectories of the diffusion-controlled reaction Eq. (46) converge to those of the reaction-only Eq. (45), and both ODEs can be used to approximate the stochastic simulations with sufficient accuracy.

The lower panel of Fig.1 shows an application of Algorithm 2 to a homogeneous system with a wide range of diffusion rates (40-fold differences). The system dynamics is always consistent with the prediction of the reaction-only Eq.(45).

Assessment of a dissociation reaction

Consider a reaction-diffusion system with constant input, where the reactants S_1, S_2 and S_3 are initially homogeneously distributed in a cube and assumed to diffuse with rate *D*. The reaction scheme

$$\begin{aligned} \phi &\xrightarrow{c_3} S_3, \\ S_3 &\xrightarrow{k_d} S_1 + S_2, \end{aligned}$$

can be modeled with the GMA equations

$$\begin{cases} \dfrac{d\left[X_1(t)\right]}{dt} = k_d \left[X_3(t)\right]^{f_3}, \\ \dfrac{d\left[X_2(t)\right]}{dt} = k_d \left[X_3(t)\right]^{f_3}, \\ \dfrac{d\left[X_3(t)\right]}{dt} = c_3 - k_d \left[X_3(t)\right]^{f_3}. \end{cases} \tag{47}$$

The dissociation reaction is concentration dependent; however it is by its nature not affected by diffusion. Therefore the dissociation simulation is formulated in the same

way in both, Algorithm 1 and Algorithm 2. The system dynamics can be predicted by the corresponding particle-based reaction-only equations, which are diffusion independent:

$$\begin{cases} \dfrac{dx_1(t)}{dt} = k_{d\_particle}(t)x_3(t), \\ \dfrac{dx_2(t)}{dt} = k_{d\_particle}(t)x_3(t), \\ \dfrac{dx_3(t)}{dt} = c_3(602.3\overline{V}) - k_{d\_particle}(t)x_3(t). \end{cases} \tag{48}$$

The results in Fig.2 confirm that the simulations with the spatial stochastic model using Algorithm 1 (or Algorithm 2) are diffusion independent and consistent with the prediction by Eq.(48).

Assessment of reversible reactions

Consider a closed reaction-diffusion system where the reactants S_1, S_2 and S_3 are initially distributed homogeneously within a cube and we assume that they diffuse with rate *D*. The reaction scheme

$$S_1 + S_2 \underset{k_d}{\overset{k_a}{\rightleftarrows}} S_3$$

can be modeled with the GMA equations

$$\begin{cases} \dfrac{d\left[X_1(t)\right]}{dt} = k_d\left[X_3(t)\right]^{f_3} - k_a\left[X_1(t)\right]^{f_1}\left[X_2(t)\right]^{f_2}, \\ \dfrac{d\left[X_2(t)\right]}{dt} = k_d\left[X_3(t)\right]^{f_3} - k_a\left[X_1(t)\right]^{f_1}\left[X_2(t)\right]^{f_2}, \\ \dfrac{d\left[X_3(t)\right]}{dt} = k_a\left[X_1(t)\right]^{f_1}\left[X_2(t)\right]^{f_2} - k_d\left[X_3(t)\right]^{f_3}. \end{cases}$$

or

$$\begin{cases} \dfrac{dx_1(t)}{dt} = k_{d\_particle}(t)x_3(t) - k_{a\_particle}(t)x_1(t)x_2(t), \\ \dfrac{dx_2(t)}{dt} = k_{d\_particle}(t)x_3(t) - k_{a\_particle}(t)x_1(t)x_2(t), \\ \dfrac{dx_3(t)}{dt} = k_{a\_particle}(t)x_1(t)x_2(t) - k_{d\_particle}(t)x_3(t). \end{cases} \tag{49}$$

Here the first set of equations represents the concentration-based GMA model, while the equations in the second set are particle-based. The diffusion-controlled reaction equations for a homogeneous system are

$$\begin{cases} \dfrac{dx_1(t)}{dt} = k_{d\_particle}(t)x_3(t) - k_{effective\_particle}(t)x_1(t)x_2(t), \\ \dfrac{dx_2(t)}{dt} = k_{d\_particle}(t)x_3(t) - k_{effective\_particle}(t)x_1(t)x_2(t), \\ \dfrac{dx_3(t)}{dt} = k_{effective\_particle}(t)x_1(t)x_2(t) - k_{d\_particle}(t)x_3(t). \end{cases} \tag{50}$$

Fig.3 shows results of simulations with the spatial stochastic model using Algorithm 1. They diverge significantly from the prediction with the reaction-only kinetic Eq.(49) for low diffusion rates. However, they are well captured by the diffusion-controlled reaction in Eq. (50). As the diffusion rate increases, the trajectories of the diffusion-controlled reaction (Eq. (50)) converge to those of the particle-based reaction-only Eq. (49), and both ODEs can be used to predict the homogeneous stochastic simulations at high diffusion rates.

Models of reactions in crowded media

Creating crowded media with Netlogo

A crowded medium can be created virtually by filling a reaction volume with inert objects (see Fig.4). In particular, using the agent-based software Netlogo (Wilensky 1999), one can create crowded media with the following algorithm:

1. Select the crowding factor $p_{crowdedness} \in [0,1)$.
2. Calculate the number of cubic space units (*patches* in Netlogo) that will be turned into impenetrable "blocks": $N_{blocking\_patch} = p_{crowdedness} \times N_{total\_patch}$.
3. Randomly select $N_{blocking\_patch}$ out of total N_{total_patch} patches as crowding blocks by setting their inner variable *avail?= false.*
4. If a molecule is located at a block (patch with *avail?= false*), move it to the nearest free (non-block) location (*i.e.*, patch with *avail?= true.*).

Within a crowded medium, the molecular diffusion can be implemented by moving a molecule for the longest possible diffusion distance until it hits a block. More specifically,

1. Randomly choose a direction in the 3D space.
2. Divide the total diffusion distance $R_{collision}$ within $\Delta t = \frac{R_{collision}^{\ 2}}{6D}$ into n (say, n=5) equal *mini steps*, each with size $\frac{1}{n} R_{collision}$.

3. Repeat moving the molecule along the chosen direction for a distance of $\frac{1}{n}R_{collision}$ and stop: if (1) n repeats are completed; or (2) the molecule arrives at a block, *i.e.*, at a patch with *avail?= false*; in this case move the molecule backward for the distance of $\frac{1}{n}R_{collision}$ along the given direction.

With a portion $p_{crowdedness}$ of total patches turned into blocks that cannot be penetrated, the available reaction volume is reduced from V to $\left(1-p_{crowdedness}\right)V$.

Quantifying crowding effects

Crowding reduces the reaction volume, the particle diffusion rate, and accessibility between reacting particles. Inspired by (Klann, Lapin et al. 2011), we quantify these crowding effects with the example of a simple enzymatic reaction model. In this model, the substrate S is created through a zero-th order reaction $\phi \xrightarrow{k_1} S$ with constant rate k_1 and is consumed by the enzymatic reaction $S+E \xrightarrow{k_2} P+E$, which is assumed to follow a simple mass action kinetic with enzyme E and association rate constant k_2. Because Methods 1 and 2 start with different assumptions, we will quantify the crowding effects with two distinct approaches. The quantification of crowding effects within the framework of Method 2 is constructed in a similar manner as in (Klann, Lapin et al. 2011), while it is different within the framework of Method 1.

Quantifying crowding effects within the framework of Method 1. Assuming an idealized, infinite diffusion rate, the reaction system can be described by the concentration-based model

$$\frac{d\left[X_S(t)\right]}{dt} = k_1 - k_2\left[X_S(t)\right]\left[X_E\right], \tag{51}$$

where $[X_E]$ represents an enzyme concentration with constant value. To simulate the system stochastically, we consider the corresponding particle-based expressions of the previous equation

$$\frac{dx_S(t)}{dt} = k_1(N_A V) - k_2(N_A V)^{-1} x_S(t) x_E . \tag{52}$$

Within the framework of Method 1, Eq. (51) or Eq. (52) only describes the reaction kinetic, while the diffusion aspects are implemented in the simulation by Brownian diffusion. The overall reaction can be mathematically described by an ODE, if the system is homogeneous and diffusion is fast. However, if the diffusion rate is not sufficiently large for this approximation, we need to consider the diffusion effect through the diffusion-controlled reaction equation

$$\frac{dx_S(t)}{dt} = k_1(N_A V) - \left(\frac{1}{k_2(N_A V)^{-1}} + \frac{1}{V^{-1} 4\pi r_{collison} \left(D_E + D_S \right)} \right)^{-1} x_S(t) x_E . \tag{53}$$

The simulation strategy for implementing the diffusion-controlled reaction in a crowded medium is the following. First, we consider the effect of the reduced reaction volume. In crowded media, the effective volume is reduced from V to $V_{effective} = V\left(1 - p_{crowdedness}\right)$ due to the occupancy of inert particles.

Two distinct approaches can be proposed to simulate a zero-th order reaction in crowded media at the microscopic level; the reduced reaction volume affects these practices differently. In the first approach, one generates substrate molecules at the same rate $k_1(N_A V)$ as in a diluted environment, which implies that, in unit time, one drops the same total number of substrate molecules into a decreased effective reaction volume $V_{effective}$ as one does with the original reaction volume V. Under this practice, the concentration-based reaction rate for the zero-th order reaction will increase from k_1 in

the original volume case to $k_1\left(1-p_{crowdedness}\right)^{-1}$ in the case of a reduced volume. In the second approach, one generates substrate molecules at a reduced rate $k_1(N_A V_{crowded}) = k_1(N_A V)\left(1-p_{crowdedness}\right)$, *i.e.*, in unit time one drops a smaller number of substrate molecules into a reduced effective reaction volume $V_{effective}$ than one does with the original reaction volume V. Under this practice, the concentration-based reaction rate for a zero-th order reaction maintains the same k_1 for both cases of the original or the reduced volume. Since the first practice is closer to what people do in controlled experiments, we will model this practice. This choice will also give us a clearer picture of how the same number of reactants will act differently in the diluted versa the crowded medium.

For completeness we also mention the effect of a reduced reaction volume on dissociation reactions, which however is not pertinent for this example: the reaction rate becomes $k_{d\_particle}(t) = k_d\left(N_A V_{effective}\right)^{1-f_3} x_3(t)^{f_3-1}$. For the simulation of a second-order bimolecular reaction in crowded media at the microscopic level, we choose the reaction rate constant as $k_2(N_A V_{effective})^{-1}$ in order to represent the effect of the increased effective concentration in the crowded medium. The concentration-based reaction rate for second-order reactions will maintain the same as k_2 in both the original volume case and the reduced volume case.

With these simulation settings, the reaction-diffusion process occurring within a fully available reaction volume (without crowding obstacles) with reduced size $V_{effective}$ is captured by

$$\begin{aligned}\frac{dx_S(t)}{dt} &= k_1(N_A V) - \left(\frac{1}{k_2(N_A V_{effective})^{-1}} + \frac{1}{V_{effective}{}^{-1} 4\pi r_{collison}\left(D_E + D_S\right)}\right)^{-1} x_S(t)x_E \\ &= k_1(N_A V) - \left(1 - p_{crowdedness}\right)^{-1}\left(\frac{1}{k_2(N_A V)^{-1}} + \frac{1}{V^{-1} 4\pi r_{collison}\left(D_E + D_S\right)}\right)^{-1} x_S(t)x_E.\end{aligned} \tag{54}$$

This result demonstrates that, due to the reduced reaction volume, the second rate term is increased by a factor called the *reduced-reaction-volume effect*

$$F_{volume} \triangleq \left(1 - p_{crowdedness}\right)^{-1}. \tag{55}$$

Second, we consider the effect of a reduced diffusion rate. When the diffusion rates of S and E are reduced from D_S and D_E to D_{S_eff} and D_{E_eff}, respectively, the diffusion-reaction Eq. (54) becomes

$$\frac{dx_S(t)}{dt} = k_1(N_A V) - \left(1 - p_{crowdedness}\right)^{-1}\left(\frac{1}{k_2(N_A V)^{-1}} + \frac{1}{V^{-1} 4\pi r_{collison}\left(D_{E\_eff} + D_{S\_eff}\right)}\right)^{-1} x_S(t)x_E. \tag{56}$$

By defining a *reduced-diffusion effect* factor

$$\begin{aligned}F_{diffusion} &\triangleq \frac{\left(\frac{1}{k_2(N_A V)^{-1}} + \frac{1}{V^{-1} 4\pi r_{collison}\left(D_{E\_eff} + D_{S\_eff}\right)}\right)^{-1}}{\left(\frac{1}{k_2(N_A V)^{-1}} + \frac{1}{V^{-1} 4\pi r_{collison}\left(D_E + D_S\right)}\right)^{-1}} \\ &= \frac{\left(1 + \frac{k_2}{N_A 4\pi r_{collison}\left(D_E + D_S\right)}\right)}{\left(1 + \frac{k_2}{N_A 4\pi r_{collison}\left(D_{E\_eff} + D_{S\_eff}\right)}\right)}.\end{aligned} \tag{57}$$

Eq. (56) becomes

$$\frac{dx_S(t)}{dt} = k_1(N_A V) - F_{volume}F_{diffusion}\left(\frac{1}{k_2(N_A V)^{-1}} + \frac{1}{V^{-1}4\pi r_{collison}\left(D_E + D_S\right)}\right)^{-1} x_S(t)x_E. \quad (58)$$

Eq. (58) says that, in order to reflect the reduced diffusion rate, one needs to multiply the second term of Eq. (53) by $F_{diffusion}$.

Third, we consider the accessibility of the reacting particles. Due to the volume exclusion by obstacles, reacting particles have a lesser chance to encounter one another. The reduced accessibility leads to a further reduction of the second term of Eq.(58) by another factor F_{access}, leading to

$$\frac{dx_S(t)}{dt} = k_1(N_A V) - F_{volume}F_{diffusion}F_{access}\left(\frac{1}{k_2(N_A V)^{-1}} + \frac{1}{V^{-1}4\pi r_{collison}\left(D_E + D_S\right)}\right)^{-1} x_S(t)x_E. \quad (59)$$

F_{access} could theoretically be derived from first principles of statistical physics; however, it is for our purposes easier to use an empirical way to estimate this factor. When the system represented by Eq. (59) reaches its steady state $x_S^{st\_crowded}$, one obtains

$$0 = k_1(N_A V) - F_{volume}F_{diffusion}F_{access}\left(\frac{1}{k_2(N_A V)^{-1}} + \frac{1}{V^{-1}4\pi r_{collison}\left(D_E + D_S\right)}\right)^{-1} x_S^{st\_crowded}x_E, \quad (60)$$

which implies

$$F_{access} = k_{2\_effective}\left(N_A V\right)^{-1}\left(\frac{1}{k_2(N_A V)^{-1}} + \frac{1}{V^{-1}4\pi r_{collison}\left(D_{E\_eff} + D_{S\_eff}\right)}\right)$$
$$= \frac{k_1 N_A V\left(1 - p_{crowdedness}\right)}{x_S^{\,st\_crowded} x_E}\left(\frac{1}{k_2(N_A V)^{-1}} + \frac{1}{V^{-1}4\pi r_{collison}\left(D_{E\_eff} + D_{S\_eff}\right)}\right). \quad (61)$$

Quantifying crowding effects within the framework of Method 2. Within the framework of Method 2, the following equation captures the system dynamics. It accounts for the combined effects of both reaction and diffusion as

$$\frac{d\left[X_S(t)\right]}{dt} = k_1 - k_2\left[X_S(t)\right]\left[X_E\right], \quad (62)$$

where $\left[X_E\right]$ represents the constant enzyme concentration.

To simulate the system stochastically, we consider the corresponding particle-based representation of the previous equation

$$\frac{dx_S(t)}{dt} = k_1(N_A V) - k_2(N_A V)^{-1} x_S(t) x_E. \quad (63)$$

First, we consider the effect of the reduced reaction volume. As explained in the previous section, for the zero-th order reaction, we choose to generate substrate molecules at the rate $k_1(N_A V)$, while for the second-order reaction, we choose the reaction rate constant as $k_2(N_A V_{effective})^{-1}$. With these settings, the homogeneous system dynamics within a reduced reaction volume is described by

$$\frac{dx_S(t)}{dt} = k_1(N_A V) - k_2(N_A V_{effective})^{-1} x_S(t) x_E$$
$$= k_1(N_A V) - k_2(N_A V)^{-1}\left(1 - p_{crowdedness}\right)^{-1} x_S(t) x_E. \quad (64)$$

By comparing the particle-based equations of the original volume case (63) and that of the reduced volume case (64), one can see that the reduced volume does not have

an effect on the zero-th order reaction, but that it does lead to an increase in the second-order reaction, which can be formulated with the factor

$$F_{volume} \triangleq \left(1 - p_{crowdedness}\right)^{-1}. \tag{65}$$

Second, we consider the effect of reduced diffusion. Because we assume that the microscopic reaction rate for the second order reaction remains the same for both, diluted and crowded, situations, we investigate how a reduced diffusion rate in crowded media will affect the macroscopic reaction rate.

Given the macroscopic rate $k_{macro} = k_2 (N_A V)^{-1} \left(1 - p_{crowdedness}\right)^{-1}$ and the collision rate $k_D = 4\pi (r_S + r_E)(D_S + D_E)$, the microscopic reaction can be calculated as

$$k_{micro} = \frac{k_D k_{macro}}{k_D - k_{macro}}. \tag{66}$$

With the reduced diffusion rate, the collision rate becomes $k_{D\_eff} = 4\pi (r_S + r_E)(D_{S\_eff} + D_{E\_eff})$, and the effective macroscopic rate is $k_{macro\_eff} = \frac{k_{D\_eff} k_{micro}}{k_{D\_eff} + k_{micro}}$. Through algebraic manipulations, as detailed in (Klann, Lapin et al. 2011), one obtains

$$k_{macro\_eff} = k_{macro} \frac{1}{1 + \frac{k_{macro}}{k_D}\left(\frac{D_S + D_E}{D_{S\_eff} + D_{E\_eff}} - 1\right)}. \tag{67}$$

This equation means that the effective macroscopic rate will be reduced by a factor

$$F_{diffusion} \triangleq \frac{1}{1+\frac{k_{macro}}{k_D}\left(\frac{D_S+D_E}{D_{S\_eff}+D_{E\_eff}}-1\right)}. \tag{68}$$

Therefore for a system in a fully available, reduced volume with reduced diffusion rate, the system dynamics becomes

$$\frac{dx_S(t)}{dt} = k_1(N_A V) - k_2(N_A V)^{-1} F_{volume} F_{diffusion} x_S(t) x_E. \tag{69}$$

Third, we consider the reduced accessibility effect. Again, the reduced accessibility between reacting particles leads to a further reduction of the bimolecular reaction rate by an additional factor F_{access}, leading to

$$\frac{dx_S(t)}{dt} = k_1(N_A V) - k_2(N_A V)^{-1} F_{volume} F_{diffusion} F_{access} x_S(t) x_E. \tag{70}$$

Similar to the previous section, instead of using statistical physics, we can determine the value of F_{access} through empirical simulation data. Namely, at steady state Eq. (70) becomes

$$0 = k_1(N_A V) - k_2(N_A V)^{-1} F_{volume} F_{diffusion} F_{access} x_S^{st\_crowded} x_E, \tag{71}$$

which implies

$$F_{access} = \frac{k_1(N_A V)^2}{k_2 x_S^{st\_crowded} x_E F_{volume} F_{diffusion}}. \tag{72}$$

As seen in Fig. 5, the reaction-diffusion dynamics in crowded media (blue curves) can be quite different from the predictions with Eq. (58) (black curves), which incorporates only the effects of a reduced reaction volume and a reduced diffusion rate. The influence of reduced accessibility between reacting molecules must be achieved through particle-based simulations and can be used as input in Eq.(59). The more

crowded the medium is, the less likely the reacting molecules will encounter one another, leading to smaller accessibility and thus a smaller effective bimolecular reaction rate. Moreover, as shown in Fig. 6, the quantification of crowding effects within the framework of Method 1 are very consistent with the corresponding results of Method 2, thereby supporting the validity of both quantification methods.

Application to binding of dansylamide and carbonic anhydrase in a crowded medium

Neff and coworkers (Neff 2010; Neff, Offord et al. 2011) investigated the adequacy of the mass action model, and of several generalizations, for reactions in artificial, crowded media. Two generalizations were studied (Bajzer, Huzak et al. 2008). The first generalization is based on generalized mass action (GMA) kinetics so that both, the association rate k_a and the dissociation rate k_d, allometrically depend on the reactant concentrations. The second generalized formulation was a fractal kinetic model where k_a and k_d depend on time, according to a Zipf-Mandelbrot distribution. To validate the models, Neff and collaborators measured the time-resolved kinetic for the binding of dansylamide to carbonic anhydrase in solutions crowded by polyethylene glycol (PEG) and Ficoll. They found that only the GMA models are adequate in both dilute and different crowded environments and therefore are to be preferred over others alternatives.

The simulation methods developed here allow us to evaluate to what degree the kinetic parameters of both mass-action and GMA models, which were measured in dilute solution, can be extrapolated to crowded media. Specifically, we can simulate the mass-action or GMA model with various diffusion rates in an unobstructed reaction volume and answer two questions. First, how does diffusion affect the system dynamics? And second, is reduced diffusion alone sufficient to create the crowding effects? To answer these questions, we create a virtual intracellular compartment with inert crowding agents

and use the parameters measured in dilute solution to run simulations in the crowded environment. The resulting simulation trajectories will be compared with experimental measurements for the crowded solution. The validity of the parameter extrapolability assumption will require consistency between the simulation results and the experimental data.

The binding of dansylamide (S_1) to carbonic anhydrase (S_2) is represented by the following reaction scheme, where S_3 is an intermediate and S_4 is the final product:

$$S_1 + S_2 \underset{k_d}{\overset{k_a}{\rightleftarrows}} S_3 \underset{k_2}{\overset{k_1}{\rightleftarrows}} S_4$$

Neff et al. found that the following GMA model best fits the experimental data, which were obtained for both dilute and crowded solutions.

$$\begin{cases} \dfrac{d\left[X_1(t)\right]}{dt} = k_d\left[X_3(t)\right]^{f_3} - k_a\left[X_1(t)\right]^{f_1}\left[X_2(t)\right]^{f_2}, \\ \dfrac{d\left[X_2(t)\right]}{dt} = k_d\left[X_3(t)\right]^{f_3} - k_a\left[X_1(t)\right]^{f_1}\left[X_2(t)\right]^{f_2}, \\ \dfrac{d\left[X_3(t)\right]}{dt} = k_a\left[X_1(t)\right]^{f_1}\left[X_2(t)\right]^{f_2} - k_d\left[X_3(t)\right]^{f_3} - k_1\left[X_3(t)\right] + k_2\left[X_4(t)\right], \\ \dfrac{d\left[X_4(t)\right]}{dt} = k_1\left[X_3(t)\right] - k_2\left[X_4(t)\right], \end{cases} \tag{73}$$

The kinetic parameters are given in Table 2. The corresponding diffusion-controlled reaction version of Eq. (73) is

$$\begin{cases} \dfrac{dx_1(t)}{dt} = k_{d\_particle}(t)x_3(t)^{f_3} - k_{effective\_particle}x_1(t)x_2(t), \\ \dfrac{dx_2(t)}{dt} = k_{d\_particle}(t)x_3(t)^{f_3} - k_{effective\_particle}x_1(t)x_2(t), \\ \dfrac{dx_3(t)}{dt} = k_{effective\_particle}x_1(t)x_2(t) - k_{d\_particle}(t)x_3(t)^{f_3} - k_1x_3(t) + k_2x_4(t), \\ \dfrac{dx_4(t)}{dt} = k_1x_3(t) - k_2x_4(t), \end{cases} \tag{74}$$

where $k_{effective\_particle}$ is defined in (42) and $k_{d\_particle}(t)$ in (21). Comparative simulation results are shown in Fig. 7.

It is surprising that the GMA model is not affected by a wide range in the degree of crowding; the stochastic simulation of the GMA models with moderate (Fig. 8a) to high (Fig. 8b) initial reactant concentrations is consistent with the reaction-only ODEs. In order to examine whether both, the mass action model and the GMA model, have this property in general, we run simulations with the mass action model and the GMA model, simulating an increased bimolecular reaction rate, knowing that only the bimolecular reaction rate is affected by the accessibility effect, but not the dissociation rate. Specifically, we quantify this robustness property by defining

$$\text{relative error} \triangleq \frac{\left|CA_{Stoch\_st} - CA_{ODE\_st}\right|}{CA_{ODE\_st}},$$

where CA_{Stoch_st} $\left(CA_{ODE\_st}\right)$ is the steady-state value of carbonic anhydrase obtained by stochastic simulation (ODE prediction). The more robust the model is, the smaller the relative error it will render. As shown in Fig. 9, if the bimolecular reaction rate of the mass action models and the GMA models is enhanced by 10, 50, 100, 200 and 300 fold, we find: 1) Higher association rates lead to more pronounced relative errors. 2) The higher crowdedness leads to a larger relative error. 3) The mass action model is more

sensitive than the GMA model in responding to the crowding effects. In contrast, for low association rates, neither the mass action model nor the GMA model is significantly affected by crowdedness over a wide range of values. Knowing that the reduced volume effect enhances the reaction rate, while effects of reduced diffusion and reduced accessibility reduce the reaction rate, this phenomena of robust reaction rates in crowded media seems to imply that there is compensation between the counteracting effects, and that the model in GMA format has stronger capacity than the mass action one to capitalize on this compensation.

Further stochastic simulations (Figure 10, upper panel) show that the dynamics of the dilute GMA model is not significantly changed by crowding within a wide range of values ($p_{crowdedness} = 0, 0.1, 0.2, 0.3, 0.4, 0.5, 0.6.$). Moreover, the stochastic simulations match well with the experimental measurements of the reaction dynamics under the PEG-6000 100 g/L solution (Figure 10, lower panel). One should note that the parameter values for the stochastic simulation cannot be directly extrapolated to other concentrations of PEG-6000, and while the unadjusted simulation results differ noticeably from data for other concentrations (results not shown), they could be adjusted to match the different situation. By contrast, the stochastic simulation and the GMA model are consistent with each other over a wide range of situations (not shown here, but demonstrated before with generic reactions).

Conclusions

The steady-state and transient kinetics of biochemical reactions are typically studied in a dilute solution that contains only reactants, products and buffers. In such studies, mass

action kinetic models are used to characterize the progress of a reaction over time. In contrast to this idealized set-up, intracellular compartments are crowded by macromolecules, organelles, and other structures, which reduce diffusion, restrict the reaction space and impose nonspecific volume exclusion effects. In spite of these variances from the idealized situation, binding reactions and enzymatic kinetics have been assumed to proceed as in aqueous solutions, and the kinetic parameters determined *in vitro* have often been presumed to be representative of intracellular systems. In this study, we analyzed this presumption and evaluated it computationally and in comparison to pertinent experimental data.

To analyze the various effects of stochasticity and crowding, we proposed two conceptually distinct, particle-based methods for the simulation of diffusion-controlled reactions in which the reaction rates depend on the reactant concentrations. In the first method, the ODEs are designed to capture the microscopic reaction mechanism under the assumption that the diffusion rate is high enough to be ignored. In this case, the microscopic reaction mechanism remains the same for different diffusion rates and crowding environments. In the second method, the ODEs are assumed to reflect the combined effects of both reaction and diffusion. If the diffusion rate can be measured, the microscopic reaction mechanism in this method can be traced back according to the theory of Smoluchowski (Smoluchowski 1917; Berg and von Hippel 1985). The two conceptually different approaches proposed here lead to different consequences. The first method can be used directly to elucidate various spatial effects, such as different diffusion rates, the effective reaction volume, and the accessibility between reacting particles. The second method can also be used to probe these effects, but only after the microscopic reaction mechanism has first been calculated for a homogenous system.

In the past, Method 1 had been used for the mass action kinetics (Pogson, Smallwood et al. 2006). However, diffusion had not been considered during validation, which led to the impression that the method is inaccurate for reactions where slow

diffusion significantly affects the system dynamics (Klann, Lapin et al. 2011). Our results indicate that consistency between the diffusion-controlled reaction ODEs and the stochastic simulations can actually be obtained, if the slow diffusion is modeled as a Brownian process. The implementation of this strategy in Method 1 was shown to be valid and accurate for a range of diffusion-reaction systems. Moreover, the particle-based nature of Method 1 renders this strategy applicable to heterogeneous systems, for instance, in an agent-based modeling framework; details will be discussed in a future publication.

Beyond assessing the performance of the proposed methods with various diffusion rates in unobstructed media, we formulated and implemented concepts for applying the same methods to diffusion-reaction systems in crowded media. As one results, we quantified the effects of crowding under the two methodological frameworks. Specifically, the crowding effects can be dissected into three contributing factors, namely a reduced reaction effect, a reduced diffusion effect, and a reduced accessibility effect. The first of these enhances the reaction rate, whereas the other two slow down the reaction. Our numerical assessments demonstrate that the quantification of crowding is consistent between the two frameworks, thereby supporting the validity of both.

The utility of the two simulation strategies was demonstrated with representative reaction schemes and with an application to experimental data characterizing the binding of dansylamide and carbonic anhydrase in crowded media. Surprisingly, the GMA models (in both dilute and sucrose solution) turned out to be very robust to a wide range of diffusion rates and different degrees of crowdedness. Specifically, when the diffusion rate was varied from 0.01 to 5 or crowding was varied from 0 to 0.4, the stochastic simulation of the GMA models was shown to be consistent with the reaction-only ODEs. In order to exam whether the GMA model possesses this property in general, we ran simulations with increased bimolecular reaction rates, arguing that only the association reaction is affected by the accessibility effect. Indeed, when the association rate in the

GMA model was increased from 1 to 10, 50, 100, 200 or 300, the GMA model with a correspondingly scaled-up association rate produces results that are not significantly affected by crowding. In contrast, the traditional mass action model with a scaled-up association rate turned out to be significantly affected by high degrees of crowding (such as 0.3, 0.4). These comparative results imply that the counteracting effects of crowding compensate each other in a fashion from which the GMA format, but not the mass action format, benefits.

Authors' Contributions

JW developed the mathematical derivations, designed and performed the simulation, and drafted the manuscript. EV supervised the research and revised the manuscript. Both authors read and approved the final manuscript.

Acknowledgements

The authors thank Dr. Kevin Neff for providing experimental data and for useful conversations about the binding of dansylamide to carbonic anhydrase. This work was supported in part by a Molecular and Cellular Biosciences Grant (EOV, PI) from the National Science Foundation. Any opinions, findings, and conclusions or recommendations expressed in this material are those of the authors and do not necessarily reflect the views of the sponsoring institutions.

References

1. Fulton, A.B., *How crowded is the cytoplasm?* Cell, 1982. **30**(2): p. 345-347.

2. Ellis, R.J., *Macromolecular crowding: an important but neglected aspect of the intracellular environment.* Current Opinion in Structural Biology, 2001. **11**(1): p. 114-119.

3. Zimmerman, S.B. and S.O. Trach, *Estimation of macromolecule concentrations and excluded volume effects for the cytoplasm of Escherichia coli.* Journal of Molecular Biology, 1991. **222**(3): p. 599-620.

4. Elowitz, M.B., et al., *Protein Mobility in the Cytoplasm of Escherichia coli.* J. Bacteriol., 1999. **181**(1): p. 197-203.

5. Weiss, M., et al., *Anomalous Subdiffusion Is a Measure for Cytoplasmic Crowding in Living Cells.* Biophysical journal, 2004. **87**(5): p. 3518-3524.

6. Zhou, H.-X., G. Rivas, and A.P. Minton, *Macromolecular Crowding and Confinement: Biochemical, Biophysical, and Potential Physiological Consequences.* Annual Review of Biophysics, 2008. **37**(1): p. 375-397.

7. Ishihama, Y., et al., *Protein abundance profiling of the Escherichia coli cytosol.* BMC Genomics, 2008. **9**(1): p. 102.

8. Grima, R. and S. Schnell, *Modelling reaction kinetics inside cells.* Essays in Biochemistry, 2008. **45**: p. 41-56.

9. van Kampen, N.G., *Stochastic Processes in Physics and Chemistry*. 2007, New York: Elsevier.

10. Dogterom, M. and S. Leibler, *Physical aspects of the growth and regulation of microtubule structures.* Physical Review Letters, 1993. **70**(9): p. 1347-1350.

11. Paulsson, J., O.G. Berg, and M. Ehrenberg, *Stochastic focusing: Fluctuation-enhanced sensitivity of intracellular regulation.* Proceedings of the National Academy of Sciences, 2000. **97**(13): p. 7148-7153.

12. Paulsson, J. and M. Ehrenberg, *Noise in a minimal regulatory network: plasmid copy number control.* Quart. Rev. of Biophys., 2001. **34**: p. 1-59.

13. Vilar, J.M.G., et al., *Mechanisms of noise-resistance in genetic oscillators.* Proceedings of the National Academy of Sciences, 2002. **99**(9): p. 5988-5992.

14. Elf, J., et al., *Near-Critical Phenomena in Intracellular Metabolite Pools.* Biophysical journal, 2003. **84**(1): p. 154-170.

15. Mayawala, K., D.G. Vlachos, and J.S. Edwards, *Spatial modeling of dimerization reaction dynamics in the plasma membrane: Monte Carlo vs. continuum differential equations.* Biophysical Chemistry, 2006. **121**(3): p. 194-208.

16. Slepchenko, B.M., et al., *Computational cell biology: spatiotemporal simulation of cellular events.* Annual review of biophysics and biomolecular structure, 2002. **31**: p. 423-41.

17. Slepchenko, B.M., et al., *Quantitative cell biology with the Virtual Cell.* Trends in cell biology, 2003. **13**(11): p. 570-6.

18. Francke, C., et al., *Why the phosphotransferase system of Escherichia coli escapes diffusion limitation.* Biophysical journal, 2003. **85**(1): p. 612-22.

19. Stundzia, A.B. and C.J. Lumsden, *Stochastic simulation of coupled reaction-diffusion processes.* J. Comput. Phys., 1996. **127**(1): p. 196-207.

20. Elf, J., A. Doncic, and M. Ehrenberg, *Mesoscopic reaction-diffusion in intracellular signaling.* Fluctuations and Noise in Biological, Biophysical, and Biomedical Systems, 2003: p. 114 - 124.

21. Grima, R. and S. Schnell, *A Mesoscopic Simulation Approach for Modeling Intracellular Reactions.* Journal of Statistical Physics, 2007. **128**(1): p. 139-164.

22. Rodríguez, J.V., et al., *Spatial stochastic modelling of the phosphoenolpyruvate-dependent phosphotransferase (PTS) pathway in.* Bioinformatics, 2006. **22**(15): p. 1895-1901.

23. Eide, J.L. and A.K. Chakraborty, *Effects of quenched and annealed macromolecular crowding elements on a simple model for signaling in T lymphocytes.* The journal of physical chemistry. B, 2006. **110**(5): p. 2318-24.

24. Hattne, J., D. Fange, and J. Elf, *Stochastic reaction-diffusion simulation with MesoRD.* Bioinformatics (Oxford, England), 2005. **21**(12): p. 2923-4.

25. Ander, M., et al., *SmartCell, a framework to simulate cellular processes that combines stochastic approximation with diffusion and localisation: analysis of simple networks.* Syst Biol (Stevenage), 2004. **1**: p. 129 - 138.

26. Lee, K.H., et al., *The immunological synapse balances T cell receptor signaling and degradation.* Science (New York, N.Y.), 2003. **302**(5648): p. 1218-22.

27. Grima, R. and S. Schnell, *A systematic investigation of the rate laws valid in intracellular environments.* Biophysical Chemistry, 2006. **124**(1): p. 1-10.

28. Stiles, J. and T. Bartol, *Monte Carlo Methods for Simulating Realistic Synaptic Microphysiology Using MCell*, in *Computational Neuroscience: Realistic Modeling for Experimentalists*, E. Schutter, Editor. 2001, CRC Press.

29. Andrews, S.S. and D. Bray, *Stochastic simulation of chemical reactions with spatial resolution and single molecule detail.* Physical biology, 2004. **1**(3-4): p. 137-51.

30. van Zon, J. and P. Ten Wolde, *Green's-function reaction dynamics: A particle-based approach for simulating biochemical networks in time and space.* J Chem Phys, 2005. **123**(23): p. 128103 - 128103.

31. Voit, E.O., *Computational analysis of biochemical systems: a practical guide for biochemists and molecular biologists*. Vol. xii. 2000: Cambridge University Press.

32. Savageau, M.A., *Biochemical systems analysis. I. Some mathematical properties of the rate law for the component enzymatic reactions.* Journal of Theorectical Biology, 1969 a. **25**(3): p. 365-9.

33. Savageau, M.A., *Biochemical systems analysis. A study of function and design in molecular biology*. Vol. xvii. 1976: Addison-Wesley.

34. Torres, N.V. and E.O. Voit, *Pathway Analysis and Optimization in Metabolic Engineering*. 2002, Cambridge, U.K.: Cambridge University Press.

35. Neff, Kevin L., et al., *Validation of Fractal-Like Kinetic Models by Time-Resolved Binding Kinetics of Dansylamide and Carbonic Anhydrase in Crowded Media.* Biophysical journal, 2011. **100**(10): p. 2495-2503.

36. Savageau, M., *Michaelis-Menten mechanism reconsidered: implications of fractal kinetics.* Journal of Theoretical Biology, 1995. **176**(1): p. 115-124.

37. Savageau, M.A., *Influence of fractal kinetics on molecular recognition.* Journal of Molecular Recognition, 1993. **6**(4): p. 149-157.

38. Bajzer, Z., et al., *Mathematical analysis of models for reaction kinetics in intracellular environments.* Mathematical Biosciences, 2008. **215**(1): p. 35-47.

39. Neff, K.L., *Biochemical reaction kinetics in dilute and crowded solutions: Predictions of macroscopic and mesoscopic models and experimental observations*. 2010, Mayo Clinic: Rochester, MN.

40. Wu, J., B. Vidakovic, and E. Voit, *Constructing Stochastic Models from Deterministic Process Equations by Propensity Adjustment* BMC Systems Biology (in press), 2011.

41. Klann, M., A. Lapin, and M. Reuss, *Agent-based simulation of reactions in the crowded and structured intracellular environment: Influence of mobility and location of the reactants.* BMC Systems Biology, 2011. **5**(1): p. 71.

42. Pogson, M., et al., *Formal agent-based modelling of intracellular chemical interactions.* BioSystems, 2006. **85**(1): p. 37-45.

43. Chandrasekhar, S., *Stochastic Problems in Physics and Astronomy.* Reviews of Modern Physics, 1943. **15**(1): p. 1-89.

44. Smoluchowski, M., *Versuch einer mathematischen Theorie der Koagulationskinetik kolloider Losungen.* Z phys Chem, 1917. **92**: p. 129 - 168.

45. Berg, O. and P. von Hippel, *Diffusion-Controlled Macromolecular Interactions.* Annu Rev Biophys Biophys Chem, 1985. **14**: p. 131 - 158.

46. Bouchaud, J.-P. and A. Georges, *Anomalous diffusion in disordered media: Statistical mechanisms, models and physical applications.* Physics Reports, 1990. **195**(4-5): p. 127-293.

47. Wilensky, U., *NetLogo*. 1999, Center for Connected Learning and Computer-Based Modeling, Northwestern University. Evanston, IL.

Table 6.1: Numerical values of parameters used in Fig.6

Method 1	$P_{crowdedness}$				
	0	0.12	0.24	0.48	0.60
D_{eff}	0.9998	0.6318	0.4001	0.2532	0.1594
F_{volume}	1	1.1364	1.3158	1.9231	2.5
$F_{diffusion}$	1.0000	0.9299	0.8375	0.7238	0.5944
F_{access}	1.0144	0.9170	0.8323	0.6019	0.5040
$F_{volume}F_{diffusion}F_{access}$	1.0143	0.96896	0.91719	0.83774	0.74889

Method 2	$P_{crowdedness}$				
	0	0.12	0.24	0.48	0.60
D_{eff}	0.9998	0.6316	0.3999	0.2530	0.1595
F_{volume}	1	1.1364	1.3158	1.9231	2.5
$F_{diffusion}$	1.0000	0.9202	0.8176	0.6950	0.5608
F_{access}	0.9898	0.9088	0.8179	0.6040	0.5094
$F_{volume}F_{diffusion}F_{access}$	0.98981	0.95029	0.8799	0.80723	0.71425

Table 6.2: Kinetic parameters obtained by weighted least-squares fitting of the GMA model in Eq. (73) for crowded and non-crowded media (adapted from (Neff 2010)). Units for k_1 and k_2 are s^{-1}. Units for k_a and k_d are $(\mu M)^{1-f_1-f_2} s^{-1}$ and $(\mu M)^{1-f_3} s^{-1}$, respectively.

	Dilute (Mass action)	**Dilute** (GMA)	**Sucrose**	**Ficoll-400**		**PEG-6000**	
				100g/L	**150g/L**	**100g/L**	**150g/L**
k_1	19.5	0.0001	2.61	111	226	0.3000	0.0100
k_2	0.21	0.2200	0.7100	12.3	26.100	0.9300	0.3600
f_1	1	0.9400	0.6500	0.9500	0.9950	0.8200	0.8100
f_2	1	1	0.74	1.04	1.07	0.8800	0.9900
f_3	1	0.94	0.29	0.22	0.27	1.1500	0.8100
k_a	1.12	0.2870	1.3444	0.1535	0.0775	0.2993	0.1109
k_d	45.9	0.2296	0.6667	9.4602	8.324	0.1911	0.4337

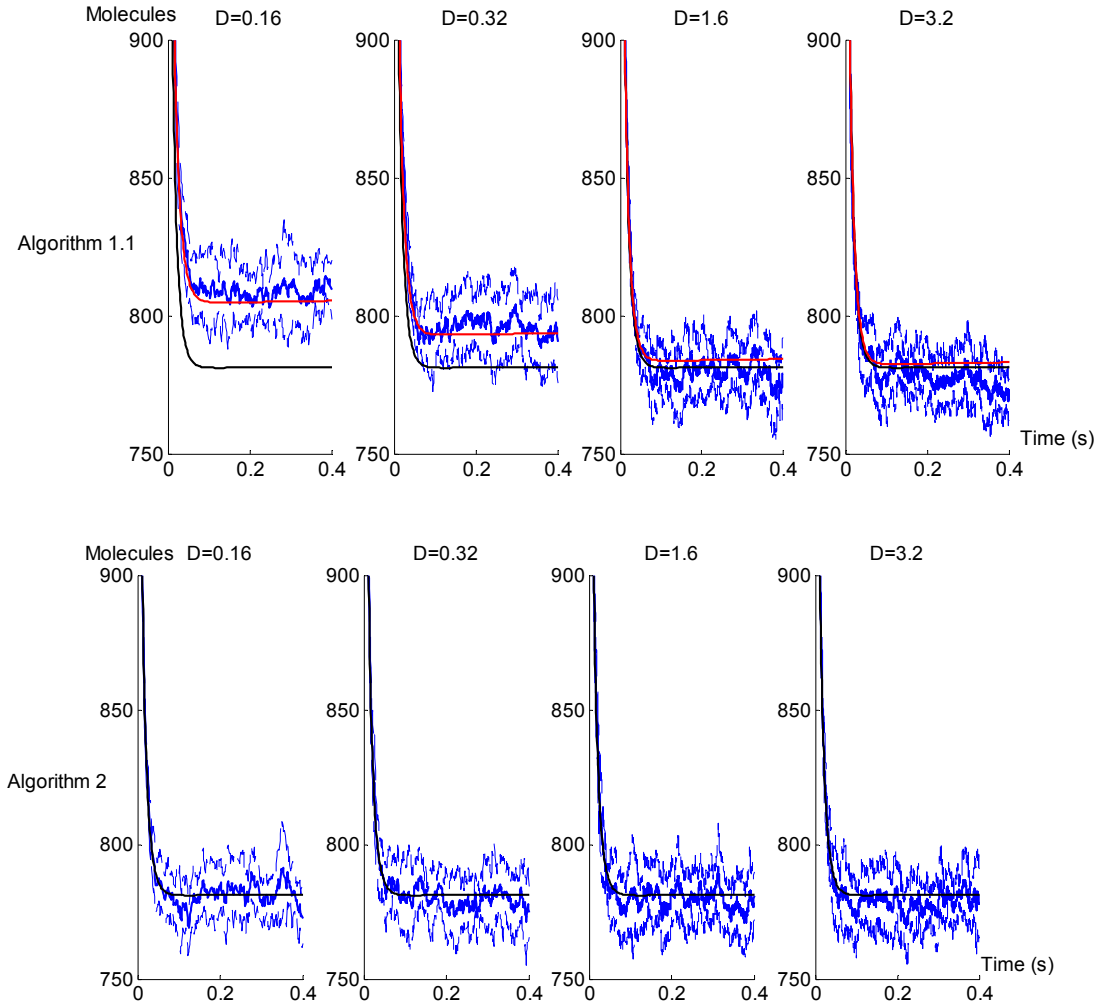

Figure 6.1. Spatial stochastic simulations of a homogeneous diffusion-reaction system. The results in the upper panel are generated by Algorithm 1: The diffusion-controlled reactions of Eq. (46) (red lines) predict quite accurately the time trajectories of S_2, which were computed with spatial stochastic simulations using Algorithm 1. By contrast, the trajectories obtained with the diffusion-controlled reaction Eq. (46) (black lines) are significantly different from the results of the particle-based reaction-only Eq.(45) at low diffusion rates; the former converge to the latter as $D \longrightarrow \infty$. The results in the lower panel are generated with Algorithm 2: The time trajectories of S_2, generated through spatial stochastic simulations using Algorithm 2, are consistent with the predictions of Eq. (45) (black lines) for all diffusion rates. Heavy blue center lines: mean of 10 spatial

stochastic simulations; thinner blue lines framing the mean: standard deviations around the mean. Diffusion rates used in the panels from left to right are: $D = 0.16, 0.32, 1.6, 3.2 \mu m^2 s^{-1}$. Other parameters are $x_1(0) = 602,\ x_2(0) = 1204,\ x_3(0) = 0,\ k_a = 50\left(\mu M\right)^{1-f_1-f_2}\ s^{-1}$, $c_1 = c_2 = 15 \mu M s^{-1},\ f_1 = 1.25,\ f_2 = 1.2,\quad r_{collision} = 0.02 \mu m$ and $V = 1 \mu m^3$. For the concentration-based GMA model (Eq. (45); top panel), the initial values are [X_1] = 1, [X_2] = 2, and [X_3] = 0.5; for comparison with the stochastic simulations, the simulation results from this model are subsequently multiplied by the corresponding number of particles, 602. The *x*-axis represents time in seconds; the *y*-axis represents the number of S_2 molecules.

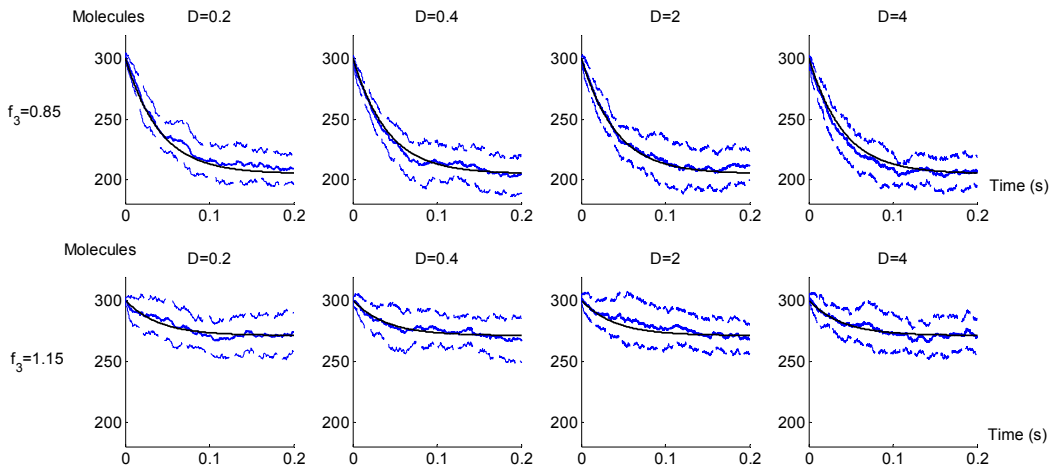

Figure 6.2. The dissociation reaction in Eq. (47) is concentration dependent, but diffusion independent. Consequently, the time trajectories of S_2, obtained with spatial stochastic simulations using Algorithm 1 or 2 are always consistent with the prediction by Eq. (48) (black lines), independent of the diffusion rate. Blue center lines: Mean of 10 spatial stochastic simulations; blue lines framing the mean: standard deviations around the mean. The diffusion rates from left to right are: $D = 0.2, 0.4, 2, 4 \mu m^2 s^{-1}$. Other parameters are $x_1(0) = 0$, $x_2(0) = 0$, $x_3(0) = 301$, $k_d = 25(\mu M)^{1-f_3}\, s^{-1}$, $c_3 = 15 \mu M s^{-1}$, $V = 1 \mu m^3$, $f_3 = 0.85$ for the upper panels and $f_3 = 1.15$ for the lower panels. For the concentration-based GMA model (Eq. (49); top panel), the initial values are [X_1] = 0, [X_2] = 0, and [X_3] = 0.5; for comparison with the stochastic simulations, the simulation results from this model are subsequently multiplied by the corresponding number of particles, 602. The *x*-axis represents time in seconds; the *y*-axis represents the number of S_3 molecules.

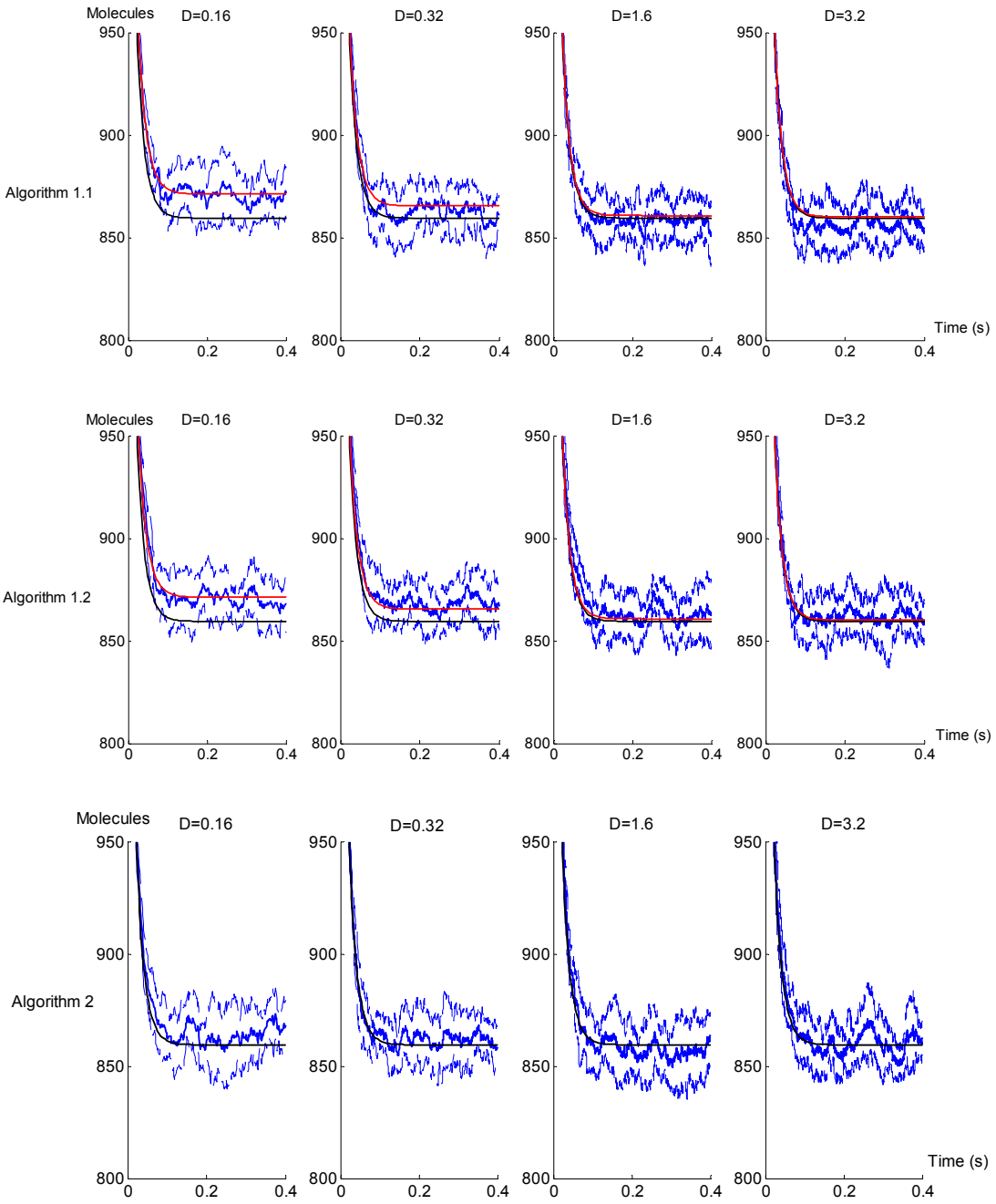

Figure 6.3. Comparison of spatial stochastic simulations of a homogeneous, reversible diffusion-reaction system with predictions from two ODEs models. The diffusion-controlled reaction Eq. (50) (red lines) rather precisely predict the averaged time trajectories of S_2, which were obtained with spatial stochastic simulations using Algorithm 1. By contrast, the trajectories obtained with the diffusion-controlled reaction

in Eq. (50) are significantly different from those of the particle-based reaction-only Eq. (49) (black lines), if the diffusion rate is low; the former converge to the latter as $D \longrightarrow \infty$. Blue center lines: Mean of 10 spatial stochastic simulations; blue lines framing the mean: standard deviations around the mean. Results from Algorithm 2 are consistent with the predictions of the particle-based reaction-only Eq. (49) (black lines). Heavy blue center lines: mean of 10 spatial stochastic simulations; thinner blue lines framing the mean: standard deviations around the mean. Diffusion rates from left to right are: $D = 0.16, 0.32, 1.6, 3.2 \mu m^2 s^{-1}$. Other parameters are $x_1(0) = 602$, $x_2(0) = 1204$, $x_3(0) = 301$, $k_a = 20(\mu M)^{1-f_1-f_2} s^{-1}$, $k_d = 10(\mu M)^{1-f_3} s^{-1}$, $r_{ij} = 0.02 \mu m$, $r_{collision} = 0.02 \mu m$, $f_1 = 1.25$, $f_2 = 1.2$, $f_3 = 0.85$ and $V = 1 \mu m^3$. For the concentration-based GMA model (Eq. (49); top panel), the initial values are [X_1] = 0, [X_2] = 0, and [X_3] = 0.5; for comparison with the stochastic simulations, the simulation results from this model are subsequently multiplied by the corresponding number of particles, 602.

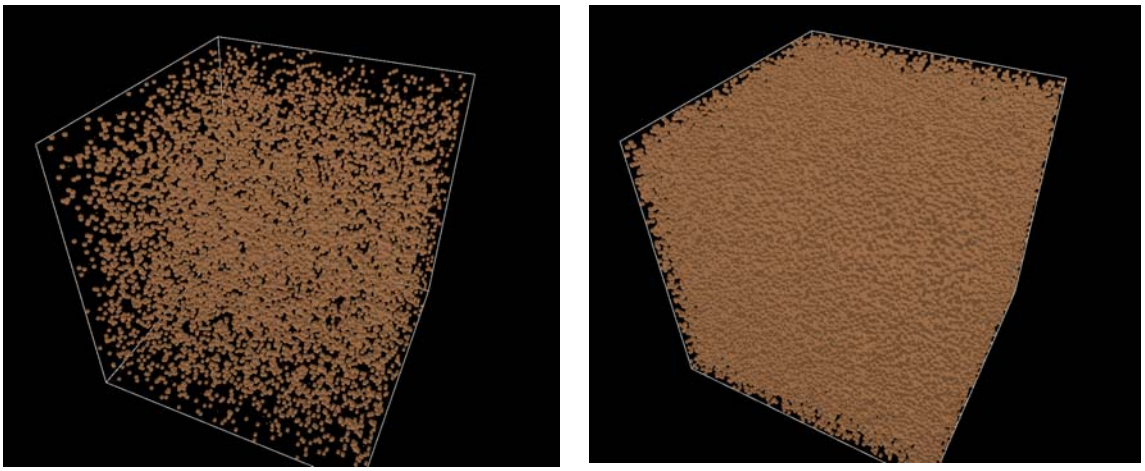

Figure 6.4. Creating a virtual, crowded medium by filling a reaction volume with inert blocks. Left: $p_{crowdedness} = 1\%$; right: $p_{crowdedness} = 10\%$.

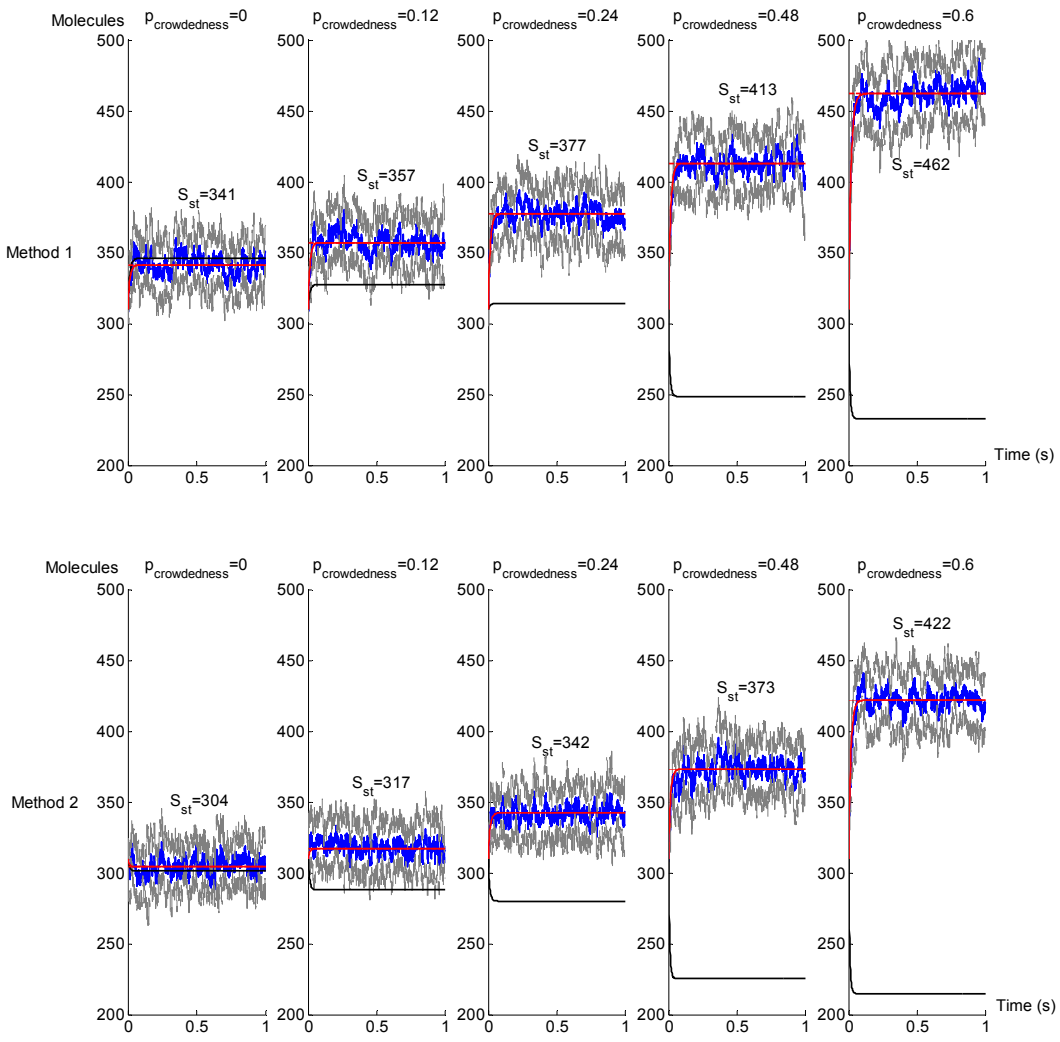

Figure 6.5. Enzymatic reaction-diffusion system in crowded media. The upper panels are generated with Method 1 (using Algorithm 1.2). Means (blue) and standard deviations (grey) are the results of 10 simulations. The black line shows the prediction of Eq. (58), which incorporates the effects of reduced reaction volume and reduced diffusion rate. Red dashed line (essentially merged with the red line): The average steady state value S_{st} which is calculated from 10 stochastic simulations by method 1. Red line: prediction of Eq.(59), which incorporates the effects of reduced reaction volume, reduced diffusion rate and reduced accessibility. The lower panels are generated with Method 2. Means

(blue) and standard deviations (grey) are from 10 simulations. Black line: prediction with ODE equation (69), which incorporates the effects of a reduced reaction volume and reduced diffusion rate. Again, the average steady-state value S_{st} is calculated from 10 stochastic simulations with Method 2. Red solid line: prediction with Eq.(70), which incorporates the effects of reduced reaction volume, reduced diffusion rate and reduced accessibility. Simulations shown from the 1st to 5th columns use $P_{crowdedness} = 0, 0.12, 0.24, 0.48$ and 0.60, respectively. The other parameters are $k_1 = 45\mu Ms^{-1}, k_2 = 45(\mu Ms)^{-1}, x_S(0) = 310, x_E = 1204,$ $D_S = D_E = 1\mu m^2 s^{-1}$, $R_{collision} = 0.02\mu m$ and $V = 1\mu m^3$. The *x*-axis represents time in seconds; the *y*-axis represents the number of substrate molecules.

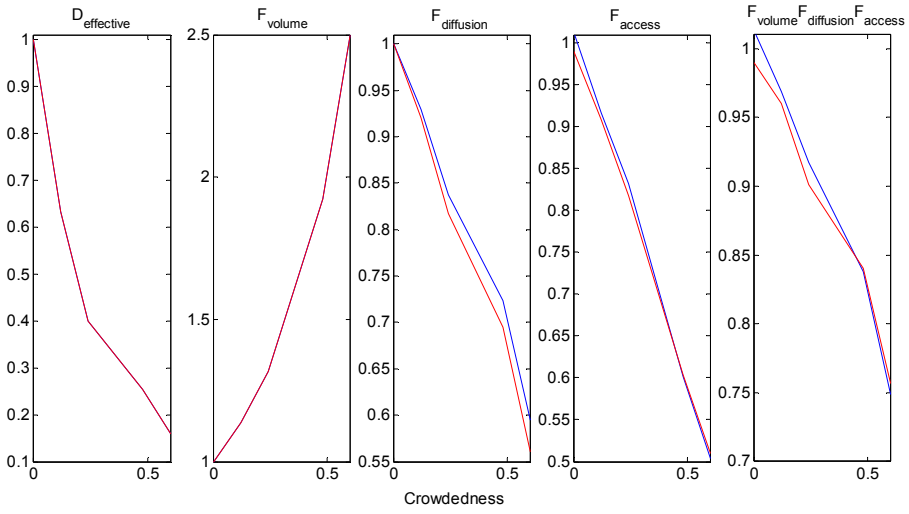

Figure 6.6. Detailed quantification of crowding effects: red lines are calculated with Method 1 and blue lines with Method 2. The *x*-axis represents the value of crowding $p_{crowdedness} = 0, 0.12, 0.24, 0.48$ and 0.60, while the *y*-axis represents the values of $D_{effective}, F_{volume}, F_{diffusion}, F_{access}$ and $F_{volume}F_{diffusion}F_{access}$ from the 1st to 5th columns of Table 1, respectively. Both axes are unit-less.

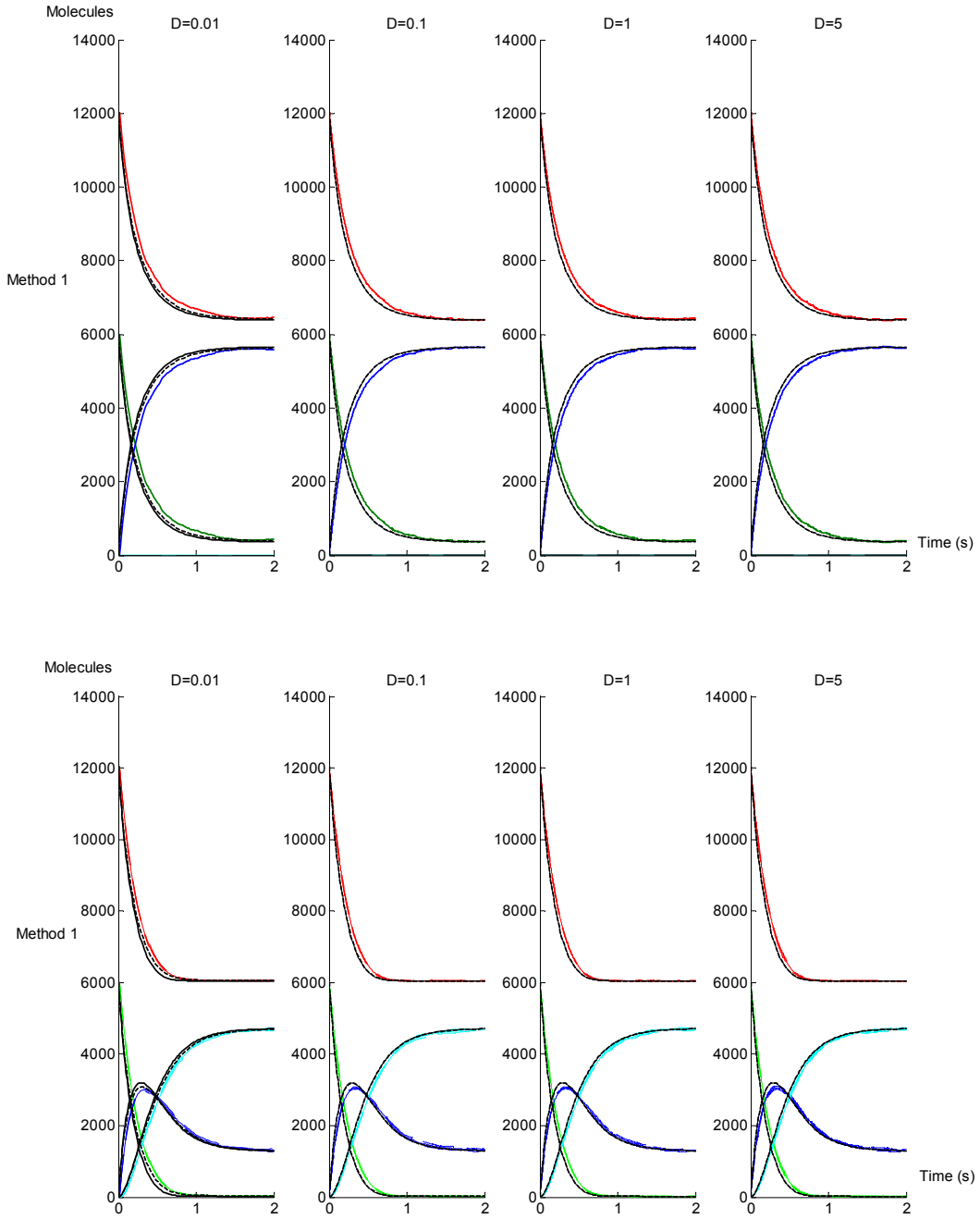

Figure 6.7. The two GMA models (for dilute and sucrose media) are not affected significantly by the diffusion rate. The upper (lower) panels display the spatial stochastic simulation of the Dilute GMA model (Sucrose GMA model) under vastly different diffusion rates. With the given parameters, the ODE predictions of the reaction-only Eq.

(73) (black solid lines) are almost identical to the diffusion-controlled reaction model in Eq. (74) (dashed black lines) for a wide range of diffusion rates. Moreover, the spatial stochastic simulations (colored lines) of a homogeneous diffusion-reaction system are rather precisely predicted by Eq. (73) (black solid lines) or Eq. (74) (dashed black lines). Green solid line: dansylamide (S_1); red: carbonic anhydrase (S_2); blue: DA-CA intermediate (S_3); cyan: DA-CA product (S_4). The diffusion rates used in the panels from left to right are: $D = 0.01, 0.1, 1, 5 \mu m^2 s^{-1}$. The other parameters are shown in the 2nd and 3rd columns of Table 2; remaining parameter values are $x_1(0) = 6023$, $x_2(0) = 12046$, $x_3(0) = 1, x_4(0) = 1$, $r_{ij} = 0.02 \mu m$, $r_{collision} = 0.02 \mu m$ and $V = 1 \mu m^3$.

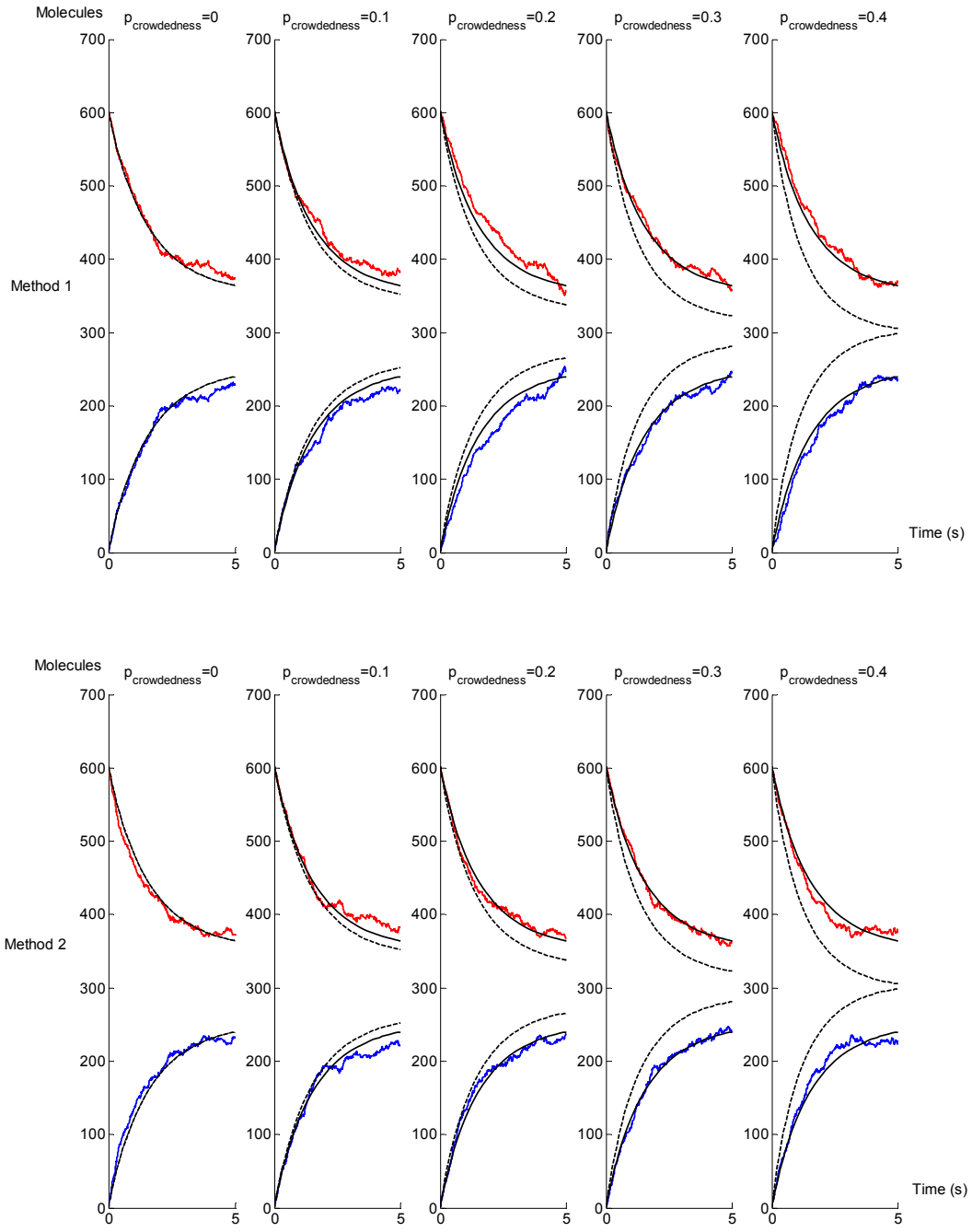

Figure 6.8a. The GMA models (for dilute conditions) are not affected significantly by a wide range of crowding parameters. The upper (lower) panels display results of simulations with Method 1 (Method 2) of the Dilute GMA model under different degrees of crowding. The spatial stochastic simulations (colored lines) of a homogeneous diffusion-reaction system are precisely predicted by reaction-only Eq. (73) (black solid

lines) but not the diffusion-reaction Eq. (74) (dashed black lines). Red: carbonic anhydrase (S_2); blue: the sum of DA-CA intermediate (S_3) and DA-CA product (S_4). The crowding rates used in the panels from left to right are: $p_{crowdedness} = 0, 0.1, 0.2, 0.3, 0.4$. The other parameters are shown at the 2nd and 3rd columns of Table 1 and $x_1(0) = 602, x_2(0) = 602, x_3(0) = 1, x_4(0) = 1,$ $r_{ij} = 0.02\mu m,$ $r_{collision} = 0.02\mu m$ and $V = 1\mu m^3$.

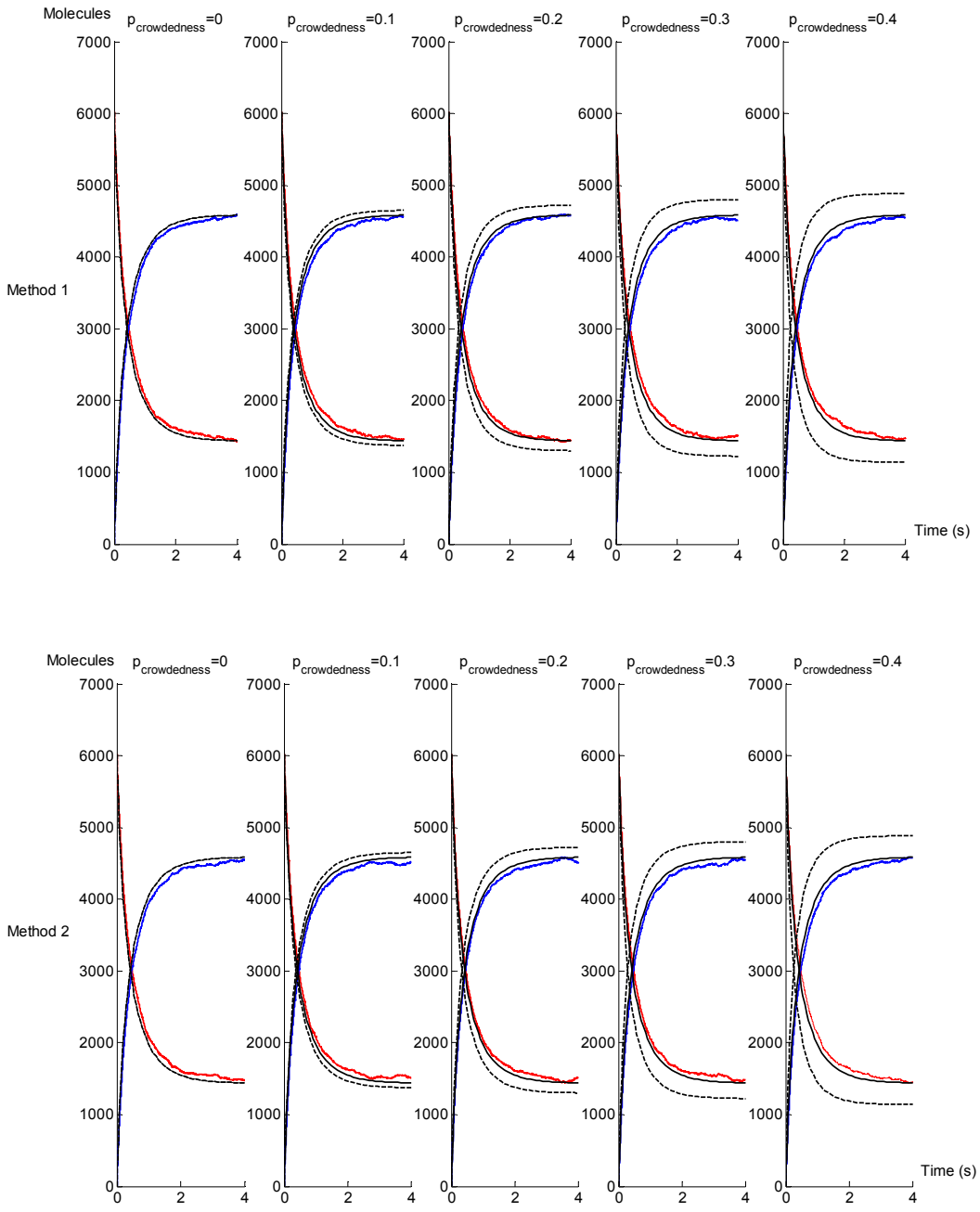

Figure 6.8b. Two GMA models (for dilute and sucrose conditions) are not affected significantly by a wide range of crowding parameters. The upper (lower) panels display results of simulations with Method 1 (Method 2) of the Dilute GMA model (Sucrose GMA model) under different degrees of crowding. The spatial stochastic simulations (colored lines) of a homogeneous diffusion-reaction system are precisely predicted by Eq.

(73) (black solid lines) but not the diffusion-reaction Eq. (74) (dashed black lines). Red: carbonic anhydrase (S_2); blue: the sum of DA-CA intermediate (S_3) and DA-CA product (S_4). The crowding rates used in the panels from left to right are: $p_{crowdedness} = 0, 0.1, 0.2, 0.3, 0.4$. The other parameters are shown at the 2nd and 3rd columns of Table 1 and $x_1(0) = 6023, x_2(0) = 6023, x_3(0) = 1, x_4(0) = 1,$ $r_{ij} = 0.02\mu m,$ $r_{collision} = 0.02\mu m$ and $V = 1\mu m^3$.

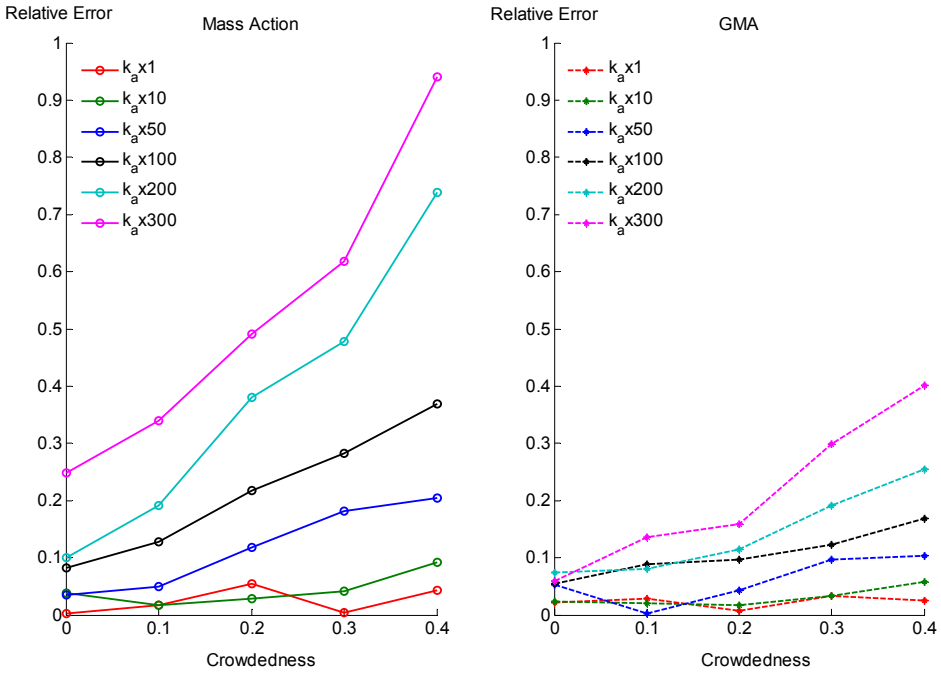

Figure 6.9. Comparison of diluted mass action models (left panel) and diluted GMA models (right panel) with escalated association rates under different degrees of crowding. The simulation results with different colors represent association reaction rates that are increased 1 (red), 10 (dark green), 50 (blue), 100 (black), 200 (dark cyan) and 300 (magenta) fold, respectively. Other parameters are shown in the 1st and 2nd columns of Table 2; furthermore: $x_1(0) = 6023, x_2(0) = 6023, x_3(0) = 1, x_4(0) = 1,$ $r_{ij} = 0.02\mu m,$ $r_{collision} = 0.02\mu m$ and $V = 1\mu m^3$. The x-axis indicates different crowding rates: $p_{crowdedness} = 0, 0.1, 0.2, 0.3, 0.4$. The y-axis exhibits the relative error in each simulation. Both axes are unitless.

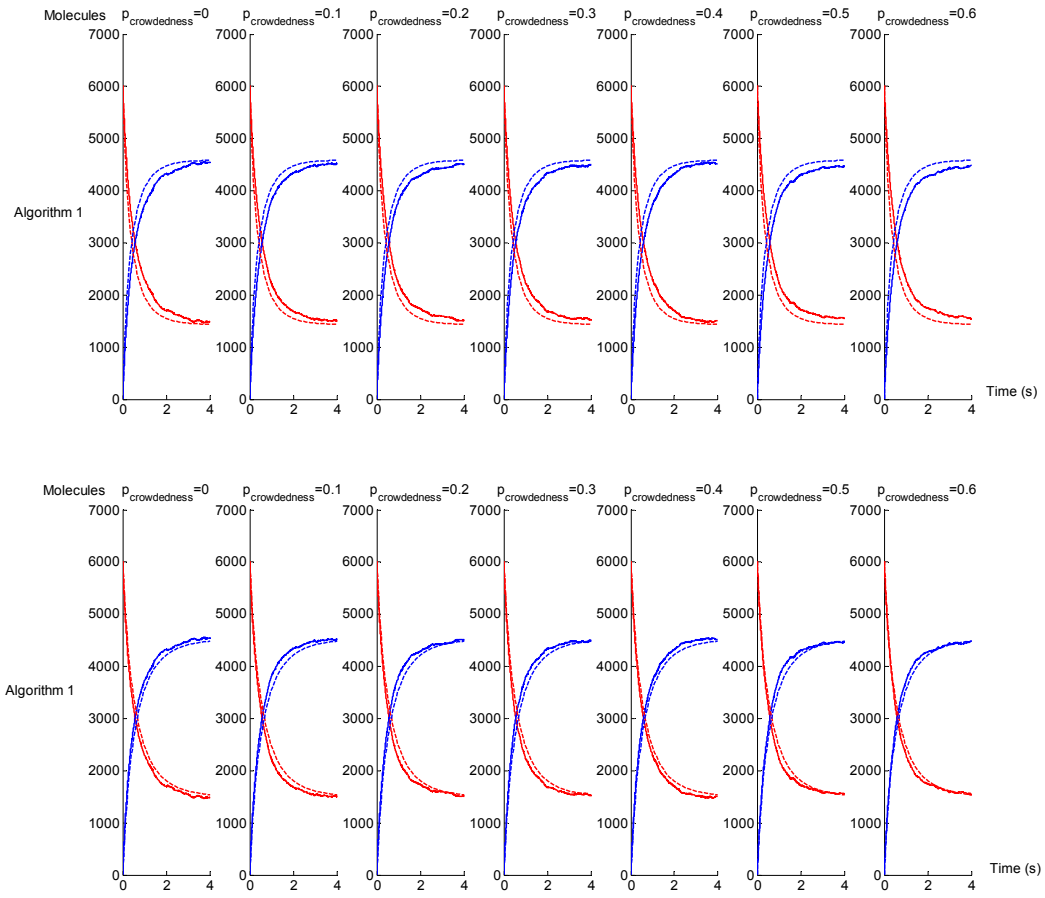

Figure 6.10. Upper panel: the GMA model for dilute conditions is not affected significantly by a wide range of crowding parameters. Lower panel: stochastic simulations with the GMA model for dilute conditions under a wide range of crowding parameters are consistent with the experimental measurements in PEG-6000 100 g/L solution (solid lines). Dashed lines show solutions with Eq. (73). Red: carbonic anhydrase (S_2); blue: the sum of DA-CA intermediate (S_3) and DA-CA product (S_4). The crowding rates used in the panels from left to right are: $p_{crowdedness} = 0, 0.1, 0.2, 0.3, 0.4, 0.5, 0.6$. The other parameters are shown at the 2nd column of Table 1 and $x_1(0) = 6023, x_2(0) = 6023, x_3(0) = 1, x_4(0) = 1,$ $r_{ij} = 0.02\mu m,$ $r_{collision} = 0.02\mu m$ and $V = 1\mu m^3$.

CHAPTER 7

SUMMARY, CONCLUSIONS, AND FUTURE WORK

Extending Biochemical Systems Theory to hybrid modeling frameworks

Several aspects of biological systems are difficult to capture with a model consisting of ordinary differential equations (ODEs). They include stochasticity, switches and delays. In the past, these aspects had to be addressed with different methodological approaches and different software packages, or it was necessary to develop new software from scratch. As a consequence, the synergisms and interrelationships between combined effects resulting from such aspects were seldom investigated, even though they are known to occur in reality with some frequency and one should expect that they may be of importance. By integrating Biochemical Systems Theory (BST) and Hybrid Functional Petri Nets (HFPN), I have developed a hybrid method that permits the simulation of biological systems containing different types of continuous and non-continuous effects, including regulation, switches, randomness, and various delays. The accuracy, efficiency and advantages of this hybrid approach were demonstrated with various examples, including representative metabolic systems, gene regulation (Chapter 2), a toggle switch (Chapter 3), and dopamine-based signal transmission (Chapter 4).

Particular attention was paid to kinetic systems that consist of few reactants and therefore have stochastic characteristics. These systems are not necessarily modeled validly with continuum representations and ODEs, because the required assumption of a well mixed, homogeneous milieu is violated. The standard alternative is Gillespie's stochastic simulation algorithm (SSA) for chemical reactions. This algorithm admits three kinds of elementary processes, namely, mass action reactions of 0^{th}, 1^{st} or 2^{nd} order. All other types of reaction processes, for instance those containing non-integer kinetic orders or following other types of kinetic laws, are assumed to be convertible to one of

the three elementary kinds, to which SSA can then be validly applied. However, the conversion to elementary reactions is often difficult, if not impossible. Within deterministic contexts, a strategy of model reduction is often employed. Such a reduction simplifies the actual system of reactions by merging or approximating intermediate steps and omitting reactants such as transient complexes, and it would be valuable to adopt a similar reduction strategy to stochastic modeling. Indeed, efforts have been devoted to manipulating the chemical master equation (CME) in order to achieve a proper propensity function for a reduced stochastic system. However, manipulations of CME are almost always complicated, and successes have been limited to relative simple cases. To address these challenges, I proposed in Chapter 5 a rather general strategy for converting a deterministic process model into a corresponding stochastic model and characterized the mathematical connections between the two. The deterministic framework was assumed to be a generalized mass action system and the stochastic analogue was in the format of the chemical master equation. The analysis identified situations: where a direct conversion is valid; where internal noise affecting the system needs to be taken into account; and where the propensity function must be mathematically adjusted. The conversion from deterministic to stochastic models was illustrated with several representative examples, including reversible biochemical reactions with feedback controls, Michaelis-Menten enzyme kinetics, a genetic regulatory motif, and stochastic focusing. The analysis demonstrated that the construction of a stochastic model for a biochemical network requires the utilization of information associated with an equation-based model. Furthermore, the proposed conversion strategy guides the model design process and ensures a valid transition between deterministic and stochastic models.

In addition to discrete and stochastic effects, biochemical processes *in vivo* almost always occur in heterogeneous, and often crowded, milieus. Nonetheless, models for such scenarios often use mass action kinetics, which, in a strict sense, are clearly limited to

biochemical reactions in dilute solution, where reactants freely diffuse and react in an unobstructed space. Indeed it had been shown that modeling diffusion-reaction kinetics in crowded environments, such as the cytoplasm, requires fractal-like ODE models. For instance, theoretical considerations had suggested generalized mass action systems as suitable formulations, and this format was indeed successfully validated in an experimental system [1, 2]. Chapter 6 discussed these situations and established two novel, particle-based methods to simulate biochemical diffusion-reaction systems within crowded environments. I distinguished two conceptually different situations. In the first, the ODEs capture a microscopic "reaction-only" mechanism, while diffusion is modeled separately. In the second case, the ODEs model the combined effects of both reaction and diffusion. This distinction led to two simulation methods that both effectively simulate and quantify crowding effects, including reduced reaction volumes, reduced diffusion rates, and reduced accessibility between potentially reacting particles. The proposed methods successfully account for fractal-like kinetics, where the reaction rate depends on the local concentrations of the molecules undergoing the reaction. Rooted in an agent based modeling framework, this aspect of the methods offers the capacity to address sophisticated intracellular spatial effects, such as macromolecular crowding, active transport along cytoskeleton structures, and reactions on heterogeneous surfaces, as well as in porous media.

Taken together, I have in this dissertation successfully developed theoretical advances, simulation methods, and algorithmic implementations that extend the deterministic continuous framework of Biochemical Systems Theory toward effects that are *a priori* difficult to model, namely different types of delays, stochasticity, discreteness, and spatial effects. These advances substantially extend the modeling repertoire for biological systems, which are by nature hybrid and span different scales in time, space, and organization.

Future developments

While this dissertation has described significant progress in the analysis of hybrid systems, further developments are needed and foreseeable in several areas.

1. **Mesoscopic methods for the simulation of reaction-diffusion systems**

The two methods developed in Chapter 6 use agent-based technique to treat every molecule as a distinct computational object and trace its position in a continuous space or on a discrete lattice over time. Focusing on this molecular level of detail, unsurprisingly, renders these methods computationally very expensive. Since the diffusion and reaction of each particle occur simultaneously, one may be able to solve this challenge by using parallel computational techniques such as GPU computing [3].

Another option might be the use of a mesoscopic method which treats molecules individually yet does not trace their exact location within subspaces of the entire volume. The computational cost for mesoscopic (microscopic) method is proportional to the compartment (molecular) amount; when the total molecular amount is much bigger than the compartments amount, the mesoscopic method is usually more efficient than the microscopic one. Among the existing mesoscopic methods, spatial Gillespie approaches usually divide the total reaction space evenly into identical subvolumes, and Gillespie-type algorithms are applied to simulate each subspace [4-7]. This strategy tends to reduce the total simulation time. To satisfy the homogeneity requirement of Gillespie's algorithms, the size of each subvolume needs to be chosen small enough so that every reactive species can be regarded as uniformly distributed. This is achieved by ensuring that the frequency of molecular diffusion events between adjacent subvolumes is much higher than the reaction frequency within each subvolume. Thus, at each time step, each molecule, represented as a point particle, either reacts within its current subvolume or

diffuses to an adjacent subvolume. The reaction probability is determined by a propensity function, while the diffusion probability is D/l^2, where D is diffusion rate and l is the subvolume side length.

Simulation efficiency could possibly also be improved by the use of a reaction propensity based on a reduced model. As shown in Chapter 5, the simulation of a full system including many reactants and reaction channels is combinatorially expensive. To counter the combinatorial explosion, the full system may be reduced by approximating, merging, or omitting intermediate reaction steps and reactants, resulting in a reduced phenomenological model. The propensity function of the reduced model can typically be computed by using power-law functions of local reactant concentrations, which can naturally be measured within each subvolume. An example of such a strategy was shown in Chapter 5, where the forward reaction was inhibited by its reaction product and the reverse reaction was accelerated by the feedback signal. These controlled effects can be quantified in a power-law function of the local concentrations of the contributing species. Therefore, a propensity function based on a reduced model may be used in the mesoscopic method to achieve low computational cost.

However, there are challenges for mesoscopic, subvolume-based methods. The first challenge is the difficulty to account for crowding effects. To the best of my knowledge, all mesoscopic methods developed so far treat molecules as point particles, and crowding effects on either reaction or diffusion have not been effectively simulated. This challenge could be solved by the technique developed in Chapter 6, which shows that the crowding effects can be quantified for a homogeneous (sub-) system. Therefore, when the crowding effects are quantified, one could use mesoscopic methods to simulate the reaction-diffusion dynamics in a crowded environment with relative low computational cost.

The second challenge is that the subvolume-based approach can give unrealistic results as the spatial discretization approaches a microscopic length scale [8, 9]. The

solutions to this challenge through propensity function adjustment have been limited to the case of bimolecular reactions abiding to the mass action law. Therefore, a future development could be to find a corresponding solution for non-mass action kinetics, such as generalized mass action representations. Chapter 6 distinguishes two interpretations of ODE-based models: In the first, the ODEs capture a microscopic "reaction-only" mechanism, while diffusion is modeled separately. In the second case, the ODEs model the combined effects of both reaction and diffusion. Because mesoscopic methods allow reactions to occur only *within* each subvolume and diffusion to occur *between* neighboring subvolumes, they impose limits on the diffusion rate. This practice is different from the case of homogeneous reactions where reacting particles freely react with one another in the total reaction volume and the diffusion rate is assumed to be infinite. The conceptual clarification in Chapter 6 could provide clues on how the unrealistic effects arise from discretization, and the particle-based methods I developed could be taken as a starting point to design reaction propensity functions with adjustment to account for the limited diffusion effect. Indeed, the subvolume-based methods corresponding to the two particle-based methods in Chapter 6 are under active development.

2. Moment-based approximation for reaction-diffusion systems with delays

The simulation of a spatial stochastic model is usually more expensive than solving corresponding ODEs, thereby making equation-based modeling computationally appealing. However, it is clear that the use of ODEs for such systems is limited in validity. In some cases, stochastic systems or subsystems can be approximated by equation-based models. An instance of such practice can be seen in [10] where spatial information is approximated by distributed time-delays and thereby a heterogeneous diffusion-reaction model can be represented by a set of delay differential equations.

However, such approaches have limitations because they are usually based on the assumption that the molecular concentration is high and noise does not propagate along reaction cascades.

When discreteness and stochastic effects cannot be ignored, the mean behavior represented by deterministic ODEs is insufficient to characterize the system dynamics, and (co-)variances as well as higher moments may need to be considered. Moment-based methods offer a promising approach for these challenges. Through solving the ODEs of moments (mean, covariance, third moments etc.), moment-based methods account for the effects of noise on the mean dynamics, thereby making it a closer approximation to multiple runs of a stochastic simulation than the mean-only ODEs. However, moment-based methods are limited to Markov-like processes where the future states of a system are totally determined by its current state. As a consequence, these methods are not directly applicable to systems with delays where the future state of the system depends on both the current state and its history.

Chapter 2 provides a technique by which a set of delay differential equations (DDEs) can be approximated by a set of ODEs with arbitrary accuracy. This computational technique makes it possible to approximate a delayed system by moment-based methods. Through experience with numerous numerical cases, I detected several advantages of moment-based method for delayed systems. In particular, the assumption of a high molecular concentration is not always required and moment-based methods can be used as a tool to assess low copy number effects. Also moment-based methods can be used to characterize how noise propagates through a reaction cascade. Specific features of moment-based methods for stochastic reaction networks with delays are currently under active investigation.

3. Moment-based parameter and structure estimation from time series data

Biological time series data are usually quite noisy. Traditional methods for the estimation of parameters and the structure of a system usually require the smoothing of the time series data as the first step in order to obtain information regarding the change rate of the variables of interest [11]. However, the smoothing step can introduce non-negligible artificial error. Moreover, after the smoothing step, only the mean information is retained and other information is lost, for instance, regarding the covariance or moments with degree higher than two. A new paradigm which does not require data smoothing would have the potential to overcome these challenges: first, time series data are used to compute all the interesting moments; and second, the moments are used to recover network structure and parameters through techniques such as Bayesian inference [12]. The advantages of this new paradigm are: 1) it does not introduce artificial error during smoothing; 2) it uses all information available from the time series data and is therefore expected to recover more features of the system than smoothing methods; 3) it can be combined with other prior information as a tool to implement new means of model selection. Within the context of BST, the challenge is that the moment-based ODEs are usually not in power-law format, so that the parameter estimation could be more challenging than the traditional mean-only analogue.

Reference

1. Savageau, M.A., *Influence of fractal kinetics on molecular recognition.* Journal of Molecular Recognition, 1993. **6**(4): p. 149-157.
2. Neff, Kevin L., et al., *Validation of Fractal-Like Kinetic Models by Time-Resolved Binding Kinetics of Dansylamide and Carbonic Anhydrase in Crowded Media.* Biophysical journal, 2011. **100**(10): p. 2495-2503.

3. Vigelius, M., A. Lane, and B. Meyer, *Accelerating Reaction-Diffusion Simulations with General-Purpose Graphics Processing Units.* Bioinformatics, 2010.

4. Stundzia, A.B. and C.J. Lumsden, *Stochastic simulation of coupled reaction-diffusion processes.* J. Comput. Phys., 1996. **127**(1): p. 196-207.

5. Elf, J., A. Doncic, and M. Ehrenberg, *Mesoscopic reaction-diffusion in intracellular signaling.* Fluctuations and Noise in Biological, Biophysical, and Biomedical Systems, 2003: p. 114 - 124.

6. Grima, R. and S. Schnell, *A Mesoscopic Simulation Approach for Modeling Intracellular Reactions.* Journal of Statistical Physics, 2007. **128**(1): p. 139-164.

7. Rodríguez, J.V., et al., *Spatial stochastic modelling of the phosphoenolpyruvate-dependent phosphotransferase (PTS) pathway in.* Bioinformatics, 2006. **22**(15): p. 1895-1901.

8. Erban, R. and J. Chapman, *Stochastic modelling of reaction–diffusion processes: algorithms for bimolecular reactions.* Phys. Biol. , 2009. **6**: p. 046001.

9. Isaacson, S., *Relationship Between the Reaction-Diffusion Master Equation and Particle Tracking Models.* J. Phys. A: Math. Theor., 2008.

10. Marquez-Lago, T., A. Leier, and K. Burrage, *Probability distributed time delays: integrating spatial effects into temporal models.* BMC Systems Biology, 2010. **4**(1): p. 19.

11. Chou, I.-C. and E.O. Voit, *Recent developments in parameter estimation and structure identification of biochemical and genomic systems.* Math. Biosc. , 2009. **219**: p. 57-83.

12. Wilkinson, D.J., *Stochastic Modelling for Systems Biology*. Mathematical and computational biology series. 2006: Chapman and Hall / CRC.

Appendix A

Derivation of the mean and variance of a power-law function of random variables

The computation of the expectation of a function of random variables is based on Taylor expansion. Specifically, a Taylor series is used to approximate the first two moments of a function f of random variable X, given that f is at least twice differentiable and the moments of X are finite. The result is the following:

$$\begin{aligned} & E\left[f(X)\right] \\ & = E\left[f\left(\mu_X + (X-\mu_X)\right)\right] \\ & = E\left[f(\mu_X) + f'(\mu_X)(X-\mu_X) + \frac{1}{2}f''(\mu_X)(X-\mu_X)^2 + \mathrm{HOT}(3)\right] \\ & \approx E\left[f(\mu_X) + f'(\mu_X)(X-\mu_X) + \frac{1}{2}f''(\mu_X)(X-\mu_X)^2\right] \\ & = f(\mu_X) + \frac{1}{2}f''(\mu_X)\sigma_X{}^2. \end{aligned} \tag{A.1}$$

Similarly,
$$\mathrm{var}\left[f(X)\right] \approx f'(\mu_X)^2\sigma_X{}^2. \tag{A.2}$$

Here $\mu_X = E\left[X\right]$ and $\sigma_X{}^2 = E\left[(X-\mu_X)^2\right] = \mathrm{var}\left[X\right]$.

To compute the expectation of power-law functions, consider first the special case $f(X) = \log(X)$ for $X > 0$. Here, $f'(X) = X^{-1}$ and $f''(X) = -X^{-2}$ for $X > 0$. In the present context, the random number X represents the amount of a given molecular species, which is positive so that $f(X) = \log(X)$ is well defined. By applying the above approximation technique to log(X), we have

$$E\left[\log(X)\right] \approx \log(\mu_X) - \frac{1}{2}\left(\sigma_X / \mu_X\right)^2 \tag{A.3}$$

$$\operatorname{var}\left[\log(X)\right] \approx \left(\sigma_X / \mu_X\right)^2 . \tag{A.4}$$

The generic power-law function of several random variables is given as $PL(\mathbf{X}) = k\prod_{s=1}^{N_s} X_s^{\,f_s}$.

The same method as before can be used to estimate its mean μ_{PL} and variance σ_{PL}, which will emerge as functions of μ_s, $\sigma_s^{\,2}$ and $\operatorname{cov}\left[X_i, X_j\right]$, with $s, i, j = 1, \ldots, N_s$.

Being a function of random variables, the function $PL(\mathbf{X})$ is itself a random variable. Therefore, we can apply the above approximation to $PL(\mathbf{X})$:

$$E\left[\log(PL)\right] \approx \log(\mu_{PL}) - \frac{1}{2}\left(\sigma_{PL} / \mu_{PL}\right)^2 \tag{A.5}$$

$$\operatorname{var}\left[\log(PL)\right] \approx \left(\sigma_{PL} / \mu_{PL}\right)^2 . \tag{A.6}$$

Taking the log of $PL(\mathbf{X})$ we obtain

$$\log\left(PL(\mathbf{X})\right) = \log k + \sum_{s=1}^{N_s} f_s \log X_s ,$$

which allows us to consider the mean and variance of $\log\left(PL(\mathbf{X})\right)$ in log-space in the following fashion:

$$
\begin{aligned}
& E\left[\log\left(PL(\mathbf{X})\right)\right] \\
&= E\left[\log k + \sum_{s=1}^{N_s} f_s \log X_s\right] \\
&= \log k + \sum_{s=1}^{N_s} f_s \mathrm{E}\left[\log X_s\right] \\
&\approx \log k + \sum_{s=1}^{N_s} f_s \left(\log(\mu_s) - \frac{1}{2}\mu_s^{-2}\sigma_s^{\,2}\right) \\
&= \log\left(k\prod_{s=1}^{N_s}\mu_s^{\,f_s}\right) - \frac{1}{2}\sum_{s=1}^{N_s} f_s\left(\sigma_s/\mu_s\right)^2
\end{aligned}
\tag{A.7}
$$

$$
\begin{aligned}
& \mathrm{var}\left[\log\left(PL(\mathbf{X})\right)\right] \\
&= \sum_{s=1}^{N_s} f_s \mathrm{var}\left[\log X_s\right] + 2\sum_{i<j}^{N_s} \mathrm{cov}\left[f_i \log X_i, f_j \log X_j\right] \\
&\approx \sum_{s=1}^{N_s} f_s \mu_s^{-2}\sigma_s^{\,2} + 2\sum_{i<j}^{N_s} f_i f_j \,\mathrm{cov}\left[\log X_i, \log X_j\right].
\end{aligned}
\tag{A.8}
$$

By combining (A.5)-(A.8), we have

$$
\mu_{PL} \approx k\prod_{s=1}^{N_s}\mu_s^{\,f_s}\exp\left(\sum_{i<j}^{N_s} f_i f_j \,\mathrm{cov}\left[\log X_i, \log X_j\right]\right) \tag{A.9}
$$

$$
\sigma_{PL}^{\,2} \approx \mu_{PL}^{\,2}\Omega. \tag{A.10}
$$

Here, $\Omega = \sum_{s=1}^{N_s} f_s \mu_s^{-2}\sigma_s^{\,2} + 2\sum_{i<j}^{N_s} f_i f_j \,\mathrm{cov}\left[\log X_i, \log X_j\right].$

In order to see the functional relationship between $\mu_{PL}, \sigma_{PL}^{\,2}$ and $\mu_s, \sigma_{ij} \triangleq \mathrm{cov}\left[X_i, X_j\right]$, one needs to express $\mathrm{cov}\left[\log X_i, \log X_j\right]$ as a function of μ_s and σ_{ij}. Using one of two alternative treatments of $\mathrm{cov}\left[\log X_i, \log X_j\right]$, we obtain two results, as shown below.

1) The first alternative is the approximation of $\mathrm{cov}\left[\log X_i, \log X_j\right]$, based on Taylor linearization of $\log X$ at μ_X, which ignores higher-order terms (HOT(2)). This strategy yields

$$\log X = \log \mu_X + \mu_X^{-1}(X - \mu_X) + \mathrm{HOT}(2) \approx \log\left(\mu_X / e\right) + X/\mu_X .$$

Thus,

$$\begin{aligned}
&\log X_i \log X_j \\
&\approx \left(\log\left(\mu_i / e\right) + X_i/\mu_i\right)\left(\log\left(\mu_j / e\right) + X_j/\mu_j\right) \\
&= \log\left(\mu_i / e\right)\log\left(\mu_j / e\right) + \log\left(\mu_i / e\right) X_j/\mu_j + \log\left(\mu_j / e\right) X_i/\mu_i + \left(X_i/\mu_i\right)\left(X_j/\mu_j\right)
\end{aligned}$$

and

$$\begin{aligned}
&E\left[\log X_i \log X_j\right] \\
&= \log\left(\mu_i / e\right)\log\left(\mu_j / e\right) + \log\left(\mu_i / e\right) + \log\left(\mu_j / e\right) + E\left[\left(X_i/\mu_i\right)\left(X_j/\mu_j\right)\right] \\
&= \log \mu_i \log \mu_j + \mathrm{cov}\left[X_i/\mu_i, X_j/\mu_j\right].
\end{aligned}$$

To compute $E\left[\log X_i\right] E\left[\log X_j\right]$, we make use of the earlier approximation

$E\left[\log X\right] \approx \log \mu_X - \frac{1}{2}\left(\sigma_X/\mu_X\right)^2$:

$$\begin{aligned}
&E\left[\log X_i\right] E\left[\log X_j\right] \\
&\approx \left(\log \mu_i - \frac{1}{2}\left(\sigma_i/\mu_i\right)^2\right)\left(\log \mu_j - \frac{1}{2}\left(\sigma_j/\mu_j\right)^2\right) \\
&= \log \mu_i \log \mu_j - \frac{1}{2}\log \mu_j \left(\sigma_i/\mu_i\right)^2 - \frac{1}{2}\log \mu_i \left(\sigma_j/\mu_j\right)^2 + \frac{1}{4}\left(\sigma_i/\mu_i\right)^2\left(\sigma_j/\mu_j\right)^2 .
\end{aligned}$$

Finally,

$$
\begin{aligned}
&\operatorname{cov}\left[\log X_i, \log X_j\right] \\
&= E\left[\log X_i \log X_j\right] - E\left[\log X_i\right] E\left[\log X_j\right] \\
&\approx \left(\log \mu_i \log \mu_j + \operatorname{cov}\left[X_i/\mu_i, X_j/\mu_j\right]\right) \\
&-\left(\log \mu_i \log \mu_j - \frac{1}{2}\log \mu_j \left(\sigma_i/\mu_i\right)^2 - \frac{1}{2}\log \mu_i \left(\sigma_j/\mu_j\right)^2 + \frac{1}{4}\left(\sigma_i/\mu_i\right)^2 \left(\sigma_j/\mu_j\right)^2\right) \qquad \text{(A.11)} \\
&= \operatorname{cov}\left[X_i/\mu_i, X_j/\mu_j\right] \\
&+ \frac{1}{2}\log(\mu_i)\left(\sigma_j/\mu_j\right)^2 + \frac{1}{2}\log(\mu_j)\left(\sigma_i/\mu_i\right)^2 - \frac{1}{4}\left(\sigma_i/\mu_i\right)^2 \left(\sigma_j/\mu_j\right)^2.
\end{aligned}
$$

Substitution of this approximation in (A.9) and (A.10) yields

$$
\mu_{PL} \approx k \prod_{s=1}^{N_s} \mu_s^{\,f_s} \exp\left(-\frac{1}{2}\sum_{s=1}^{N_s} f_s \left(\sigma_s/\mu_s\right)^2 + \frac{1}{2}\Omega\right) \qquad \text{(A.12)}
$$

$$
{\sigma_{PL}}^2 \approx {\mu_{PL}}^2 \Omega, \qquad \text{(A.13)}
$$

where

$$
\begin{aligned}
\Omega &\approx \sum_{s=1}^{N_s} f_s \left(\sigma_s/\mu_s\right)^2 + 2\sum_{i<j}^{N_s} f_i f_j \{\operatorname{cov}\left[X_i/\mu_i, X_j/\mu_j\right] \\
&+ \frac{1}{2}\log(\mu_i)\left(\sigma_j/\mu_j\right)^2 + \frac{1}{2}\log(\mu_j)\left(\sigma_i/\mu_i\right)^2 - \frac{1}{4}\left(\sigma_i/\mu_i\right)^2 \left(\sigma_j/\mu_j\right)^2\}.
\end{aligned}
$$

2) An alternative way to calculate $\operatorname{cov}\left[\log X_i, \log X_j\right]$ is to assume that $\left(X_1, \ldots, X_s\right)$ is log-normally distributed (*i.e.*, $\left(\log X_1, \ldots, \log X_s\right)$ is normally distributed). Using this assumption, Law and Kelton (Law and Kelton 2000) showed that

$$\mathrm{cov}\left[\log X_i, \log X_j\right] = \log\left(1 + \frac{\sigma_{ij}}{\mu_i \mu_j}\right). \tag{A.14}$$

By substituting this equation into (A.9) and (A.10), one obtains

$$\mu_{PL} \approx k \prod_{s=1}^{N_s} \mu_s^{f_s} \prod_{i<j}^{N_s} \left(1 + \frac{\sigma_{ij}}{\mu_i \mu_j}\right)^{f_i f_j} \tag{A.15}$$

$$\sigma_{PL}{}^2 \approx \mu_{PL}{}^2 \Omega. \tag{A.16}$$

Here, $\Omega = \sum_{s=1}^{N_s} f_s \left(\frac{\sigma_s}{\mu_s}\right)^2 + 2\sum_{i<j}^{N_s} f_i f_j \log\left(1 + \frac{\sigma_{ij}}{\mu_i \mu_j}\right)$.

The first set of expressions for μ_{PL} and $\sigma_{PL}{}^2$ (A.9 and A.10) provides an easy numerical implementation if data for the computation of $\mathrm{cov}\left[\log X_i, \log X_j\right]$ are available. The second set of expressions for μ_{PL} and $\sigma_{PL}{}^2$ (A.11 and A.13) gives a clear picture of how they are related to μ_s, σ_s and σ_{ij}; however, the price for this insight is the inaccuracy introduced during the approximation. The third set (A.15 and A.16) also provides a functional form of μ_{PL} and $\sigma_{PL}{}^2$ on $(\mu_s, \sigma_s, \sigma_{ij})$, but requires the assumption of log-normality.

Reference

1. Law, A.M. and W.D. Kelton, *Simulation Modeling and Analysis*. 3 ed. 2000, Boston: Mc.Graw Hill.

Appendix B

Computation of approximate mean and covariance for a generic propensity function to be used in stochastic simulations

Following a procedure similar to one proposed in (Lee, Kim et al. 2009), we derive an ODE system of the mean and covariance of the number of molecules. For a chemical reaction system with N_r reactions and N_s species, the governing equation is the chemical master equation (CME; Equation (21)). With simplified notation $P(\mathbf{x},t) \triangleq P(\mathbf{x},t \mid \mathbf{x}_0,t_0)$, CME becomes

$$\frac{\partial P(\mathbf{x},t)}{\partial t} = \sum_{r=1}^{N_r}\left[\alpha_r(\mathbf{x}-\mathbf{v}_r)P(\mathbf{x}-\mathbf{v}_r,t) - \alpha_r(\mathbf{x})P(\mathbf{x},t)\right]. \tag{B.1}$$

By multiplying (B.1) with x_s and then summing over all the possible states $\mathbf{x}$, we obtain

$$\sum_{\mathbf{x}} x_s \frac{\partial P(\mathbf{x},t)}{\partial t} = \sum_{r=1}^{N_r}\sum_{\mathbf{x}} x_s\left[\alpha_r(\mathbf{x}-\mathbf{v}_r)P(\mathbf{x}-\mathbf{v}_r,t) - \alpha_r(\mathbf{x})P(\mathbf{x},t)\right]. \tag{B.2}$$

Because the sum in the first term of the right-hand side covers all **x**, we are allowed to renumber terms and to replace $\mathbf{x}-\mathbf{v}_r \to \mathbf{x}$, which yields

$$\begin{aligned}\frac{\partial E[X_s]}{\partial t} &= \sum_{r=1}^{N_r}\sum_{\mathbf{x}}\left[(x_s+\mathbf{v}_{r,s})\alpha_r(\mathbf{x})P(\mathbf{x}_r,t) - x_s\alpha_r(\mathbf{x})P(\mathbf{x},t)\right] \\ &= \sum_{r=1}^{N_r}\sum_{\mathbf{x}}\left[v_{r,s}\alpha_r(\mathbf{x})P(\mathbf{x}_r,t)\right] \\ &= \sum_{r=1}^{N_r} v_{r,s}E[\alpha_r(\mathbf{X})],\end{aligned} \tag{B.3}$$

where $v_{r,s}$ is the s^{th} component of vector $\mathbf{v}_r$.

In order to obtain the second central moment, we denote $\mu_s(t) = E\left[X_s(t)\right]$, multiply eqn.(A.1) by $(x_i - \mu_i)(x_j - \mu_j)$, and sum over all possible states. The result is

$$\begin{aligned}&\sum_{\mathbf{x}}(x_i-\mu_i)(x_j-\mu_j)\frac{\partial P(\mathbf{x},t)}{\partial t}\\&=\sum_{r=1}^{N_r}\sum_{\mathbf{x}}(x_i-\mu_i)(x_j-\mu_j)\left[\alpha_r(\mathbf{x}-\mathbf{v}_r)P(\mathbf{x}-\mathbf{v}_r,t)-\alpha_r(\mathbf{x})P(\mathbf{x},t)\right].\end{aligned} \tag{B.4}$$

Again transforming the first term of the left-hand side with the replacement $\mathbf{x} - \mathbf{v}_r \to \mathbf{x}$ we obtain

$$\begin{aligned}&\frac{\partial E\left[(X_i-\mu_i)(X_j-\mu_j)\right]}{\partial t}\\&=\sum_{r=1}^{N_r}\sum_{\mathbf{x}}[(x_i+v_{r,i}-\mu_i)(x_j+v_{r,j}-\mu_j)\alpha_r(\mathbf{x})P(\mathbf{x},t)\\&-(x_i-\mu_i)(x_j-\mu_j)\alpha_r(\mathbf{x})P(\mathbf{x},t)]\\&=\sum_{r=1}^{N_r}\sum_{\mathbf{x}}[v_{r,i}(x_j-\mu_j)+v_{r,j}(x_i-\mu_i)+v_{r,i}v_{r,j}]\alpha_r(\mathbf{x})P(\mathbf{x},t)\\&=\sum_{r=1}^{N_r}\left\{v_{r,i}E\left[(X_j-\mu_j)\alpha_r(\mathbf{X})\right]+v_{r,j}E\left[(X_i-\mu_i)\alpha_r(\mathbf{X})\right]+v_{r,i}v_{r,j}E\left[\alpha_r(\mathbf{X})\right]\right\},\end{aligned} \tag{B.5}$$

where $i, j = 1, \ldots, N_s$. With these results, we can now approximate the propensity function $\alpha_r(\mathbf{x})$ using a second-order Taylor expansion at $\mathbf{X} = \boldsymbol{\mu}$, which leads to the following result:

$$\alpha_r(\mathbf{x}) \approx \alpha_r(\boldsymbol{\mu}) + \sum_{s=1}^{N_s}\frac{\partial \alpha_r(\boldsymbol{\mu})}{\partial X_s}(X_s-\mu_s) + \frac{1}{2}\sum_{m,n=1}^{N_s}\frac{\partial^2\alpha_r(\boldsymbol{\mu})}{\partial X_m \partial X_n}(X_m-\mu_m)(X_n-\mu_n). \tag{B.6}$$

The approximation becomes exact when $\alpha_r(\mathbf{x})$ is a linear or quadratic function, which is the case for elementary reactions. Furthermore, its expectation is

$$E\left[\alpha_r(\mathbf{X})\right] \approx \alpha_r(\boldsymbol{\mu}) + \frac{1}{2}\sum_{m,n=1}^{N_s} \frac{\partial^2 \alpha_r(\boldsymbol{\mu})}{\partial X_m \partial X_n} E\left[(X_m - \mu_m)(X_n - \mu_n)\right]. \tag{B.7}$$

Similarly,

$$\begin{aligned} & E\left[(X_i - \mu_i)\alpha_r(\mathbf{X})\right] \\ & \approx \sum_{s=1}^{N_s} \frac{\partial \alpha_r(\boldsymbol{\mu})}{\partial X_s} E\left[(X_i - \mu_i)(X_s - \mu_s)\right] \\ & + \frac{1}{2}\sum_{m,n=1}^{N_s} \frac{\partial^2 \alpha_r(\boldsymbol{\mu})}{\partial X_m \partial X_n} E\left[(X_i - \mu_i)(X_m - \mu_m)(X_n - \mu_n)\right]. \end{aligned} \tag{B.8}$$

Substituting eqns. (B.5) and (B.6) into (B.1) and (B.3), we obtain

$$\begin{aligned} & \frac{\partial E\left[X_s\right]}{\partial t} \\ & \approx \sum_{r=1}^{N_r} v_{r,s} \left\{ \alpha_r(\boldsymbol{\mu}) + \frac{1}{2}\sum_{m,n=1}^{N_s} \frac{\partial^2 \alpha_r(\boldsymbol{\mu})}{\partial X_m \partial X_n} E\left[(X_m - \mu_m)(X_n - \mu_n)\right] \right\} \end{aligned} \tag{B.9}$$

and

$$\begin{aligned} & \frac{\partial E\left[(X_i - \mu_i)(X_j - \mu_j)\right]}{\partial t} \\ & = \sum_{r=1}^{N_r} \{ v_{r,i} \sum_{s=1}^{N_s} \frac{\partial \alpha_r(\boldsymbol{\mu})}{\partial X_s} E\left[(X_j - \mu_j)(X_s - \mu_s)\right] \\ & + v_{r,i} \frac{1}{2}\sum_{m,n=1}^{N_s} \frac{\partial^2 \alpha_r(\boldsymbol{\mu})}{\partial X_m \partial X_n} E\left[(X_j - \mu_j)(X_m - \mu_m)(X_n - \mu_n)\right] \\ & + v_{r,j} \sum_{s=1}^{N_s} \frac{\partial \alpha_r(\boldsymbol{\mu})}{\partial X_s} E\left[(X_i - \mu_i)(X_s - \mu_s)\right] \\ & + v_{r,j} \frac{1}{2}\sum_{m,n=1}^{N_s} \frac{\partial^2 \alpha_r(\boldsymbol{\mu})}{\partial X_m \partial X_n} E\left[(X_i - \mu_i)(X_m - \mu_m)(X_n - \mu_n)\right] \\ & + v_{r,i} v_{r,j} \left[\alpha_r(\boldsymbol{\mu}) + \frac{1}{2}\sum_{m,n=1}^{N_s} \frac{\partial^2 \alpha_r(\boldsymbol{\mu})}{\partial X_m \partial X_n} E\left[(X_m - \mu_m)(X_n - \mu_n)\right] \right] \}. \end{aligned} \tag{B.10}$$

Finally, we denote $\sigma_{ij} = E\left[(X_i - \mu_i)(X_j - \mu_j)\right]$ and

$\sigma_{ijk} = E\left[(X_i - \mu_i)(X_j - \mu_j)(X_k - \mu_k)\right]$ and obtain the mean and second central moment as

$$\frac{\partial \mu_s}{\partial t} \approx \sum_{r=1}^{N_r} v_{r,s} \left\{ \alpha_r(\boldsymbol{\mu}) + \frac{1}{2} \sum_{m,n=1}^{N_s} \frac{\partial^2 \alpha_r(\boldsymbol{\mu})}{\partial X_m \partial X_n} \sigma_{mn} \right\}$$

$$\frac{\partial \sigma_{ij}}{\partial t} \approx \sum_{r=1}^{N_r} \{ v_{r,i} \sum_{s=1}^{N_s} \frac{\partial \alpha_r(\boldsymbol{\mu})}{\partial X_s} \sigma_{js} + v_{r,j} \sum_{s=1}^{N_s} \frac{\partial \alpha_r(\boldsymbol{\mu})}{\partial X_s} \sigma_{is} + v_{r,i} v_{r,j} \left[\alpha_r(\boldsymbol{\mu}) + \frac{1}{2} \sum_{m,n=1}^{N_s} \frac{\partial^2 \alpha_r(\boldsymbol{\mu})}{\partial X_m \partial X_n} \sigma_{mn} \right]$$
$$+ v_{r,i} \frac{1}{2} \sum_{m,n=1}^{N_s} \frac{\partial^2 \alpha_r(\boldsymbol{\mu})}{\partial X_m \partial X_n} \sigma_{jmn} + v_{r,j} \frac{1}{2} \sum_{m,n=1}^{N_s} \frac{\partial^2 \alpha_r(\boldsymbol{\mu})}{\partial X_m \partial X_n} \sigma_{imn} \}.$$

If the system is assumed to have a symmetric distribution such as multivariate normal distribution (Kurtz 1978), then the third central moment is zero and we can obtain closed-form expressions for the mean and covariance equations, namely

$$\frac{\partial \mu_s}{\partial t} \approx \sum_{r=1}^{N_r} \mathbf{v}_{r,s} \left\{ \alpha_r(\boldsymbol{\mu}) + \frac{1}{2} \sum_{m,n=1}^{N_s} \frac{\partial^2 \alpha_r(\boldsymbol{\mu})}{\partial X_m \partial X_n} \sigma_{mn} \right\} \tag{B.11}$$

$$\frac{\partial \sigma_{ij}}{\partial t} \approx \sum_{r=1}^{N_r} \left\{ v_{r,i} \sum_{s=1}^{N_s} \frac{\partial \alpha_r(\boldsymbol{\mu})}{\partial X_s} \sigma_{js} + v_{r,j} \sum_{s=1}^{N_s} \frac{\partial \alpha_r(\boldsymbol{\mu})}{\partial X_s} \sigma_{is} + v_{r,i} v_{r,j} \left[\alpha_r(\boldsymbol{\mu}) + \frac{1}{2} \sum_{m,n=1}^{N_s} \frac{\partial^2 \alpha_r(\boldsymbol{\mu})}{\partial X_m \partial X_n} \sigma_{mn} \right] \right\}. \tag{B.1}$$

Reference

1. Lee, C.H., K.-H. Kim, and P. Kim, *A moment closure method for stochastic reaction networks.* The Journal of chemical physics, 2009. **130**(13): p. 134107-15.
2. Kurtz, T.G., Stoch. Proc. Appl. , 1978. **6**: p. 223.